



**HAL**  
open science

# Treatise on the Meandering of Vortices

Tobias Bölle

► **To cite this version:**

Tobias Bölle. Treatise on the Meandering of Vortices. Fluid Dynamics [physics.flu-dyn]. Institut Polytechnique de Paris, 2021. English. NNT : 2021IPPAX038 . tel-03307146

**HAL Id: tel-03307146**

**<https://theses.hal.science/tel-03307146>**

Submitted on 29 Jul 2021

**HAL** is a multi-disciplinary open access archive for the deposit and dissemination of scientific research documents, whether they are published or not. The documents may come from teaching and research institutions in France or abroad, or from public or private research centers.

L'archive ouverte pluridisciplinaire **HAL**, est destinée au dépôt et à la diffusion de documents scientifiques de niveau recherche, publiés ou non, émanant des établissements d'enseignement et de recherche français ou étrangers, des laboratoires publics ou privés.



INSTITUT  
POLYTECHNIQUE  
DE PARIS

NNT : 2021IPPAX038

Thèse de doctorat



# Treatise on the Meandering of Vortices

Thèse de doctorat de l'Institut Polytechnique de Paris  
préparée à l'École polytechnique

École doctorale n°626 de l'Institut Polytechnique de Paris (IP Paris)  
Spécialité de doctorat : Mécanique des fluides et des solides, acoustique

Thèse présentée et soutenue à Meudon, le 3 Juin 2021, par

**TOBIAS BÖLLE**

Composition du Jury :

Pierre Brancher Professeur des universités, Université Paul Sabatier / IMFT, France	Président du Jury
Gert J. F. van Heijst Professeur, TU Eindhoven, Pays-Bas	Rapporteur
Stéphane Le Dizès Directeur de l'IRPHE, Institut de Recherche sur les Phénomènes Hors Équilibre, France	Rapporteur
Carlos del Pino Professeur, Université de Málaga, Espagne	Examineur
Laurent Jacquin Professeur, École polytechnique Directeur scientifique, ONERA, France	Directeur de thèse
Denis Sipp Directeur de Recherche, ONERA, France	Co-directeur de thèse
Jean-Christophe Robinet Professeur des universités, Arts et Métiers ParisTech, France	Invité (encadrant)
Vincent Brion Ingénieur de recherche, ONERA, France	Invité (encadrant)



## Acknowledgements

First of all, I would like to thank a lot my two thesis advisers Laurent and Denis for initially suggesting me the subject of vortex meandering, which turned out to be a very challenging and interesting topic, covering very different areas of physics, fluid mechanics, mathematics and experiments. The liberty they let me in choosing my approaches and their confidence cannot be acknowledged enough.

I am grateful to Laurent, whose great background in physics in general and the problem of vortex meandering in particular was always a great source of inspiration. His motivation and support in the right moments were very helpful.

I will never forget the long and intense discussions we had with Denis (especially concerning the JFM), where he put into question many of my ideas. I recognise that he was mostly right with his suggestions – although I was sometimes frustrated and did not want to hear it – and I wish to say that he taught me a lot! It was a real pleasure to work with him and to try to defend my ideas against his extremely valuable criticism and ingenuity.

Of course, the greatest thanks go to my supervisor Vincent who was always there for me in all respects and at all time. His passion and expertise were of highest value for the preparation of this thesis; I enjoyed a lot the many discussions we had and the experience he shared with me. I hope that there will be a way to continue this work one day together.

Eventually, I would like to thank Jean-Christophe for his implication in the preparation of this thesis; what started as a collaboration finally turned into an additional supervision. I am very grateful for all the discussions we had (mostly together with Denis and Vincent) and which helped to improve my studies. His impressive background in fluid mechanics and mathematics was always an important source.

It was finally to a large part the fellow PhD and post-doc students at ONERA to whom I am thankful for the very good time that I passed at Meudon. Remaining particularly good souvenirs are the very friendly welcome of Nicolas with whom I had the pleasure to share the office during the first couple of months and the many long discussions with Navrose over all problems of fluid mechanics; it was him who reminded me that PhD means Doctor of Philosophy. I also would like to thank Jahnavi and Catherine for the many exhaustive discussions we had on turbulence, its modelling and mathematics. I will always remember these good moments we passed.

And last but not least, I am very grateful for the investment, excellent suggestions and comments of all jury members. Thanks a lot GertJan van Heijst and Stéphane Le Dizès for the interest in reading my manuscript and the valuable remarks. And of course many thanks to Pierre Brancher and Carlos del Pino for their curious questions and suggestions.



# Contents

<b>1</b>	<b>Introduction</b>	<b>1</b>
<b>2</b>	<b>Characterization of vortex meandering</b>	<b>3</b>
2.1	Canonical configuration and experimental parameter space . . . . .	3
2.1.1	Geometric parameters – characterization of the observation domain and boundary conditions . . . . .	4
2.1.2	Fluid parameters – characterization of the flow field . . . . .	7
2.1.3	The typical evolution of wing wakes . . . . .	8
2.2	Vortex notions in the present context . . . . .	9
2.2.1	The dynamic–kinematic duality of vortices . . . . .	10
2.2.2	Partition of the fluid domain . . . . .	12
2.2.3	The scales of vortex dynamics . . . . .	15
2.3	What is vortex meandering? A first definition . . . . .	18
2.4	Specific characterization of trailing-vortex meandering . . . . .	20
2.4.1	Characterization in physical space . . . . .	21
2.4.2	Characterization in frequency space . . . . .	26
<b>3</b>	<b>Discussion of the possible mechanisms</b>	<b>35</b>
3.1	Extrinsic dynamics . . . . .	36
3.2	Intrinsic dynamics . . . . .	40
<b>4</b>	<b>First mechanism: Brownian meandering?</b>	<b>45</b>
4.1	A dimensional argument: the scaling law . . . . .	45
4.2	Derivation from the Navier–Stokes equations . . . . .	49
<b>5</b>	<b>Second mechanism: return to order!</b>	<b>51</b>
5.1	Organization and low-dimensionality in wing wakes . . . . .	51
5.1.1	Is there a universal scaling law of the meandering frequency? . . . . .	52
5.1.2	Is meandering a stochastic or coherent dynamics? . . . . .	52
5.2	An analogy between vortices and rotating turbulence . . . . .	61
5.2.1	Entrainment and persistence: is there fluid exchange with the free stream? . . . . .	62
5.2.2	Transition from three- to two-dimensional dynamics: a different view on the wake evolution . . . . .	63
<b>6</b>	<b>Third mechanism: energy amplification via mother–daughter interplay</b>	<b>69</b>
6.1	Vortex–turbulence interaction . . . . .	69
6.1.1	The distinct characteristics of vortex and free-stream dynamics . . . . .	70
6.1.2	Bi-directional vortex–turbulence coupling . . . . .	73
6.2	Energy transfer and the mother–daughter mechanism . . . . .	76
6.2.1	The integral fluctuation–energy balance . . . . .	76

6.3	Linear receptivity . . . . .	86
6.3.1	Analysis in frequency space: the resolvent . . . . .	88
6.3.2	Analysis in time domain: transient growth . . . . .	89
<b>7</b>	<b>Some final thoughts</b>	<b>97</b>
<b>8</b>	<b>Conclusion</b>	<b>99</b>
	<b>Bibliography</b>	<b>101</b>
<b>A</b>	<b>Details of the experiments</b>	<b>113</b>
A.1	Presentation of the experimental configuration . . . . .	113
A.2	Symbols of the experiments in figs. 2.2, 2.4 and 3.1 . . . . .	114
A.3	Details of the experiments in fig. 4.3 . . . . .	115
A.4	Details of the experiments in fig. 5.7 . . . . .	115
<b>B</b>	<b>Brownian meandering</b>	<b>117</b>
<b>C</b>	<b>The linear receptivity of vortices in frequency space</b>	<b>123</b>
<b>D</b>	<b>Long French résumé</b>	<b>153</b>

## Recurrent notations and definitions

$b$	Wing span	$\mathbf{X}(t)$	Vortex centre (random process)
$\tilde{b}$	Spacing of the trailing-vortex pair	$\mathbf{x}(t)$	Realization of vortex-centre random experiment
$c$	Chord length	$x, y, z$	Coordinates of the <i>earth-fixed frame</i>
$d$	Dimension of physical space (= 2 or 3)	$x_1, x_2$	Coordinates of the <i>laboratory-fixed frame</i>
$E_u(\omega)$	Power spectral density of the signal $u(t)$	$\alpha$	Angle of incidence
$f$	Real-valued frequency ( $\in \mathbb{R}$ )	$\alpha_z$	Streamwise wavenumber
$i, j, \dots$	Other indices ( $\in 0, \dots, \infty$ )	$\alpha, \beta, \dots$	Spatial indices ( $\in 1, \dots, d$ )
$L^2(A)$	Space of square-integrable functions on $A$	$\delta$	Correlation dimension
$M$	Fluid domain	$\Gamma(r)$	Circulation
$q$	Swirl number (defined in (2.13))	$\Gamma_0$	Initial circulation
$r_0$	Dispersion radius	$\Gamma_\infty$	Circulation at infinity ( $:= \Gamma(r \rightarrow \infty)$ )
$r_1$	Core radius	$\mu_X$	Probability density of the random variable $X$
$r_2$	Support radius	$\nu$	Kinematic viscosity
$R_c$	Chord-based Reynolds number	$\rho_u(\tau)$	Autocorrelation of the signal $u(t)$ for the time lag $\tau$
$R_\Gamma$	Circulation-based Reynolds number	$\sigma(t)$	Vortex centre standard deviation ( $\in \mathbb{R}^2$ )
$R_\delta$	Axial-velocity-deficit-based Reynolds number	$\sigma(L)$	Spectrum of the linear operator $L$
$S$	Strouhal number	$\Omega_0$	Mean angular velocity on the vortex axis
$s$	Complex-valued frequency ( $\in \mathbb{C}$ )	$\omega$	Real-valued angular frequency ( $= 2\pi f$ )
$T$	Time interval	DNS	Direct Numerical Simulation
$t_c$	Advection time ( $:= cU_\infty^{-1}$ )	HWA	Hot-Wire Anemometry
$t_r$	Rotation time ( $:= \Omega_0^{-1}$ )	LDV	Laser Doppler Velocimetry
$\mathbf{u}(t, \mathbf{x})$	Root-mean-square velocity	PIV	Particle Image Velocimetry
$\mathbf{U}, \mathbf{u}$	Mean and fluctuation velocity	POD	Proper Orthogonal Decomposition
$U_\infty$	Free-stream velocity	PSD	Power Spectral Density
$\mathbf{W}, \mathbf{w}$	Mean and fluctuation vorticity		

– A tilde  $\sim$  between two statements  $a$  and  $b$ :  $a \sim b$  – means that  $a$  and  $b$  are of the same order.

– If they are approximately the same, we write  $a \approx b$ .

These two notions are mathematically not well defined.

–  $a := b$  means that  $a$  is equal to  $b$  by definition.

– The big-O notation (Landau symbols), e.g.  $f(x) = O(g(x))$  ( $x \rightarrow x_0$ ), is defined in Dahmen & Reusken (2008, p. 20).

– Sets are denoted as:  $(a, b)$  = 'all real elements between  $a$  and  $b$ , the limits not being included';  $[a, b]$  is the same but with the limits included;  $\{a, b, \dots\}$  = 'list of given elements'.

– Angle brackets are used for all types of averages:  $\langle a \rangle$  denotes either the mathematical expectation (probability measure  $\mu$ ), the ensemble average or the time average.

– An asterisk superscript  $*$  denotes complex conjugation.

– Subscript  $_0$  = theoretical values;  $_1$  = evaluation at core radius (e.g.  $U_1, \Gamma_1$ ).

– The real and imaginary part of a complex number  $z$  are  $z_r$  and  $z_i$ , such that  $z = z_r + iz_i$ , and  $i^2 = -1$  the imaginary unit.

– In the case of Eulerian observables (e.g. the velocity or vorticity field), capital letters,  $\mathbf{U}$  (say), denote the mean flow and lowercase letters fluctuations, such that  $\mathbf{U} + \mathbf{u}$  is the Reynolds decomposition of the whole velocity field. In contrast, the vortex centre random process is denoted with the capital letter  $\mathbf{X}(t)$ , while a particular realization is  $\mathbf{x}(t)$ ; the mean centre position is  $\langle \mathbf{X}(t) \rangle$ .

– Concatenation of a matrix  $\mathbf{A}$  with a vector  $\mathbf{x}$  or another matrix  $\mathbf{B}$  indicates a matrix-vector (resp. matrix-matrix) product  $\mathbf{A}\mathbf{x} := \sum_l A_{kl}x_l$ ; the same as  $\mathbf{A}f$  means application of the operator  $\mathbf{A}$  to the function  $f$ .

– Scalar products are defined as follows:

$$(\mathbf{a}, \mathbf{b})_{\mathbb{C}^n} := \sum_{l=1}^n a_l b_l^*$$

$$(\mathbf{a}, \mathbf{b})_{\mathbb{R}^n} := \sum_{l=1}^n a_l b_l$$

$$(\mathbf{a}, \mathbf{b})_{L^2(A)} := \int_A d^m x \sum_{l=1}^n a_l(\mathbf{x}) b_l^*(\mathbf{x})$$

The induced norms are denoted as  $\|\mathbf{a}\|_{\mathbb{R}^n}^2 := (\mathbf{a}, \mathbf{a})_{\mathbb{R}^n}$  and the like.

The modulus of a scalar  $z \in \mathbb{C}$  (or  $\mathbb{R}$ ) uniformly reads  $|z| := \sqrt{z z^*}$  (or  $:= \sqrt{z^2}$ ), as the case may be.

# 1 | Introduction

Wenn jene suchenede Lust in mir ist, die nach  
Unentdecktem die Segel treibt, wenn eine  
Seefahrer-Lust in meiner Lust ist: Wenn je mein  
Frohlocken rief: »die Küste schwand , – nun fiel mir  
die letzte Kette ab – das Grenzenlose braust um  
mich, weit hinaus glänzt mir Raum und Zeit,  
wohlan! wohlauf! altes Herz!«

---

— F. Nietzsche: Also sprach Zarathustra

The mean and turbulence characteristics of (trailing) vortices are of considerable importance, determining lifetime, persistence and breakdown. However, the 'actual' or 'true' turbulence activity is overshadowed by an undulation of the 'vortex' which adds significant (fictitious) Reynolds stresses without impacting mixing, diffusion and persistence.

In the scope of (first-order) lifting-line theory, 'trailing vortices are straight lines' (Prandtl, 1918, p. 25),<sup>1</sup> while the reality is shown in fig. 1.1 – Fixed-point measurements of the 'actual' velocity fields in wind-tunnel experiments are obscured by the phenomenon of vortex wandering or meandering, manifesting as an erratic side-to-side motion<sup>2</sup> at a given downstream position (Green & Acosta, 1991, p. 107; Devenport *et al.*, 1996, p. 73). From a practical point of view, this apparently random oscillation has a significant effect on 'measured' vortex data, essentially resulting in an increased core radius, while the peak tangential velocity is decreased (Corsiglia *et al.*, 1973, p. 756; Baker *et al.*, 1974, pp. 331–332). Jacquin *et al.* (2001, p. 1) state that vortex meandering constitutes 'the main manifestation of unsteadiness . . . observed in wind-tunnel experiments'.

The phenomenon is recurrently observed since the 1970s (Corsiglia *et al.*, 1973), however, 'vortex meandering' . . . still escapes our understanding in spite of its universal character' (Jacquin *et al.*, 2005, p. 400). Still about five years ago, Edstrand *et al.* (2016, pp. 1–2) state that 'although this phenomenon has been observed in experiments for decades, the underlying mechanism that causes the wandering remains uncertain'.

One of the most puzzling controversies is the duality between apparently stochastic meandering motion, while at the same time the evolution of wing wakes is remarkable in that it is not associated with global decay but rather with the establishment of orderliness and the progressive concentration of vorticity and energy in the vortex. Indeed, it is typical of vortex experiments that, concomitantly with overall energy decay, non-axisymmetric complex waves develop in the core (Hussain *et al.*, 2011, p. 309). Vortex meandering is typically characterized as this coherent low-frequency motion which seems to be universal for (wind-tunnel-generated) vortices (Devenport *et al.*, 1996, pp. 67, 73).

As of this writing, the two essential problems in this context can be formulated as – *What is vortex meandering and why do vortices meander?*

---

<sup>1</sup>In Prandtl, L.; Betz, A. (editor: A. Dillmann): *Vier Abhandlungen zur Hydrodynamik und Aerodynamik*. Göttinger Klassiker der Strömungsmechanik. Vol. 3.

<sup>2</sup>The meaning of the word 'motion' is defined in Truesdell (1954, p. 29) and Engel & Nagel (2000, p. 533).

In this regard, they are concerned with two fundamental questions, namely the manifest nature (*Sein*) and the dynamic causality (*Werden*). In other words, the objective of the present study is to answer the question – *What are the main characteristics and governing mechanisms of vortex meandering?*

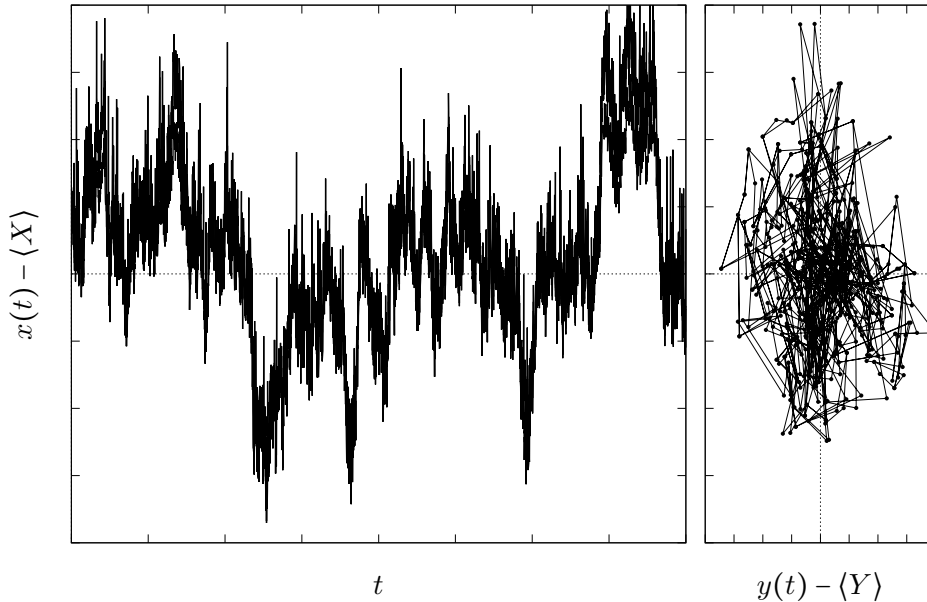


Figure 1.1: Vortex meandering in a measurement plane at  $z = 26c$  of the PIV measurements presented in appendix A.1. (a) Lateral vortex-centre displacement in the  $x$ -coordinate over time  $t$  (duration of the 'actual' experiment). (b) Vortex-centre scattering in the plane.

**Outline.** This question leads us to globally structuring the following treatise into two blocks, dealing with the characterization (chapter 2) and governing mechanisms (chapters 3–6) of vortex meandering, respectively. In some sense, chapter 2 is a preparation for the following chapters 3–6 in the sense that we first must know *what* the phenomenon *is*, before we can make any attempt to explain it.

The first block (chapter 2) is divided into four parts. To start with, it will be necessary to present the minimal experimental configuration needed to observe the phenomenon and introduce the relevant notation. From a semantic point of view, vortex meandering concerns the particular motion of a fluid object – the vortex. In order to make sense of this expression, we define what is meant by a vortex in the scope of the present study and what meandering consists of. This first general definition of the meandering motion is then refined for the case of trailing vortices in the last part of chapter 2. This analysis leads to the identification of three fundamental characteristics indispensably associated with the meandering of (trailing) vortices. Any comprehensive model therefore must explain at least these three aspects of the dynamics.

In the first part of the second block (chapter 3), we confront the previously suggested explanation approaches with these minimal characteristics. This discussion leads us to the conclusion that the meandering dynamics shares important aspects of intrinsic and extrinsic mechanisms and propose to model it in terms of a generalized receptivity. We then proceed to propose models for the three main meandering characteristics in chapters 4–6. We terminate with some final thoughts and a conclusion in chapters 7–8.

In the words of J. W. von Goethe – Was also ist des Pudels Kern?

## 2 | Characterization of vortex meandering

The formation of large, isolated vortices is an extremely common, yet spectacular phenomenon in unsteady flow. Its ubiquity suggests an explanation on statistical grounds.

---

— L. Onsager: Statistical Hydrodynamics

The objective of this chapter is to answer the question, *what is vortex meandering?* A clear statement of what the problem consists of, is necessarily the first step in explaining it. This is beautifully expressed by F. Nietzsche (*Also sprach Zarathustra*) –

Habe ich – noch ein Ziel? Einen Hafen, nach dem mein Segel läuft?  
Einen guten Wind? Ach, nur wer weiss, wohin er fährt, weiss auch, welcher  
Wind gut und sein Fahrtwind ist.<sup>1</sup>

To this end, we review the literature in conjunction with the exploration of an experimental database gathered at ONERA, which is shortly presented in appendix A.1. The thus deduced universal characteristics form the basis for the subsequent discussion of the governing mechanisms and modelling approaches.

### 2.1 Canonical configuration and experimental parameter space

L'expérience est la source unique de la vérité : elle seule peut nous apprendre quelque chose de nouveau ; elle seule peut nous donner la certitude.

---

— H. Poincaré: La Science et l'hypothèse

Before formulating an operational definition of vortex meandering in sections 2.2–2.4, it is necessary to recall the general circumstances under which the phenomenon is observed – that is, under which it is custom to refer to it.

Vortex meandering is a robust feature of trailing-vortex experiments observed for various models and wing shapes, such as rectangular full-wing (Corsiglia *et al.*, 1973; Baker *et al.*, 1974) and half-wing configurations (Devenport *et al.*, 1996; Roy & Leweke, 2008; Edstrand *et al.*, 2016) as well as Delta wings (Gursul & Xie, 2000), fins (Beresh *et al.*, 2010) and flat plates (Rokhsaz *et al.*, 2000; Navrose *et al.*, 2019) and model aeroplanes

---

<sup>1</sup>Have I – still a goal? A haven towards which my sail is set? A good wind? Ah, he only who knows where he sails, knows what wind is good, and a fair wind for him.

(Jacquin *et al.*, 2001). This variety of vortex generators suggests that the *occurrence* of meandering is not restricted to a particular shape, geometry or configuration of the vortex generator. Closer inspection even suggests that the mean characteristics of vortex meandering are essentially unaffected by these geometric details<sup>2</sup> and, therefore, can be studied for a canonical rectangular half-wing flow sketched in fig. 2.1. Or, more drastically, all that is needed to observe vortex meandering is the existence of a vortex (perhaps embedded into an unsteady flow).

We assume an incompressible fluid with constant, homogeneous material properties. The problem to solve are the incompressible Navier–Stokes equations (viscosity  $\nu \geq 0$ )

$$(2.1) \quad \partial_t \mathbf{u} = \mathbf{N}_\nu(\mathbf{u}, p), \quad \text{div } \mathbf{u} = 0, \quad \text{in } M \subset \mathbb{R}^3$$

subject to boundary conditions on  $\partial M$  and an initial condition in  $M$ . The choice of boundary conditions and fluid parameters will be discussed below.

While there is no unanimous agreement whether meandering manifests for trailing vortices in the atmosphere, as a matter of fact it *is* observed in experiments. The present work focuses on explaining experimental meandering. The first step, namely abstracting experiments into a mathematical model, is guided by the question: *What is indispensable?* More precisely, we explore the possibility of geometrical restrictions. Is there a correlation between the experimental configuration (chord length, wing profile, aspect ratio, angle of incidence) and the meandering characteristics? If so, what are the minimum requirements for the setup to observe meandering? Or, can we conceive of an experiment where we suppress meandering only by the geometrical arrangement (e.g. placing a particular model in a particular way)?

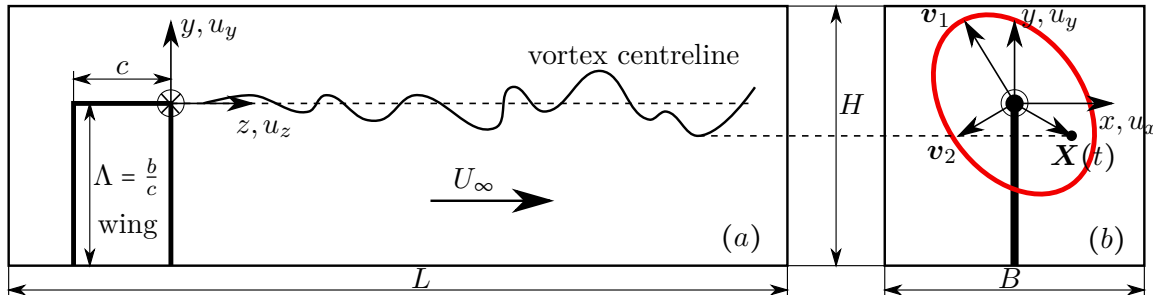


Figure 2.1: Schematic of the experimental setting (wind-tunnel dimensions  $L, B, H$ ), showing a bottom-mounted half wing (chord length  $c$  and aspect ratio  $bc^{-1}$ ). (a) Side view in the  $y - z$ -plane, showing the meandering vortex centreline. (b) Cross-plane cut, showing the instantaneous vortex-centre position  $\mathbf{X}(t)$  and the variance ellipse (red) spanned by the eigenvectors  $\mathbf{v}_1, \mathbf{v}_2$  of the covariance tensor of the vortex-centre position.

### 2.1.1 Geometric parameters – characterization of the observation domain and boundary conditions

A schematic of the canonical configuration is shown in fig. 2.1. Unless the particular facility is of importance, we shall conveniently refer to wind tunnels synonymously for all experiments. Length and width of the experimental facility are denoted  $L$  and  $\sqrt{H^2 + B^2}$ , respectively; the geometry of the facility may be cylindrical.

<sup>2</sup>Nevertheless, some footprint of the vortex generator in the meandering characteristics can be expected, as it is responsible for the vortex formation; for instance, the angle of incidence determines the circulation. The statement must be understood in the sense that, as soon as the circulation (and perhaps other parameters) is fixed, the mere origin becomes unimportant.

– The geometrical details of the vortex generator are not discussed in this work. If necessary, we merely assume a rectangular shape, defined by the chord length  $c$  and span  $b$ ; the aspect ratio is defined by  $bc^{-1}$ .

– We assume a Cartesian coordinate system  $\{x, y, z\}$  with  $z$  pointing in the direction of the free-stream velocity  $U_\infty$ ,  $y$  outwards along the trailing edge and  $x$  in order to obtain a right-handed system (the corresponding unit vectors are  $\{e_x, e_y, e_z\}$ ). The corresponding velocity components  $u_i$  are labelled alike. Unless stated otherwise, capital letters (of velocity and vorticity) indicate mean values with respect to a sensible average. Angle brackets  $\Phi = \langle \phi \rangle$  are used to denote all kinds of averages (mathematical expectation, ensemble or time average) and we assume all prerequisites to be fulfilled for their equivalence. Lower-case letters  $\varphi$  usually stand interchangeably for fluctuations<sup>3</sup> or perturbations<sup>4</sup> such that  $\phi = \Phi + \varphi$ .

– The circulation of the velocity  $\mathbf{u}$  around the closed curve  $\partial S$  (infinitesimal element  $ds$  and tangent vector  $\mathbf{t}$ ) is defined by (Truesdell, 1954, p. 10; Landau & Lifšic, 1959, p. 12; Batchelor, 2000, p. 93)

$$(2.2) \quad \Gamma := \oint_{\partial S} ds (\mathbf{t}, \mathbf{u})_{\mathbb{R}^3} = \int_S d^2x (\mathbf{n}, \nabla \times \mathbf{u})_{\mathbb{R}^3}.$$

Herein, the surface  $S$  (infinitesimal element  $d^2x$  and normal  $\mathbf{n}$ ) is bounded by  $\partial S$ . The second identity in (2.2) is a consequence of Stokes' theorem, stating that the circulation of a quantity around a closed circuit equals the flux of its curl across any surface bounded by the circuit (Truesdell, 1954, p. 13).

**Geometry and orientation of the vortex generator.** Placing a solid object in the fluid flow changes the boundary conditions and thus impacts the flow field, depending on form and orientation of the object.

– The shape of the vortex generator is essentially determined by the wing profile. Various profiles (including flat plates) and further geometric details (such as rounded tips) have been examined (e.g. Giuni, 2013). Since we are not aware of any reasonable (lift producing) configuration which does *not* result in vortex meandering, this topic is not further discussed here.

– The aspect ratio in meandering experiments published since its first observation scatters almost continuously among  $bc^{-1} \in [2, 8.7]$ . The smallest aspect ratio  $bc^{-1} = 1$  is documented for the fin experiments of Beresh *et al.* (2010). Vortex meandering is reported in all cases with no obvious trends or correlations.

– The angle of incidence is varied in the range of  $\alpha \in [0^\circ, 12^\circ]$  whereas mostly  $\alpha = 5^\circ \dots 10^\circ$  yielding a no-stall regime. We have considerable evidence that larger angles of incidence lead to reduced meandering amplitudes.

These geometrical parameters describing shape and orientation of the vortex generator can be combined to yield the circulation  $\Gamma$  which is an – perhaps the most – important quantity characterizing the wake intensity (Gerz *et al.*, 2002, pp. 185, 189; Jacquin *et al.*, 2003, p. 578).<sup>5</sup> Its dependence on the form and the orientation ( $\alpha =$  angle of incidence) of the wing is reflected in

$$(2.3) \quad \Gamma = \frac{2C_L}{\pi bc^{-1}} U_\infty b \quad \rightarrow \quad \frac{\Gamma}{U_\infty c} \sim C_L(\text{shape}, \alpha, R_c)$$

<sup>3</sup>Latin *fluctuātiō*, restless motion, indecisiveness (*unruhige Bewegung, Unentschlossenheit*; Stowasser, p. 212).

<sup>4</sup>Latin *perturbō*, to confuse or disarrange (*in Unordnung bringen*; Stowasser, p. 378).

<sup>5</sup>Since vorticity is generated at the boundaries, i.e. the object, (Batchelor, 2000, p. 266) the circulation is a measure of the *integral* effect of the vortex generator.

showing that the lift coefficient  $C_L$  is a function of the (complicated) dependencies on the vortex-generator geometry, inclination, and fluid-flow conditions ( $R_c$  is the chord-based Reynolds number defined in (2.5)).<sup>6</sup> Assuming potential theory and using the Kutta–Joukowski theorem (see also Landau & Lifšic, 1959, pp. 153–155), Prandtl (1923, p. 180) shows that

$$(2.4) \quad \Gamma(\alpha) \sim \sin \alpha,$$

indicating that the circulation increases nonlinearly with the angle of incidence  $\alpha$ . Relation (2.4) is confirmed in the experiments of Roy & Leweke (2008, p. 17) for the range of  $\alpha \in [0^\circ, 12^\circ]$ , as extrapolated from the discrete set  $\alpha \in \{6^\circ, 9^\circ, 12^\circ\}$ .

Albeit, for the question of vortex meandering, it would seem that these factors independently are of secondary importance, while mere vortex generation counts. The important parameter is probably the circulation. Of course, for a particular configuration  $\Gamma = \Gamma(\text{shape})$ , however, we expect that the reproducible (statistical) aspects of meandering should be unaffected by modifications of the shape – which for the rest leave invariant the circulation. Even more, we postulate that meandering should be similar if the vortex origin is not a wing (again leaving circulation unchanged), e.g. a tornado (Singh & Uberoi, 1976, p. 1862 arrive at a similar conclusion).

#### Conclusion 2.1.1: Restriction to the wake flow

We come to the conclusion that – for questions concerning the statistics of meandering – we can restrict to the wake region assuming the existence of a vortex with given circulation.

**Deducing boundary conditions from the wind-tunnel dimensions.** Comparing experimental arrangements from the first observation in the 1970s until today, we observe the striking trend that earlier studies emphasized large-dimensional settings and long downstream measurement distances (up to about 31 wing spans) while more recent experiments are carried out in wind-tunnels with comparably smaller cross-sectional dimensions and significantly shorter measurement distances.

Taken together, we have experimental evidence for vortex meandering over a downstream range of roughly  $zc^{-1} \in [0.5, 165]$ . From the very terminology, *vortex* meandering concerns the motion of a *vortex*. There is agreement that the vortex formation is terminated within one to two chord lengths from the wing. While this range might be crucial for the origin of meandering, the absence of a well-defined vortex suggests that we cannot speak of vortex meandering in this range. The upper limit of the observation interval should be bounded by the onset of cooperative instabilities of the counter-rotating vortex system. The onset of the Crow (1970) instability in realistic landing conditions is  $z_{crow} \approx 30b = 0.5b^2$  (Fabre & Jacquin, 2004, p. 259). Hence, we expect meandering to be dominant roughly in  $z \in [c, b^2]$ , where the upper bound follows from the Crow instability (see also Jacquin *et al.*, 2001, p. 17).

Jammy *et al.* (2014, p. 352) resume that ‘no causal relation between meandering amplitude and domain size is known’. In order to assess the influence of the wind-tunnel walls on the development of an isolated vortex more quantitatively, tab. 2.1 lists the characteristic dimensions normalized with the vortex-core radius  $r_1$  (defined in (2.15)). The shortest distance for half-wing configurations is typically half the aspect ratio, varying over one order of magnitude for the listed experiments. For sufficiently short distances the wall-boundary-layer turbulence might be entrained into the vortex during roll up (Jacquin *et*

<sup>6</sup>NASA on <https://www.grc.nasa.gov/WWW/K-12/airplane/liftco.html>, called 27 Oct 2020.

Table 2.1: Wing and wind-tunnel dimensions normalized with the vortex-core radius  $r_1$ .

	$br_1^{-1}$	$Lr_1^{-1}$	$Br_1^{-1}$	$ Hr_1^{-1}$
Devenport <i>et al.</i> (1996)	290	1200	300	300
Jacquín <i>et al.</i> (2001)	–	1071	300	385
Roy & Leweke (2008)	60	300	74	100
Bailey & Tavoularis (2008)	29	240	34	50
Edstrand <i>et al.</i> (2016)	50	–	47	71
Bailey <i>et al.</i> (2018)	69	488	80	120

*al.*, 2001; Beresh *et al.*, 2010). The remaining dimensions equally spread over one order of magnitude, being at least roughly 50 core radii away. Experiments with a very narrow test section are presented in Vandernoot *et al.* (2008, fig. 2). Bailey *et al.* (2018, p. 726) judge a distance of about  $26r_1$  between the (mean) vortex axis and the side walls sufficient to exclude strong effects from the boundaries. This is consistent with our (linear) studies (cf. sec. 6.3) which suggest that an interaction of the vortex with its surrounding is restricted to a fairly narrow free-stream layer (less than  $10r_1$ ) around the vortex. The idea was spelt out that wind-tunnel walls could be modelled analogously to free-stream perturbations.<sup>7</sup> This would then imply, however, that (linear) meandering dynamics is not a consequence of the core excitation by the walls.

As already conjectured by Corsiglia *et al.* (1973, p. 756), assessment of the available experimental results suggests that the model scale as well as the wind-tunnel dimensions have negligible influence on the phenomenon.

### Conclusion 2.1.2: Canonical configuration

We are unable to discern any geometrical trends (see also Sarpkaya & Daly, 1987, p. 401). Thus, meandering can be studied for the canonical setting of an isolated vortex (e.g. trailing from a rectangular half wing) in a laterally unbounded domain within downstream distances between about one to two chords and the onset of cooperative instabilities.

### 2.1.2 Fluid parameters – characterization of the flow field

We are tempted to ask the same question as in sec. 2.1.1: can we conceive of an ensemble of fluid parameters which prevents meandering? What are the governing fluid parameters?

**Global parameters.** For the most part, the phenomenon of vortex meandering was observed in experiments at sufficiently low Mach numbers that the flow can be considered as incompressible (in air of about 290K the Mach number is typically of the order of  $M := U_\infty a^{-1} \sim 10^{-1}$ ,  $a$  = the speed of sound in the medium). The compressible study of Beresh *et al.* (2010, p. 604) found no Mach-number dependence in the range  $M = 0.5 \dots 0.8$ .

By appeal to fig. 2.1, we define the chord-based Reynolds number

$$(2.5) \quad R_c := \frac{U_\infty c}{\nu}$$

<sup>7</sup>By A. Antkowiak and P. Brancher (IMFT Toulouse) according to a private communication with V. Brion (ONERA Meudon).

with the chord length  $c$  and the free-stream velocity  $U_\infty$ . Reynolds numbers in wind-tunnel experiments usually range among

$$R_c \in [2 \times 10^4, 10^7] \quad \text{whereas mostly} \quad R_c \sim 10^5.$$

At this Reynolds number the boundary-layer flow at the wind-tunnel walls is turbulent.<sup>8</sup> In some experiments the wing was tripped to accelerate transition of the flow past the wing (e.g. Devenport *et al.*, 1996, p. 70; Bailey & Tavoularis, 2008, p. 284).

The mean measures of vortex meandering would seem to be at best weakly affected by the Reynolds number (Sarpkaya & Daly, 1987, p. 399; Del Pino *et al.*, 2011, p. 5). This apparent independence might be a consequence of the fact that the considered range is systematically above a critical value (Gursul & Xie, 2000, fig. 3 and p. 350). Solitons observed on vortices in rotating turbulence (Hopfinger *et al.*, 1982; Maxworthy *et al.*, 1985) might be characteristic of meandering in the lower Reynolds-number range (as also simulated by Navrose *et al.*, 2019, pp. 417–418). This possibility is further discussed in sec. 6.3.2.

**Free-stream parameters.** The strength of the ambient turbulence is measured in terms of the turbulence intensity (Schlichting, 1997, p. 511)

$$(2.6) \quad \frac{\mathbf{u}(t, \mathbf{x})}{U_\infty} := \frac{\sqrt{\frac{1}{d} \langle \|\mathbf{u}(t, \mathbf{x})\|_{\mathbb{R}^d}^2 \rangle}}{U_\infty} \quad (d = 1, 2, 3).$$

This is the spatio-temporal standard deviation of the Eulerian velocity field. In meandering experiments, the turbulence intensity varies between

$$\frac{\mathbf{u}}{U_\infty} \in [0.05\%, 1.5\%] \quad \text{whereas mostly} \quad \frac{\mathbf{u}}{U_\infty} \lesssim 0.5\%$$

if no additional grids are installed. In this case, the free-stream fluctuation velocity (2.6) can be modelled as a nearly stationary (or streamwise homogeneous) stochastic process with invariant standard deviation  $\mathbf{u} = \text{const}$ . Grid-turbulence experiments achieve turbulence intensities up to  $\mathbf{u}(0)U_\infty^{-1} = 2.5 \dots 6.8\%$  at the wing position (with the wing removed), depending on the grid size (Bailey & Tavoularis, 2008; Pentelov, 2014; Bailey *et al.*, 2018, pp. 725–726). The integral scales in these experiments range between one and three core radii at the wing position.

### 2.1.3 The typical evolution of wing wakes

For the sake of later reference, we briefly recall the common classification of the different regimes of wing-wake flow. Jacquin *et al.* (2001, pp. 5–6) [J] classify the wake as being composed of the following four regions according to the distance from the wing (see also Gerz *et al.*, 2002, pp. 184, 194, who provide additional typical fluid-flow characteristics) [G]. The streamwise extent of the regions depends on the Reynolds number (García-Ortiz *et al.*, 2019, p. 183).

1. **Near wake** [ $zc^{-1} \sim 1$ ]. The flow field is characterized by the coexistence of the trailing vortex rolling up at the tips, a spanwise shear layer at the trailing edge and a streamwise boundary-layer momentum deficit (Bailey *et al.*, 2006, p. 1282). The dynamics may contain variable contributions from boundary-layer separation, roll up,

---

<sup>8</sup>Given that the inflow is at least one chord upstream of the leading edge and the critical Reynolds number for boundary-layer transition  $R_{z,crit} := (zU_\infty\nu^{-1})_{crit} \sim 10^5 \dots 10^6$  readily yields  $R_c \geq R_{z,c}$  (Schlichting, 1997, p. 418).

vortex merging, instabilities, etc.[G]. Irrespective of this multitude of contributing flow features and dynamics, the net effect always is the emergence and formation of small highly concentrated vortices from all surface discontinuities [J].

Several experiments indicate that the roll up is essentially terminated in the near wake (Del Pino *et al.*, 2011, p. 5:  $zc^{-1} \approx 2 \dots 3$ , depending on the vortex strength; Iungo, 2017, p. 1782:  $zc^{-1} \approx 1$ ).

The roll up continues until the full merging of the shear layer vorticity into the vortex by diffusion; this state is called a fully-developed vortex (Bailey *et al.*, 2006, p. 1283).

2. **Intermediate wake** [ $zb^{-1} \leq 10$ ]. Roll up and vortex merging leading to the establishment of two strong counter-rotating vortices [J] of approximately equal strength [G]. The intermediate wake is characterized by a strong interaction of the vortex with the wake (Edstrand *et al.*, 2018, p. 861). While wake and vortex are significantly coupled (in the streamwise velocity component) close to the wing (up to  $1.5c$ ), down-wash induced uncoupling of the vortex from the remainder of the wake is accomplished at  $zc^{-1} = 5$  latest, such that ‘the wake insignificantly affects the transversal motion, implying that the wake is unnecessary to model the base flow for the wandering motion’ (Edstrand *et al.*, 2016, pp. 7, 9).
3. **Far wake** [ $10 \leq zb^{-1} \leq 100$ ]. No major changes and emergence of linear (cooperative) instabilities [J].
4. **Dispersion region** [ $zb^{-1} > 100$ ]. Instability-induced strong interaction between the two vortices, topological changes, decreasing circulation, breakdown [J]. In the far wake, ‘the impact of the atmosphere on the wake vortices becomes dominant ... [with a] huge spectrum of energy containing and interacting scales’ (Gerz *et al.*, 2002, pp. 184, 194).

### Conclusion 2.1.3

We thus come to the conclusion that all we need to observe vortex meandering is a vortex; probably at high Reynolds number and embedded into an unsteady free stream. This leaves us with the question: what is a vortex? and when does it meander?

## 2.2 Vortex notions in the present context

... tourbillon ... pour signifier toute la matière qui tourne ainsi en rond autour de chacun de ces centres

— R. Descartes: Principes de la Philosophie. III

The word ‘vortex’ (German, *Wirbel*; French, *tourbillon*) from the Latin *vertō*,<sup>9</sup> meaning to turn or revolve, as such, has an intuitive meaning to everyone (Lugt, 1979, pp. 309–310). Despite ‘vortices’ being ubiquitous in fluid flows and are commonly attributed primary kinematic and dynamic importance, there seems to exist no universally accepted definition and we are unable to identify unambiguously vortices in a given complex fluid flow in general (Haller *et al.*, 2016, p. 136). In the special case of *trailing*-vortex flow, matter seems clearer, though not completely unequivocal. We do not strike for a universal definition of a vortex here, rather we seek an operational definition which is sharp enough for the present

<sup>9</sup> *drehen, wenden* (Stowasser, p. 546).

purpose. On the one hand, definitions are necessary to develop a physical theory, while on the other hand, it seems that ambiguity of even essential notions is an unavoidable – and perhaps stimulating – fact (Heisenberg, 1959, pp. 237–262).

### 2.2.1 The dynamic–kinematic duality of vortices

The essential point we want to make regarding the nature of vortices is, that they have a dynamic and a kinematic identity. Which is perhaps even the most characteristic aspect of vortices. By a dynamic identity is meant, that we can associate a vortex unambiguously with a distinguished state (at least in theory) of the dynamical system governed by the Navier–Stokes equations. However, at the same time, we identify a vortex with a definite fluid volume consisting of the same particles (Haller *et al.*, 2016, pp. 136–138). We suggest that the *manifestation* of a vortex is where both definitions overlap.

**The dynamic vortex: characterization of the mean field.** The *dynamic*-vortex definition does not pose a serious problem. Let the dynamical system (2.1) be associated with some function space; at any time, the dynamic vortex is a distinct element (state) of this space.

**Definition 2.1.** The dynamic vortex is defined as the trajectory  $\mathbf{W}(t)$  (the mean vorticity) in the function space of the admissible dynamics.

**Remark 2.1.** We find it more appropriate to associate the vortex with the vorticity  $\mathbf{W}$  and think of the velocity  $\mathbf{U}$  (where  $\nabla \times \mathbf{U} = \mathbf{W}$ ) as being induced by the vortex. This identification implies that vortices are typically strongly spatially confined (having practically compact support; Helmholtz, 1858; Saffman, 1992) while they have non-local influence.

**First model: the Lamb–Oseen vortex.** For the present purpose, it is sufficient to introduce the Lamb–Oseen (or Gaussian or Hamel) vortex which is the analytical solution of the two-dimensional vorticity equation in  $\mathbb{R}^2$  for the initial condition of  $\delta$ -localized vorticity of initial circulation  $\Gamma_0$ . The length scale (Batchelor, 1964, p. 652)

$$(2.7) \quad r_0(t) := 2\sqrt{\nu t} = 2\sqrt{\nu \frac{z}{U_\infty}} \quad \text{yields the similarity variable} \quad \eta(t) := \frac{r}{r_0(t)} = \frac{r}{2\sqrt{\nu t}}.$$

The vorticity of the Lamb–Oseen vortex then follows from a heat equation, (Barenblatt, 1996, p. xii)

$$(2.8) \quad W_z(t, r) = \frac{\Gamma_0}{4\pi\nu t} e^{\eta^2(t)} = \frac{2\Gamma_0}{2\pi r_0^2} e^{\eta^2(t)},$$

which leads to the integral vorticity (or circulation)

$$(2.9) \quad \Gamma(t, r) = \Gamma_0(1 - e^{\eta^2(t)}).$$

The induced azimuthal and angular velocities are

$$(2.10) \quad U_\theta(t, r) = \frac{\Gamma(t, r)}{2\pi r} = \frac{\Gamma_0}{2\pi} \frac{1 - e^{\eta^2(t)}}{r}, \quad \Omega(t, r) = \frac{U_\theta(t, r)}{r} = \frac{\Gamma_0}{2\pi} \frac{1 - e^{\eta^2(t)}}{r^2}.$$

In theoretical vortex dynamics of the Lamb–Oseen vortex in a parallel approximation, we non-dimensionalize (2.8)–(2.10) with

$$(2.11) \quad r_0 := 1 \quad \text{and} \quad \Gamma_0 := 2\pi \quad \text{thus} \quad \mathcal{U} = \frac{\Gamma_0}{2\pi r_0}, \quad \Omega_0 = \frac{\Gamma_0}{2\pi r_0^2}.$$

The Choice  $r_0 = 1$  is arbitrary and fixes the vortex age.

**Remark 2.2.** In extension to remark 2.1, we see that for Lamb–Oseen vortices  $W_z(t) \in L^2(0, \infty)$  and  $\Omega(t) \in L^2(0, \infty)$  (appearing in the perturbation equation), while the effect (*Wirkung*)  $U_\theta(t) \notin L^2(0, \infty)$ .

**Second model: the Batchelor vortex.** For the Batchelor vortex, we add the Gaussian axial velocity (Batchelor, 1964)

$$(2.12) \quad U_z(t, r) = q^{-1}(t)e^{r^2(t)}.$$

Isolated line vortices without inflexion point are destabilized by the superposition of a sufficiently strong axial mean-velocity in the core. The stability problem is thus parametrized by the ratio of the azimuthal and the axial velocity scales called swirl number (Batchelor, 1964, p. 653; Lessen *et al.*, 1974, p. 755). Instead of the original definition it is common practice to work with the equivalent swirl number (Fabre, 2002, p. 31)

$$(2.13) \quad q(t) := \frac{\pi}{2} \frac{U_{\theta,1}(t)}{|U_z(t, 0) - U_z(t, r \rightarrow \infty)|} \quad (\delta U_z(t) \neq 0),$$

where  $U_{\theta,1}(t) := \max_r U_\theta(t, r)$  denotes the maximum azimuthal velocity and  $\delta U_z(t) := U_z(t, 0) - U_z(t, r \rightarrow \infty)$ .<sup>10</sup>

The maximum azimuthal velocity and the axial-velocity deficit are shown in fig. 2.2 as fractions of the free-stream velocity for the experiments listed in appendix A.2. Despite the considerable variance, we assume the mean values

$$(2.14) \quad \frac{U_{\theta,1}}{U_\infty} \approx \frac{1}{4} \quad \text{and} \quad \frac{|\delta U_z|}{U_\infty} \approx \frac{1}{8}$$

indicated by horizontal lines, for later reference.

The objective of the present study is not in the characterization and description of the vortex mean fields but in the meandering dynamics. We shall therefore content us in stating that generally the Lamb–Oseen and Batchelor vortex are accepted as fair approximations of trailing vortices (e.g. Heaton & Peake, 2007, p. 272; Stout & Hussain, 2016, p. 354). A further discussion can be found in appendix C.

**The kinematic vortex.** Vortices combine important aspects of being a distinguished dynamic object of the phase space (cf. def. 2.1), while at the same time being associated with the same fluid mass (Lugt, 1979; Provenzale, 1999, p. 55; Haller *et al.*, 2016, p. 137), which is a kinematic Lagrangian characteristic.

By a vortex, we think of an objectively identifiable cylindrical (up to reasonable topology-preserving deformations which ‘almost’ preserve axisymmetry) subset of the fluid domain of concentrated axially oriented mean vorticity (cf. also Saffman, 1992, p. 63). The mean kinematics of a vortex thus represent rotation about the  $z$ -axis. Superposition of an axial or radial mean-velocity component is possible as long as the overall kinematics is ‘dominated’ by rotation (this is subjective but otherwise we give the fluid flow another name, e.g. jet). For the sake of visualization, we think of a vortex as a rotating mass of fluid with cylindrical geometry embedded in the surrounding free stream. In the case of trailing vortices, this definition of a vortex is not problematic; there remains however some flexibility as to where the vortex ‘ends’, i.e. the definition of the (radial) vortex boundary is ambiguous.

<sup>10</sup>The experimentally inaccessible theoretical velocity scale  $\mathfrak{U}$  (cf. (2.11)) is related to the maximum value by  $U_{\theta,1} = \frac{\Gamma_1}{2\pi r_1} \approx \frac{0.716\Gamma_0}{2\pi \cdot 1.12(2\sqrt{\nu t})} \mathfrak{U} = \frac{0.716}{1.12} \mathfrak{U} \approx 0.64 \mathfrak{U}$  (Saffman, 1992, p. 254).

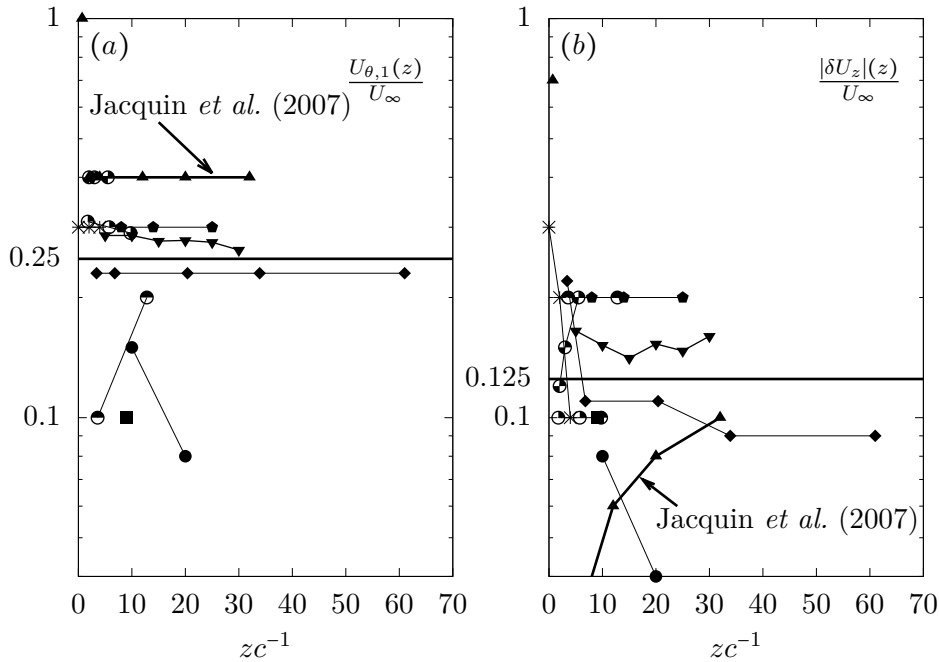


Figure 2.2: Downstream variation of the maximum azimuthal velocity (a) and the axial-velocity deficit (b). While  $U_{\theta,1} \approx \text{const}$  over  $z$  the axial velocity in the core admits larger values in the very proximity of the wing then drops rapidly to a small and rather constant value (cf. appendix A.2). The approximate mean values are shown by straight lines.

**Definition 2.2.** The *kinematic vortex* is defined as the material fluid sub-volume rotating around the same axis.

Definition 2.1 would be of little value if it would not coincide with what we identify as the vortex in experiments.

**Conjecture 2.1.** *The actual manifestation of a vortex in terms of a rotating fluid mass (def. 2.2) always spatially coincides with the fluid volume carrying (practically all of) the mean vorticity (def. 2.1). We therefore drop the specification attributes and simply refer to the vortex as the fluid volume where both definitions coincide.*

We shall loosely speak of vortices in order to refer to their manifestation and expect them to coincide with the volumes to be introduced in defs. 2.4–2.5. (See also the discussion in Spalart, 1998, pp. 115–117.)

### 2.2.2 Partition of the fluid domain

Vortex meandering is observed in subsets of Euclidean space of various extents (e.g. wind tunnels or perhaps the atmosphere). This suggests that we can define some universal *fluid domain* as the subset of this larger embedding space in which the fluid motion of interest is going to be observed and which is subjected to some conservation laws. Conservation of integral observables (e.g. energy, vorticity) is equivalent to the condition that there is no net exchange of these observables between the fluid domain and the embedding space (see also Landau & Lifšic, 1959, footnote on p. 50).

**Definition 2.3.** The *fluid domain* is defined as the subset  $M$  of  $\mathbb{R}^d$  ( $d = 2, 3$ ) having no integral mass, energy and vorticity flux over its lateral boundary  $\partial M$ .

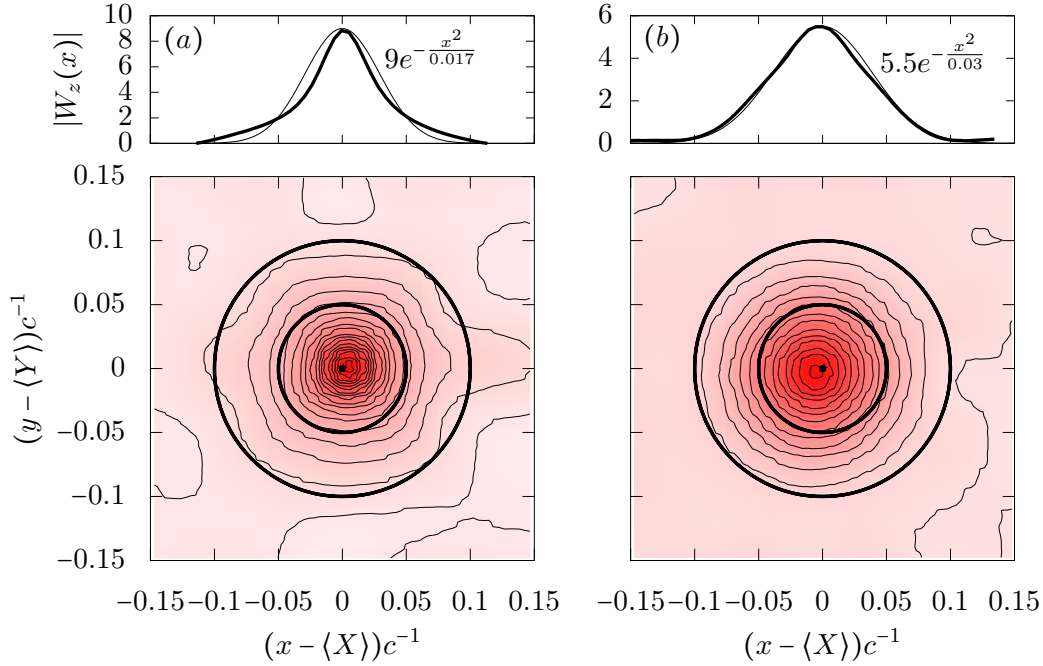


Figure 2.3: Module of the mean vorticity  $|W_z(\mathbf{x})|$  at  $zc^{-1} = 4$  in (a) and  $zc^{-1} = 26$  in (b). Inner and outer circle representing the vortex core and support. Profile along  $x$  through the centre (thick line) and fitted Gaussian (thin line). The vorticity is normalized with  $t_c^{-1} := U_\infty c^{-1}$ . (From the PIV measurements presented in appendix A.1.)

The entire fluid-flow field can roughly be classified into a core region, a surrounding layer and an external flow which is essentially irrotational. Several 'vortex-core' definitions and characteristic length scales are discussed in Jacquin *et al.* (2001, p. 3) and Fabre (2002, § 2.2). These studies conclude that realistic (trailing-vortex) cores have at least two length scales.

Let us assume that it is always possible to define a dichotomy of the fluid domain into a subset  $V(t)$  which we identify with the *vortex* and its set complement  $F(t) = M \setminus V(t)$ , called the *free stream*. Since the vortex obeys an unsteady motion these volumes occupy different parts of the fluid domain for all  $t$ . Let  $\mathbf{X}(t)$  denote the vortex centre (loosely, the central point of  $V(t)$ ), which we define below. For all  $t$ , we assume the following decomposition:

$$M = V(t) \cup S(t) = V_1(t) \cup V_2(t) \cup F(t).$$

The vortex core<sup>11</sup>  $V_1(t)$ , also referred to as internal or viscous core, roughly corresponds to the fluid volume which is in solid-body rotation about the instantaneous vortex centre ( $W_z(r) \sim 2\Omega(r) \Leftrightarrow U_\theta(r) \sim r$ ). In an earth-fixed frame of reference  $\mathbf{x} = (x, y)$ , the radius is defined by  $r := \|\mathbf{x} - \mathbf{X}(t)\|_{\mathbb{R}^2}$  with respect to the instantaneous vortex centre.

**Definition 2.4.** The *vortex core* is defined as the subset  $V_1(t) := \pi r_1^2(t)$  of the fluid domain centred about the instantaneous vortex centre, where

$$(2.15) \quad r_1(t) := \arg \max_r U_\theta(t, r(t))$$

defines the core radius.

We only consider axisymmetric vortices for which the core radius uniquely defines the vortex core and the two notions are equivalent. Definition 2.4 is used in Corsiglia *et al.*

<sup>11</sup>Latin *cor*, heart or spirit (*Herz, Geist*; Stowasser, p. 126).

(1973), Baker *et al.* (1974, p. 330), Singh & Uberoi (1976, p. 1858), Devenport *et al.* (1996, p. 74), Heyes *et al.* (2004, p. 4), Van Jaarsveld *et al.* (2011, p. 222) and Bailey *et al.* (2018, p. 726). Spalart (1998, p. 116) concludes ‘that  $r_1$  and the associated ‘peak velocity’  $U_1$  have received too much attention . . . ;  $r_1$  cannot be called *the* core radius.’ In meandering experiments the vortex-core radius is typically (see also Bailey *et al.*, 2018, p. 726)

$$(2.16) \quad \frac{r_1}{c} \approx 5 \times 10^{-2}.$$

The external or inviscid core is defined as the fluid volume which essentially contains all of the mean vorticity (see also Van Jaarsveld *et al.*, 2011, p. 216). We shall call this volume the (vortex) support<sup>12</sup>  $V_2(t)$ . Batchelor (1964, p. 647) calls  $V_2$  the vortex core.

**Definition 2.5.** The *vortex support* is defined as the subset  $V_2(t) := \pi r_2^2(t)$  of the fluid domain centred about the instantaneous vortex centre where

$$(2.17) \quad r_2(t) := \arg \min_r \{\Gamma(t, r(t)) = 0.98\}$$

defines the support radius.

Fabre (2002, p. 24) refers to  $r_1$  and  $r_2$  as the internal and external radii, respectively – emphasizing the difficulty in defining the latter.

**Remark 2.3.** Unless stated otherwise, we define  $r_2(t) := 2r_1(t)$  as motivated from the Lamb–Oseen vortex. Probably the same argument has been used by Bandyopadhyay *et al.* (1991, p. 1629), who define the core radius as the radius used in the computation of the reference circulation. While formally at infinity (surrounding the entire vorticity), twice the radius of the maximum azimuthal velocity is a sensible working definition.

This volume is used by Sarpkaya & Daly (1987, p. 401), Roy & Leweke (2008, p. 4) and Del Pino *et al.* (2011, p. 5). The latter two studies identify the core with the vorticity, respectively dye, containing region. This emphasizes the above mentioned dynamic–kinematic duality of vortices, being vorticity support and distinguished material (Lagrangian) object at the same time. Two-layer structure and localization of vorticity in the support is evidenced in figs. 2.3 and 5.5.

**Remark 2.4.** Our definition of a vortex (def. 2.1) based on the vorticity readily implies that the circulation (i.e. the integrated vorticity) is a measure for the *vortex strength*. The *de facto* confinement of vorticity to the vortex support (conj. 2.1 and def. 2.5) guarantees that it is finite (assuming it being continuous on the support). Conventionally, the vortex strength is defined as the circulation at two times the core radius (Maxworthy *et al.*, 1985, p. 148; Heyes *et al.*, 2004, p. 4; Van Jaarsveld *et al.*, 2011, p. 224). According to Iungo (2017, p. 1789), ‘the vortex strength is the principal parameter that controls vortex meandering’. We shall elaborate on this statement in chap. 4.

The mutual interaction between vortex and surrounding (organization and excitation) seems to be of restricted reach in practice (cf. rem. 6.1).

**Definition of the vortex centre.** The vortex centre is not defined uniquely. Probably the most natural and widespread way is to assume Lamb–Oseen-like mean profiles and then identify the vortex centre with the point of zero cross-flow velocity or peak-vorticity location (Devenport *et al.*, 1996, p. 90; Heyes *et al.*, 2004, p. 4; Bailey & Tavoularis, 2008, p. 292). Measurements on a discrete grid might make a fit to analytic vortex profiles

---

<sup>12</sup>Latin *supportō*, to carry (Stowasser, p. 498).

necessary (Roy & Leweke, 2008, p. 2; Deem *et al.*, 2013, p. 227). The dual material character of vortices is reflected in the identification procedure of Del Pino *et al.* (2011, p. 5), who identify the centre of mass of the dye concentration with the vortex centre. That is, assuming that vorticity and fluid-particle concentrations are strictly correlated (cf. conj. 2.1).

Instead of fitting the discrete data to an analytic profile, integral vortex-centre definitions might be employed. Van Jaarsveld *et al.* (2011, p. 220) define the vortex centre as the maximum cross-plane stream function (assuming near streamwise invariance;  $\partial_z u_z \approx 0$ ).

A dynamics-based definition of the vortex centre exploits the common observation (regardless of geometry and Reynolds number) that the maximum of the azimuthal root-mean-square (rms) velocity

$$\mathbf{u}_{\theta, \max}(t) := \max_{\mathbf{x}} \sqrt{\langle (u_{\theta}(t, \mathbf{x}) - U_{\theta}(\mathbf{x}))^2 \rangle}$$

is attained in the vortex centre  $\mathbf{X}(t)$ :  $\mathbf{u}_{\theta, \max}(t) = \mathbf{u}_{\theta}(\mathbf{X}(t))$  (Gursul & Xie, 2000, p. 348).

In the present study, we identify the vortex centre with the barycentre of the vorticity field on  $M$  (formally identifying mass with total vorticity), viz.

$$(2.18) \quad \mathbf{X}(t) := \frac{1}{\Gamma} \int_M d^2x \mathbf{x} w_z(t, \mathbf{x}), \quad \Gamma := \int_M d^2x w_z(t, \mathbf{x}), \quad \forall t \geq 0,$$

see also Saffman (1992, p. 66). Since meandering is an essentially transversal motion, we take the fluid domain  $M$  (def. 2.3) to be a subset of  $\mathbb{R}^2$  for which  $\mathbf{e}_z$  is everywhere normal. In particular,  $M$  is supposed to contain  $V(t)$  (the vortex volume) for all times and does not cross the symmetry plane ( $y = -b/2$ , cf. fig. 2.1). Since the bulk of the vorticity is highly concentrated in the vortex (while the free stream is almost irrotational) a variation of the integration domain does not significantly alter the centre of gravity in practice.

### 2.2.3 The scales of vortex dynamics

**Taylor's hypothesis.** Experiments suggest to take the chord  $c$  and the free-stream velocity  $U_{\infty}$  as reference scales. For the following estimates, we shall use the typical experimental values of  $c \approx 10^{-1}$  m and  $U_{\infty} \approx 10$  ms $^{-1}$  (e.g. Devenport *et al.*, 1996). In this scale system, the advection time scale is defined by

$$(2.19) \quad \mathbf{t}_c := \frac{c}{U_{\infty}} \approx 10^{-2} \text{ s}.$$

By Taylor's hypothesis (Rotta, 1972, pp. 71–72; Tennekes & Lumley, 1973, p. 253)

$$\frac{t}{\mathbf{t}_c} = \frac{tU_{\infty}}{c} = \frac{z}{c},$$

which establishes a duality between temporal and spatial evolution in the streamwise direction. Taylor's hypothesis holds in good approximation for perturbations of characteristic velocity which is much less than  $U_{\infty}$  (see also Monin & Yaglom, 1975, p. 11). As a matter of fact, vortex meandering *is* usually assumed to be associated with very small velocity (cf. assumption 2.2). Jacquin *et al.* (2001, p. 21 and fig. 22) state that ‘the low-frequency perturbations associated to meandering are convected at the free-stream velocity’.

**Further advection time scales.** According to Ash & Khorrami (1995, p. 321), it is advantageous to use the dispersion radius  $r_0$  and the centreline axial-velocity excess or defect  $|\delta U_z| \neq 0$  as the reference scales. This yields the characteristic time scale for Batchelor-like vortices

$$(2.20) \quad \mathbf{t}_{\delta} := \frac{r_0}{|\delta U_z|} \approx 5 \times 10^{-3} \text{ s},$$

using  $r_1 \approx 1.12 r_0$  and (2.14) and (2.16). We eventually introduce the advection time scale

$$\mathbf{t}_{r_1} := \frac{r_1}{U_\infty} \approx 5 \times 10^{-4} \text{ s.}$$

**The rotation time scale.** The natural time scale issuing from the Lamb–Oseen scales (and perhaps of vortex dynamics in general) is the rotation or turn-over time (for values in Devenport *et al.*, 1996; Bailey & Tavoularis, 2008)

$$(2.21) \quad \mathbf{t}_r := \frac{1}{\Omega_0} \approx \frac{r_1}{U_{\theta,1}} = 2\pi \frac{r_1^2}{\Gamma_1} \approx 5 \times 10^{-4} \text{ s,}$$

where  $r_1$  is defined in (2.15) as the approximate end of the rigid-body rotation (operational definition). The corresponding circulation  $\Gamma_1$  is an approximation of  $\Gamma_\infty$ .

**Relations between the time scales.** We are let to the time-scale sequence

$$(2.22) \quad \mathbf{t}_{r_1} \approx \frac{\mathbf{t}_r}{4} \approx \frac{\mathbf{t}_c}{20},$$

meaning that  $\mathbf{t}_{r_1}$  is four times shorter than  $\mathbf{t}_r$  and twenty times shorter than  $\mathbf{t}_c$ . That is, within one advection time unit  $\mathbf{t}_c$  the vortex completes about five rotations and advects an equivalent of approximately twenty core radii. Or in yet other words, it takes five rotation periods to advect the vortex by one chord length at  $U_\infty$ .

### Conclusion 2.2.1: Time–space correspondence

In experiments the equivalence  $1 c \leftrightarrow 5 \mathbf{t}_r$  approximately holds.

This scaling is consistent with the estimate of Heaton (2007b, p. 505) that  $t t_r^{-1} = 500$  (i.e.  $z c^{-1} \approx 100$ ) corresponds to about 25 wing spans.

**Remark 2.5** (A comment on the time scales.). The velocity gradient imposes two natural time scales for vortices. Namely, rotation  $\mathbf{t}_r^{-1} = \Omega_0$  is the characteristic scale of the rotating, energy-redistributing, stabilizing dynamics, while shear  $\mathbf{t}_s^{-1} \sim r d\Omega/dr$  characterizes energy amplification (Bölle *et al.*, 2020).

**Reynolds numbers of isolated vortex dynamics.** For the characterization of the vortex dynamics two Reynolds numbers are conventionally employed (e.g. Mayer & Powell, 1992, p. 104; Fabre, 2002, p. xi).

– In the discussion in sec. 2.1.1 we concluded that the circulation is an important wake parameter, which also turns out to be fundamental for analytical vortex models, introduced in sec. 2.2.1. While theoretical approaches are based on the initial circulation  $\Gamma_0$  (see (2.11)), in experiments the circulation at infinity  $\Gamma_\infty$  (in practice at a radius deemed sufficiently large) is used (cf. def. 2.5 and rem. 2.3).<sup>13</sup> We thus define the circulation-based Reynolds number

$$(2.23) \quad R_\Gamma := \frac{\Gamma_0}{2\pi\nu}.$$

While the Reynolds number is of the order of  $R_\Gamma \sim 10^7 \dots 10^8$  in real aerodynamic applications, this value is not realized in experiments (Jacquin *et al.*, 2001, p. 5). Over a

<sup>13</sup>As a matter of fact, the initial circulation  $\Gamma_0$  is proportional to the angular velocity on the vortex axis  $\Omega_0$  and identical to the circulation at infinity  $\Gamma_\infty$ .

streamwise range  $5 \leq zc^{-1} \leq 30$  and angles of incidence  $2.5^\circ \leq \alpha \leq 7.5^\circ$ , Devenport *et al.* (1996, p. 81) find

$$\frac{\Gamma_0}{\nu} \in [10^4, 6 \times 10^4] \sim 10^4 \dots 10^5,$$

which is the correct order of magnitude across various experiments (Bandyopadhyay *et al.*, 1991, p. 1627; Jacquin *et al.*, 2001, pp. 6, 8; Beninati & Marshall, 2005, pp. 248–249; Roy & Leweke, 2008, tab. 1; Iungo *et al.*, 2009, tab. 1; Van Jaarsveld *et al.*, 2011, p. 221; Iungo, 2017, p. 1785; Bailey *et al.*, 2018, p. 725).

– In the light of the above introduced scales, we can also define a Reynolds number with the axial-velocity deficit,

$$(2.24) \quad R_\delta(z) := \frac{|\delta U_z(z)| r_0(z)}{\nu}.$$

Fixing  $\delta U_z := \text{const}$  and  $r_0 := \text{const}$  is known as the parallel approximation.

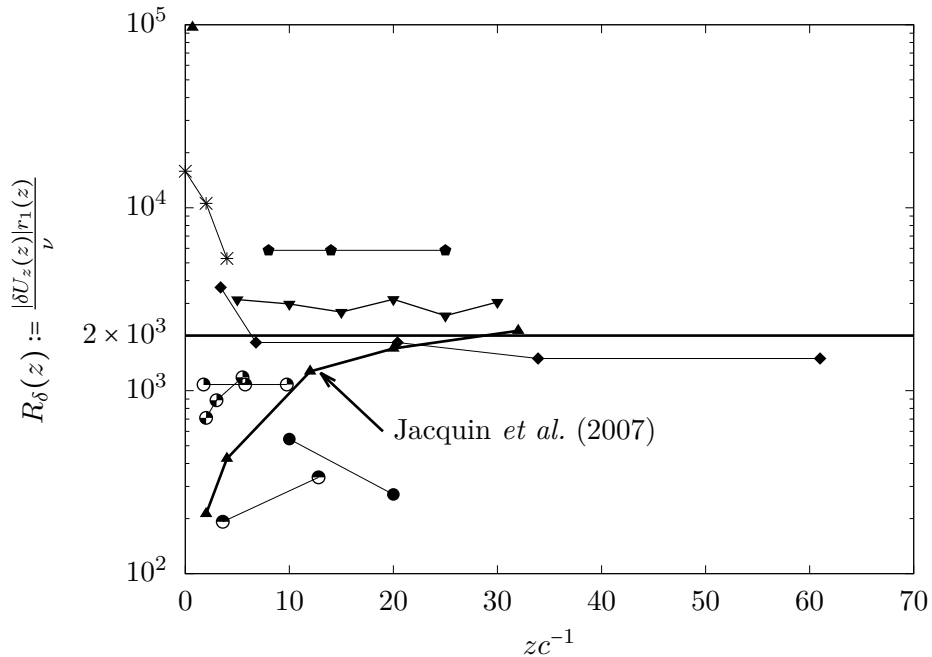


Figure 2.4: Downstream variation of the Reynolds number  $R_\delta(z)$  in experiments (cf. appendix A.2).

Unlike the circulation-based Reynolds number – essentially invariant for typical experiments – the downstream variation of (2.24) is shown in fig. 2.4 for the experiments listed in appendix A.2. From this, we see that the average Reynolds number is  $R_\delta \approx 2 \times 10^3$ , although this value is subject to considerable variation, especially for  $zc^{-1} \lesssim 10$ . The largest Reynolds number  $R_\delta \approx 10^5$  is reported in the experiment of Chow *et al.* (1997).<sup>14</sup> The Reynolds number during landing of a commercial aircraft is estimated as  $R_\delta \approx 3 \times 10^5$  (Fabre & Jacquin, 2004, p. 259).

**Symmetries of the velocity field (dynamics).** We assume statistical stationarity over the measurement duration to hold in all measurement planes ( $z = \text{const}$ ). Thus, the (lowest-order) statistics are independent of the origin of time and temporal averages are meaningful (Rotta, 1972).

<sup>14</sup>This is a consequence of the significant axial-velocity excess of  $\delta U_z U_\infty^{-1} \approx 0.7$  and the estimated core radius of  $r_1 c^{-1} \approx 0.03$  (Chow *et al.*, 1997, p. 53)

The experiments of Green & Acosta (1991, p. 119) indicate that the vortex is axisymmetric beyond  $zc^{-1} = 2$ . This implies stochastic homogeneity of the mean in  $\theta$ . It should be emphasized though that the variance (kinetic energy) has dominant contributions from  $m = 1$  hence is not stochastically homogeneous. Stochastic axisymmetry is corroborated by the observation that on the mean centreline the cross-flow variances equal,  $\langle u_r u_\theta \rangle = \langle u_r u_z \rangle$  while  $\langle u_\theta u_z \rangle = 0$  (uncorrelated) (Beninati & Marshall, 2005, p. 249 at  $zc^{-1} = 25$ ).

Statistical homogeneity in  $z$  only holds approximately for the azimuthal component of the mean velocity while it is not true for the mean axial velocity. Also, it is a fundamental characteristic of meandering that the variance (velocity and vortex centre) changes in the streamwise direction. Perhaps, the dynamics approaches some state of approximate invariance or symmetry (Beninati & Marshall, 2005, p. 247).

### 2.3 What is vortex meandering? A first definition

Einer verbindet die Vorstellung eines gewissen Wortes mit einer Sache, der andere mit einer anderen Sache.

---

— I. Kant: Kritik der reinen Vernunft

We restrict our attention to the dynamics of *isolated slender line vortices*. That is, vortices of elongated linear topology that do not close on themselves (no circular geometry) and where the characteristic transversal length scale is much smaller than the longitudinal length scale. These characteristics are representative of trailing vortices and tornadoes, for instance, however, exclude vortex rings or vorticity concentrations of similar aspect ratio (Stout & Hussain, 2016, p. 354). We call longitudinal, axial or streamwise  $z$ -coordinate and expect only slow variation and gradients in this direction. The plane defined by the normal  $\mathbf{e}_z$  and spanned by  $\mathbf{e}_x, \mathbf{e}_y$  (resp.  $\mathbf{e}_r, \mathbf{e}_\theta$ ) accommodates the lateral motion.

We define vortex meandering as follows (cf. also Gursul & Xie, 2000, p. 348).

**Definition 2.6.** Vortex meandering is the lateral, topology-preserving displacement of the vortex. In other words, meandering designates a displacement of the vortex as a whole.

The notion of a vortex in the present context has been introduced in sec. 2.2. The word 'meandering'<sup>15</sup> origins from the Greek  $\mu\acute{\alpha}\lambda\lambda\alpha\delta\omicron\varsigma$ <sup>16</sup> and, in its common use, designates the lateral displacement of a trajectory generated by some flow (in a functional-analytic sense). Our trajectory is defined by the evolution of the vortex, supposed to be a discernible object throughout. Meandering is then defined to be the contribution to the whole vortex motion which corresponds to a lateral displacement of the vortex *as a whole*. That is, displacements which do not change the topology (filamentation, merging, break down, ...). It should be emphasized that 'meandering' is an expression of foremost poetic usage, bearing the connotation of some 'randomness' or 'complexity', since otherwise we would have merely decided to call it 'oscillation' or the like.

**Translation into a mathematical model.** This definition indicates that, from the outset, vortex meandering describes an inherently *kinematic* phenomenon of a distinguished fluid volume. Let  $V \subset \mathbb{R}^d$  ( $d = 2, 3$  is the dimension of the fluid domain or the projection on the cross plane) be the fluid volume identified with the vortex. Meandering is then formally defined as

$$M(t) : V \mapsto M(t)V = V(t) \text{ s.t. } V(t) \text{ preserves its topology for all } t \geq 0$$

---

<sup>15</sup>The same phenomenon instead of being called 'meandering' is referred to as vortex *wandering*, too.

<sup>16</sup>Which was the name given to the patron deity of the Maiandros river (modern Turkey).

and  $t \mapsto M(t)$  is the meandering semigroup ( $\text{vol } V, \text{fracatal dim } V \neq f(t)$ ). Displacement as a whole implies that deformation (also topology preserving) is irrelevant for meandering. We can therefore identify the motion of the entire vortex with the motion of one point in  $V(t)$ . Conventionally, we chose the vortex centre  $\mathbf{X}(t)$ . Assuming bijectivity between the meandering motion of the whole vortex and the measured centreline time series, we can establish a characterization of meandering which does not rely on the notion of the vortex, but its centreline.

**Conjecture 2.2.** *Vortex meandering is equivalent to the vortex-centre time series.*

**Remark 2.6.** While the assumption of a rigid-body displacement of the vortex may be true for the low frequencies, the high frequencies are likely due to core turbulence which does not displace the vortex but solely cause fluctuation of the centreline inside the core (as presumably observed by Beresh *et al.*, 2010, p. 608; meandering correction left invariant the mean profiles). We might say that the centreline is material to first order. This is consistent with the observation that for low turbulence intensity meandering becomes less discernible (as it merges with the turbulent motion of the centreline inside the core).

**Definition of the meandering amplitude.** Let the vortex centre  $X_l(t)$  ( $l = 1, 2$ ) be a stochastic process. The meandering amplitude is conventionally defined as follows (Devenport *et al.*, 1996, pp. 74, 76; Rokhsaz *et al.*, 2000, p. 1026; Bailey & Tavoularis, 2008, p. 292; Deem *et al.*, 2013, p. 220).

**Definition 2.7.** The meandering amplitude is defined as the standard deviation of the vortex centre

$$(2.25) \quad \sigma_l(t) := \sqrt{\langle (X_l(t) - \langle X_l(t) \rangle)^2 \rangle}, \quad l = 1, 2.$$

**Remark 2.7.** For zero mean, the stationary variance is

$$(2.26) \quad \sigma^2 := \|\mathbf{X}\|_{L^2(\mathbb{R})}^2 = \int_{\mathbb{R}} dt \|\mathbf{X}(t)\|_{\mathbb{R}^2}^2 = \int_{\mathbb{R}} d\omega \|\hat{\mathbf{X}}(\omega)\|_{\mathbb{R}^2}^2 = \|\hat{\mathbf{X}}\|_{L^2(\mathbb{R})}^2.$$

By Plancherel's theorem the integral signal energies in time and frequency domain are identical (see also Bailey *et al.*, 2018, p. 734). This suggests that the bulk contribution to meandering may be estimated from the (pre-multiplied) power spectral density (cf. sec. 2.4.2).

Fundamentally, meandering is not stationary, meaning that the amplitude (2.25) depends on time (whereas  $t = zU_{\infty}^{-1}$  here). Nevertheless, except in the near wake and in grid-turbulence studies, the meandering amplitude is typically found to be a fraction of the core radius

$$(2.27) \quad \frac{\sigma}{c} \approx \frac{1}{2} \frac{r_1}{c} \approx 2 \times 10^{-2}$$

over the experimentally accessible measurement length.

**Meandering conserves the mean core circulation.** From the definition of the circulation in (2.2), we define the mean core circulation of an axisymmetric vortex in the earth-fixed reference frame by

$$(2.28) \quad \Gamma_1(z) := \Gamma(z, r_1(z)) = 2\pi r_1(z) U_{\theta,1}(z) \quad \text{where} \quad U_{\theta,1}(z) := U_{\theta}(r_1(z)).$$

We speculate that  $\Gamma_1$  is conserved:

**Conjecture 2.3.** *The mean core circulation is invariant in  $z$ .*

**Corollary 2.1.** *Conjecture 2.3 implies that the growth of  $r_1(z)$  and the decay of  $U_{\theta,1}(z)$  mutually balance for all  $z$ .*

Evidence for streamwise invariance of the core circulation is provided by the experiments of Corsiglia *et al.* (1973, p. 756), Devenport *et al.* (1996, p. 75), Iungo *et al.* (2009, tab. 1) and Van Jaarsveld *et al.* (2011, p. 223 and fig. 8b).

**Meandering is a universal feature of vortex flow.** Del Pino *et al.* (2011, p. 1) resume that vortex meandering is a typical feature of wing-tip vortices, having broad application in aerodynamic and marine engineering as well as in propulsion and generator turbines, for instance. Unlike its universal observation in wind-tunnel or water-channel experiments no final consensus seems to exist whether the phenomenon definitely occurs under real free-flight conditions (see e.g. Beresh *et al.*, 2010, p. 599, Jammy *et al.*, 2014, p. 351 and Bailey *et al.*, 2018, p. 722 for opposite statements).<sup>17</sup> Nonetheless, meandering (def. 2.6) is documented in geophysical systems such as tornadoes (e.g. Aref & Flinchem, 1984; Lund & Snow, 1993; Nolan & Farrell, 1999). Also, Vadarevu (2017, pp. 24, 122) resumes that turbulent boundary-layer bursting involves meandering vortices which, additionally, are characteristic of all exact invariant states documented for wall-bounded flows. In fact, ‘small-scale polarized structures are unavoidable companions of coherent structures’<sup>18</sup> (Melander & Hussain, 1993b, pp. 2001, 2002) which suggests that meandering is a natural phenomenon rather than a strangeness. Lateral vortex motion is documented in rotating flow experiments (Hopfinger *et al.*, 1982; Maxworthy *et al.*, 1985), inlet vortices (Wang & Gursul, 2012), in simulations (McWilliams, 1984; Zurheide *et al.*, 2009; Jammy *et al.*, 2014) and for optical vortices (Gu, 2013).

**Conjecture 2.4.** *Meandering according to def. 2.6 is a universal feature of vortices.*

## 2.4 Specific characterization of trailing-vortex meandering

I soon understood that there was little hope of developing a pure, closed theory, and, because of absence of such a theory, the investigation must be based on hypotheses obtained on processing experimental data.

---

— A. N. Kolmogorov: Selected Works

The definition of vortex meandering in def. 2.6 is still too vast to be of practical utility. Of course, we could call any vortex deformation whatsoever ‘meandering’, but there is no point in doing so if we intend to understand what we observe in experiments. We use

---

<sup>17</sup>An essential open question related to this controversy is whether meandering is boundary-condition induced (presence of wind-tunnel walls) or whether atmospheric turbulence is sufficient.

<sup>18</sup>The word ‘structure’ derives from the Latin *structūra*, meaning assemblage (*Zusammenfügung*; Stowasser, p. 484). According to the dictionary, ‘structure is the order, arrangement, connection and organization of simpler elements’ (see also chap. 5 and Bohm & Peat, 1987, pp. 141–144). In this sense, the notion of a ‘coherent structure’ (from the Latin *cohaereō*, to consist of (*mit anderem zusammenhängen*; Stowasser, p. 95)) would appear either redundant or inconsistent. In the present work, a structure is understood as the ordered appearance of a spatio-temporal field  $u(t, \mathbf{x})$  (say). In the similar vein, we use occasionally the word ‘mode’, from the Latin *modus*, amount, kind (*Maß, Art, Weise*; Stowasser, p. 320) and the word ‘pattern’, from the Latin *patrōnus*, outline, plan, model (*Schutzherr, Verteidiger*; Stowasser, p. 366) to refer to the shape of a mode.

terminology against the backdrop of our experience with the intention to (necessarily ambiguously) try to grasp a complex idea (Heisenberg, 1959). And here, as already remarked after def. 2.6, the expression 'meandering' implies a certain complexity and irregularity of the motion. In what follows, we concentrate on trailing vortices and strike for a refined characterization in this particular case.

### 2.4.1 Characterization in physical space

Characterization of meandering in physical space essentially serves the purpose to elucidate amplitude and velocity (or what is the same here, kinetic energy) systematics. We do so by means of a stochastic model.

#### The stochastic meandering model: the centreline is a random process

Due to the broadband spectral signature of whatsoever time series typically considered equivalent to the meandering motion<sup>19</sup> (Jacquin *et al.*, 2001, p. 11) and the lack of distinct frequencies (Corsiglia *et al.*, 1973, p. 754; Rokhsaz *et al.*, 2000, p. 1027), meandering is commonly modelled as a random process.

**Assumption 2.1.** *The vortex centreline is a vector-valued stochastic process  $t \mapsto \mathbf{X}(t) \in \mathbb{R}^2$ , the joint-probability distribution  $\mu_{\mathbf{X}}^t$  of which is a priori unknown and not stationary.*

For the conventional interpretation, let us consider a measurement plane at some fixed  $z = \text{const}$  and conduct one vortex-meandering (random) experiment. The realization of the centreline time series  $\mathbf{x}(t)$  is shown in fig. 2.5a for the  $x$ -component. By the law of large numbers, we expect the relative occurrences to converge (in an appropriate sense) to the probability distribution  $\mu_{\mathbf{X}}$ , as shown in fig. 2.5b; the mean is denoted  $\langle \mathbf{X} \rangle$  and the standard deviation  $\sigma_{\mathbf{X}}$ .

**Linearity, reversibility and correction.** While large-amplitude meandering may be irreversible, typical meandering (viz. amplitudes of the order of the core radius, cf. (2.27)) can be corrected for and is thus *reversible* (Devenport *et al.*, 1996, p. 73). This implies that vortex dynamics is *linearly additive* consisting of (i) the meandering motion and (ii) the core dynamics, with no nonlinear coupling between these two components! The meandering correction of Devenport *et al.* (1996, p. 73) is based on the following assumption.

**Assumption 2.2.** *Meandering is independent of any turbulent motion and meandering velocities are negligible compared to vortex-generated velocities.*

Independence implies additivity such that meandering is simply linearly superposed without affecting the core turbulence and vice versa. The spectral separation between meandering and core turbulence activity (as evidenced e.g. from filtering; Frisch, 1995, pp. 22–26) would seem to corroborate this hypothesis (Jacquin *et al.*, 2001, p. 16; Beninati & Marshall, 2005).<sup>20</sup> If turbulence in the core was significant compared to velocity fluctuations due to meandering, the equivalence between the vortex-centre and the meandering motion might break down. This could be either because the conventional vortex-centre

<sup>19</sup>Namely, Eulerian fluctuation velocity on the mean centreline, leading POD expansion coefficients or the vortex centre.

<sup>20</sup>A priori, in nonlinear systems, all scales are coupled and vortex meandering would be expected to interfere with the core turbulence. In this case, linear filtering would be problematic (Abarbanel *et al.*, 1993, pp. 1377–1388; Bradley & Kantz, 2015, p. 7). Albeit, the effective separation of the two dynamics by a linear filter does not imply that vortex meandering itself is a linear dynamics. Rather, it indicates a product dynamical system composed of two non-interacting (nonlinear) subsystems (Eckmann & Ruelle, 1985, p. 648).

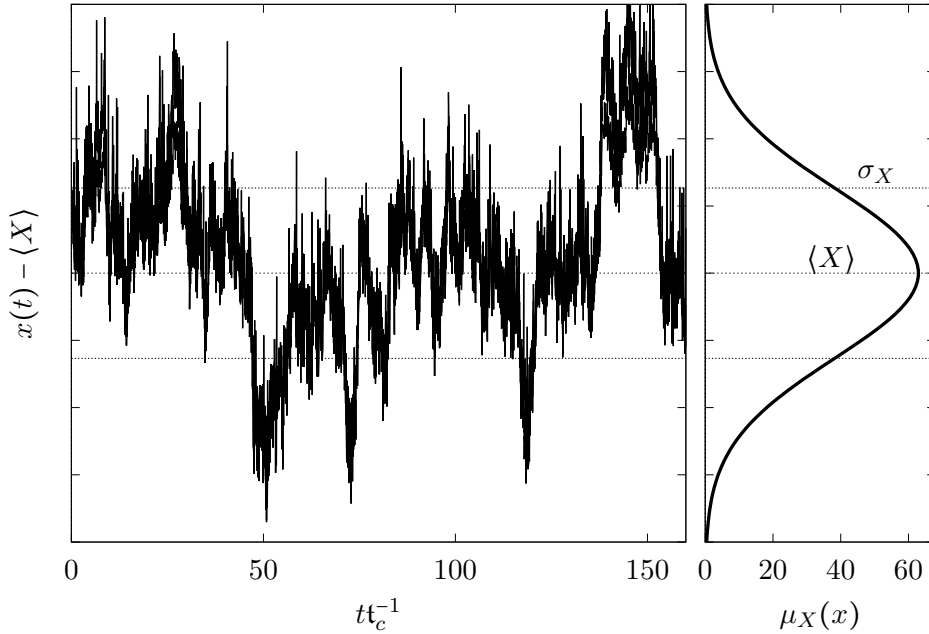


Figure 2.5: The conventional experiment. (a) Vortex-centre time series of the  $X$  coordinate in the fixed measurement plane at  $zc^{-1} = 26$  in the PIV measurements presented in appendix A.1. (b) The reconstructed Gaussian marginal probability density showing the mean and standard deviation.

identification procedures become ambiguous (Bailey & Tavoularis, 2008, pp. 290, 293), or because the core turbulence is strongly fluctuating without actually displacing the vortex. Generally, it is assumed that ‘on the vortex axis, . . . any deviations from zero velocity are due only to vortex wandering’ (Deem *et al.*, 2013, p. 226). Negligible meandering as compared to mean velocities leaves intact the mean profiles. In a monochromatic idealization this implies small-amplitude or low-frequency deflections. In other words, this means that meandering is the solid-body displacement of the vortex as a whole (def. 2.6), consistent with experimentally observed cross-correlation at  $zb^{-1} = 4.78, 5$  and various vertical stations (Jacquin *et al.*, 2001, p. 20).

The Lagrangian point of view of meandering suggests to refer to any  $\mathbf{X}(t) \in \mathbb{R}^2$  as a possible *state* of the system (and  $\mathbf{x}(t)$  is a particular realization). A measurable function  $F \in L^2(\mathbb{R}^2)$  mapping a state into some real-valued scalar is called an *observable*.<sup>21</sup> Under assumption 2.2, the effect of meandering corresponds to a linear integral operator<sup>22</sup> on the observables which can be inverted (reversed) (Devenport *et al.*, 1996, p. 74)

$$\begin{aligned} \mathsf{T}_\mu : L^2(\mathbb{R}^2) &\rightarrow L^2(\mathbb{R}^2) \\ F(\mathbf{x}) &\mapsto (\mathsf{T}_\mu F)(\mathbf{x}) := \int_{\mathbb{R}^2} d^2y \mu_X(\mathbf{y}) F(\mathbf{x} - \mathbf{y}) \quad \forall \mathbf{x} \in \mathbb{R}^2. \end{aligned}$$

Suppose the vortex-centre location in the cross plane is a vector-valued random process and  $\mu_X(\mathbf{x})$  the associated probability density function. Then, the above model means that the actually measured velocity (say) at a fixed probe location  $U_m(\mathbf{x}) = (\mathsf{T}_\mu U)(\mathbf{x})$  is given by the convolution of the ‘true’ velocity field  $U$  (which would be observed in a frame following the meandering motion) with the probability density function of the centreline

<sup>21</sup>Example observables are the mean velocity or Reynolds stress.

<sup>22</sup>Fredholm of the first kind, thus Hilbert–Schmidt (Kato, 1980, pp. 230, 262–264).

position

$$(2.29) \quad U_m(\mathbf{x}) = (U * \mu_{\mathbf{X}})(\mathbf{x}) \quad \forall \mathbf{x} \in \mathbb{R}^2.$$

This model goes back to Baker *et al.* (1974) and was substantially refined by Devenport *et al.* (1996). A priori, the probability density function associated with vortex meandering is unknown but was assumed to obey an isotropic Gaussian distribution parametrized by an eddy viscosity by Baker *et al.* (1974, p. 331), suggesting an isotropic eddy-diffusivity parametrization  $\nu_t \approx 2.5 \dots 5 \nu$  for the surrounding turbulence (the larger value corresponding to a larger Reynolds number  $R_c$ ). Devenport *et al.* (1996, p. 76) relaxed the isotropy assumption to the non-isotropic bivariate Gaussian distribution

$$(2.30) \quad \mu_{\mathbf{X}}(\mathbf{x}) = \frac{1}{2\pi\sigma_x\sigma_y\sqrt{1-e^2}} \exp\left[-\frac{1}{2(1-e^2)}\left(\frac{x^2}{\sigma_x^2} + \frac{y^2}{\sigma_y^2} - \frac{2exy}{\sigma_x\sigma_y}\right)\right],$$

where  $\sigma_x, \sigma_y$  are the standard deviations of the centreline position and  $e := \text{Cov}(X, Y)/(\sigma_x\sigma_y)$  denotes the correlation coefficient (measure for anisotropy). The experiments of Heyes *et al.* (2004, p. 5), Bailey & Tavoularis (2008, p. 295 validity extends to isotropic grid turbulence), Deem *et al.* (2013, p. 227) and Edstrand *et al.* (2016, p. 3) as well as the statistical simulations of the Lamb–Oseen vortex due to Iungo *et al.* (2009, p. 437) confirm the assumption that the vortex centreline obeys a bivariate Gaussian distribution in the transverse plane (cf. also figs. 2.5 and 2.6). The effect of meandering as modelled by (2.29) and (2.30) is equivalent to the application of a Gaussian filter smoothing the original 'true' signal. At any fixed position in space the actual measurement constitutes a weighted average in space and time (Baker *et al.*, 1974, p. 331; Green & Acosta, 1991, p. 107; Devenport *et al.*, 1996, p. 73; Iungo *et al.*, 2009, p. 435).

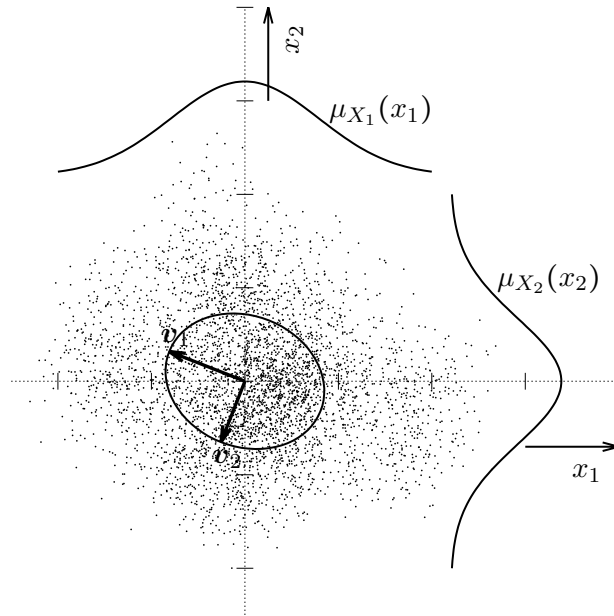


Figure 2.6: Experimentally (cf. appendix A.1) detected cloud of realizations of  $\mathbf{x}(t)$  for some fixed  $t > 0$  and the associated marginal probability densities obeying normal distributions  $\mathcal{N}(0, \sigma_{X^i})$  ( $t$  fixed). The principal axes  $\mathbf{v}_1, \mathbf{v}_2$  spanning the standard-deviation ellipse.

The normal distribution maximizes entropy among all continuous distributions and hence, knowing only the first two stochastic moments, requires the least a-priori inform-

ation. Examination of the second stochastic moment generally provides considerable insight into the nature of random processes; if the actual probability distribution is normal, knowledge of the first two stochastic moments is equivalent to knowing the probability distribution (Lumley, 1970, p. 68).

Consider the centreline random process  $\mathbf{X}(t)$  in a measurement plane at  $z = \text{const}$  (a possible realization being shown in fig. 2.5) and suppose it to have zero mean (i.e.  $\langle \mathbf{X}(t) \rangle = 0$ ).<sup>23</sup> We then define the covariance operator<sup>24</sup> (cf. Lumley, 1970, pp. 20, 24)

$$(2.31) \quad \mathbf{C} = \langle \mathbf{X} \otimes \mathbf{X} \rangle \quad \Leftrightarrow \quad C_{\beta\gamma} = \langle X_{\beta} X_{\gamma} \rangle \quad (\beta, \gamma = 1, 2).$$

For  $\mathbf{C}$  being symmetric real-valued, the spectral theorem guarantees orthogonal diagonalization ( $T = \text{transpose}$ )  $\mathbf{C} = \mathbf{V} \mathbf{\Sigma}^2 \mathbf{V}^T$  with real-valued eigenvalues.<sup>25</sup> Geometrically, the eigenvectors designate the principal axes of the centreline position and the eigenvalues represent the mean-square fluctuation in this direction. This is shown in fig. 2.6 and also in figs. 6.6–6.7. From  $\|\boldsymbol{\sigma}\|_{\mathbb{R}^2}^2 = \text{tr } \mathbf{C} = \text{tr } \mathbf{\Sigma} = \sum_{\beta=1}^2 \sigma_{\beta}^2$ ,<sup>26</sup> the meandering amplitude defines an ellipse in the measurement cross plane spanned by the eigenvectors and centred about the mean vortex position. Representation of the centre motion in the principal axes results in uncorrelated expansion coefficients (Karhunen–Loève theorem).

The convolution in (2.29) is invertible such that, in principle, the original ‘true’ signal can be recovered from the measured velocity. Deconvolution is discussed by Iungo *et al.* (2009, p. 437) and Deem *et al.* (2013, § 6). Since the bivariate probability density function (2.30) is stochastically independent along the principal axes, the total deconvolution can be accomplished by a sequence of one-dimensional deconvolutions (Iungo *et al.*, 2009, p. 450).

**A note on the anisotropy of meandering.** Anisotropy of vortex meandering is expressed by the cross-correlation  $e$  in (2.30). According to Iungo (2017, p. 1785), the correlation coefficient is the meandering parameter with the largest experimental uncertainty. This is reflected in the rather diverging results. Vanishing correlation upon high-pass filtering would seem to indicate that anisotropy is solely due to the meandering motion; this was indeed observed by Iungo *et al.* (2009, p. 443) while it is not the case in Beninati & Marshall (2005, p. 256). Increasing the Reynolds number in the range  $R_c \sim 5 \times 10^6 \dots 10^7$ , Roy & Leweke (2008, p. 5 and fig. 11) observe tilting of the standard-deviation ellipse from vertical to horizontal. Iungo *et al.* (2009, p. 449) conclude that, quite generally, the meandering amplitude is larger in the spanwise direction. The experiments of Bailey & Tavoularis (2008, p. 310) find vanishing correlation, implying isotropic Gaussian meandering. We make a similar observation in figs. 2.5 and 2.6.

### Conclusion 2.4.1

Meandering is assumed to be (stochastically) independent of the core-turbulence dynamics and its statistics  $\mathbf{X}(t) \sim \mathcal{N}(0, \boldsymbol{\sigma}_{\mathbf{X}}(t))$  is commonly found to obey a normal distribution. This latter result may be a consequence of the central limit theorem, discussed in appendix B.

<sup>23</sup>The parameter  $t$  is thought to either represent time (conventional interpretation) or the index of the random experiment (Lagrangian point of view), related by the ergodic hypothesis (cf. appendix B).

<sup>24</sup>Where  $\otimes$  is the tensor product in  $\mathbb{R}^2$ .

<sup>25</sup>The result is equivalent to singular value decomposition (also called principal axes or proper orthogonal decomposition) of  $\mathbf{X}$ .

<sup>26</sup>The trace  $\text{tr } \mathbf{C}$  is defined in Kato (1980, pp. 18, 523).

### Amplitude downstream evolution

Amplitude growth of the vortex unsteadiness downstream of the wing is an established fact already recognized in the first study by Corsiglia *et al.* (1973, p. 752). This growth was long believed to be roughly linear (Devenport *et al.*, 1996, p. 80; Heyes *et al.*, 2004, p. 6; Deem *et al.*, 2013, p. 227). Iungo *et al.* (2009, p. 436) seem to be the first to point towards a square-root amplitude growth. We shall postpone further discussion of the scaling to chap. 4 and merely recall some general characteristics here.

**At which downstream position does meandering first occur?** Whereas the low-aspect-ratio fin experiments of Beresh *et al.* (2010, p. 604) report a significant non-zero meandering amplitude already at the trailing edge, it is not entirely clear whether this observation translates to other geometries, e.g. to wings with larger aspect ratios. In the particular first case, the vortex is born in the boundary layer. Extrapolation of linearly fitted curves for the downstream amplitude growth obtained by Heyes *et al.* (2004, fig. 10) seem to support the findings of Beresh *et al.* (2010) for a rectangular wing model: for grid turbulence of increasing length scale the meandering amplitude seems to retain increasing non-zero initial values. The experimental results of Del Pino *et al.* (2011, fig. 10) suggest that the meandering amplitude admits very weak but finite values at the tip.

On the other hand, Jacquin *et al.* (2001, p. 24) find velocity correlations to vanish when approaching the model thus concluding that meandering is not an immediate consequence of wing-surface flow unsteadiness. Non-vanishing correlations of low-frequency perturbations of the vortex downstream with disturbances contained in the near-field and the 0.5 *b*-fuselage, however, are observed (Jacquin *et al.*, 2001, pp. 21, 23 and figs. 23c, 24).<sup>27</sup> This would seem to indicate sustained forcing rather than an initial-value problem. In accordance, Edstrand *et al.* (2016, p. 7) show curves of the integral perturbation kinetic energies associated with the most energetic POD modes (Berkooz *et al.*, 1993) that, when extrapolated to the trailing edge, drop to zero, too.

Irrespective the precise spatial origin of the phenomenon, there seems to be decided evidence that the meandering amplitude is growing (monotonously) downstream. Being usually negligible within downstream distance of  $zc^{-1} \lesssim 2$  (Green & Acosta, 1991, p. 108; Green, 1995, p. 445), amplitudes become significant a few chord lengths downstream (Iungo *et al.*, 2009, p. 448; Del Pino *et al.*, 2011, p. 1). Beyond  $zc^{-1} \approx 5$  amplitudes are non-negligible and vortex meandering is an issue (Devenport *et al.*, 1996, p. 67; Edstrand *et al.*, 2016, p. 3). It should be mentioned though that closer examination of the near field due to Del Pino *et al.* (2011, p. 5 and fig. 10) revealed that until about  $zc^{-1} \approx 2 \dots 3$  the meandering amplitude behaves not necessarily monotonically. As already stated above, we think that it is difficult to speak of meandering (def. 2.6) in this downstream range.

### Meandering depends on local rather than upstream turbulence: history counts.

The grid-turbulence study of Heyes *et al.* (2004, pp. 6–7 and fig. 10) shows that the downstream amplitude growth is correlated with the decay of the free-stream turbulence. This implies weaker amplitude-growth rates for increased initial turbulence intensities as a consequence of the convergence towards a universal 'no-grid value' (Heyes *et al.*, 2004, p. 8). Comparing the spatial energy distributions across the core shown in Beninati & Marshall (2005, figs. 8 and 12) for the no-grid and grid-turbulence case, the latter tends to promote the concentration of energy in the core at the first station at  $zc^{-1} = 8$ . Enhanced ambient turbulence causes an increased amplitude at the first station, while at  $zc^{-1} = 25$  the distributions admit very similar shape and magnitude. These observations indicate, that free-stream turbulence has an essentially *local* effect and that sufficiently far downstream

<sup>27</sup> *Cum hoc ergo propter hoc* – correlations do not imply causality.

meandering asymptotes towards a *universal* state independent of the background flow and the *upstream* turbulence intensity.

As a corollary of the proportionality between meandering amplitude and turbulence intensity (discussed in chap. 4 in detail) it follows that meandering must vanish in the absence of any free-stream turbulence. This contradicts the possibility of sustained or even increasing meandering in decaying turbulence. For this reason, Bailey *et al.* (2018, p. 734) postulate that rather than on the *local* conditions, the meandering amplitude should depend on a scale taking into account the entire *history*. At least for a linear system, this corresponds to a convolution integral as the response to sustained forcing or, what is the same, the resolvent in complex frequency space.

### Energy concentration in the vortex core

In what follows, let us assume that the Eulerian velocity (as detected in a measurement plane in experiments)  $\mathbf{u}(t, \mathbf{x})$  is a random process (actually, a field).

The first stochastic moment (mean velocity) is structurally unaffected by Gaussian meandering (Birch, 2012, p. 5; Jammy *et al.*, 2014, p. 360). This is plain if the 'true' vortex (in the co-meandering frame)<sup>28</sup> is Gaussian, since then it is invariant under Gaussian convolution. Devenport *et al.* (1996, appendix) further show that sufficiently strong meandering smooths arbitrary vortices to an apparently Gaussian in the laboratory frame. To the contrary, second-order statistics (Reynolds stresses and fluctuation kinetic energy) are known to be highly sensitive and significantly affected by meandering (Jammy *et al.*, 2014, p. 360). In other words, meandering is said to be associated with fictitious Reynolds stresses in the laboratory frame.

### Sharp fluctuation-velocity excess in the core, cumulating on the mean centreline.

It is characteristic of meandering experiments that the Eulerian-velocity unsteadiness peaks on the mean centreline while it drops to a small quasi-constant level in the surrounding (Green & Acosta, 1991, p. 133; Gursul & Xie, 2000, pp. 348–349). The measured Eulerian-velocity fluctuations in the core are believed to be primarily due to the meandering motion (Baker *et al.*, 1974, p. 328).

The typical signature of meandering consists of the progressive concentration of fluctuation kinetic energy in the core downstream of the wing, with the main contribution from the transversal components (Devenport *et al.*, 1996, pp. 80, 99). Beyond about three wing spans, energy is contained almost exclusively in the core (Jacquin *et al.*, 2007, pp. 5, 7 and figs. 6, 7). This and the fact that the spectral signature remains nearly unchanged afterwards led Beninati & Marshall (2005, p. 255) to conjecture that within about  $zc^{-1} \in [14, 25]$  'the total turbulent kinetic energy in the core seems to reach an asymptotic state'.

PIV experiments of Yeung & Lee (1999, p. 484) report meandering amplitudes of the order of the core radius which corresponds to a meandering velocity of about 4% of the free-stream velocity (estimation based on the image sampling rate). Baker *et al.* (1974, p. 328) and Jacquin *et al.* (2003, p. 577) resume that, while at least until  $zb^{-1} \approx 10$  meandering is characterized by small-amplitude core displacements, it is associated with large velocity fluctuations due to the significant gradients close to the vortex axis.

### 2.4.2 Characterization in frequency space

Vortex meandering is commonly perceived as a low-frequency, long-wavelength coherent motion of the vortex core in space and time (e.g. Jammy *et al.*, 2014). Although having

<sup>28</sup>That is, a frame of reference following the meandering motion of the vortex centre, see appendix B for details.

probably contributions from several frequencies, there seems to be nevertheless the expectation that it is possible to identify *the* meandering frequency which would reduce the phenomenon to an essentially monochromatic oscillation.

**Definitions.** Analysis in frequency space is conventionally based on the power spectral density (PSD) of some representative time series at a fixed measurement station. Representative here means that the time series is thought to be equivalent to the meandering motion in the sense discussed in sec. 2.3. Let  $u(t)$  be such a signal – assumed to be the realization of a stationary random process registered at a fixed point  $\boldsymbol{x}$  of the fluid domain. For instance, different centreline velocities, POD expansion coefficients and the vortex-centre time series have been considered. For arbitrary  $t \geq 0$ , the autocorrelation is defined by (Tennekes & Lumley, 1973, p. 210; Monin & Yaglom, 1975, p. 3)<sup>29</sup>

$$(2.32) \quad \rho_u(\tau) := \lim_{T \rightarrow \infty} \frac{\langle u^*(t)u(t+\tau) \rangle}{\langle u^2 \rangle} \quad \forall \tau \geq 0.$$

Due to stationarity, the origin of time  $t$  does not matter and we can normalize with the constant variance  $\mathbf{u}^2 = \langle u^2 \rangle = \text{const}$  of the random process.

The integral  $\mathbf{t}_u := \int_0^\infty d\tau \rho_u(\tau)$  defines an integral scale which is conventionally assumed to be finite (Tennekes & Lumley, 1973, p. 210); this is plausible since an infinite integral scale would indicate a correlation of the signal with itself at arbitrarily distant times (see also Rotta, 1972, pp. 25–27). We conclude that  $\rho \in L^1(\mathbb{R})$  (i.e. an integrable function) such that its Fourier transform exists, called power spectral density  $E_u(\omega)$ .<sup>30</sup> The Fourier-transform pair reads (Rotta, 1972, p. 30)

$$(2.33) \quad \rho_u(\tau) = \int_{\mathbb{R}} d\omega e^{i\omega\tau} E_u(\omega), \quad E_u(\omega) = \frac{1}{2\pi} \int_{\mathbb{R}} d\tau e^{-i\omega\tau} \rho_u(\tau).$$

**Proposition 2.1.** *The correlation function is a real, symmetric function, majorized by unity at the origin that decays faster to zero than  $\tau^{-1}$  as  $\tau \rightarrow \infty$ . The power spectral density is a continuous, symmetric, positive, real function.*

*Proof.* See Tennekes & Lumley (1973, pp. 201–206, 210–214) and Monin & Yaglom (1975, pp. 1–8).  $\square$

It is common practice in vortex-meandering experiments, to trace the graph of the power spectral density over some *Strouhal number*  $S$ . With regards to the scales introduced in sec. 2.2.3, we define  $S_c := fcU_\infty^{-1}$  ( $f$  = frequency); other Strouhal numbers are defined alike.

Physically, the power spectral density represents the energy partition (per unit time) over frequency of the given signal (by the Wiener–Khinchin theorem; Eckmann & Ruelle, 1985, p. 628). However, logarithmic plots over the frequency warp (*verzerrern*) the perception of the energy partition over different frequency ranges; this is a purely visual issue. The visually correct proportionality of the relative energy content in a certain frequency band and the corresponding integrated area under  $E_u(f)$  is retained if the power spectral density is pre-multiplied by the frequency  $f$  (Pope, 2000, p. 242). The integral is understood here in the sense of Riemann (Riesz & Sz-Nagy, 1956, pp. 19–21); then accounting for the non-uniform spacing of a logarithmic abscissa the energy reads<sup>31</sup>

$$\langle u^2 \rangle = \int df E_u(f) = \int d \ln f f E_u(f),$$

<sup>29</sup>Due to stationarity, the average is defined as the temporal mean over  $(0, T)$  for  $T \rightarrow \infty$  (Rotta, 1972, p. 19).

<sup>30</sup>The power spectral density is commonly simply referred to as the ‘spectrum’; although confusion with the spectrum  $\sigma(\mathbf{A})$  of a linear operator  $\mathbf{A}$  is unlikely, we stick to the full expression or call it ‘power spectrum’.

<sup>31</sup>It is readily shown that  $df = d(\ln f) f$  holds for the line element.

where integration is over an arbitrary frequency interval.

The spectral characteristics of the meandering dynamics are best elucidated by comparing power spectral densities at different points along the radial coordinate approaching the vortex axis from its periphery keeping  $z$  fixed, and on the centreline along the streamwise coordinate; these two cases are shown in figs. 2.7 and 2.8, respectively.

### The universal meandering spectral signature

Power spectral densities registered at fixed positions along a radial coordinate approaching the core show gradual dominance of an inactive core motion (i.e. meandering) at low frequencies (below  $S_c \sim 10$ ), while smaller turbulence structure (above  $S_c \sim 10$ ) is an order less than in the wake (see fig. 2.7). This characteristic suggests that the vortex core is a fluid volume which generates little or no turbulence of its own (Devenport *et al.*, 1996, p. 94 and fig. 21).

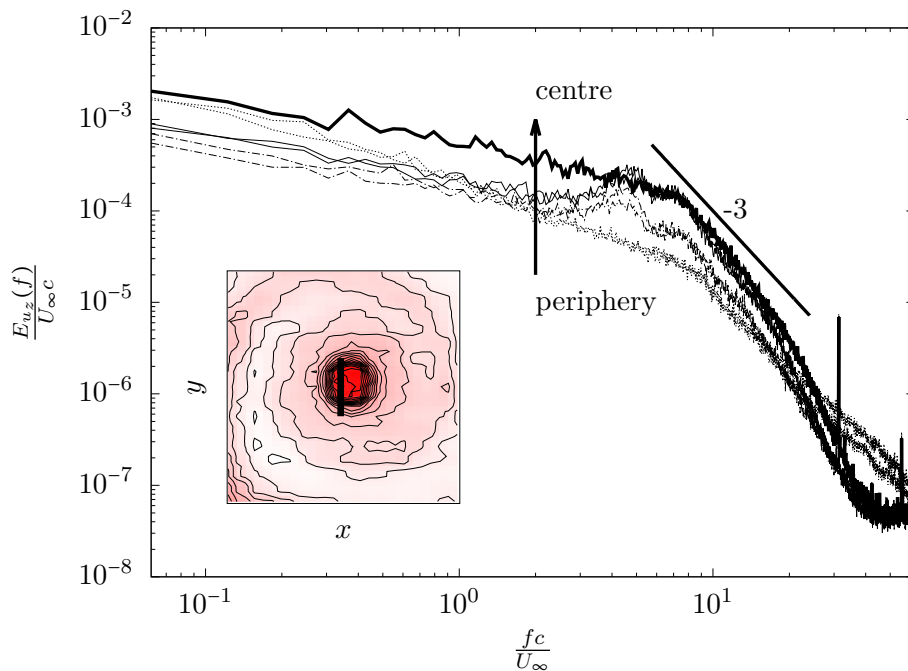


Figure 2.7: Power spectral densities at  $z b^{-1} = 3$  obtained from hot-wire measurements along the core-traversing line indicated in the inset (LDV of the axial velocity component). Same line styles reveal flow symmetry as the measurement points approach the centre from the core periphery. (See appendix A.1.)

Beninati & Marshall (2005, p. 251) state that for all stations downstream of  $z c^{-1} = 8$  perturbations with  $S_c \ll 2$  correspond to meandering. Typically the power spectral density admits a sharp energy excess for frequencies smaller than  $S_c \approx 1$  with the bulk of the kinetic energy (typically 95%) below this threshold (Jacquin *et al.*, 2001, p. 11; Devenport *et al.*, 1996, p. 80). Beninati & Marshall (2005, pp. 251–252) find the bulk of the kinetic energy to be contained in a frequency band of  $S_c \in [2, 100]$  which corresponds to wavelengths of the order of the core diameter and about 2% thereof, while the energy content in the typical meandering frequency  $S_c \approx 0.2$  was found to be insignificant.<sup>32</sup>

Bailey & Tavoularis (2008, p. 298) suggest that the typical signature of vortex meandering in frequency space consists of a plateau in the power spectral density for  $S_c \lesssim 1$

<sup>32</sup>The fact that they relate these perturbations to rather short wavelengths (order of the core diameter) stems from the fact that their core is a factor ten larger than usual, while  $S_c$  is of the same order as usual.

followed by a drop of constant slope that kinks followed by a drop of higher slope. This principal partition is consistent with the findings of Devenport *et al.* (1996, p. 93), Jacquin *et al.* (2001, p. 37) for axial velocity spectra and Roy & Leweke (2008, pp. 26–28) for the leading POD expansion-coefficient time series of the dye concentration ( $\sim$  vorticity)<sup>33</sup> and reasonably applies to fig. 2.7.

The (first) slope in the power spectral density obeys a power law of the generic form  $f^\beta$  where the exponent is usually of the value  $\beta \approx -3$  (Devenport *et al.*, 1996, p. 93; Beninati & Marshall, 2005, p. 252). This power-law decay suggests two-dimensional turbulence-like blocking of the three-dimensional energy cascade at high frequencies (Jacquin *et al.*, 2001, p. 14). However, this does not imply that low-frequency dynamics (such as meandering) is two dimensional.

Meandering is characterized by a high level of fluctuation kinetic energy, with the typical signature that, when approaching the core, the contribution to the total energy of the low-frequency modes increases (Devenport *et al.*, 1996, p. 94; Jacquin *et al.*, 2001, p. 16). This is clearly visible in fig. 2.7, showing measurement positions symmetrically approaching the centre (thick continuous line) from the vortex periphery (thin dashed lines). Moreover, the power spectral densities themselves are almost identical for the same radial distance  $\pm r$  from the centre: this suggests a certain rotation symmetry, or isotropy. Iungo *et al.* (2009, pp. 437, 440) observe that despite the wake turbulence vanishing downstream, low-frequency unsteadiness in the vortex core persists. As evidenced by filtering, the low-frequency fluctuations are restricted to the core (at six chords) but do not extend to the wake spiral (cf. sec. 2.4.1). For the core unsteadiness at six chords being dominated by low-frequency fluctuations, Iungo *et al.* (2009) conclude that ‘they cannot thus be considered as the result of a real turbulence activity’.

Applying gradually increased high-pass filters to the Reynolds stresses shows that long-wavelength perturbations are concentrated in the core and gradually increase in energy content, essentially affecting the transverse velocity components while the axial fluctuations are mainly of short-wavelength (Beninati & Marshall, 2005, pp. 253–255 and figs. 12, 13). Confinement of the long-wavelength perturbations to the core while they are negligible outside the core is consistent with the observation of meandering corrections and contributions being negligible beyond  $rc^{-1} > 0.1$  (Devenport *et al.*, 1996, p. 83).

The spectral separation of the characteristic meandering frequencies and turbulence scales suggests independence (Tennekes & Lumley, 1973, p. 65; Devenport *et al.*, 1996, p. 73; Jacquin *et al.*, 2001, p. 16).

**Conjecture 2.5.** *The effect of meandering on the vortex development is almost certainly negligible.*

Conjecture 2.5 is equivalent to the assumption that meandering merely consists of a linear superposition of a deflection kinematics that has no impact on the core turbulence or any other vortex dynamics (cf. also ass. 2.2). In other words, everything happens as if there was no meandering if we gather data in a reference frame following the meandering motion. Meandering thus simply corresponds to a linear coordinate transformation.

#### Conclusion 2.4.2: Spectral signature

The spectral signature of meandering consists of a low-frequency plateau (roughly  $S_c \lesssim 10$ ) with growing energy content downstream, followed by an inertial range with  $\sim f^{-3}$  slope, characteristic of two-dimensional turbulence. The low-frequency (meandering) perturbations are confined to the vortex core.

<sup>33</sup>This same approach is employed by Del Pino *et al.* (2011, p. 8).

### Is there *one* meandering frequency?

The broadband spectral signature without discernible peaks evidenced in fig. 2.8*a* suggests that the signal does not show any dominant frequency but that meandering is largely stochastic (Corsiglia *et al.*, 1973, p. 754; Rokhsaz *et al.*, 2000, p. 1026). A multi-frequency characteristic is also implied in the observation that, although small-scale turbulence in the core decays more rapidly than long-wavelength perturbations, significant small-scale fluctuations remain detectable until  $zc^{-1} = 25$  (Beninati & Marshall, 2005, pp. 252, 255).

Although meandering time series undoubtedly have broadband spectral signature, Bailey *et al.* (2018, p. 734) resume that ‘there seems to be a general agreement that the meandering of the vortex has a relatively long wavelength’. Despite this common long-wavelength inference, we are not aware of any sufficiently resolved experiment providing details about the actual streamwise wave form of the vortex (see also Bailey *et al.*, 2011, p. 1). Although identifying a characteristic frequency, Del Pino *et al.* (2011, p. 9) conclude that meandering may probably be characterized by more than one frequency. At least, there seems to be agreement that meandering is (essentially) assembled from frequencies in the range  $0.1 \leq S_c \leq 5$  (Devenport *et al.*, 1996, p. 99; Jacquin *et al.*, 2001, p. 11; Roy & Leweke, 2008, p. 7; Iungo *et al.*, 2009, pp. 437, 440).

Attempts at extracting *one* characteristic meandering frequency are due to e.g. Roy & Leweke (2008, p. 6), Del Pino *et al.* (2011, p. 8) and Bailey *et al.* (2018). It would appear that this expectation of the existence of one meandering frequency is borne by two observations, namely (i) that meandering visualizations appear to be much more organized than the time series suggests<sup>34</sup> and (ii) the existence of a sharp peak in the pre-multiplied power spectral densities. This peak is centred around a frequency of  $S_c \approx 1$  in the experiments of Jacquin *et al.* (2001, p. 37) (see also fig. 2.8*b*). What is remarkable, is that the same signature and peak value is reported by Jacquin *et al.* (2005, fig. 12 on p. 412) for the tip- and flap-vortices of an aeroplane model as obtained in experiments at ONERA ( $zb^{-1} = 1$ ) and TU Munich ( $zb^{-1} = 5.56$ ) as well as by Bailey *et al.* (2018, p. 736) for grid-turbulence experiments.

For definiteness, we use the following definition for the meandering frequency.

**Definition 2.8.** The meandering frequency is defined by

$$(2.34) \quad f_m := \arg \max_f f E_u(f) \quad \text{on a log-scale abscissa,}$$

as the argument of the maximum of the graph of the pre-multiplied PSD.

**Remark 2.8.** At present, we have no direct access to the streamwise waveform of meandering. We therefore infer the meandering wavelength from Taylor’s hypothesis, viz.  $\lambda c^{-1} := S_c^{-1}$ .

This suggests that meandering is characterized by a dominant frequency (Bailey & Tavoularis, 2008) which seems, moreover, to be universal across various experiments.

**Conjecture 2.6.** *It exists a dominant universal meandering wavelength  $\lambda c^{-1} \approx 2 \dots 3$  ( $\lambda r_1^{-1} \approx 40 \dots 60$  using (2.15)), independent of the free-stream conditions. Since this wavelength is much larger than the integral (grid) turbulence scale, free-stream turbulence cannot be the source of meandering.*

---

<sup>34</sup>For instance, in the FAR-Wake presentation ‘Experiments on vortex meandering’ of C. Roy and T. Leweke held at the International Workshop on Fundamental Issues related to Aircraft Trailing Wakes, 27–29 May 2008, Marseille, France, pp. 2–5.

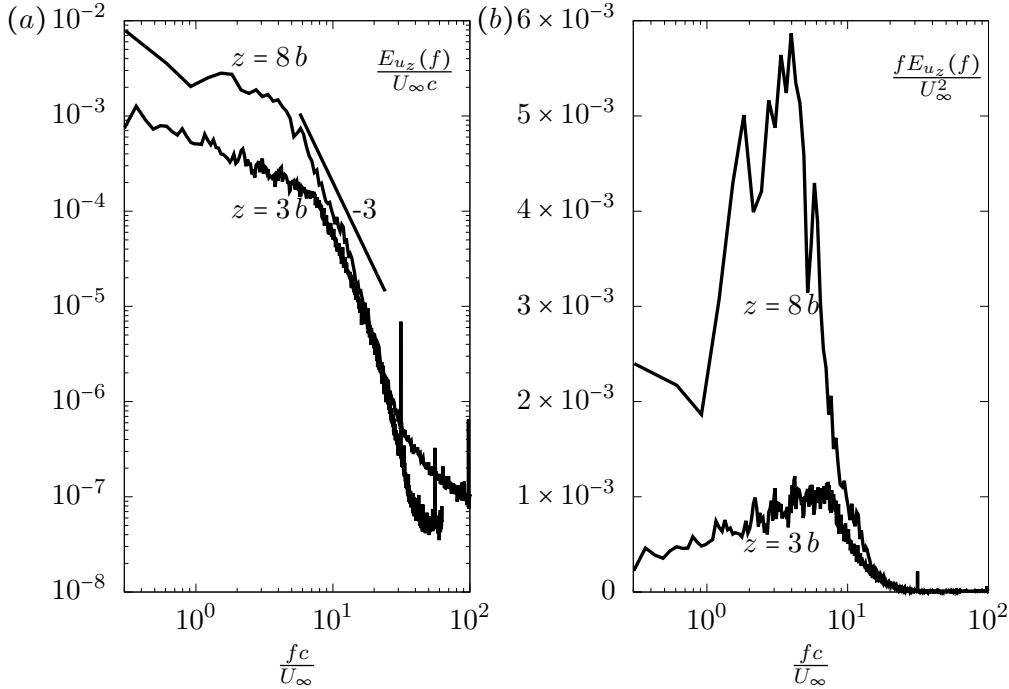


Figure 2.8: (a) Power spectral densities of the streamwise Eulerian velocity component  $u_z(\mathbf{X}(z))$  on the respective mean centrelines at  $z b^{-1} = 3$  and  $z b^{-1} = 8$  obtained from hot-wire measurements (see appendix A.1). (b) Same as (a) but frequency pre-multiplied.

Conjecture 2.6 (originally spelt out by Bailey & Tavoularis, 2008, p. 311) qualitatively extends to other experiments ( $\lambda r_1^{-1} \approx 120$  at  $z c^{-1} = 11.2$  in Roy & Leweke, 2008, p. 7; Beresh *et al.*, 2010, p. 599;  $\lambda r_1^{-1} \approx 30 \dots 60$  in the wind tunnel and less  $50 r_1$  in water-channel LIF in Bailey *et al.*, 2018, pp. 738–739). Unlike conj. 2.6, it should be noted that an order of magnitude shorter wavelengths  $O(1 \dots 3 r_1)$  have been identified with the bulk core unsteadiness, too (Bandyopadhyay *et al.*, 1991; Beninati & Marshall, 2005).

**The characteristic frequency closer to the wing.** The near-wake experiments of Chow *et al.* (1997, p. 60) identify a characteristic meandering frequency<sup>35</sup> of about  $S_c \approx 10^{-2}$  at  $z c^{-1} \leq 0.678$ .<sup>36</sup> This frequency in the near wake is two orders of magnitude smaller than stated in conj. 2.6 (postulated for the extended near field). Similarly, Del Pino *et al.* (2011, p. 9 and fig. 23) report a meandering frequency associated with the most-energetic POD mode of  $S_c \approx 2.5 \times 10^{-2}$  ( $\lambda c^{-1} \approx 40$ , which is an order of magnitude larger than conj. 2.6), asymptotically for  $2 \lesssim z c^{-1} \leq 4$ , independent of the angle of incidence and Reynolds number. Slightly farther downstream at  $z c^{-1} = 5$ , Edstrand *et al.* (2016, p. 8) identify<sup>37</sup>  $S_c \approx 10^{-1}$  which is intermediate between the near-wake findings and conj. 2.6.

This very-long-wave characteristic in the near wake is also stated for the unsteady behaviour of inlet vortices, the characteristic meandering wavelength of which is estimated to be  $\lambda r_1^{-1} \sim 10^3$  (Wang & Gursul, 2012, p. 16).

Unlike the above experiments associating meandering with longer wavelengths in the near wake than suggested by conj. 2.6, Bailey *et al.* (2018, fig. 7a) identify an order-of-

<sup>35</sup>Chow *et al.* (1997, p. 33) refer to McAlister & Takahashi (1991) for this value.

<sup>36</sup>The corresponding amplitude was estimated to be of the order  $\sigma c^{-1} \sim 10^{-4}$  which corresponds to  $\sigma r_1^{-1} \sim 10^{-2}$  assuming  $r_1 c^{-1} \sim 10^{-2}$ .

<sup>37</sup>This value corresponds to the frequency of the least stable eigenvalue in a spatial stability analysis of a fitted Batchelor vortex.

magnitude smaller dominant frequency  $S_c \sim 10$  ( $S_r := fr_1 U_\infty^{-1} \sim 10^{-1}$ ), corresponding to  $\lambda c^{-1} \sim 10^{-1}$ , for the smallest ambient turbulence intensity at  $zc^{-1} = 3.75$ .

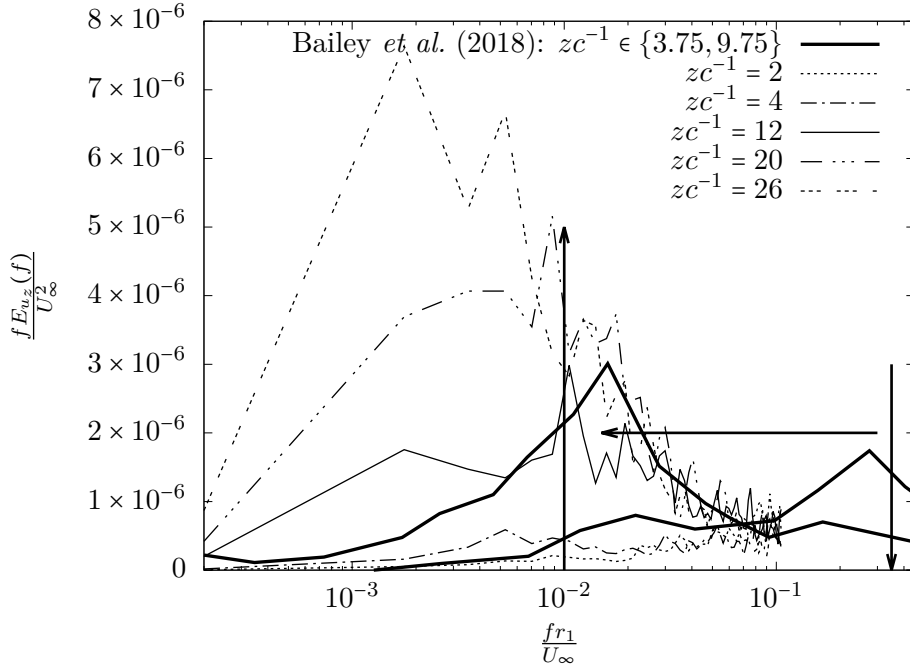


Figure 2.9: Frequency shift. Pre-multiplied power spectral densities of the streamwise Eulerian velocity component  $u_z(\langle \mathbf{X}(z) \rangle)$  in the respective mean vortex centres in the measurement planes  $zc^{-1} \in \{2, \dots, 26\}$  obtained from PIV (cf. appendix A.1). Thick lines (lower;  $zc^{-1} = 3.75$ ) show rescaled pre-multiplied PSD of the vortex centreline of Bailey *et al.* (2018). Arrows highlight trends in the frequency shift of the energy-containing scales.

**Spectral peak shift and convergence of the characteristic frequency.** While the identification of one meandering frequency seems too ambitious, we can identify universal trends. Most notably, Bailey *et al.* (2011, p. 4) resume that ‘the wavelength of low-frequency/long-wavelength motion increases gradually with streamwise distance from the wing’. In the light of the above discussion, we should rather state that the available data provides evidence for a general convergence of the pre-multiplied PSD towards a single sharp peak centred around the frequency of conj. 2.6 (see also Bailey *et al.*, 2011, p. 5; Bailey *et al.*, 2018, p. 737). We can resume these findings as follows.

**Conjecture 2.7.** *At least for low free-stream turbulence intensity there is a spectral shift in the dominant (meandering) frequency downstream. In all cases, the dominant (meandering) frequency converges towards the universal asymptotic value given in conj. 2.6.*

This spectral shift is visualized in the pre-multiplied power spectral densities of Bailey *et al.* (2011, fig. 6a) and Bailey *et al.* (2018, fig. 7a) (reproduced and compared to PIV in fig. 2.9). Assuming Taylor’s hypothesis, the first peak (at  $zc^{-1} = 3.75$ ) in these experiments could be a manifestation of linear transient growth by the resonance mechanism of Antkowiak & Brancher (2004) (Bailey *et al.*, 2018, p. 736). A qualitative assessment of areas and magnitudes in the pre-multiplied power spectral densities of these experiments might suggest some ‘feeding mechanism’ from the primary to the secondary peak downstream. Albeit, the energy budget (cf. fig. 6.4) precludes this interpretation as all energy to the perturbation space is provided by the mean flow.

**Conclusion 2.4.3: Trends rather than concrete values**

Meandering comes with an intricate duality between 'disorder' (broadband signature) and 'order' (coherent, recurrent properties). The apparent orderliness seems to increase downstream and progressively converge towards a universal behaviour. If a distinguished frequency (wavelength) exists, it seems to be subject to a shift (at least for low ambient turbulence intensity). At present, all we can say is that meandering is expected to correspond to the plateau  $S_c \lesssim 10$  (cf. conclusion. 2.4.2).

**Independence of the meandering and free-stream scales**

While the dependence of the meandering amplitude on the free-stream turbulence intensity seems to be undoubted (cf. sec. 2.4 and chap. 4), it appears to be uncoupled from the free-stream turbulence scales. The variety of measurement techniques (PIV, LDV, hot wire, ...), facilities (wind tunnel, water channel, ...), flow conditions and post-processing schemes (zero-crossing, deconvolution, ...) to assess the effects of meandering, readily suggests a certain robustness of the experimental findings discussed so far. Bailey *et al.* (2018, p. 734) draw the following conclusion.

**Conjecture 2.8.** *The meandering amplitude is disconnected from the integral length scales of the free-stream turbulence.*

Independence of the spectral signature with respect to changes in the free-stream conditions implies that free-stream turbulence can only excite inherent vortex modes (see also conj. 5.1). Borrowing terminology from stability theory, (strong) vortices behave similar to oscillators despite being asymptotically stable (Huerre & Monkewitz, 1990, p. 475).

**Characterization of the dynamics.** Probably the most remarkable feature of vortex meandering is its intrinsic linearity with respect to the remainder of the core dynamics in the sense that there seems to be no interaction between these two dynamics. For this reason, the meandering motion is conventionally termed inactive, meaning that it does not constitute a true turbulence activity.

**Conclusion 2.4.4: Dynamical independence**

The spectral separation of the meandering motion and core turbulence is taken as evidence that the two dynamics are independent and, moreover, that meandering is essentially irrelevant for the vortex development. Unlike the lack of interaction with the core dynamics, meandering depends on the free-stream turbulence *intensity*, while it seems to be insensitive to the free-stream *scales*.

We emphasize the importance of the second part of this conclusion! At present, all experiments seem to indicate that the *large-scale, slow* meandering motion is externally excited by *short-scale, fast* random dynamics of the free stream. Furthermore, as regards the statistics, the intricate scale interactions (i.e. the 'details') of the free stream are largely irrelevant and meandering only depends on the random *net* effect of the external excitation. This model has striking parallels with the Langevin equation describing Brownian motion (e.g. Yaglom, 1962, p. 69); we postpone further discussion to chaps. 4 and 6.

**Characterization of the phenomenology.** The absolute phenomenological foundation of (trailing-)vortex meandering can be boiled down to the following three cornerstones. They are indispensable for the phenomenon in the sense that meandering does not manifest

without showing all of them; however, they are not disjoint, but rather seem to causally overlap.

**Conclusion 2.4.5: The three pillars of vortex meandering**

The meandering (of trailing vortices) is characterized by

- (1) the amplitude growth downstream of the vortex generator,
- (2) a broadband spectral signature with energy accumulation in a low-frequency band approximately below  $S_c \approx 10$ : stochastic-coherent duality, and
- (3) the progressive energy concentration in the core.

We shall call these three key aspect the *three pillars of vortex meandering*.

### 3 | Discussion of the possible mechanisms

Aller guten Dinge Ursprung ist tausendfältig.

---

— F. Nietzsche: Also sprach Zarathustra

We terminate the review part of this mémoire by discussing the explanation approaches put forth as of this writing.

For low turbulence intensities the characteristic power spectral densities computed on the mean centreline might show several peaks (e.g. Jacquin *et al.*, 2001, p. 37 as compared to the flat spectra of fully-developed turbulence). This led Jacquin *et al.* (2001, p. 25) and Bailey & Tavoularis (2008, p. 298) to conclude that vortex meandering most likely has multiple sources. Different effects (such as stratification, ambient and core turbulence, etc.), however, are not linearly additive (Sarpkaya & Daly, 1987, p. 399). Increasing the turbulence intensity, this source multitude would seem to be lost and meandering becomes dominated by only one source (Bailey & Tavoularis, 2008, p. 299).

As regards the thus far proposed mechanisms, the principal controversy is most beautifully and clearly introduced by quoting H. Hesse (*Siddhartha*) –

Die meisten Menschen, Kamala, sind wie ein fallendes Blatt, das weht und dreht sich durch die Luft, und schwankt, und taumelt zu Boden. Andre aber, wenige, sind wie Sterne, die gehen eine feste Bahn, kein Wind erreicht sie, in sich selber haben sie ihr Gesetz und ihre Bahn.<sup>1</sup>

Anticipating the conclusion of this chapter, this black–white distinction seems not to hold. Rather, meandering would be like a falling star (*Sternschnuppe*) in this metaphor: bearing strong internal dynamics, while at the same time being influenced by the surrounding.

The discussion of the meandering characteristics in sec. 2.4 suggests that vortices combine characteristics of ‘amplifier-’ and ‘oscillator-like’ flows (although not in the strict sense of Huerre & Monkewitz, 1990, p. 475). On the one hand, proportionality of the meandering amplitude with respect to the free-stream turbulence intensity and the broadband, apparently stochastic spectral signature is indicative of an *extrinsic* mechanism. On the other hand, meandering seems to scale on the circulation while it is independent of the free-stream turbulence scales. Together with a certain universality of the characteristic meandering scales suggests an *intrinsic* mechanism. Also there is the controversy whether meandering persists for (ideally) vanishing free-stream turbulence. If very low values of  $u$  are seen as practically no free-stream turbulence, the only possibility remains an inherent mechanism.

---

<sup>1</sup>Most people, Kamala, are like a falling leaf, which is blown and is turning around through the air, and wavers, and tumbles to the ground. But others, a few, are like stars, they go on a fixed course, no wind reaches them, in themselves they have their law and their course.

We will therefore categorize the ensemble of previous explanation approaches into two families. The first class of extrinsic mechanisms presumes that meandering is essentially the response to external sources, while the second family of intrinsic mechanisms seeks to explain the phenomenon through inherent vortex dynamics. The review of Jacquin *et al.* (2005, p. 413) concludes with stating that essentially mechanisms of the second family (namely, linear dynamics) and receptivity to external turbulence should be further concerned (see also Del Pino *et al.*, 2011, p. 2).

### 3.1 Extrinsic dynamics

Daß ich erkenne, was die Welt  
Im Innersten zusammenhält,  
Schau' alle Wirkenskraft und Samen,  
Und tu' nicht mehr in Worten kramen.

J. W. von Goethe: Faust

The predominant perception of vortex dynamics and meandering can be formulated as follows: Unlike turbulence inside the core being damped by rotation, it is wrapped into filaments outside the core, forming strong aligned secondary coherent structures which buffet the core (Beninati & Marshall, 2005, p. 244). This contains the recurrent conclusions that core and free-stream dynamics are distinct and the former is laminarising. The vortex organizes the surrounding fluid flow and the emerging filaments contribute to passive buffeting of the core again. However, it is never clearly stated how this should really work.

**Excitation by free-stream unsteadiness.** Historically the first explanation for meandering sought its origin in the flow unsteadiness inherent in wind-tunnel experiments (Corsiglia *et al.*, 1973, pp. 753, 754). Corsiglia *et al.*'s reasoning is based on essentially identical spectral signature of meandering and isotropic turbulence. We have compelling evidence that the meandering power spectral density differs in important aspects from isotropic turbulence (cf. sec. 2.4.2). Despite this inconsistency, the hypothesis remains that *vortex meandering is the mere result of an excitation by the wind-tunnel free-stream turbulence*. In some sense, this hypothesis marks one extreme of the range of explanation approaches which reduces the phenomenon to a completely external mechanism. The assumption that meandering persists even in the absence of any free-stream turbulence defines the other extreme of entirely inherent dynamics which shall be discussed in sec. 3.2.

This hypothesis is corroborated by the experimental observation of significantly less meandering upon systematic reduction of the free-stream turbulence intensity (e.g. Baker *et al.*, 1974, p. 331; below  $uU_\infty^{-1} \approx 0.5\%$ ). For values of about  $uU_\infty^{-1} = 0.2 \dots 0.3\%$  (no grid), Bailey & Tavoularis (2008, p. 290) state that the effect of meandering was essentially negligible within  $zc^{-1} \in [3.75, 9.75]$ .

On the other hand, in a private communication with L. Jacquin (2018, ONERA Palaiseau), the opinion was spelt out that meandering subsists even in virtually turbulence-free ambient flow. Meandering is still observed for free-stream turbulence levels of  $uU_\infty^{-1} \approx 0.1\%$  (e.g. Devenport *et al.*, 1996; Jacquin *et al.*, 2001). Such low levels are not expected to have dominant dynamical significance by Jacquin *et al.* (2001, p. 14).

The present study suggests that the mere intensity is not the most interesting parameter, but that rather the 'form' counts.<sup>2</sup> We have the tendency to reduce the significance of excitations to their magnitude (quantity), while we neglect their structure or pattern (quality). In fact, the case of a resonant excitation is a prominent example showing that

<sup>2</sup>This is, by the way, a fundamental property of linear theories in general.

first and foremost the 'kind' of excitation plays a role. What matters is the 'correct type' of excitation together with a continuous supply of energy. This remark equally applies to the Reynolds–Orr equation which tells us that perturbation shape, not magnitude counts.

**The limit of zero angle of incidence.** According to (2.3)–(2.4), changes in the angle of incidence engender modifications of the circulation and therewith impact the vortex dynamics. Albeit, meandering seems to persist even at  $\alpha = 0$ , where actually no vortex forms at all (Baker *et al.*, 1974, footnote on p. 331). This observation led several researchers to argue that meandering is caused mainly by the free-stream turbulence since it is not linked to the presence of a vortex (e.g. Baker *et al.*, 1974, p. 331; Devenport *et al.*, 1996, p. 68).<sup>3</sup> On the other hand, we have substantial experimental evidence that the meandering amplitude grows with downstream distance, seemingly contradicting a purely passive buffeting effect in decaying or stationary free-stream turbulence, suggesting some vortex-induced mechanism, instead (see also Del Pino *et al.*, 2011, p. 2; Edstrand *et al.*, 2016, p. 2).

The stabilizing effect of rotation is visible in the meandering of wakes and vortices (compare Foti *et al.*, 2016, figs. 7, 8 with Bailey *et al.*, 2018, fig. 3). This might be taken as evidence to conjecture that *a mean axial core velocity is a necessary requirement for meandering while mean rotation has a purely stabilizing effect.*

Further support to this hypothesis comes from the direct numerical simulations of the core dynamics due to Melander & Hussain (1994, p. 34), stating that a (self-induced) axial flow is crucial. In a concomitant study emphasizing vortex–turbulence interaction, Melander & Hussain (1993a, p. 2676) come to the conclusion that 'even though axial transport is slow relative to the swirl velocity it is of central importance', notably essentially contributing to the organization of the surrounding turbulence. Also, Iungo (2017, p. 1789) reports a 'drastic' reduction of the meandering amplitude for vortices with smaller axial velocity deficit (in fact almost constant for  $\pm 15\%$  defect). Comparing this finding to related studies of turbine-hub wake meandering, Iungo concludes that this amplitude dependence on the axial velocity deficit suggests that axial shear within the core might play an important role, most likely involving a significant non-linear interaction.

**The scale separation.** The typical scaling behaviour suggests that meandering should be excited by external forcing, with the main source being the turbulence contained in the wrapping shear layers (Devenport *et al.*, 1996; Iungo, 2017, p. 1789). While we have compelling evidence that meandering amplitudes are affected by variations of the background-turbulence level, there seems to be no final conclusion whether vortex-core perturbations should be induced by turbulence contained in the free stream or from the shear layer rolling up around the core (Heyes *et al.*, 2004, p. 8; Beresh *et al.*, 2010, p. 605).

At the same time, meandering and free-stream turbulence are spectrally separated in the sense that the characteristic meandering frequencies are substantially lower than the turbulent ones (Bailey & Tavoularis, 2008, p. 297). Even more, typically there is no significant energy present in the flow (with and without grid) that is of the same order of the final long-wavelength perturbations (Beninati & Marshall, 2005, p. 255). This scale separation between free-stream turbulence and meandering suggests almost independence (Miyazaki & Hunt, 2000; Jacquin *et al.*, 2001, p. 16). In some cases, three-dimensional instabilities in the shear layer may lead to wake fluctuations, e.g. in the flow past delta wings. However, it remained unclear whether these low-energetic shear-layer instabilities

<sup>3</sup>As a matter of fact, *jet meandering* is a known geophysical phenomenon (e.g. of the Gulf stream; Samelson & Wiggins, 2006, p. 8) and is also observed in aerodynamic wakes (e.g. behind wind turbines; Larsen *et al.*, 2008).

(respectively perturbations) are sufficient to trigger very large core fluctuations (Menke & Gursul, 1997, p. 2966).

With regards to the energy argument of Beninati & Marshall and Menke & Gursul, we refer back to our above argument. Moreover, this reasoning seems to be based on the wrong perception that there is an energy transfer from the free stream to the vortex (see chap. 6 for further discussion). The issue of distinct scales finds its origin in the expectation of a linear dynamics, where the excitation and response frequencies are identical. If frequency 'selection' (if there is one) was nonlinear, this expectation could prove wrong.

**Kelvin–Helmholtz instability.** A definite correlation between the Kelvin–Helmholtz instability of the shear layer and vortex meandering was suggested by Gursul & Xie (2000, pp. 348, 350). Namely, *vortex meandering is due to nonlinear interaction of the trailing vortex with several secondary vortices generated by the Kelvin–Helmholtz instability of the vortex sheet shed from the trailing edge*. This meandering scenario assumes the generation of small-scale vortices by a Kelvin–Helmholtz instability of the shear layer that are advected around the primary trailing vortex, causing a displacement of the latter due to mutual Biot–Savart induction. This multiple nonlinear interaction of a system of several vortices results in a chaotic dynamics of the primary vortex (Gursul & Xie, 2000, p. 350 referring to Sen, 1997). Unsteadiness of the secondary vortices is essential, whereas stationary small-scale vortex structures (e.g. due to steady instabilities) cannot cause meandering (Gursul & Xie, 2000, p. 350).

Conversely, Bailey *et al.* (2018, p. 737) indicate that ‘the action of vortices from the free stream can make at most a small contribution to the overall meandering motion of the main vortex’. Although such vortices are experimentally observed their streamwise spacing of  $2 \dots 6 r_1$  is consistent with small-wavelength meandering only, however, unlikely to cause the long-wavelength characteristic.

Though perhaps a valid scenario for delta wings, meandering is observed in the absence of a shear-layer Kelvin–Helmholtz instability. With regards to the general problem, the assumption of a Kelvin–Helmholtz instability seems not justified and even unnecessary. In fact, in the light of the previous discussion it would seem sufficient to concentrate on the general interaction of a vortex with surrounding disturbances naturally contained in the free stream. In this interpretation, the Kelvin–Helmholtz scenario can be considered a particular sub-situation of a more generic receptivity approach.

**Entrainment.** While free-stream turbulence is probably a source of meandering in experiments, another mechanism must be active if we suppose that vortices meander under real flight conditions in an ideally quiescent earth atmosphere, too. Considering that vortex formation happens close to a rigid body (airplane, missile, wall), low-speed turbulent fluid from the boundary layer might be entrained during roll up (Beresh *et al.*, 2010, p. 600). This *turbulence entrainment of the wall-boundary layer could be an additional source of meandering*, which remains pertinent in real conditions (e.g. for missiles) (Beresh *et al.*, 2010, p. 608). Entrainment-induced meandering, however, does neither exclude possible other sources such as free-stream turbulence or shear-layer instabilities, nor does it provide a statement of its importance (Beresh *et al.*, 2010, p. 610).

Entrainment is observed in jet–vortex flow and depends crucially on the initial spacing of the jet with respect to the wing tip (Jacquin *et al.*, 2007, p. 9). The behaviour is discrete in the sense that entrainment is possible or even unavoidable for jet locations close to the wing tip, while it is completely prohibited otherwise. In the latter case the jet is rolled up analogously to any other free-stream disturbances. The possibility of entrainment will be further discussed in sec. 5.2.1.

Jacquin *et al.* (2001) installed a half-model configuration, employing a solid separation wall at the model symmetry plane ( $y = \text{const}$ ). Fluid flow past the separating wall developed a fully-developed turbulent boundary layer of standard thickness  $\delta c^{-1} \approx 1$  ( $2\delta\tilde{b}^{-1} \approx 0.3$  normalized with the vortex-centre position; similar to Beresh *et al.*, 2010, fig. 3). Hence, the vortex core is well outside the boundary layer (distance of about  $2c$  or  $20r_1$  between core and boundary-layer edge). This setup left the meandering characteristics essentially unaffected in the sense that the power spectral densities for the full- and half-model configurations were essentially identical. This suggests that significant influence of the wind-tunnel walls on vortex meandering can be discarded (Jacquin *et al.*, 2001, p. 15).

Albeit, Beresh *et al.* (2010, p. 602) emphasize that the vortex core behaves like an entrainment barrier *on average*, while the *instantaneous* velocity fields show core penetration by turbulence patches spiralling in.

Beresh *et al.* (2010, pp. 608–609) suggest that turbulence is lifted from the boundary layer due to the inherent rotational motion, admitting that this mechanism is unable to explain the finite meandering amplitudes at the trailing edge and that it is inconsistent with the characteristic time scale for transport inside a turbulent boundary layer. Thus, conjecturing that ‘some other means must exist by which the wind-tunnel wall boundary layer influences the vortex meander’. Immediate transferability to wings with higher aspect ratios may not be given though (Beresh *et al.*, 2010, p. 610).

**Confinement and boundary conditions.** As stated above, it exists no unanimous agreement whether vortex meandering is a mere artefact of the unavoidable spatial confinement in experiments which does not manifest under realistic flight conditions. According to Jammy *et al.* (2014, pp. 352, 354), meandering depends sensibly on the boundary conditions, viz. *meandering is caused by initial and boundary conditions inherently imposed by the wind tunnel*. As to further investigate this hypothesis, Jammy *et al.* (2014, p. 353) conduct a temporal DNS of the parallel Batchelor vortex in decaying homogeneous isotropic turbulence at  $R_\Gamma = 4 \times 10^3$ , considering periodic and symmetric lateral boundary conditions, respectively. While different boundary conditions indeed change the magnitude and qualitative evolution of the perturbation kinetic energy, the meandering-corrected second-order statistics closely match (Jammy *et al.*, 2014, p. 356). This suggests that meandering is the only contribution to the total core perturbation which is sensibly affected by changes in the boundary conditions.

However, it should be noted that none of the tested boundary conditions attempted to model the wind-tunnel walls as a no-slip wall but both intended to simulate a laterally infinite domain.

The present study indicates that regions of the fluid domain that really concern vortex dynamics seem to be restricted to some close neighbourhood (in  $r$ ,  $z$  and  $t$ ). Everything that lays farther away does not have significant influence on the dynamics. This short-reach influence region of vortex dynamics (organization and excitation: resolvent) rather precludes significant dependence on boundary conditions as long as they do not penetrate the ‘interaction layer’ around the vortex. The magnitude of different experimental configurations, all yielding similar behaviour, seems to indicate that boundary conditions do not matter too much.

The rapid adjustment of the free stream to the presence of the vortex suggests that the particular initial condition is not crucial either.

**Model vibrations.** For the sake of completeness, we should mention that Jacquin *et al.* (2001, p. 14) put forth the principal possibility of *vortex meandering being related to the propagation of wind-tunnel model vibrations*. However, further analysis led Jacquin *et al.* (2001, p. 24) to conclude that the influence of model-vibration induced perturbations

on meandering is weak, whereas its contribution to linear instabilities may be significant. Model vibrations as a source of vortex meandering have been excluded in the experiments of Iungo *et al.* (2009) (see also Iungo, 2017, p. 1789) and Beresh *et al.* (2010, p. 609). The experimental setup of Beninati & Marshall (2005, pp. 246, 251) was designed particularly to prevent any model vibrations.

## 3.2 Intrinsic dynamics

Alle Versuche des Verstehens bedürfen ja der  
Hilfsmittel, der Theorien, der Mythologien, der  
Lügen.

— H. Hesse: Der Steppenwolf

The opposed evolution – decaying (or stationary) free-stream turbulence as compared to increasing core integral kinetic energy – would seem to indicate a vortex-induced meandering mechanism. While at this point often instabilities are put forth, this reasoning is unnecessarily restrictive and we should rather think of resonant excitation. The pseudo-spectrum provides a map (*Karte*) of the possible pseudo-resonant amplification by decaying perturbations off the spectrum. (Parts of the theory are introduced in sec. 6.3 and a comprehensive treatise can be found in Trefethen & Embree, 2005.) In the scope of a linear dynamics, intrinsic mechanisms (sometimes called core dynamics; e.g. Melander & Hussain, 1994) are inextricably linked with the discrete spectrum of the linearised Navier–Stokes operator (e.g. Arendt *et al.*, 1997). Restriction to the discrete spectrum prevents all interaction with the free stream, which, in fact, is governed by the (inviscid) continuous spectrum (this is discussed in appendix C; see also Roy & Subramanian, 2014).

### Self-induction and circulation dependence

Considering a single vortex filament, Rokhsaz *et al.* (2000, p. 1023) employ a first order kinematic approach to derive an equation of motion  $dA/dt = \beta A$ ,  $\mathbb{C} \ni \beta = \beta(\Gamma) \sim \Gamma$ , for the temporal amplitude function of the filament  $A(t)$ . Solution by separation of the variables yields temporally oscillating solutions with the amplitude growing or decaying exponentially in time. Since  $\beta_r = \beta_r(\Gamma) \sim \Gamma$  the amplitude growth depends on the vortex strength. Thus, Rokhsaz *et al.* (2000, p. 1027) suggest that *vortex meandering is self induced due to the Biot–Savart law*.

This explanation for the observed amplitude growth can almost certainly be rejected from the compelling evidence of a reciprocal relation between amplitude and circulation (Devenport *et al.*, 1996; Heyes *et al.*, 2004; Bailey & Tavoularis, 2008; Roy & Leweke, 2008; Iungo *et al.*, 2009; Beresh *et al.*, 2010; Iungo, 2017). In other words, a strong vortex resists deflection by external impacts (Devenport *et al.*, 1996, p. 100). This relation is quantified in (4.1) and fig. 4.2.

Heyes *et al.* (2004, p. 6 and fig. 8) and Iungo *et al.* (2009, p. 450) report a linear relation between the meandering amplitude and vortex strength. The studies of Devenport *et al.* (1996, p. 80), Roy & Leweke (2008, p. 5) and Beresh *et al.* (2010, p. 604) show results for the variation of the meandering amplitude over the (wing) angle of incidence. This relation seems to be generally non-linear, principally consistent with (2.4).

The experimental fact that meandering amplitudes reduce for increasing vortex strength (Bailey & Tavoularis, 2008, p. 311) (*idem*, angles of incidence) is usually argued to provide strong support to the conjecture that meandering can be thought of as the vortex being buffeted by an external source (Devenport *et al.*, 1996, p. 80). If it was an exclusively

intrinsic mechanism, we would expect meandering to scale on the characteristic vortex scales alone.

### Isolated-vortex instability

Jacquín *et al.* (2001, p. 19) and Jacquín *et al.* (2003) compare estimates of the characteristics of (isolated-)vortex instabilities with their spectra, concluding that the broadband spectrum may be the consequence of many simultaneously active instability mechanisms. However, although their spectrum revealed possible signatures of several instabilities, the measurement distance up to  $zb^{-1} = 9$  was judged insufficient to finally identify the governing mechanism for meandering and a definite relation could not be established.

Among the principally possible instabilities, the deflection characteristic of meandering readily suggests the following hypothesis.

**Conjecture 3.1.** *Vortex meandering is related to a linear instability of  $|m| = 1$  symmetry.*

Conjecture 3.1 is put forth by Edstrand *et al.* (2016, p. 2) due to the strikingly similar patterns of the leading POD modes of the coherent part in a triple decomposition of the velocity field with the (spatially) least stable mode of a Batchelor vortex fitted at  $zc^{-1} = 5$ . The actual result of the linear stability analysis by Edstrand *et al.* (2016, p. 8) yields at worst a (*marginally*) *stable* mode but *no* spatial instability for the considered configuration. Thus, conj. 3.1 is, in fact, solely based on the visual resemblance of the respective modes obtained and the monotonic energy growth of the leading-order POD modes with  $z$ . In fact, this structural similarity together with perturbation-energy growth alone provided sufficient evidence for Edstrand *et al.* (2016, p. 8) to claim that all indices ‘strongly point towards an instability as the underlying mechanism for vortex meandering; the type of instability, however, is still subject to debate’. The problem here might be a confusing use of the terminology of what precisely is meant by an ‘instability’. Stricto sensu, there is no instability in the sense of Lyapunov.

Isolated vortices can principally be destabilised by either a centrifugal instability or an axial-flow-induced instability (Stout & Hussain, 2016, p. 354; Viola *et al.*, 2016, p. 525; see also Gallay & Smets, 2019, 2020 for a recent account). We shall only give a brief account here on the relevance of the loss of (temporal) stability due to the vortex comprising an axial mean-flow component. The prototype reference flow in this case is given by the Batchelor vortex.<sup>4</sup> The dispersion relation in this case reads (the azimuthal wave number  $|m|$  is assumed to be unity)

$$(3.1) \quad s = s(\alpha, q, R) \in \mathbb{C}.$$

The parameters  $\alpha, q, R$  are taken to be real valued and the perturbation ansatz such that  $s_r$  represents the temporal growth rate.

From fig. 2.4, we see that the average Reynolds number is  $R_\delta \approx 2 \times 10^3$ , although this value is subject to considerable variation, especially for  $zc^{-1} \lesssim 10$ .

A reference state is called stable here, if it is *asymptotically* stable, i.e. Lyapunov stable and the perturbed state tends asymptotically to the reference state as  $t \rightarrow \infty$  (Joseph, 1976, p. 26; Yudovich, 1989, p. 100). Asymptotic stability is equivalently to the discrete spectrum of the linearised Navier–Stokes operator. We note that the signature of the discrete spectrum extends to the nonlinear problem (Monin & Yaglom, 1971, p. 157):<sup>5</sup>

**Proposition 3.1.** *Linear stability implies non-linear stability.*

<sup>4</sup>To be precise, the Batchelor vortex is no fixed point of the Navier–Stokes equations but a slowly diffusing solution of the boundary-layer approximation. For dynamics which are fast compared to the slow diffusion, it is assumed essentially equivalent to a fixed point, also called  $q$  vortex (Fabre & Jacquín, 2004).

<sup>5</sup>The proposition that linear *instability* implies nonlinear *instability* is less obvious, see e.g. Georgescu (1985), Friedlander *et al.* (1997), Friedlander & Yudovich (1999) and Friedlander *et al.* (2006).

**The swirl number.** As the definition suggests, the swirl number (2.13) should increase with vortex strength (i.e. the angle of incidence) for otherwise fixed conditions. This is indeed observed in the experiments of Devenport *et al.* (1996, p. 81) for fixed  $R_c$  and  $zc^{-1} = 10$ :

$$q \approx 1.85 \dots 7.85 \quad \text{for } \alpha = 2.5^\circ, \dots, 7.5^\circ \quad \text{at } R_\delta \approx 1500 \dots 2000.$$

Similarly, varying the angle of incidence  $\alpha = 4^\circ, \dots, 12^\circ$  at  $zc^{-1} = 9$ , Chigier & Corsiglia (1972, fig. 3) find  $q \approx 1.57 \dots 7.85$  followed by a drop to  $q \approx 4.2$  for the highest angle of incidence (probably due to stall). Keeping the angle of incidence fixed the swirl number seems to be rather unaffected by changes in the Reynolds number  $R_c$  (Devenport *et al.*, 1996, tab. 1).

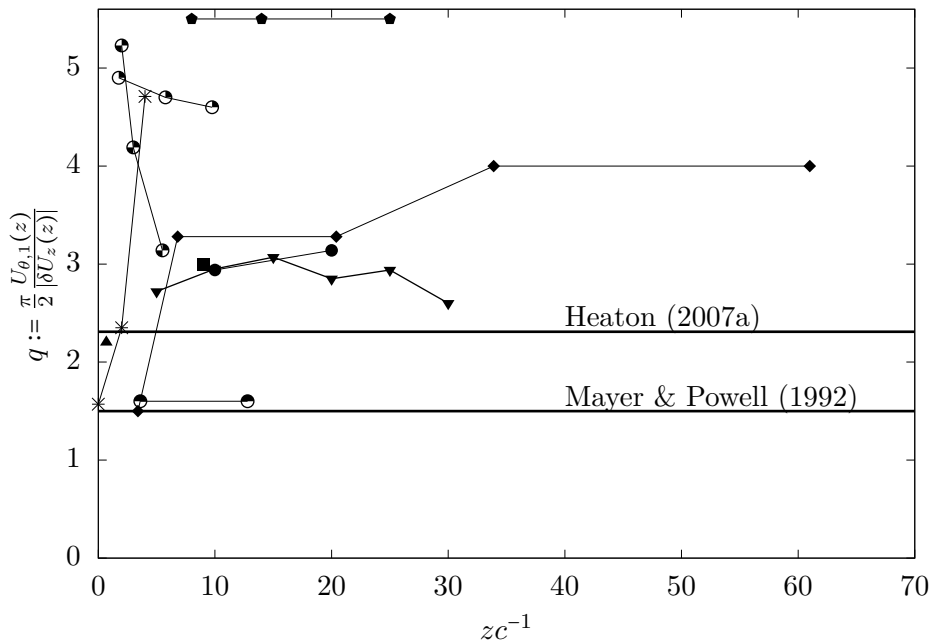


Figure 3.1: Variation of the swirl number (2.13), compared to the viscous and inviscid neutral stability limits to helical perturbations (for the experiments listed in appendix A.2). The swirl numbers computed from the experiments of Jacquin *et al.* (2007) (cf. also appendix A.1) can be estimated from fig. 2.2 to be  $q > 6$  for all measurement positions and are thus not shown.

The (monotonous) downstream growth of the core kinetic energy and meandering amplitude might be taken as evidence that experimental meandering is the result of flow transition as observed in various shear flows (Schlichting, 1997). A possible scenario assumes an initial instability of the laminar vortex followed by some kind of a transition eventually resulting in the turbulent state corresponding to experimental meandering. This perception would require vortex instability in the near wake of  $zc^{-1} \leq 3$  (say).

The downstream variation of the swirl number is shown in fig. 3.1. The horizontal lines indicate the viscous (Mayer & Powell, 1992) and inviscid (Heaton, 2007a, p. 327) neutral stability limits of helical perturbations to the Batchelor vortex.

Reducing the question of vortex stability to the swirl number, the experimental results are not conclusive. While some studies find swirl numbers of  $q \approx 2 \dots 3$  for  $zc^{-1} \leq 2$  (Green & Acosta, 1991, fig. 14; Chow *et al.*, 1997, pp. 53, 55), others report a weakly unstable condition  $q \approx 1.25 \dots 1.5$  for  $zc^{-1} \approx 1$  (Chigier & Corsiglia, 1971, figs. 4–6; Jacquin *et al.*,

2001, p. 15). These values of the swirl number are close to the inviscid critical value which, however, may be viscously weakly destabilised at the given Reynolds number (Fabre & Jacquin, 2004, p. 248). Despite the possibility of initial growth the swirl number in both experiments is rapidly stabilised to values of  $q \approx 4.71$ .

Beyond approximately  $zc^{-1} = 5$ , the swirl number would seem to stabilise at a value of  $q \approx 3 \dots 4$  (Devenport *et al.*, 1996, p. 81; Fabre & Jacquin, 2004, p. 259; Edstrand *et al.*, 2016, p. 4). This might be indicative of the vortex reaching a persistent equilibrium state for which  $q \geq 1.5$  (Jacquin & Pantano, 2002, p. 167). Systematically larger swirl numbers of  $q \approx 5.5$  can be estimated for the experiments of Beninati & Marshall (2005, p. 248). Downstream stabilisation in the sense of rapidly increasing  $q$  is also observed in spatial direct numerical simulations of the non-parallel Batchelor vortex (Heaton *et al.*, 2009, p. 144 and fig. 3, as well as similar simulations due to Jacquin & Pantano, 2002, p. 163 and Viola *et al.*, 2016, figs. 1–2).

The only experiment known to us being persistently in a potentially unstable configuration over  $zc^{-1} \in [3.6, 12.8]$  at an angle of incidence  $\alpha = 5^\circ$  is due to Pentelov (2014, figs. 5.21 and 5.25); in this case,  $q \approx 1.6$ .

**Growth rates.** Since some experiments indicate weakly unstable conditions shortly behind the wing, we should estimate the growth rates<sup>6</sup> in order to decide on their pertinence. For this purpose, we must express the time scale used in stability studies in terms of experimentally accessible scales. The experimental scales of least uncertainty which are pertinent for vortex meandering are probably the chord length  $c$  and free-stream velocity  $U_\infty$ .

The temporal growth rates  $s_r$  of the viscous modes of Khorrami (1991) and Fabre & Jacquin (2004) decay as  $s_r = O(R_\delta^{-1})$  and  $s_r = O(R_\delta^{-1/3})$  as  $R_\delta \rightarrow \infty$ , respectively. In either case, the maximum growth rate is bounded above by  $s_{r,max} \sim 10^{-2} \tau_\delta^{-1}$  for finite Reynolds numbers (Heaton, 2007a, p. 326). Converting scales,  $s_{r,max} \sim 10^{-1} \tau_c^{-1}$  which corresponds to a growth length of  $zc^{-1} = (U_\infty s_{r,max}^{-1}) c^{-1} \sim 10$ . That is, perturbation growth by one unit happens, at best, over a downstream distance of ten chord lengths. Except possibly for cruise conditions at very low angle of incidence in a quiescent environment, growth of viscous instabilities of a Batchelor-like vortex is too slow to be of practical importance for meandering. Even in the parameter range where viscous instabilities are active, they are less important on the time scale where inviscid mechanisms are active (Heaton & Peake, 2007, p. 285).

The maximum growth rate of an inviscid instability is  $s_r = 0.46$  (Mayer & Powell, 1992; Heaton, 2007a, p. 326). Repeating the same estimates as above, this instability develops over a time scale of  $s_r \sim 4.6 \tau_c^{-1}$  which corresponds to a growth length of  $zc^{-1} \sim 0.5$ . Nevertheless, Reynolds numbers in experiments are finite (fig. 2.4) and these inviscid instabilities are damped in practice. Non-linear integration of these instabilities by direct numerical simulation shows that the developing fine-scale turbulence is stabilised and the core relaminarises (Jacquin & Pantano, 2002).

### Cooperative instabilities

Jacquin *et al.* (2001, p. 14) suggest the following.

**Conjecture 3.2.** *Vortex meandering is associated with a linear cooperative instability.*

Already Baker *et al.* (1974, p. 331) presumed that *far downstream* some meandering may be induced by mutual vortex instability of the trailing-vortex pair while they estimated it to be

<sup>6</sup>The modulus of a complex number  $u(t) = \hat{u}e^{st}$ ,  $s \in \mathbb{C}$ , is  $|u(t)| = \hat{u}e^{\text{Re}(s)t}$ . Let  $\hat{u} := 1$  without loss of generality, then the amplitude at time  $t$  is  $A(t) = e^{\text{Re}(s)t}$ . Thus, the time  $t$  to attain a certain amplification  $C = \ln A$  becomes  $t = Cs_r^{-1} \sim s_r^{-1}$  or  $(t = zU_\infty^{-1}) zc^{-1} \sim (U_\infty s_r^{-1})c^{-1}$ .

most certainly negligible at downstream positions less than  $zc^{-1} \leq 60$ . Trailing vortices in free-flight measurements show neither significant growth nor decay about 20 wing spans (i.e.  $zc^{-1} \lesssim 160$ ) from the trailing edge. For about this distance the trailing vortices of a full-wing setting can, in good approximation, be assumed to develop independently (Devenport *et al.*, 1996, p. 68). This is consistent with the time scale of cooperative instabilities  $\sim \tilde{b}^2 \Gamma^{-1} \sim \tilde{b}^3$ ;  $\tilde{b}$  is the vortex separation and the circulation (through lift) is inversely proportional to vortex spacing (Jacquin *et al.*, 2001, p. 5). Eventually, according to Beninati & Marshall (2005, pp. 246, 251), their experimental set-up was designed especially to prevent cooperative instabilities. This and particularly the fact that the phenomenon is observed already shortly behind the wing (see sec. 2.4), cooperative instabilities as a necessary prerequisite for vortex meandering are excluded. It should be noted that conj. 3.2 was eventually rejected by Jacquin *et al.* (2005, p. 412), too.

The near wake is typically characterized by the coexistence of several vortices (e.g. Jacquin *et al.*, 2001). Bailey *et al.* (2006, pp. 1285–1286) find the vortex positions to be independent of the free-stream turbulence intensity in their experiment. However, arrangement and number of the vortices depend strongly on the geometry of the vortex generator and are not universal. Observed  $n$ -vortex instability in a particular setting is therefore most likely not representative in general. The universal observation (e.g. trailing from canonical rectangular wing) would seem to be inconsistent with the systematic formation of certain vortex systems.

### Conclusion 3.2.1: Linear stability

We conclude that vortex destabilisation due to the vortex comprising an axial mean-velocity component is largely irrelevant: meandering is not a direct consequence of an axial-flow-induced linear instability. While viscous instabilities can be excluded due to swirl-number restrictions and extremely weak growth, inviscid instabilities are shown to be insignificant due to finite Reynolds numbers and nonlinear stabilisation. The only potential exceptions might be for small angles of incidence or very close to the trailing edge, within one chord say. Albeit, in this case validity of the theoretical model of an isolated parallel Batchelor vortex in an infinite fluid container is certainly doubted. Eventually, even if all conditions are fulfilled and an instability is possible, it is probably overpowered by the dynamics resulting from the nonnormality of the linearised operator (Heaton, 2007b).

Ad idem, Fabre & Jacquin (2004, p. 259) conclude that (at least in the experiment of Jacquin *et al.*, 2001) *vortex meandering is not due to a viscous instability* of vortices comprising an axial velocity, but conjecture that:<sup>7</sup>

**Conjecture 3.3.** *Vortex meandering is due to the (transient) excitation of Kelvin waves in the vortex core by the surrounding turbulence.*

This mechanism does not follow the rigid separation into intrinsic or extrinsic mechanisms adopted thus far but assumes a contribution from both. Indeed, meandering would seem to be likely associated with a generalized (spatio-temporal) receptivity problem of the vortex core with respect to free-stream disturbances. We postpone a further discussion to chap. 6.

<sup>7</sup>This proposition can already be found in Jacquin *et al.* (2003, p. 590).

## 4 | First mechanism: Brownian meandering?

Es ist der Einblick in eine neue Welt. Statt der erwarteten Kirchhofruhe bemerkt er einen äußerst lebhaften, munteren Tanz . . .

---

— M. Planck: Dynamische und statistische Gesetzmäßigkeit

At the end of sec. 2.4, we concluded that meandering (of trailing vortices) is characterized by three pillars. The first pillar – downstream amplitude growth – is the subject of the present chapter. The here suggested theory is best motivated with the aid of fig. 4.1, showing the Brownian motion of a suspended particle (taken from the famous experiment of J. Perrin, 1913, p. 166). Comparing this trajectory to realizations of experimental vortex meandering shown in fig. 4.2, we propose that, had we access to measurement planes spaced more closely and over a longer downstream range, the trajectories shown in fig. 4.2 would be indistinguishable (in its characteristics) from the path shown in fig. 4.1. What we want to show henceforth resumes in the following conjecture and corollary.

**Conjecture 4.1.** *The vortex-centre random process  $t \mapsto \mathbf{X}(t) \subset \mathbb{R}^2$  is a Brownian motion.*

**Corollary 4.1.** *If we assume – what we do! – that there exists a bijection between  $\mathbf{X}(t)$  and what we call meandering, vortex meandering is a Brownian motion, too. The meandering vortex volume (presumably comparable to the core or support) is then material and the vortex behaves like a fluid particle.*

### 4.1 A dimensional argument: the scaling law

Auch spielt das Zufällige, Unberechenbare, Inkommensurable eine zu große Rolle. Unsere Gesetze fußen nur auf Wahrscheinlichkeiten, auf Statistik, nicht auf Kausalität, treffen nur im allgemeinen zu, nicht im besonderen.

---

— F. Dürrenmatt: Das Versprechen

It should probably be recalled that the ‘meandering amplitude’ is defined as the standard deviation of the vortex-centre position in def. 2.7. In the following, we recall some heuristic modelling, augmented by dimensional arguments, which leads to a simple scaling law for the meandering amplitude; reminiscent of Brownian motion (as already motivated at the end of sec. 2.4).

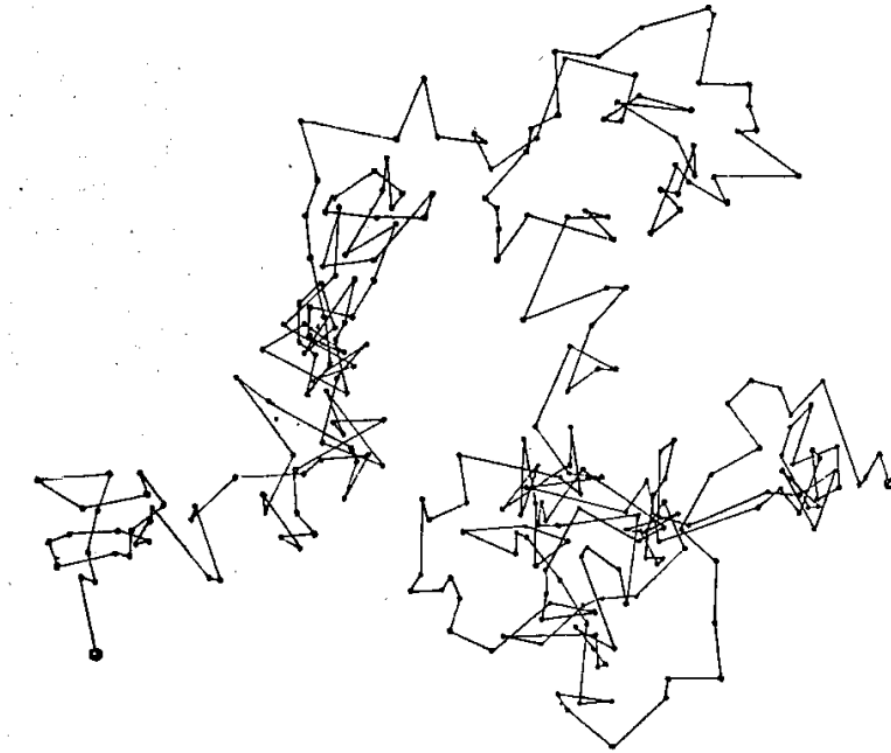


Figure 4.1: Brownian motion of a suspended particle traced under the microscope by J. Perrin (1913, p. 166).

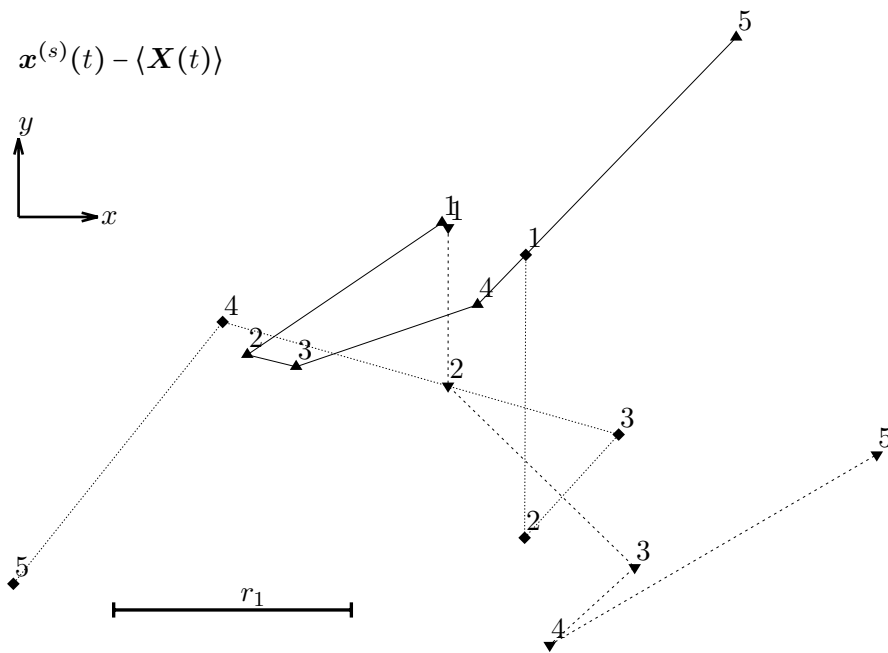


Figure 4.2: Centred vortex centre (from the PIV measurements presented in appendix A.1). Time is defined by  $t = zU_\infty^{-1}$  and the points  $\{1, 2, \dots, 5\}$  label subsequent measurement planes at  $zc^{-1} \in \{2, 4, \dots, 26\}$ . The shown realizations correspond to  $s \in \{10^0(\blacktriangle), 10^2(\blacktriangledown), 10^3(\blacklozenge)\}$  ( $s$  is the index of the 'random experiment' defined in appendix B). The core scale  $r_1$  is shown for comparison.

**Experimental evidence for  $\sigma \sim u$ .** It is universally observed that meandering amplitudes increase when the vortex is immersed in ambient turbulence of enhanced kinetic energy (Baker *et al.*, 1974, p. 331; Heyes *et al.*, 2004, fig. 10; Beninati & Marshall, 2005; Bailey & Tavoularis, 2008, p. 291 and fig. 6; Van Jaarsveld *et al.*, 2011, p. 222; Hussain *et al.*, 2011, p. 314; Bailey *et al.*, 2018, p. 733). Amplitude modification as a consequence of increased free-stream turbulence intensity is obvious in the Laser Induced Fluorescence (LIF) visualisations of the water-tunnel experiments of Bailey *et al.* (2018, p. 731) (also refer to Pentelow, 2014, §5.1). Besides the absolute deflection amplification, strong local distortions of the vortex axis for higher turbulence intensities manifest (Bailey *et al.*, 2018, p. 729).

**Brownian motion.** The dynamics leading to vortex meandering are twofold: namely, a balance between external driving and internal resistance. This is reminiscent of Brownian motion. The essentials of Brownian motion, namely that it is the ‘outcome of rival tendencies’ – *ordering vs disordering forces* –, is very concisely illustrated by Schrödinger (1992, p. 12).

Without specifying the receptivity mechanism, Bailey & Tavoularis (2008, p. 293) speculate that ‘the ‘beating-about’ of the vortex by the free-stream turbulence and induction by nearby eddies might result in velocity fluctuations in the core. On the other hand, the vortex naturally resists deformation so that meandering-velocity amplitudes bounded above by amplitude of free-stream fluctuation velocity amplitudes’. This must be understood in the sense that vortex only resists deformation but does not ‘own-meander’.

Dimensional analysis of the two-trailing-vortex system subject to grid turbulence in the far field (emphasizing cooperative instabilities, decay and breakdown) due to Sarpkaya & Daly (1987, pp. 401–402) yields

$$\frac{H}{\tilde{d}_0} = H \left( \frac{U_\infty t}{\tilde{d}_0}, \varepsilon, \frac{l}{\tilde{d}_0} \right)$$

for the elevation  $H$  of the vortex pair, normalized with the initial vortex-core spacing  $\tilde{d}_0$ . The dissipation rate  $\varepsilon$  defined in Sarpkaya & Daly (1987, eq. (8)) and  $l$  denotes the integral length scale. The elevation was found to be insensitive with respect to the Froude and Reynolds number. Further investigation suggested that the dissipation rate  $\varepsilon$  is the governing parameter for the determination of the vortex deflection amplitude, while the integral length scale of the surrounding turbulence  $l$  only plays a minor role (Sarpkaya & Daly, 1987, p. 403). The dissipation rate can always be estimated as  $\varepsilon \sim \mathfrak{U}^3 \tau^{-1}$  (Tennekes & Lumley, 1973, p. 68).

Rokhsaz *et al.* (2000, p. 1026) proposed  $\sigma = \sigma(z, \Gamma)$  as the general lawfulness (*Gesetzmäßigkeit*). From purely dimensional arguments, we derive: –

**Conjecture 4.2.** *Take the experimental evidence that the meandering amplitude  $\sigma$  grows for stronger free-stream turbulence intensity  $u$  and downstream  $z$  of the wing. The amplitude decreases as the vortex strength  $\Gamma$  increases. In general,  $\sigma \sim u^a z^b \Gamma^{-c}$  for  $a, b, c > 0$ , and for dimensional reasons  $\sigma r_1^{-1} \sim u \times (t/\Gamma)^{1/2}$ .*

– Baker *et al.* (1974, eq. (9)) suggested the amplitude growth  $\sigma^2(z) = 2\nu_t z/U_\infty$  ( $\nu_t$  is a scalar characteristic of the *ambient* turbulence) to follow a law similar to vortex diffusion.

– Van Jaarsveld *et al.* (2011, p. 222) propose that the standard deviation of the vortex-centre location can be described analogously to that of a passive scalar in homogeneous turbulence. This problem was first solved by G. I. Taylor (1921). In this case, the characteristic time scale corresponds to that of the ambient turbulence field, which Van Jaarsveld

*et al.* (2011, p. 222) suggest to substitute by the vortex-turnover time  $t_r$ . Then,

$$(4.1) \quad \sigma(t) \sim u\sqrt{t_r t} \sim u\sqrt{\frac{r_1^2 t}{\Gamma_1}} \Leftrightarrow \frac{\sigma(t)}{r_1} \sim u\sqrt{\frac{t}{\Gamma_1}}$$

or equivalently

$$\frac{\sigma(t)}{r_1} \sim u\sqrt{\frac{t}{r_1 U_{\theta,1}}} \sqrt{\frac{U_{\theta,1}}{U_{\theta,1}}} = \frac{u}{U_{\theta,1}} \sqrt{\frac{U_{\theta,1} t}{r_1}} \sim \frac{u}{U_\infty} \sqrt{\frac{t}{t_r}}.$$

The last form indicates that vortex meandering is proportional to the ambient turbulence intensity and the residence time of the vortex in the turbulent surrounding. Bailey *et al.* (2018, p. 734 and fig. 5) match their results obtained in two facilities with this linear (with respect to the free-stream turbulence intensity) amplitude law which supports ‘van Jaarsveld’s observation that the vortex turnover time is an important scaling parameter for the meandering amplitude’. This is also shown in fig. 4.3.

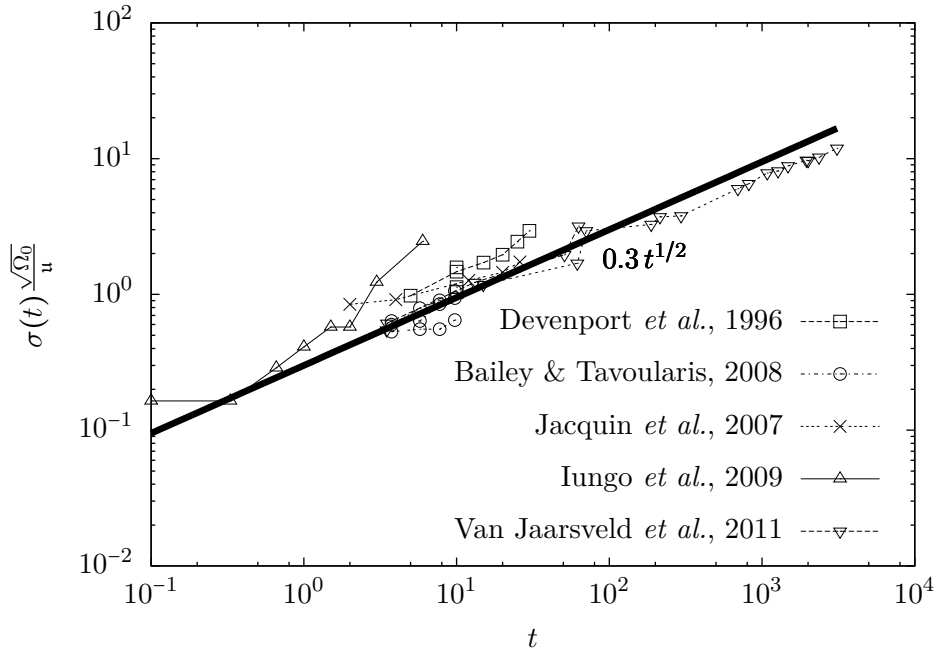


Figure 4.3: Temporal ( $t = zU_\infty^{-1}$ ) evolution of the normalized vortex-centre standard deviation  $\sigma(t)$  according to (4.1) (solid line) and compilation of experiments (symbols).

From the importance of the rotation time as a scaling parameter of vortex meandering, Bailey *et al.* (2018, pp. 724, 745) conclude the following.

**Conjecture 4.3.** *Vortex wandering scales on intrinsic vortex rather than external turbulence scales.*

Bailey *et al.* (2018, p. 733) stress that Taylor’s theory assumes *homogeneous* turbulence (i.e. statistics independent of  $z$ , implying e.g.  $u = \text{const}$ ) which is not the case in grid-turbulence experiments, where  $u = u(z)$  decays downstream ( $-1.3$  power law; cf. (6.1)).

**A comment on two-dimensional turbulence.** It is characteristic of two-dimensional turbulence to gradually concentrate vorticity in several ‘vortices’ which ‘meander’ around (McWilliams, 1984, 1990). Most likely, this vortex motion is ‘true’ meandering in the sense

of def. 2.6. Yet, the situation is different with respect to trailing-vortex meandering in that normally more than one 'dominant vortex' forms. The dynamics is therefore likely due to the interaction of several vortices of comparable strength and the governing mechanisms might differ from the here discussed.

## 4.2 Derivation from the Navier–Stokes equations

The attempt at deriving a Brownian meandering motion directly from the Navier–Stokes equations is appended in appendix B. Brownian meandering is also evidenced in fig. 4.4, where the diffusion of the normal probability density according to  $\sigma(t) \sim t^{1/2}$  is shown. In appendix B, we suggest that the universal Gaussian statistics (see also sec. 2.4) may be an artefact of the central limit theorem.

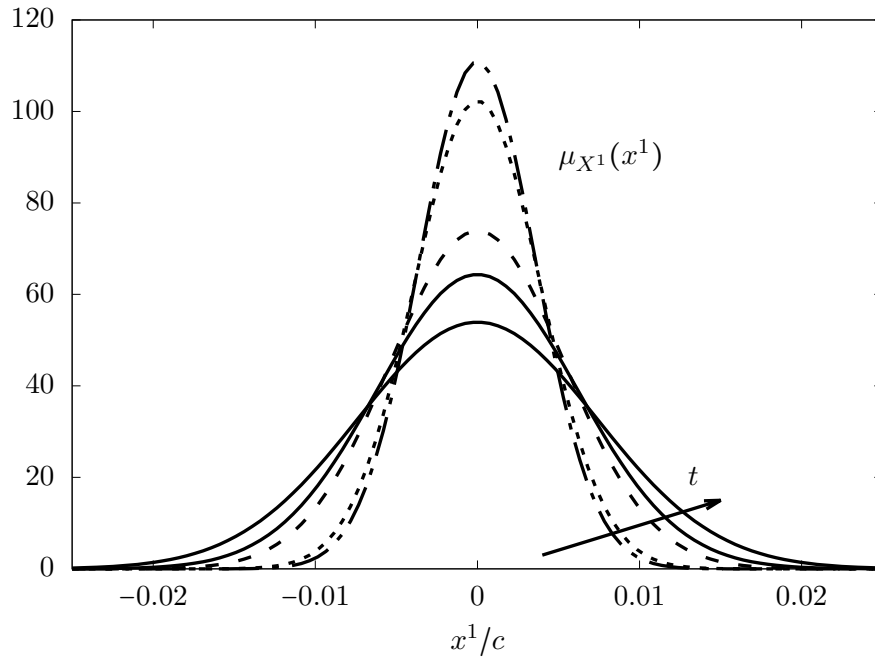


Figure 4.4: Diffusion of the marginal probability density  $\mu_{X_1}^t(x_1) \sim \mathcal{N}(0, \sigma_{R_1}^1 t^{1/2})$  for the five measurement stations in the experiment (cf. appendix A.1 and B).



## 5 | Second mechanism: return to order!

Es ist aber immer auch etwas Vernunft im Wahnsinn.

---

— F. Nietzsche: Also sprach Zarathustra

At the end of sec. 2.4, we identified some sort of stochastic-coherent duality as one of the cornerstones characterizing vortex meandering. By this figurative description, we intended to put into one concept the fact that meandering involves scales spreading over several orders of magnitude, all the same having a somewhat well-ordered appearance. That there is always a regular skeleton underlying manifesting irregularity is precisely the content of the above quotation from F. Nietzsche and, in fact, characteristic of chaotic rather than stochastic dynamics (see the definition of chaos in Devaney, 1989, p. 50).

On the basis of the general trends of the meandering dynamics worked out in sec. 2.4.2, we conjecture that (trailing-)vortex meandering obeys a *return-to-order* principle. Bohm & Peat (1987, p. 141) state that – ‘as with order, so with structure, there can be no complete definition’. To get an idea, recall that the word ‘order’ has its root in the Latin *ōrdō*, meaning row, rank, regular arrangement<sup>1</sup>. As such, it describes the *state* of an ensemble of elements in which the parts are subject to certain uniform, established proportions yielding structural regularity or form. Bohm (1980, pp. 146–149) defines order in terms of similar differences. That is, a system<sup>2</sup> is highly ordered if it has very few degrees of freedom or free parameters that characterize it (see also Bohm & Peat, 1987, p. 116). In the present context, the degrees of freedom are identified with the dynamically active modes (viz. the span of the supporting phase-space volume). In order to emphasize the intention or desire of the system towards order, we may employ the word ‘orderliness’. According to the dictionary, the suffix ‘-ly’ means ‘having qualities of, of the form or nature of’.

Eventually, the word ‘organization’ is sometimes used with a similar meaning (e.g. Bandyopadhyay *et al.*, 1991; Jacquin *et al.*, 2001, p. 1; Bailey *et al.*, 2018, pp. 734–744). The word ‘organization’ derives from the Greek *ὄργανον*, meaning instrument, tool. Rather than a state, it bears the connotation of a *process* that assembles parts to a viable whole.

### 5.1 Organization and low-dimensionality in wing wakes

No one knows what entropy really is, so in a debate you will always have the advantage.

---

— J. von Neumann to C. Shannon.

---

<sup>1</sup>*Reihe, Schicht, Ordnung* (Stowasser, p. 355).

<sup>2</sup>The word ‘system’, from the Greek *σύστημα*, means ‘the whole assembled from connected elements’.

The following section is guided by the questions – *What does the broadband continuous power spectrum tell us about the meandering dynamics?* And – *How can we quantify the apparent increase of orderliness?*

### 5.1.1 Is there a universal scaling law of the meandering frequency?

In chap. 4, we have shown how the meandering amplitude results from a balance between external excitation and internal resistance. Considerable evidence for the idea of an externally determined frequency selection (amplifier-like dynamics; Huerre & Monkewitz, 1990, p. 475) is typically seen in the scaling  $\lambda \sim c$  of the characteristic meandering wavelength (i.e. the peak frequency); cf. conj. 2.6. Proportionality to the chord length  $c$  suggests that (part of) the meandering scales with the model dimension (Jacquin *et al.*, 2005, p. 413).

At the same time, universality and convergence irrespective of the turbulence conditions (conj. 2.6–2.7) is seen as an indicator for a vortex-induced selection principle. Experience tells us that the vortex strength is one of the key parameters of meandering (e.g. in chap. 4). It would appear that it is in this spirit that Bailey *et al.* (2018, p. 739) ‘assert with some confidence’ that the meandering wavelength scales on the vortex turnover time  $\lambda \sim \tau_r$ .

On the other hand, Devenport *et al.* (1996, p. 96) find the power spectral densities to collapse, when scaled on the parameters of the two-dimensional unrolled-up wake though not when scaled on the core parameters. This suggests an externally induced meandering frequency by the surrounding flow. This scaling, to the best of our knowledge, has never been confirmed. The vortex-surrounding, energy-containing turbulence structures are typically associated with integral length scales of  $0.1 \dots 5 r_1$  (Beninati & Marshall, 2005, pp. 245, 251; Bailey *et al.*, 2018, p. 737). This turbulence scale is about an order of magnitude smaller than the characteristic meandering wavelength postulated in conj. 2.6 (see also Bailey & Tavoularis, 2008, p. 298 and fig. 13). Comparison with the ‘eddy-travelling distance’ (estimated to be  $1 \dots 2 \times 10^2 r_1$ ; Bailey *et al.*, 2018, p. 737) shows that these two turbulence scales constitute, at best, lower and upper bounds for the true meandering wavelength. This scale independence (and furthermore invariance with respect to the turbulence intensity) provides evidence that (see also sec. 2.4.2 and Bailey *et al.*, 2011, p. 5):

**Conjecture 5.1.** *Free-stream turbulence only excites inherent vortex modes, while it does not cause the development of new modes.*

### 5.1.2 Is meandering a stochastic or coherent dynamics?

There is the ongoing controversy as to whether the meandering dynamics is stochastic or coherent. To begin with, understanding these attributes without rigour, the essential question seems to be whether meandering is either an externally induced phenomenon lacking intrinsic dynamics or a fundamentally vortex-induced mechanism manifesting through inherent vortex modes.

**Experimental evidence.** The existence of organized periodic motion underlying meandering is inferred from non-vanishing cross-correlation of the meandering amplitudes. Cross correlation, weak periodicity and identical wavelengths in  $x, y$  indicates the existence of a helical pattern of long-wavelength, organized meandering co-rotating with the vortex (Bailey *et al.*, 2011, p. 5). Correlation analysis of Singh & Uberoi (1976, pp. 1860–1862) suggests that among the distinguished core fluctuations ( $m = 0, 1$ ) more energy is in the low-frequency helical  $|m| = 1$  core perturbation.

On the other hand, Bailey *et al.* (2018, p. 743) find a cross correlation of  $\rho_{XY} < 0.1$  ( $X$  and  $Y$  are the Cartesian components of the vortex centre), stating that almost uncorrelated

axes coordinates imply negligible contribution from helical axis motion. Zero-crossing analysis of Bailey & Tavoularis (2008, p. 310) suggests that the *meandering motion is incompatible with dominant helical or sinusoidal modes*.

As shown in fig. 2.8 the meandering energy spreads over scales in the range of three orders of magnitude and although well-defined peaks in the pre-multiplied power spectral densities exist, Bailey *et al.* (2018, pp. 735–736, 740) conclude that the corresponding relative energy content (within  $\pm 50\%$  of the peak value) only constitutes a small fraction of the total energy. From this and the Gaussian Lagrangian centreline-velocity probability density function, Bailey *et al.* infer that ‘meandering was largely stochastic [and] . . . motions with frequencies at or near the most probable values were rare’.

At the same time, the fact that meandering seems to affect vortices in general and that, moreover, the characteristics are essentially universal, irrespective of the details of the initial and boundary conditions, suggests the existence of some supporting structure in phase space which accommodates vortex meandering (Guckenheimer, 1986, p. 17). For the ease of understanding, we call this supporting phase-space volume the ‘meandering attractor’, emphasizing though that this terminology is not necessarily mathematically rigorous here, and that further analysis would be required for its confirmation.

### Low dimensionality of the meandering attractor

The above discussion shows that the main evidence for the association of meandering with a stochastic dynamics stems from the difficulty to identify one particular (expectedly helical) mode in experiments together with the fact that the phenomenon is associated with a broadband continuous power spectral density (as shown in sec. 2.4.2). While the inference of randomness from the power spectrum is common practice (Schlichting, 1997, p. 409), it strictly allows the identification of quasi-periodic<sup>3</sup> dynamics, at best, whereas little information can be gained for more complicated flows (Malraison *et al.*, 1983, p. 897; Guckenheimer, 1986, pp. 16, 21, 24). In view of a quasi-periodic motion, the physical system is perceived as the superposition of an ensemble of *independent* oscillators (Eckmann & Ruelle, 1985, p. 618). This is a linear representation of the inherently nonlinear Navier–Stokes dynamics. In fact, according to Eckmann & Ruelle (1985, p. 619),

if we are confronted experimentally with a continuous power spectrum, there are two possibilities: We are either in the presence of a system that ‘explores’ an infinite number of dimensions in phase space, or we have a system that evolves nonlinearly on a finite-dimensional attractor.

In other words, experimentally observed broadband continuous power spectra can be due to (i) a *linear* superposition of a *large* number of *independent* modes (oscillators) or (ii) the *nonlinear interaction* of a *small* number of modes. The latter situation was shown to apply to several fluid flows, such as Taylor–Couette flow and Rayleigh–Bénard convection, while it seems not to hold for grid turbulence, for instance (Swinney & Gollub, 1986, pp. 448–450). This problem can be approached by appeal to nonlinear time-series analysis (Grassberger *et al.*, 1991; Kantz & Schreiber, 2004; Bradley & Kantz, 2015). A primary objective here is to discriminate deterministic chaos from random noise.

**Assumption 5.1.** *We assume that experimental vortex meandering is either a deterministically chaotic or stochastic dynamics. In the former case, we assume the existence of a finite phase-space volume where the motion takes place and call it attractor.*

<sup>3</sup>That is, the motion corresponds to the phase trajectory on a torus of incommensurable frequencies (Eckmann & Ruelle, 1985, p. 631; Landau & Lifšic, 1959, pp. 109–110).

**Phase-space reconstruction.** While the Navier–Stokes equations formally define a dynamical system on an infinite-dimensional phase space, the dynamics is in practice restricted to a finite (presumably small) phase-space volume (Eckmann & Ruelle, 1985, p. 618; Guckenheimer, 1986, p. 24; Foias *et al.*, 2001). Suppose this volume is  $m$ -dimensional, then Packard *et al.* (1980, p. 713) argue that the measurement of *any*  $m$  independent (in some appropriate sense) quantities captures the whole dynamics uniquely. Moreover, all such complete sets are conjectured to be diffeomorphically equivalent. This is the essence of *Takens’ embedding theorem* (Takens, 1981) which allows the reconstruction of a full nonlinear dynamical system from an experimental time series. This a very remarkable result, that all the geometrical and statistical information of the whole dynamical system is already contained in the scalar time series registered at a fixed measurement point in experiment! In practice, delay coordinates are used (Packard *et al.*, 1980, p. 713; Malraison *et al.*, 1983, p. 898; Swinney & Gollub, 1986, p. 449; Bradley & Kantz, 2015, p. 2).

Let  $u(t) \in \mathbb{R}$  be the experimentally measured time series. We then construct the delay vector  $\mathbf{z}_t := (u(t), u(t + \tau), \dots, u(t + (n - 1)\tau)) \in \mathbb{R}^n$  with the fixed delay  $\tau > 0$ .<sup>4</sup> The delay vector  $\mathbf{z}_t$  describes a trajectory in the phase space  $\mathbb{R}^n$ ;  $n$  is called embedding dimension, for which  $n \geq 2m + 1$  is required ( $m$  is the dimension of the ‘actual’ dynamics) (Swinney & Gollub, 1986, p. 449). As motivated above, in order to yield a complete picture of the supporting phase-space structure, the measurement of  $m$  independent quantities is required. Linear independence between the components is assured by setting  $\tau$  as the first zero of the autocorrelation function of the signal (Bradley & Kantz, 2015, p. 3). Guckenheimer (1986, p. 25) recommends to set the delay as about one fourth of the characteristic oscillation of the system.

**Attractor dimension.** We shall estimate the attractor dimension in terms of the correlation dimension (Grassberger & Procaccia, 1983a; Grassberger & Procaccia, 1983c). Let there be given the trajectory  $\{\mathbf{z}_t\}_{t=1}^N$  in the embedding space  $\mathbb{R}^n$ . The correlation function  $C(\epsilon)$  is proportional to the number of pairs  $(s, t)$  whose distance  $\|\mathbf{z}_s - \mathbf{z}_t\|$  is less than  $\epsilon$ . Grassberger & Procaccia (1983a, p. 346) establish that  $C(\epsilon) \sim \epsilon^\delta$  in the limit as  $\epsilon \rightarrow 0$  and call  $\delta$  the correlation dimension (for details see Grassberger & Procaccia, 1983c). We therefore have (see also Eckmann & Ruelle, 1985, pp. 620–621, 647):

**Definition 5.1.** The correlation function is defined as

$$(5.1) \quad C(\epsilon) := \lim_{N \rightarrow \infty} \frac{1}{N^2} \sum_{s,t=1}^N \Theta(\epsilon - \|\mathbf{z}_s - \mathbf{z}_t\|)$$

where  $\Theta(f) := (1 + \operatorname{sgn} f)/2$  (Heaviside function). It follows the correlation dimension

$$(5.2) \quad \delta = \lim_{\epsilon \rightarrow 0} \frac{\log C(\epsilon)}{\log \epsilon} \quad (N \text{ large}).$$

**Remark 5.1.** The correlation dimension is a lower bound of the information and fractal dimension (Grassberger & Procaccia, 1983a, p. 348; Grassberger & Procaccia, 1983c, pp. 191, 196–198).

**Remark 5.2.** Different norms may be used to define the radius  $\|\mathbf{z}_s - \mathbf{z}_t\|$  of the hypersphere (Malraison *et al.*, 1983, p. 898; Eckmann & Ruelle, 1985, p. 647). Calculations with the 1-, Euclidean and maximum norm led to comparable results in the present study so that we assume the Euclidean norm in the following (see e.g. Lax, 2007, for definitions).

<sup>4</sup>Time-delay coordinates are analogous to the use of position and its derivatives in classical mechanics (Packard *et al.*, 1980, p. 713; Swinney & Gollub, 1986, p. 449; Abarbanel *et al.*, 1993, pp. 1336, 1343).

The essential point for the present analysis is that stochastic dynamics is associated with a space-filling trajectory. That is, if meandering was stochastic, we expect the correlation dimension to be always identical with the embedding dimension –  $\delta = n$  (Grassberger & Procaccia, 1983c, pp. 191–192, 204, 206; Malraison *et al.*, 1983, p. 898). On the other hand, if  $\delta$  stabilizes at a constant value less than  $n$ , we would expect that  $\delta$  is representative of the dimension of the supporting phase-space structure and that the dynamics is not stochastic.

**Dimension estimates from the meandering experiment.** To estimate the attractor dimension of experimental vortex meandering, the analysis in sec. 6.2 suggests that the leading POD expansion coefficient  $a_1(t) := (\mathbf{u}(t), \phi_1)_{L^2(M)}$  constitutes a representative time series. (We recall that  $a_1(t)$  is equivalent to the component of the vortex-centre time series along the principal axis.) Guckenheimer (1986, p. 25) states that spatially different regions may have different dynamics so that time series at different points would be required to capture the whole of the system. This is likely the case here for the vortex and the free stream. However, since the interest is in vortex meandering, we assume the selected time series to be representative.

In practice, the correlation dimension (5.2) is evaluated graphically by appeal to a log-log plot. This is shown in fig. 5.1 for PIV measurements at  $zc^{-1} = 26$  (cf. appendix A.1). The graph of the correlation function over the radius always admits a characteristic ‘S-like’ shape (the upper arc approaching unity is not resolved in fig. 5.1). For small  $\epsilon$  the plateau results from the fact that each element is correlated only with itself, while for large  $\epsilon$  all elements are correlated and  $C(\epsilon) \rightarrow 1$  as  $\epsilon \rightarrow \infty$ . The correlation dimension is identical with the slope of the branch connecting the two plateaus as  $\epsilon \rightarrow 0$  and  $\epsilon \rightarrow \infty$ .

The delay is fixed at  $\tau = 150\tau_s$  ( $\tau_s = 3 \times 10^{-4}$  s is the experimental sampling period) with regards to the above recommendations. Increasing the embedding dimension  $n$ , the correlation dimension is found to stabilize at approximately  $\delta \approx 6$ , independent of  $n$ , the norm and the delay. Further analysis is required to definitely establish this dimension, however, the general trends strongly suggest that meandering (at  $zc^{-1} = 26$ ) is not stochastic but rather a deterministic dynamics, restricted to a comparably small phase-space volume.

The frequency content of the PIV measurements (sampling rate  $f_s = 3$  kHz) is roughly restricted to the plateau in the power spectra (cf. sec. 2.4.2 and appendix A.1). This is presumably enough to capture the essence of the meandering dynamics, while it excludes the core dynamics. We did not have access to a frequency-resolved time series, but would expect the correlation function to admit a kink (or ‘knee’), allowing the identification of two correlation dimensions (Ben-Mizrachi *et al.*, 1984). This behaviour is characteristic of product dynamics where the whole dynamical system is assembled from two non-interacting subsystems (Eckmann & Ruelle, 1985, pp. 647–648). Detection of this characteristic would provide strong support to the common assumption that vortex meandering and core dynamics are independent. This has already been anticipated in footnote 20 on p. 21.

**Downstream evolution of the dimension.** The same analysis as for  $zc^{-1} = 26$  above is repeated for the other measurement planes at  $zc^{-1} \in \{2, 4, 12, 20\}$ , whereas the delay  $\tau$  is successively decreased (as the first zero of the correlation function and the characteristic period). The resulting correlation dimensions are shown in fig. 5.2, revealing a monotonic decrease from  $\delta \approx 15$  at  $zc^{-1} = 4$  to  $\delta \approx 6$  at  $zc^{-1} = 26$ . We emphasize that the calculations of the first value (at  $zc^{-1} = 2$ ) seemed not to converge towards a final dimension, while, at the same time, they remained smaller than the embedding dimension. This suggests that already at the first measurement station the dynamics is not stochastic, while it has probably not yet converged to the meandering attractor either. However, irrespective of the definite values, we clearly observe a decreasing trend, implying that the vortex dynamics is confined to ever smaller volumes in phase space.

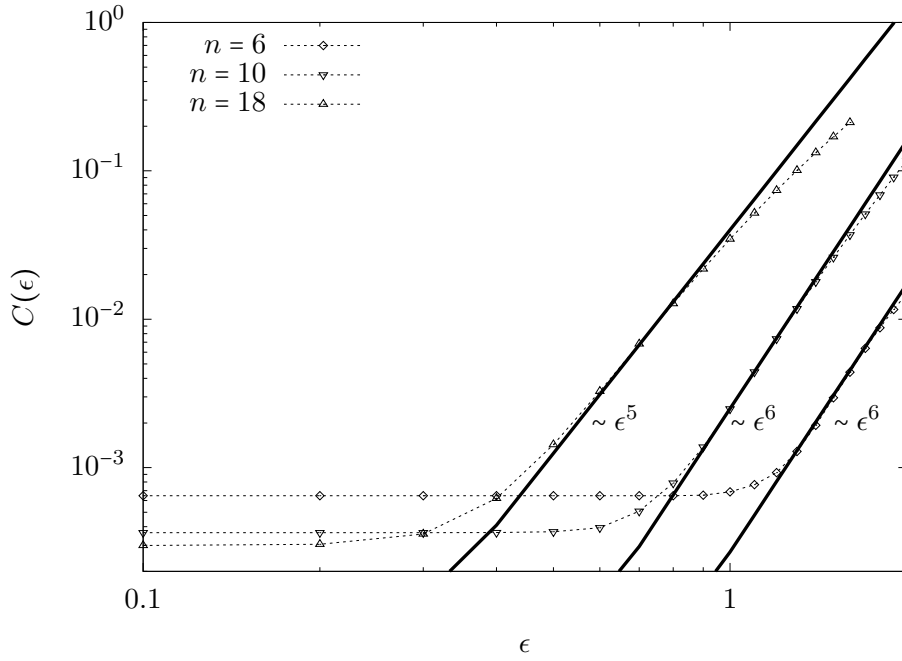


Figure 5.1: Correlation function  $C(\epsilon)$  based on the leading POD expansion coefficient over the radius  $\epsilon$  at  $zc^{-1} = 26$ . Embedding dimension  $n$ , time lag  $\tau = 150\tau_s$ , Euclidean 2-norm. (For the PIV measurements presented in appendix A.1.)

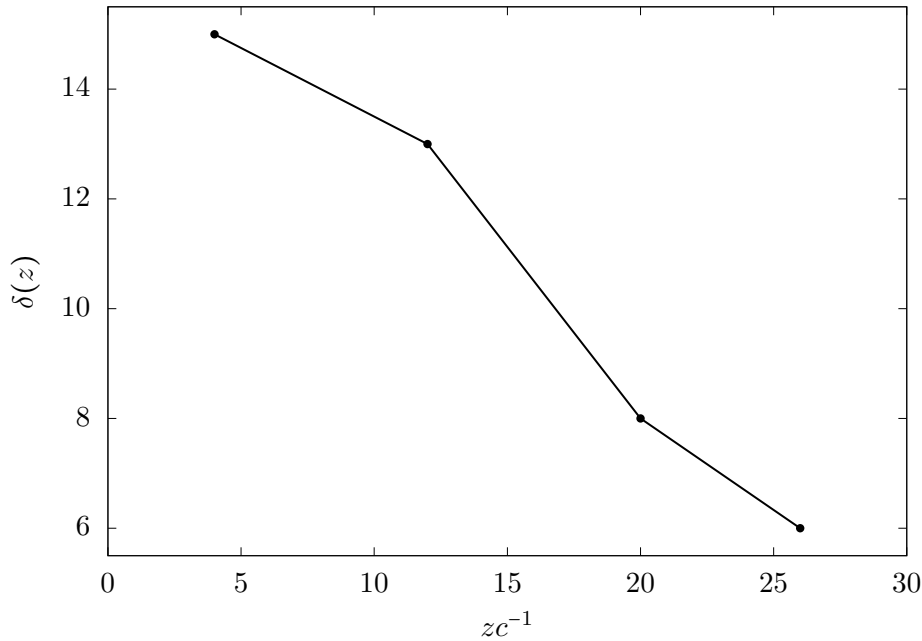


Figure 5.2: Downstream evolution of the correlation dimension. (For the PIV measurements presented in appendix A.1.)

As the wing wake evolves, the formation of a strong isolated vortex is compatible with relaminarisation. The overall vortex dynamics obeys a 'return-to-order'-principle – i.e. the emergence of a gradually more organized state out of a complex dynamics –, rather than the classical 'route to turbulence'. This is the opposite of the transition (to turbulence) problem (Schlichting, 1997, § 15; Yaglom, 2012). Although this conclusion seems fairly trivial, it is

not the commonly held point of view, which sees trailing-vortex dynamics as the gradual evolution of a laminar state close to the wing towards a fully-turbulent dynamics further downstream (i.e. framed in the classical transition problem) (e.g. Antkowiak & Brancher, 2004, p. 4; Stout & Hussain, 2016, p. 354). It is likely that all attempts to explain vortex meandering through intrinsic dynamics are in fact based on this perception.

**Kolmogorov–Sinai entropy.** Nonlinear time series analysis is appealing since it puts the analysis of experimental data on a solid and rigorous mathematical foundation. Much more analysis could be done on the experimental time series. For instance, the present framework is straightforwardly extended to compute the Kolmogorov–Sinai entropy (Grassberger & Procaccia, 1983b). Since the Kolmogorov–Sinai entropy equals the sum of the positive Lyapunov exponents (Bradley & Kantz, 2015, p. 5), zero entropy indicates non-chaotic dynamics.

### Increasing orderliness of the phase support: recurrence plots

An important aspect of time-series analysis lies in the identification of redundancies. An approximate repetition is called recurrence (Kantz & Schreiber, 2004, p. 43). The analysis by means of recurrence plots has been proposed by Eckmann *et al.* (1987) (see Kantz & Schreiber, 2004, pp. 43–46 and Marwan *et al.*, 2007 for details). As in def. 5.1, we define the correlation matrix by

$$(5.3) \quad C_{st}(\epsilon) := \Theta(\epsilon - \|z_s - z_t\|) \quad (s, t = 1, \dots, N).$$

As a matter of fact, the qualitative structure and statistics of recurrence plots are unaffected by the embedding dimension (Iwanski & Bradley, 1998; March *et al.*, 2005). Even more, embedding can lead to spurious correlations, manifesting as faulty small-scale structure in the recurrence plots (Marwan *et al.*, 2007, pp. 251–253). Therefore, since the information can be extracted directly from the unembedded time series (March *et al.*, 2005, pp. 173–174), we consider the scalar time series  $z_t = a_1(t)$  ( $n = 1$ ) in the following.

The recurrence plot is obtained by drawing the matrix  $C_{st}(\epsilon)$  with black colour (= 1) indicating recurrence (with respect to the norm and  $\epsilon$ ) and white (= 0) meaning no recurrence. This is shown in fig. 5.3 for  $zc^{-1} \in \{2, 26\}$ . The structure of the recurrence plot is practically not affected by the choice of  $\epsilon$  within reasonable limits.

The essential point here for regarding recurrence plots is, that the *particular* system behaviour can be inferred from *typical* patterns.<sup>5</sup> Eckmann *et al.* (1987, p. 974) distinguish large-scale *typology* and small-scale *texture*. A comprehensive classification of the various patterns and corresponding dynamics can be found in Marwan *et al.* (2007, pp. 248–251).

If meandering was associated with a dominant periodic motion, the recurrence plots should reveal a (quasi-)periodic typology. That is, the structure should be dominated by diagonal lines, yielding a chequerboard arrangement. This is clearly not the case in fig. 5.3 and does not manifest for the measurement planes lying in between either. For  $zc^{-1} \in \{4, 12, 20\}$  the structure smoothly transitions between the limits shown in fig. 5.3. This observation is consistent with the before said and provides further evidence that there does not exist *one* meandering frequency. It would seem that the phenomenon cannot be reduced to a monochromatic or even quasi-periodic motion.

At the first measurement station ( $zc^{-1} = 2$ ) the recurrence plot is characterized by a homogeneous typology and a texture of single isolated points. This indicates a strongly fluctuating motion as typically associated with a stationary uncorrelated random processes

<sup>5</sup>This is, by the way, one of the fundamental ideas underlying the dynamical-system approach to turbulence (Lanford, 1982, p. 347).

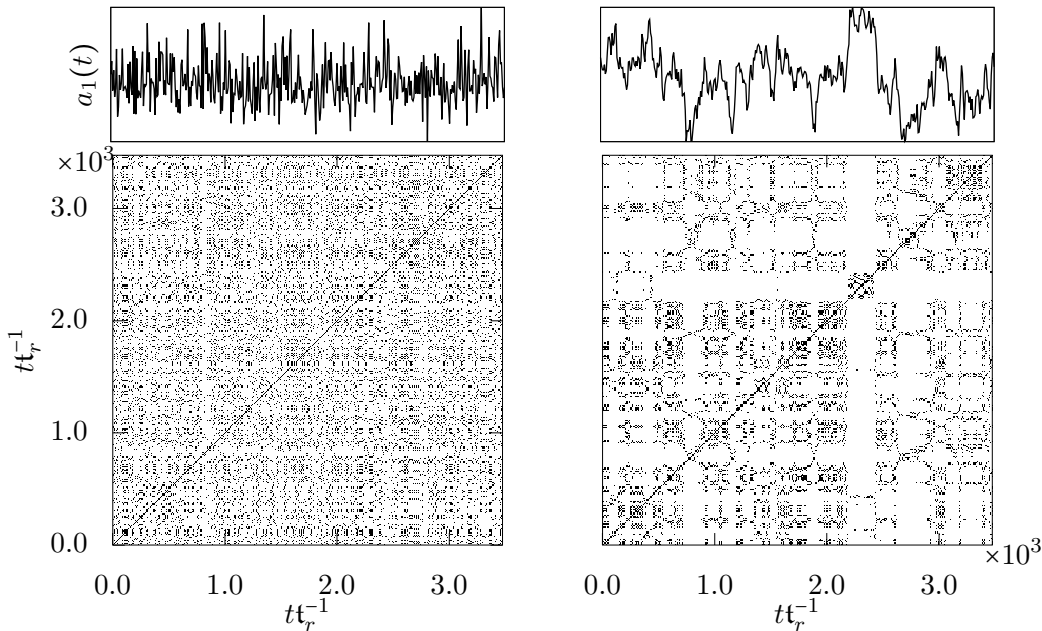


Figure 5.3: Time series (top row) and recurrence plots (bottom row) at  $zc^{-1} = 2$  (left column) and  $zc^{-1} = 26$  (right column). Radius  $\epsilon = 6 \times 10^{-2}$  and turnover time  $t_r = 2\pi r_1^2 \Gamma_1^{-1} \approx 4 \times 10^{-4}$  s (Jacquin *et al.*, 2007, pp. 4–5). (For the PIV measurements presented in appendix A.1.)

(noise). Dynamics without any recurrence are likely to be transient; that is, the initial condition was not yet in the attracting set and the motion continuous to settle (Kantz & Schreiber, 2004, p. 44). It is very probably that this dynamics does not yet correspond to vortex meandering as defined in sec. 2.3. Quite generally, we cannot speak of meandering before about  $zc^{-1} \approx 4$ ; the upstream dynamics is transient and has not yet relaxed to the ‘meandering attractor’.<sup>6</sup>

In agreement with all previous results, comparison of the recurrence plots and time series at the first and last measurement stations (i.e.  $zc^{-1} = 2, 26$ ) in fig. 5.3 suggests a gradual evolution towards increasing order. The disrupted typology visible at  $zc^{-1} = 26$  is indicative of non-stationary data (like Brownian motion) with abrupt changes between rare events. Texture in form of horizontal or vertical (white) bands implies that the state is trapped for some time and changes only slowly. This behaviour may indicate a laminar dynamics (Marwan *et al.*, 2007, table 1 on p. 251). It suggests that experimentally observed meandering *is* analogous to the phase-space meandering between different elementary solutions. This idea is very close to the suggestion of Hopf (1948).

### Quantification of organization and persistence: entropy

The notion of entropy<sup>7</sup> was coined by R. Clausius as a measure of irreversibility and disorder. For a closed thermodynamic system, the second law of thermodynamics states that the entropy cannot decay (Atkins, 1984, p. 78). In other words, the disorder or chaos in a closed system (without energy input from the outside) must inevitably increase (or stag-

<sup>6</sup>We emphasize that this conclusion by no means implies that the dynamics and wake–vortex interactions in the near field are of no importance for vortex meandering. It merely means that the very phenomenon does not yet exist as such.

<sup>7</sup>From the Greek εν, inside and τροπέ, reversal.

nate) and maximum disorder is attained when all degrees of freedom of the system under consideration have equal probability. This brings us naturally to the work of L. Boltzmann and W. Gibbs to whose legacy we owe the relation between (macroscopic) entropy and probabilities of the (microscopic) dynamics (see Truesdell, 1984, pp. 1–48 for details).

To the best of our knowledge, it was E. Schrödinger who first proposed the existence of distinguished (living) organisms which correspond to spatio-temporally confined regions of matter where entropy *decreases* (Schrödinger, 1992, pp. 70–74). A particularly striking formulation for this is due to N. Wiener (1988, p. 12) –

In Gibb’s universe order is least probable, chaos most probable. But while the universe as a whole, if indeed there is a whole universe, tends to run down, there are local enclaves whose direction seems opposed to that of the universe at large and in which there is a limited and temporary tendency for organization to increase. Life finds its home in some of these enclaves.<sup>8</sup>

The notion of entropy is by no means restricted to (classical) thermodynamics and statistical mechanics but straightforwardly extends to other subject matters (e.g. information theory; Shannon, 1948; Wiener, 1988 and biology; Schrödinger, 1992).

**Definition of the entropy.** In sec. 2.2, we identified the vortex with a definite state, namely the mean flow. Now, in a thermodynamic analogy, let us identify the mean flow (i.e. the vortex) with a heat bath (*Wärmebad*), i.e. a (practically) inexhaustible reservoir of energy. This identification is justified by the experimental evidence that the mean flow has several orders of magnitude larger kinetic energy than the perturbations (cf. fig. 6.4 and discussion). A sketch of this can be found in fig. 6.12.

The totality of all admissible perturbations define the system, which, in the present context, is an (infinite-dimensional) function space,  $L^2(M)$  for definiteness, called phase space.<sup>9</sup> ( $L^2(M)$  is separable; Riesz & Sz-Nagy, 1956.) Analogously to statistical mechanics, the system is characterized on the macroscopic level by its (*macro*) *state* (e.g. kinetic energy) which can always be associated with a certain point in the phase space, called *phase point* or *micro state* (Landau & Lifšic, 1980, p. 2). The symbolic or coordinate-free representation  $\mathbf{u}(t) \in L^2(M)$  is equivalent to an infinite-dimensional vector with components  $a_l(t) := (\mathbf{u}(t), \phi_l)_{L^2(M)}$  ( $l = 1, \dots, \infty$ ) with respect to a given basis  $\text{span}\{\phi_l\}_{l=1}^\infty = L^2(M)$  for all  $t$ . In a dissipative system, the number of dynamically active modes will always be finite, such that  $\mathbf{a}(t) \in \mathbb{R}^m$ , where  $m$  denotes the effective degrees of freedom (Swinney & Gollub, 1986, pp. 448–449; Foias *et al.*, 2001, pp. 115–123). All micro states which lay on the same energy surface (*Energieschale*) are macroscopically indistinguishable in the sense that they lead to the same macroscopic kinetic energy; the family of equivalent systems constitutes the canonic ensemble (*kanonisches Ensemble*).

---

<sup>8</sup>As regards the notion of life, Wiener (1988, p. 32) continues that

... the problem as to whether the machine is alive or not is, for our purpose, semantic and we are at liberty to answer it one way or another ... If we wish to use the word 'life' to cover all phenomena which locally swim upstream against the current of increasing entropy, we are at liberty to do so.

An abstract notion of 'life' can also be found in Dürr (2009, p. 141) –

Wir können auch sagen: Das Pendel wird an diesem Punkt »lebendig«. Es tritt in Kontakt mit dem Informationsfeld des Ganz-Einen.

(We can also say: the pendulum comes 'alive' at this point. It makes contact with the information field of the All-One.)

This idea of living bears the important aspect of communication between the considered element and all of the surrounding in the very perception of wholeness.

<sup>9</sup>This corresponds to the notion of a 'system' as defined by G. Nickel (Engel & Nagel, 2000, pp. 533–534).

We then chose the eigenvectors of the covariance operator<sup>10</sup>  $\{\phi_l\}_{l=1}^{\infty}$  as a basis of the system such that  $\mathbf{u}(t) = \sum_{l=1}^{\infty} a_l(t)\phi_l$  is a possible state. (Representing the distribution of the actual micro state over the various degrees of freedom in the statistical-mechanics analogy.) One and the same macroscopic energy of the system  $E(t) := \|\mathbf{u}(t)\|_{L^2(M)}^2$  can evidently result from an infinite combination of micro states  $\mathbf{a}(t) \in \mathbb{R}^{\infty}$  constituting the same energy surface. The energy of the  $l$ -th mode is  $E_l(t) := a_l^2(t) = \lambda_l(t)$  ( $\lambda_l$  is the eigenvalue belonging to  $\phi_l$ ) and the relative energy content becomes

$$(5.4) \quad p_l(t) := \frac{E_l(t)}{\sum_{k=1}^{\infty} E_k(t)} = \frac{\lambda_l(t)}{\sum_{k=1}^{\infty} \lambda_k(t)}.$$

Equation (5.4) serves as a measure for the probability to find the system in this particular micro state.<sup>11</sup> We then define the entropy by (Landau & Lifšic, 1980, p. 26)

$$(5.5) \quad H(t) := - \lim_{m \rightarrow \infty} \frac{1}{\log m} \sum_{l=1}^m p_l(t) \log p_l(t)$$

The entropy has been defined essentially identically by Aubry *et al.* (1991, pp. 701–702) and Sirovich (1991, p. 141).

**Downstream evolution of the entropy in the experiment.** Figure 5.4 shows the downstream evolution of the entropy (5.5) for two different systems. In the top panel, the mean flow (energy  $\lambda_0(t)$ , see sec. 6.2) is added to the system, while in the bottom panel the entropy is computed for the perturbations alone.

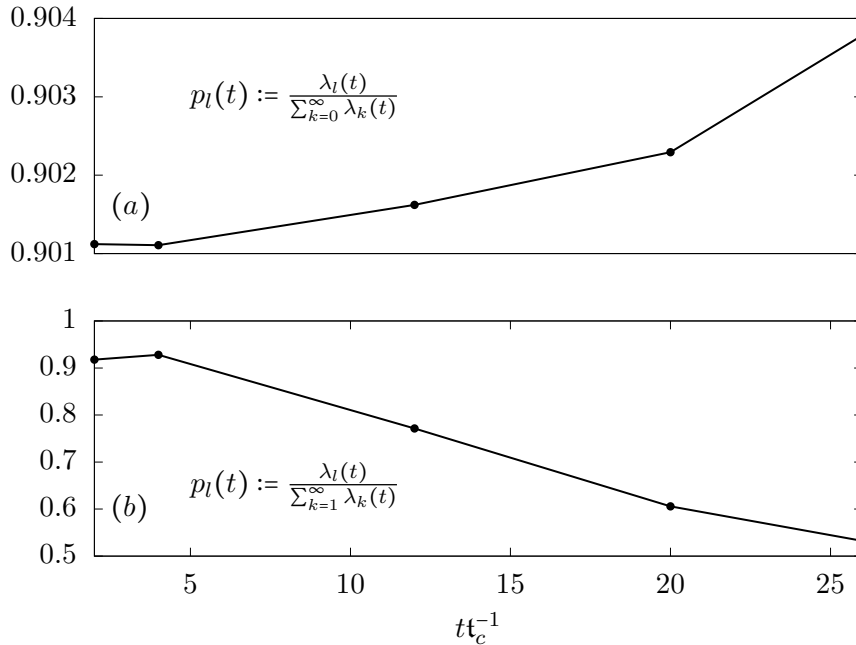


Figure 5.4: Downstream evolution of the entropy. (a) The system including the mean increases its entropy according to the second law of thermodynamics. (b) Identifying the system with the perturbation space, the entropy decreases downstream. (For the PIV measurements presented in appendix A.1.)

<sup>10</sup>Derived from POD, see sec. 6.2.

<sup>11</sup>That (5.4) indeed qualifies for a probability follows from the normalization to unity and additivity.

Including the mean flow, the system is closed and the entropy increases downstream according to the second law of thermodynamics. We recall that the state of maximum disorder corresponds to the equipartition of the energy over all degrees of freedom (POD modes here), while the maximum possible order is reached if all energy is concentrated in one single mode. It is readily verified that these two limits correspond to  $H = 1$  and  $H = 0$ , respectively.<sup>12</sup> Increasing entropy is consistent with the spreading of energy shown in fig. 6.3; while at the first measurement station practically all energy is contained in the mean flow, it gradually feeds into the perturbation space. This means that in the system including the mean flow, progressively more degrees of freedoms get involved and the system increases its disorder.

On the other hand, the bottom panel of fig. 5.4 shows that the entropy decreases when the system is identified with the perturbations alone. This is an open system which receives energy from the mean flow. Again, on the microscopic level, the observed increase in order conforms with fig. 6.3 in that initially all modes have approximately equal probability (i.e. energy) which progressively concentrates in the leading degrees of freedom (modes).

Since L. Boltzmann, entropy is regarded as a measure for disorder. However, the above discussion shows, that what entropy really quantifies here is the *dispersal* or *spread of energy* among the micro states (or modes). This interpretation was put forth, among others, by Atkins (1984, p. 78) and is related to the idea of information entropy (Shannon, 1948). The link to disorder is established by supposing that, as energy disperses, the number of dynamically active modes increases and, thus, the order decreases.

**Conclusion 5.1.1: The 'life' of vortices – return to order**

A vortex is an enclave of order (like a ship) embedded in a sea of disorder or chaos; the embedding free-stream or grid turbulence is highly complex and nonlinearity important. Meandering is the competition between external excitation and internal resistance ('steering of the ship'). There is no distinct meandering frequency, rather the dynamics alternate between different elementary solutions, being trapped in their neighbourhood for a while before being repelled.

## 5.2 An analogy between vortices and rotating turbulence

When is a piece of matter said to be alive? When it goes on 'doing something', moving, exchanging material with its environment, and so forth, and that for much longer period than we would expect an inanimate piece of matter to 'keep going' under similar circumstances.

— E: Schrödinger: What is Life?

The objective of this section is to provide evidence that vortices are associated with material fluid volumes (thus having no mass exchange with their surrounding) and that the core dynamics is two-dimensional turbulence. In this regard, we ask – *How closed are vortices to the transport of physical observables (mass, momentum and energy)?*

<sup>12</sup>Uniform probability of all  $m$  degrees of freedom,  $p_l = m^{-1}$  for all  $l$  yields  $H = -\frac{1}{\log m} \sum_{l=1}^m \frac{1}{m} \log \frac{1}{m} = \frac{1}{\log m} \frac{1}{m} \log m \sum_{l=1}^m 1 = 1$ . One degree of freedom is a sure event,  $p_1 = 1$  and  $p_l = 0$  for  $l > 1$  yields  $H = -\frac{1}{\log m} 1 \log 1 = 0$ .

### 5.2.1 Entrainment and persistence: is there fluid exchange with the free stream?

In contrast to other free shear flows, turbulent vortices decay at a nearly viscous rate (i.e. Lamb–Oseen-like,  $r_0(t) \sim \sqrt{\nu t}$ ), resulting in remarkably long persistence (Lingevitch & Bernoff, 1995, p. 1015; Cotel, 2002, p. 2933; Pradeep & Hussain, 2010; Van Jaarsveld *et al.*, 2011, p. 223). Jacquin & Pantano (2002, p. 160) suggest two possible mechanisms for persistence, namely either (i) a rapid laminarisation principle in the core effectively preventing turbulence to exist inside a vortex or (ii), given turbulence inside the vortex to exist, some kind of a shielding or protecting mechanism that prevents momentum transport across the lateral border and hence entrainment of the surrounding flow. Thus,

the main mechanism that must be accounted for to understand turbulence in a vortex is the coupling between rotation and shear.

Perturbation dynamics in rotating flow shows some striking similarity to the propagation of gravity waves in a stably stratified fluid. Along vortices, the equivalent dynamics consists of the propagation of Kelvin waves (dispersive inertia waves) (Jacquin *et al.*, 2003, p. 580). The ability of wave transport is a common intrinsic property of various vortices (Wu *et al.*, 2006, p. 406). These core waves can be intense without having appreciable Reynolds stress which would be required for faster than laminar decay (Hussain *et al.*, 2011, p. 309). (Typical turbulence models impinge the Reynolds-stress tensor to molecular diffusion, attributing it a principal effect of fluid mixing.) The fluctuation-energy equation shows that attenuation via the production term is possible depending on the alignment of the Reynolds stress with the mean-velocity gradient (Bölle *et al.*, 2020).

Takahashi *et al.* (2005) state that *no external turbulence can penetrate the core* directly but is effectively blocked due to the strong rotational motion of the vortex. The numerical studies of Jacquin & Pantano (2002, p. 162) indicate that short-wave perturbations to the Batchelor vortex lead to the formation of a dispersion buffer surrounding the core ( $q$  dependence). Inside the dispersion buffer perturbations are transformed into non-amplified propagating waves hardly interacting with the base flow. Any disturbance present in the core must traverse this region before it can diffuse, suggesting that the dispersion buffer is responsible for the confinement of turbulence in the core (Jacquin & Pantano, 2002, p. 163). This ‘dynamical barrier’ due to differential rotation is believed to govern the core contamination in the jet–vortex experiments of Jacquin *et al.* (2007, p. 5 and fig. 4; p. 9 and fig. 8). Depending on the spacing between jet and wing tip, either no penetration of the jet plume into the core at all or immediate entrainment and conservation of the contaminant in core (for the closest spacing) are observed (see also p. 38).

On the other hand, Bandyopadhyay *et al.* (1991, p. 1633) state that ‘the vortex core is not a benign solid body of rotation but has a dynamic nature’, intermittently exchanging momentum (ejection of fluid packets) with the outer region (this seems to be observed in the experiments of Beresh *et al.*, 2010). This exchange of momentum, vorticity and energy between the core and the free stream is governed by azimuthally aligned filaments (of opposite polarization) wrapped around the vortex core. By the Biot–Savart law each filament pair contributes a radial velocity, causing entrainment and scalar mixing across the lateral vortex boundary (Melander & Hussain, 1993a, p. 2684). Due to conservation of linear momentum, intermittent ejection of fluid patches causes the remainder of the core to bend in the opposite direction, resulting in the observed wave-like character (Green, 1995, p. 445). Due to strong rotational motion, turbulent patches absorbed in the core region are partially relaminarised. Some further discussion in this respect can be found on p. 75.

**Vortices are associated with entrainment barriers.** Exchange of fluid between the vortex and the surrounding free stream, either by entrainment or ejection, is a matter of radial transport across the vortex boundary. Generally, the ability of significant radial momentum transport in the core is an inevitable requirement for faster than laminar decay by viscous diffusion. To approach this question, Bradshaw (1969) devised an analogy between flows with curved streamlines and stratification. The central parameter of Bradshaw’s analogy is the Richardson number,<sup>13</sup> representing the local strength of an analogous stratification in rotating flow (see also Cotel, 2002, p. 2933). Cotel & Breidenthal (1999, p. 3026) suggest that in stratified turbulence the transport of mass, momentum and energy across a thin interface depends on the four parameters, Richardson, Reynolds, Schmidt or Prandtl and persistence number. However, streamlines are not Galilean invariant which renders these approaches subjective to the particular observer with respect to elementary symmetry groups of physics.

Respecting Galilean invariance, Provenzale (1999, p. 55) resumes that ‘vortices induce regular Lagrangian motion inside their cores and are highly impermeable to inward and outward particle fluxes’ (see also Haller *et al.*, 2016, p. 137 for further discussion). It appears that rotation imposes powerful barriers to radial transport of mass and momentum, thus separating significantly different Lagrangian behaviour inside the vortex from that in the external field (Provenzale, 1999, p. 67).

Since vortices exchange little fluid with their surrounding, it is proposed here to model the vortex boundary by an impenetrable but flexible wall. This is shown schematically in fig. 5.5, where, *ad hoc*, we assume the boundary to be (roughly) at the support radius  $r_2$ . The vortex then corresponds to a flexible material cylinder or tube containing practically all vorticity and inside which the motion is dominated by rotation.<sup>14</sup>

### 5.2.2 Transition from three- to two-dimensional dynamics: a different view on the wake evolution

Turbulence evolution in a rotating rigid cylinder has been studied experimentally by Hopfinger *et al.* (1982), Maxworthy *et al.* (1985) and Hopfinger & Van Heijst (1993).

**The mean Rossby number.** A strong rotational motion is known to have a stabilizing effect on the dynamics in many circumstances. As such, rotation tends to organize the motion, driving the dynamics towards an equilibrium state. In that, it counteracts fluctuation (and therewith turbulence) growth, hence rotation promotes relaminarisation – the return to order. Thus, the observations of turbulent vortex cores at short downstream distances seems not to be inconsistent with a laminar core dynamics further downstream (cf. sec. 6.1) as a consequence of the rotation-induced inherent relaminarisation property of the vortex core. The non-dimensional group associated with rotation in the Navier–Stokes equations is the Rossby number and is defined as the ratio of the rotation to the advection time scale. We thus define

$$(5.6) \quad \text{Ro}_\delta := \frac{t_r}{t_\delta} = \frac{|\delta U_z|}{2r_0\Omega_0} \approx 0.32 \frac{|\delta U_z|}{U_{\theta,1}} = \frac{1}{2q}$$

as the reciprocal of the swirl number  $q$  (up to a constant factor) (Wu *et al.*, 2006, p. 647, Alekseenko *et al.*, 2007, p. 168; Lesieur, 2008, p. 48).

<sup>13</sup>As noticed by Holzäpfel *et al.* (2002, p. 298) and Cotel (2002, p. 2933), the original definition of the Richardson number by Bradshaw (1969, p. 179) is erroneous since it relies on different frames of reference.

<sup>14</sup>The idea of defining vortices as rotation-dominated fluid volumes in a flow underlies various identification criteria (Truesdell, 1954, p. 107; Okubo, 1970; Weiss, 1991, p. 275; Hunt *et al.*, 1988, p. 196; Jeong & Hussain, 1995).

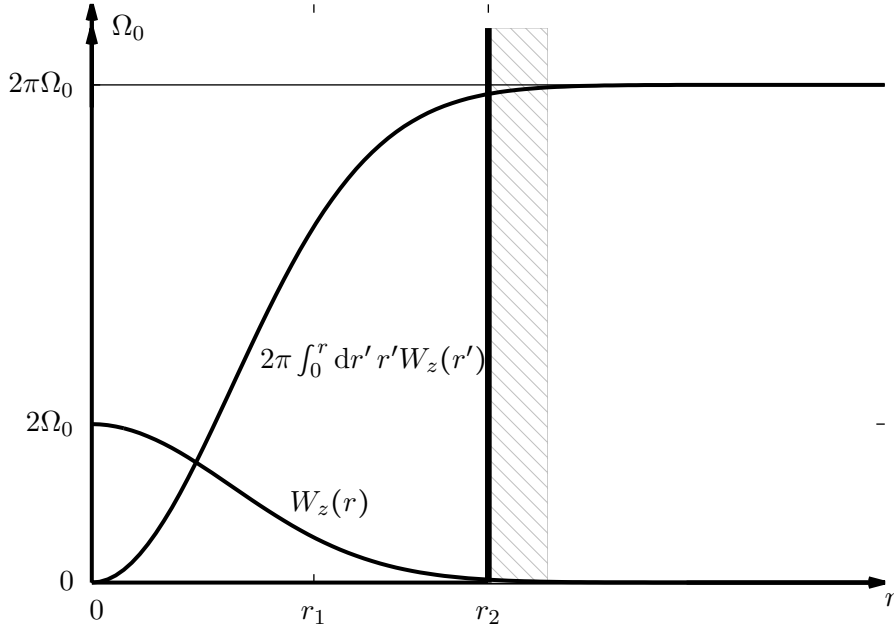


Figure 5.5: Vorticity profile of the Lamb–Ossen vortex  $W_z(r)$  and the vorticity integral  $\Gamma(r)$  reaching the asymptotic value at approximately  $r_2$ . The equivalent fluid container delimited by  $r_2$  modelled as an impenetrable wall and the angular velocity  $\Omega_0$  on the vortex axis.

Equation (5.6) differs slightly from the definition of Bandyopadhyay *et al.* (1991, p. 1630) and Devenport *et al.* (1996, p. 92). The latter study reports  $|\delta U_z|U_{\theta,1}^{-1} \approx 0.5$  (this value also follows from (2.14)) which corresponds to  $\text{Ro}_\delta \approx 0.15$ . (The dynamics is rotation dominated if  $\text{Ro} \ll 1$ .) Bandyopadhyay *et al.* (1991, p. 1631) conclude that the essential parameter governing the turbulence structures is the Rossby rather than the Reynolds number, while Green (1995, p. 445) states that both effects are significant.

The Rossby number (5.6) characterizes linear stability of the (Batchelor) vortex. From fig. 3.1, we can see that the dynamics indeed typically stabilizes downstream. However, this seems not to be the most relevant, since  $\text{Ro}_\delta(z)$  remains almost always in the parameter range of linear stability. The essential conclusion to be drawn from fig. 3.1 then is that conventional trailing-vortex experiments are unaffected by linear instabilities of the isolated vortex (as already concluded in sec. 3.2).

**The transition Rossby number.** In order to characterize the transition from three-dimensional, turbulence-like to two-dimensional, rotation-dominated dynamics, we define the (transition) Rossby number

$$(5.7) \quad \text{Ro}_t(z) := \frac{\mathbf{u}_z(z)}{2\Omega_0 \mathbf{l}(z)}$$

analogously to Hopfinger *et al.* (1982, p. 512). Herein,  $\mathbf{u}_z(z)$  is the root-mean-square velocity in the mean vortex-centre location and  $\mathbf{l}(z)$  denotes some representative perturbation length scale, which we assume to have the same dependence on  $z$  as the core radius, viz.  $\mathbf{l}(z) \sim z^{1/2}$ . Since  $\Omega_0 \sim \Gamma_\infty$  is approximately constant, the principal behaviour of (5.7) is reflected by  $\text{Ro}_t(z) \sim \mathbf{u}_z(z)z^{-1/2}$ , shown in fig. 5.6. Superposed in fig. 5.6 is the  $\sim z^{-1}$ -decay that applies close to the grid in rotating-turbulence experiments (Hopfinger *et al.*, 1982, p. 515). We can see that the Rossby-number decay in the present experiment in the near

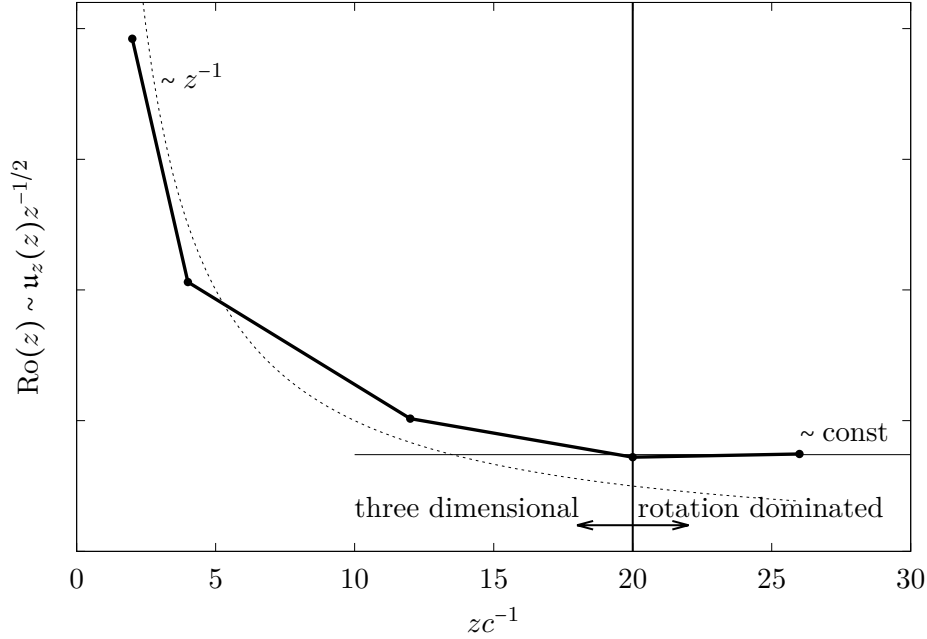


Figure 5.6: Transition Rossby number as a function of  $z$  assuming  $l(z) \sim z^{1/2}$  for the integral scale of the vortex dynamics. Comparison with a  $z^{-1}$ -decay close to the wing and a constant asymptotic which determines the transition to rotation-dominated dynamics (Hopfinger *et al.*, 1982, p. 515). (For the PIV measurements presented in appendix A.1.)

wake follows a similar law. At about 20 chord lengths, the Rossby number settles to a constant value which is indicative of rotation-dominated dynamics beyond this point. The corresponding  $z$ -position is called the transition distance (Hopfinger *et al.*, 1982, p. 515).

The decay of the streamwise component of the rms velocity in the mean vortex centre is also observed in Green & Acosta (1991, pp. 122, 123), Jacquin *et al.* (2001, fig. 10) and Beninati & Marshall (2005, figs. 7, 9). This tendency is consistent with the idea of downstream laminarisation (cf. also sec. 6.1).

**Comparison with the features of rotating turbulence.** Hopfinger *et al.* (1982, p. 511) observe that, as the background rotation rate  $\Omega_0$  is decreased, the mean flow substantially deviates from a rigid-body rotation (which holds for the fastest rotation rate) and the mean vorticity progressively drifts towards the centre.<sup>15</sup> This can be observed in fig. 2.3 which suggests that, with respect to Hopfinger *et al.*'s definition of the Rossby number, trailing vortices should be comparably slowly rotating cylinders.

As a key feature, rotating turbulence tends to locally accumulate vorticity in elongated structures roughly aligned with the rotation axis (Hopfinger *et al.*, 1982, pp. 506, 516–517; Maxworthy *et al.*, 1985, pp. 141, 147). If the background rotation rate  $\Omega_0$  is decreased for otherwise unchanged conditions, some of the vorticity concentrations become retrograde (counter-rotating in the co-rotating frame), the total number of vortices decreases while their size increases. The strength of the local vorticity accumulations typically exceeds the background vorticity (Hopfinger *et al.*, 1982, p. 510). In a formal analogy, we propose to associate the vortex mean flow (fig. 2.3) with Hopfinger *et al.*'s background vorticity and the leading POD mode (figs. 6.6–6.7) with their vorticity concentrations. In this

<sup>15</sup>Disregarding vorticity concentration at the tank wall, an extrapolation of the mean vorticity profile in Hopfinger *et al.* (1982, fig. 5,  $Ro_g = 33.2$ ) is compatible with the Lamb–Oseen vortex shown in fig. 5.5 when the tank radius is identified with  $r_2$ .

analogy, trailing vortices correspond to the slowly-rotating limit, where only a dipole pair of vorticity concentrations emerges whose magnitude exceeds the mean flow, which deviates substantially from a rigid-body rotation. The gradual (in  $z$ ) emergence of strong elongated vortex filaments in the vortex (viz. the leading perturbation modes) becomes evident in the instantaneous vorticity snapshots shown in fig. 6.8 (as compared to the instantaneous streamlines of Hopfinger *et al.*, 1982).

The above discussion suggests that the vortex-support radius  $r_2$  is a characteristic length scale of vortex dynamics. Indeed, fig. 5.7b shows that the (normalized) power spectra taken from various experiments match fairly well when normalized with  $r_2$ . This is clearly not the case when normalized with the chord length  $c$  (fig. 5.7a).

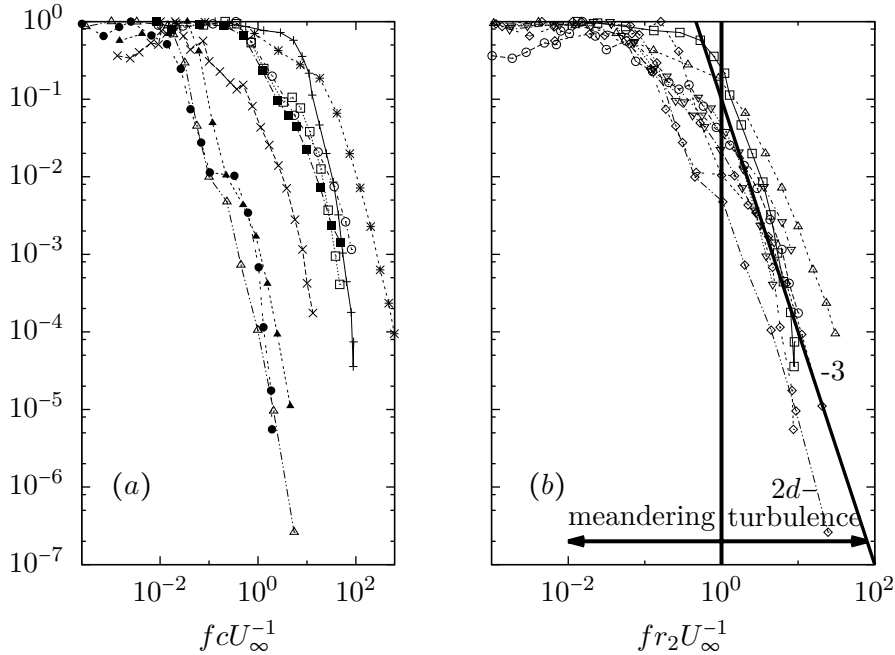


Figure 5.7: Rescaled (to unity) power spectral densities. (a) Chord length  $c$  as length scale. (b) Support radius  $r_2$  as length scale. The proposed meandering and core regimes are indicated as well as the  $-3$  power-law in the inertial range. Experiments are detailed in appendix A.4.

**Triple decomposition of the meandering motion.** Meandering (i.e. the vortex displacement as a whole) is associated only with the low frequencies. The high frequencies constitute core turbulence unable to displace the vortex ('local fluctuations'). Due to strong rotation, the core turbulence is (or becomes) two dimensional, thus favours the generation of vorticity (dipole) concentration. This is a triple decomposition  $\mathbf{X}(t) = \langle \mathbf{X}(t) \rangle + \mathbf{X}_m(t) + \mathbf{X}_{2d}(t)$  of the vortex centreline. This decomposition has conceptual similarity with the triple decomposition of the velocity field (proposed by Reynolds & Hussain, 1972; Hussain, 1986, appendix A) and has been applied to the analysis of vortex meandering by Bailey & Tavoularis (2008, p. 311), who propose to decompose vortex meandering into a *deterministic* and a *random* contribution due to the surrounding turbulence and associated with the wind-tunnel geometry, respectively. The latter since they found the characteristic meandering wavelength being of the same order as the half-wing aspect ratio and the gap between tip and opposite wall. This seems not to be generally true. A velocity triple decomposition is also employed to identify the coherent meandering motion by Edstrand *et al.* (2016, p. 4). In this approach, the mean flow is perturbed by a

coherent meandering motion and random fluctuations which are, by definition, free from meandering.

**Energy condensation in two-dimensional turbulence.** The emergence of local vorticity concentrations is not only characteristic of rotating turbulence but also fundamental for two-dimensional turbulence (Hopfinger & Van Heijst, 1993, p. 241). Kraichnan (1967) conjectured that two-dimensional turbulence in a closed container without large-scale dissipation tends to concentrate energy and enstrophy at the integral scale (the container size,  $r_2$  here), analogously to a Bose–Einstein condensate (see also Kraichnan & Montgomery, 1980; Hossain *et al.*, 1983; Boffetta & Ecke, 2012). The resulting perturbation pattern is that of a vorticity dipole (Boffetta & Ecke, 2012, pp. 440–441).

**Conjecture 5.2** (Meandering scenario). *A vortex is a flexible, material fluid tube inside which the motion is dominated by rotation. This configuration inherently favours the emergence of elongated vorticity concentrations and convergence towards two-dimensionality. Two-dimensional turbulence condenses energy at the integral scale, viz.  $\sim r_2$ . The formation of the leading dipole perturbation pattern is thence intrinsic and the deformation follows from the fact that the vortex tube is flexible.*



## 6 | Third mechanism: energy amplification via mother–daughter interplay

Die stillsten Worte sind es, welche den Sturm bringen. Gedanken, die mit Taubenfüßen kommen, lenken die Welt.

---

— F. Nietzsche: Also sprach Zarathustra

The previous chapter 5 (and the discussion in sec. 2.2) suggest that vortices are distinct material entities of the fluid domain. At the same time, they remain a part of the whole and their evolution is governed by the mutual 'communication' with the surrounding free stream. The 'tension' between the part and the whole is a fundamental aspect of ancient Greek philosophy<sup>1</sup> (Heisenberg, 1959, p. 91) and profoundly influences science ever since (Heisenberg, 1969; Bohm, 1980). Indeed, in chap. 3, we concluded that vortex meandering probably results from an intricate combination of intrinsic and extrinsic dynamics.

The objective of this chapter is in the detailed characterization and modelling of the third meandering pillar elucidated at the end of chap. 2 – the progressive energy concentration in the core. For this purpose, the present chapter is organized in three parts. First, we review some fundamental properties of vortex–turbulence interaction in sec. 6.1, which are augmented by a detailed analysis of the energy evolution in the experiments presented in appendix A.1 in sec. 6.2. As already anticipated, we propose to model the meandering dynamics in terms of a generalized receptivity, which we discuss in sec. 6.3. The proposed model is essentially similar to the mother–daughter mechanism of Boberg & Brosa (1988). An important aspect of this model is that it puts the emphasis on form rather than magnitude and information transfer rather than physical penetration. This idea of a high-energetic large-scale organism being directed by a low-energetic small-scale influence of a highly subtle nature is beautifully expressed in the introducing quotation of F. Nietzsche.

### 6.1 Vortex–turbulence interaction

That the exchange of material should be the essential thing is absurde.

---

— E: Schrödinger: What is Life?

Although there is considerable acceptance among researchers that meandering is some sort of a passive core buffeting, Bailey *et al.* (2018, pp. 723, 724) state that the (precise)

---

<sup>1</sup>The cradle of modern Western culture and thinking (Schrödinger, 1996).

link between meandering and free-stream turbulence has not been established yet. It is true that very few studies go beyond this qualitative statement. In particular, there seems to be no agreement whether meandering persists in the absence of any free-stream turbulence.

**Is vortex dynamics generic? The notions of a vortex vs eddy.** ‘Well-organized, elongated vortices (coherent structures) commonly occur in turbulent flows and dominate phenomena of technological interest, such as entrainment, mixing, drag, and aerodynamic sound’ (Pradeep & Hussain, 2006, p. 251). Vortices might be conceived as the organizing cells embedded into the surrounding fluid flow, having the power to organize and determine. This perception is generic, ‘the turbulence evolution in the vicinity of a relatively large-scale vortex structure is a ubiquitous problem affecting most high-Reynolds number flows at some scale’ (Beninati & Marshall, 2005, p. 244). This is essentially the same idea as put forth in the self-similar cascade argument of Melander & Hussain (1993a, fig. 19).

Beyond uni-directional organization, ‘many flow problems involve the *interaction* of one (a few) prominent large scale coherent structures with small scale turbulence; trailing-vortex wake is a prominent example. These problems are still today not understood’ (Hussain *et al.*, 2011, p. 304). On the other hand, Jacquin (2005, p. 397) stresses the fact that there are important differences between ‘eddies’ in turbulent flow and ‘trailing vortices’, notably, short vs long lifetime and the existence of an energy cascade vs the concentration of energy. Indeed, Jacquin (2005, p. 397) claims that ‘the concentration of the vertical momentum behind a wing into big and weakly interacting vortices is the opposite of a turbulent process’.

### 6.1.1 The distinct characteristics of vortex and free-stream dynamics

Globally, wing wakes are characterized by the rapid decay of in-coherent background turbulence due to viscous diffusion concomitantly with the persistence of coherent vorticity (Melander & Hussain, 1993a, p. 2673). This rapid wake-turbulence decay as opposed to maintained core unsteadiness led Singh & Uberoi (1976, fig. 6) to conclude that wake and vortex are not associated. The dynamics inside the vortex is characterized by high vorticity and low momentum, while outside the vortex dynamics is highly turbulent with only very low vorticity. Apparently, vortex-dominated flow has the tendency to separate dynamic regimes into spatially disjoint regions of the fluid domain.<sup>2</sup> We shall contrast the (universal) characteristics in the free stream and vortex core below.

**The typical evolution of wake turbulence outside the vortex.** Turbulence in the wake can be separated into an ambient and an aircraft-induced contribution. Whereas the former can, in principle, be formally absent (e.g. perfectly quiescent atmosphere), the latter constitutes the lower turbulence bound always present due to boundary-layer separation and mounted devices, inevitable, at the typically high Reynolds numbers (Gerz *et al.*, 2002, p. 190).

The fluid flow outside the core is dominated by the remainder of the wing wake which rolls up into an ever increasing spiral pattern. The wake spiral ‘simply’ decays downstream and there seems to be no large region of axisymmetric or vortex-rotation-generated and sustained turbulence around the core (Devenport *et al.*, 1996, abstract and figs. 7, 8*d, e* on pp. 87–88). This free-stream organization is generic in the sense that initially random, isotropic, homogeneous, solenoidal fine-scale turbulence adjusts to the presence of a laminar vortex column embedded within few rotations (Melander & Hussain, 1993a, p. 2671).

---

<sup>2</sup>We note that this intrinsic separation associated with vortices extends to Lagrangian aspects as discussed e.g. in sec. 2.2 and has implications on the modelling of the dynamics in sec. 6.3.

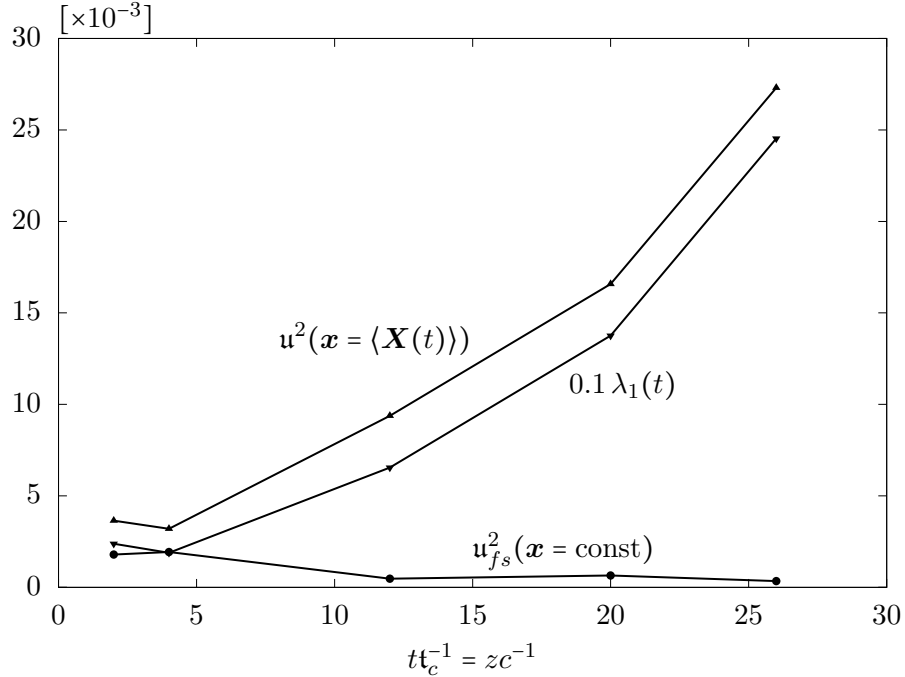


Figure 6.1: Downstream growth of the kinetic energy on the instantaneous mean centreline  $u^2(\langle \mathbf{X}(t) \rangle)$  and of the integral kinetic energy associated with the first POD mode  $\lambda_1(t)$  (scaled by a factor of  $10^{-1}$ ) as compared to almost stationary turbulence intensity  $u_{fs}^2$  at an arbitrary fixed point in the vortex periphery. All quantities are normalized with  $U_\infty^2$ . (For the PIV measurements presented in appendix A.1.)

In any case, we assume that the free stream is characterized by only one representative velocity scale  $u_{fs}$  called turbulence intensity (if unambiguous, we drop the subscript).

In general, experiments are conducted with a uniform background flow in an essentially unbounded fluid domain (i.e. the walls are far away). In this case, the velocity gradient vanishes such that there is no production of turbulent kinetic energy. While redistribution of energy between different parts of the fluid domain remains possible, the integral free-stream turbulence in the whole fluid domain must decay monotonously. The downstream evolution of grid turbulence (of characteristic grid scale  $M$ ) is characterized by a decrease in intensity and increase in integral length scale (Batchelor, 1953; Rotta, 1972, pp. 107–112; Tennekes & Lumley, 1973, pp. 71–73; Pope, 2000, pp. 158–160). Experiments of vortex–turbulence interaction report power-law behaviour according to

$$(6.1) \quad u_{fs}^2(z) \sim \left(\frac{z}{M}\right)^{-1.3} \quad \text{and} \quad l_{fs}(z) \sim \left(\frac{z}{M}\right)^{0.4}.$$

These laws are confirmed in the experiments of Sarpkaya & Daly (1987, p. 400), Bailey *et al.* (2006), Bailey & Tavoularis (2008, pp. 288–289) and Van Jaarsveld *et al.* (2011, fig. 3). The turbulent kinetic energy in the free stream is approximately independent of the grid details beyond  $10M$  (Rotta, 1972, p. 110; Beninati & Marshall, 2005, p. 248). If no grids are installed the turbulence intensity is nearly stationary.

The integral-energy decay of the core-surrounding spiral becomes obvious from the leading POD modes, revealing gradual diminishing structure within  $zc^{-1} = 0.1 \dots 4$  (Del Pino *et al.*, 2011, figs. 16, 17; Edstrand *et al.*, 2016, fig. 4).

Figure 6.1 shows the downstream evolution of the turbulence intensity  $u_{fs}U_\infty^{-1}$  at an arbitrary but fixed point in the vortex periphery of the PIV measurements presented in

appendix A.1. As the wake spiral dissipates, the turbulence intensity settles to an almost constant value of about  $u_{fs}U_\infty^{-1} \approx 3\%$ .

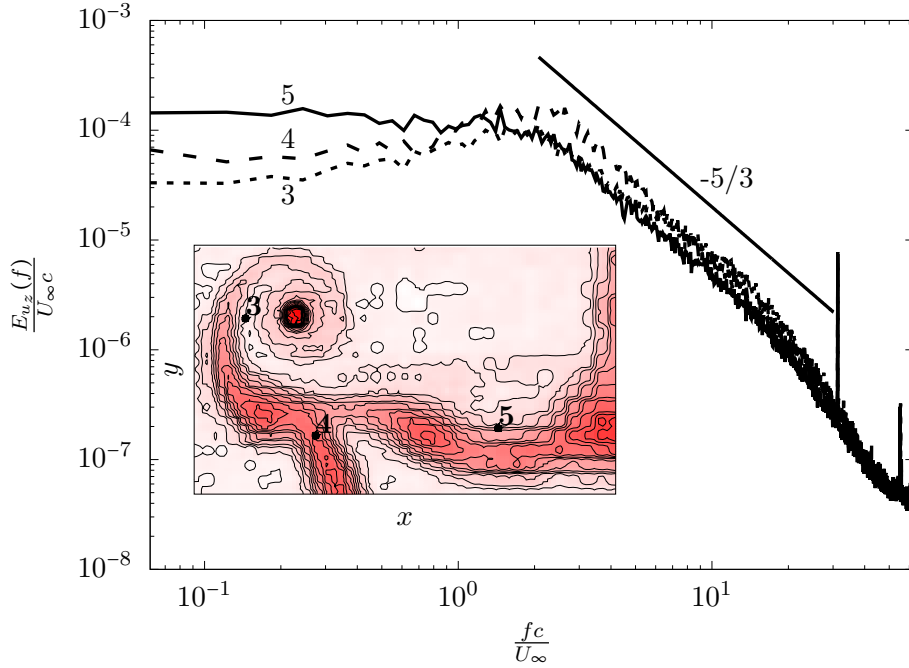


Figure 6.2: Power spectral densities at  $zb^{-1} = 3$  obtained from hot-wire measurements at the points indicated in the inset (LDV of the axial velocity component); cf. appendix A.1.

**The typical evolution of vortex-core unsteadiness.** Trailing vortices support core-velocity fluctuations until far downstream. The root-mean square velocity  $\mathbf{u}(t, \mathbf{x})$  (or turbulent kinetic energy) peaks on the mean centreline and remains at a nearly constant level after an initial decay irrespective of the free-stream-turbulence intensity (Beninati & Marshall, 2005, pp. 250, 252). This decay behaviour is the characteristic signature of meandering but not fully-developed equilibrium turbulence (Jacquin *et al.*, 2001, p. 11 and fig. 10).

Despite the concentration of fluctuation kinetic energy in the core, there seems to be no consensus as of this writing whether the dynamics in the vortex core is laminar or turbulent. Turbulence entrainment in the core during roll up of the turbulent boundary layer of the wing (Chow *et al.*, 1997 as referred to by Devenport *et al.*, 1996, p. 68; Spalart, 1998 as cited by Bailey & Tavoularis, 2008, p. 282; Beninati & Marshall, 2005, p. 255) is the only inevitable source of turbulence in (trailing) vortices. For certain configurations, turbulence development inside the vortex via some instability mechanism might be an additional potential sources (Jacquin & Pantano, 2002, p. 160). However, whereas turbulent core dynamics may be conceivable in the near wake, Corsiglia *et al.* (1973, p. 754) find a laminar-like appearance in the vortex core beyond  $zc^{-1} \gtrsim 48$ . Already at  $zc^{-1} = 22.9$ , Heyes *et al.* (2004, p. 6) observe a laminar vortex core with all unsteadiness being entirely associated with vortex meandering. Laminar core flow is also suggested by the numerical simulations (Ragab & Sreedhar, 1995; Zeman, 1995; see also Devenport *et al.*, 1996, p. 69).

The fact that the characteristic core length scale increases at a nearly viscous rate while the maximum mean azimuthal velocity decays at a similar rate (in the co-meandering frame) is typically taken as evidence for the core dynamics being laminar, whereas core turbulence is insignificant (Rokhsaz *et al.*, 2000, p. 1026; Van Jaarsveld *et al.*, 2011, pp. 223,

233). According to Birch (2012, p. 1) there is ‘compelling evidence that turbulence [in the core] plays only a passive role in vortex development’.

While the question of whether the core dynamics is laminar or turbulent can perhaps not be answered (because it is probably ill-posed), we have considerable experimental evidence that the core dynamics is relaminarising downstream. This characterization of vortex dynamics in terms of trends rather than hard facts is consistent with the conclusions drawn in sec. 2.4 and the particular tendency of trailing-vortex dynamics to increase its orderliness (discussed in chap. 5). The experiments of Singh & Uberoi (1976, p. 1858) confirm that initial turbulence in the vortex core decays downstream, however seemingly periodic disturbances of axisymmetric and helical type persist in the extended near field ( $zc^{-1} = 13 \dots 40$ ). Farther downstream the vortex core motion loses periodicity again, passing to a chaotic state. In the far field, Singh & Uberoi (1976, p. 1862) observe large spatial excursions of the vortex core with the fluctuation kinetic energy being essentially concentrated at the vortex axis admitting a broad peak. Experiments and simulation indicate that small-scale turbulence has little effect on the evolution of an isolated vortex which, at least in the far field, always evolves as if the dynamics was laminar. Linear instability is at best transient, or in other words ‘isolated axisymmetric vortices, far from their source, are laminar’ (Jacquin *et al.*, 2001, p. 15). In fig. 6.9, we see that the velocity fluctuations are essentially concentrated in the core, while at the same time diffusion at an almost viscous rate suggests progressive downstream relaminarisation of the core dynamics. The common conclusion drawn from this concomitancy is that the vortex core cannot be a region of turbulence activity or production but rather velocity fluctuations are a manifestation of a passive motion (Devenport *et al.*, 1996, p. 69) – the meandering motion.

Scaling of the core-velocity fluctuations on the wake (rather than core) parameters (at  $zc^{-1} = 10$ ) is considered as evidence for laminar core dynamics without turbulence production by Devenport *et al.* (1996, p. 96). Consequently, all velocity fluctuations in the core must inevitably be inactive passive motions due to buffeting by the surrounding wake turbulence. Most of the turbulence in the core (as detected in the laboratory frame) is an artefact of meandering associated with fictitious Reynolds stresses. After transformation to a co-meandering frame of reference, they can effectively be removed, in stark difference to the wake turbulence which is unaffected by the transformation (Heyes *et al.*, 2004, p. 8; Beresh *et al.*, 2010, p. 606). This corresponds essentially to a laminar vortex surrounded by turbulence, subjected to intermittent interaction and rotation-induced stabilization in the core (Beresh *et al.*, 2010, p. 606).

### 6.1.2 Bi-directional vortex–turbulence coupling

There are major differences between turbulent trailing vortices and other shear flows: contrary to the uni-directional energy cascade in classical turbulence theory, there is considerable evidence for significant interaction in both directions causing *momentum and energy transport* between large-scale coherent structures and fine-scale turbulence (Jacquin, 2005, p. 397). This bi-directional dynamical coupling might be true of all ‘coherent structures’ generating sufficiently strong local shear (Melander & Hussain, 1993a, pp. 2669, 2675).

**The different vortex–turbulence interaction regimes.** ‘Single vortices have a very long lifetime except when embedded in strong ambient turbulence’ (Gerz *et al.*, 2002, p. 195). Depending on the external turbulence intensity vortices are observed to axisymmetrise ceasing to be turbulent, develop bending waves sustaining azimuthally wound secondary fluctuation modes or disappear altogether (Melander & Hussain, 1993a, p. 2681). This finding conforms with the simulations of Marshall (1997) who investigates the dynamics of periodic vortex rings around a columnar vortex, finding standing waves and vorticity

stripping for weak and strong external turbulence, respectively (Beninati & Marshall, 2005, p. 245 and idem in Marshall & Beninati, 2005; Holzäpfel *et al.*, 2003).

**The typical vortex-induced organization of the free stream.** The wrapping and near-azimuthal alignment of elongated, cylindrical, ribbon-like vorticity modes around the core is a typical feature of vortex–turbulence interaction (Van Jaarsveld *et al.*, 2011, p. 233). From their characteristic shape, these free-stream modes are also referred to as filaments, threads (Melander & Hussain, 1993a) or worms (Jiménez *et al.*, 1993). Typical here means that the emergence of these patterns is observed for various configurations, namely in the roll up of experimental trailing vortices and numerical vortex–turbulence interaction studies. In the latter, this pattern emerges irrespective of the chosen initial turbulence structure (including white noise) and even without spectral separation to the vortex, provided it persists (Melander & Hussain, 1993a, p. 2671). It can be thought that these characteristics principally extend to general ‘coherent structures’ which tend to organize the surrounding fluid, increasing anisotropy at all scales in their vicinity and bi-directional interaction (Melander & Hussain, 1993a, p. 2685; Melander & Hussain, 1994, p. 34). Numerical experiments indicate that the filaments are stacked along the vortex core with alternating polarization (Melander & Hussain, 1993a, p. 2676).<sup>3</sup>

The observed organization is due to the vortex-induced shear and hence of effectively finite extent, prescribing geometrical constraints similar to two-dimensional vorticity dynamics and turbulence (Melander & Hussain, 1993a, pp. 2674, 2687). The short-reach impact is reflected in the jet–vortex interaction experiments of Jacquin *et al.* (2007, p. 9) who find faster wrapping of the jet around the core the closer the jet is to the wing tip. Characteristic aspects of the free-stream organization such as pairing, dipole motion and axi-symmetrization are reminiscent of two-dimensional turbulence. The filaments are stretched by the large-scale vortex structure, thereby increasing the (odd) symmetry of the flow about the axis and characteristic length scale of the in-coherent fluctuations (McWilliams, 1984; Melander *et al.*, 1987, p. 149; Melander & Hussain, 1993a, pp. 2671, 2674). The organization of in-coherent small scales by a large-scale coherent structure is essentially inviscid (Melander & Hussain, 1993a, pp. 2671, 2676). It should be noted though that besides the inviscid organization leading to larger scales (two-dimensional characteristic), inviscid mechanisms generating smaller scales are also at work, e.g. filamentation, vorticity shedding by the vortex, secondary threads tearing vorticity from the main vortex and vortex stretching (Melander & Hussain, 1993a, p. 2676).

The thus far discussed free-stream organization characteristics are essentially obtained from numerical experiments. However, there is evidence that similar organization holds for trailing-vortex experiments, such that it can be assumed that similar dynamics is at play. The wrapping of the vortical free-stream (turbulence) structure around the core is observed in the LIF visualisation of Bailey *et al.* (2018, p. 737) at  $zc^{-1} \approx 6$  and is also visible in the experiments of Beresh *et al.* (2010, figs. 3, 4 and 15) for  $0.5 \lesssim zc^{-1} \lesssim 4$  in the mean and instantaneous velocity and kinetic-energy fields. Self-similarity of the wake scaling implies that the turbulence structure outside the core varies only slightly in the streamwise direction (Devenport *et al.*, 1996, p. 89). A secondary vortex structure in the core periphery (at roughly 4...5 core radii) is still observed at  $xc^{-1} \approx 27$  (Corsiglia *et al.*, 1973, p. 756) and  $xc^{-1} = 40$  (Bandyopadhyay *et al.*, 1991, p. 1631). Visualization in this latter experiments suggests the winding of a vortex pair around the trailing vortex helically ‘in opposite cork-screw fashion’.

---

<sup>3</sup>Filament polarization is defined as  $\log_2 |w_R| |w_L|^{-1}$ ,  $w_L \neq 0$ , where  $w_R, w_L$  denote right and left-propagating eigenfunctions of the curl operator (Melander & Hussain, 1993a, p. 2683).

The emergence of perturbation structure in the core periphery (at less than about 3 core radii) also manifests in the presence of a secondary peak in turbulent kinetic energy for  $zc^{-1} \leq 8$ . Near azimuthal alignment close to the vortex edge is reflected in the anisotropy of the spectra (Beninati & Marshall, 2005, pp. 250, 252). This maximum in Reynolds stress (after high-pass filtering), attained in a ring between approximately one to two core radii, is not sustained by the vortex and rapidly attenuated (Devenport *et al.*, 1996, pp. 99–100 and fig. 28).

It is likely that these organization characteristics extend to still other configurations, e.g. in geophysics. While vortex-induced organization is probably of great importance for several questions (such as mixing), we should not felicitate us too early, as the mere organization may not be compatible with energy production (Reynolds–Orr equation). Even more, it is most likely not! Since energy production (between mean and perturbations) works both ways, this then would mean that the more the free stream is organized it should attenuate core perturbations (Landau damping) (see also Pradeep & Hussain, 2006). In this sense it is perhaps the fact that the free-stream turbulence decays sufficiently fast that prevents an energy back flow while the core is a wave guide.

**Excitation of core perturbations: the buffeting picture.** Devenport *et al.* (1996, pp. 95–97) find the power-spectral-density graphs of the velocity fluctuation on the mean centreline at different streamwise measurement stations to collapse when non-dimensionalised with scales of the two-dimensional unrolled-up portion of the wake, while the core fluctuations appear independent from the core parameters. Therefore, Devenport *et al.* conclude that the *core dynamics is laminar while the measured velocity fluctuations are a result of inactive motions due to buffeting by the surrounding, rapidly decaying spiral-wake turbulence* (Devenport *et al.*, 1996, p. 96; Beninati & Marshall, 2005, pp. 244, 255; Marshall & Beninati, 2005, p. 242; Jammy *et al.*, 2014, p. 367). Remarkably, a highly energetic free stream, instead of forming new structures, ‘simply’ tends to bend and distort the vortex (Holzäpfel *et al.*, 2003). The attribute ‘inactive’ means that meandering-associated fluctuations do not contribute to turbulence production and that the effect can be linearly superposed, i.e. does not change the topology but ‘simply’ displaces (see also Jammy *et al.*, 2014, pp. 352, 354). Meandering has no *dynamic* contribution or coupling but is a merely additional *kinematic* feature (see sec. 2.4).

It seems that this perception of meandering has its origin in the work of Bandyopadhyay *et al.* (1991, p. 1633) who proposed that turbulence is transferred from the free stream to the core by means of *intermittent momentum transport*, all the same as core fluid is ejected into the surrounding. This exchange between the core and the free stream is governed by organized structures surrounding the core (see also Beninati & Marshall, 2005, p. 244), as detailed in sec. 5.2.1. Similarly, Fabre *et al.* (2006, pp. 266–267) suggest that perturbations can be introduced into the vortex core by critical-layer waves which enable a ‘communication’ between the core and regions located outside the core. Consequently, they are physically significant in all situations where a *transfer of energy* occurs between the vortex core and its surroundings. . . . an external perturbation can transfer its energy to the core [transient growth].

Bending (Kelvin) waves can be excited by energetic small-scale azimuthal perturbations in the free stream (Melander & Hussain, 1993a, pp. 2683, 2687; Van Jaarsveld *et al.*, 2011, p. 233). Beninati & Marshall (2005, p. 253) conclude that the observed core bending wave – of characteristic wavelengths and energies substantially greater than the exciting external turbulence – are essentially a manifestation of (*energy*) *backscatter* from the small (free-stream) scales to the vortex.

Similarly, Bailey *et al.* (2018, p. 744) conclude that ‘stochastic meandering is the result of . . . *momentum exchanges* between the vortex and coherent structures (‘eddies’) from the

free stream'.<sup>4</sup> Bailey *et al.* suggest that the vortex–turbulence interaction time scale is the turnover time.

In this section, we provided evidence that there is no energy (perhaps also momentum) transfer. However, the existence of a control instance which rules the communication between core and free stream is probably correct. This is the mother–daughter mechanism (sketched in fig. 6.12) to be described hereafter.

## 6.2 Energy transfer and the mother–daughter mechanism

So lässt sich nicht abweisen, dass die Welt unendliche Interpretationen in sich schließt, ohne dass man zu einer endgültigen gelangen könnte.

— F. Nietzsche: Die fröhliche Wissenschaft

The meandering amplitude obeys a Brownian motion (cf. chap. 4). However, the energy (and momentum) transfer to the perturbation space seems to be more intricate than in molecular Brownian motion where this happens via (randomly) impacting atoms. Rather, vortices are subject to a mother–daughter excitation mechanism (Boberg & Brosa, 1988), illustrated in fig. 6.12.

### 6.2.1 The integral fluctuation-energy balance

**Proper orthogonal decomposition.** The idea of the proper orthogonal decomposition (POD) is closely related to the paradigm of coherent structures, namely, the objective identification of the deterministic structure underlying stochastic or chaotic dynamics (e.g. Lumley, 1981, pp. 215–220; Sirovich, 1989, p. 126; Holmes *et al.*, 1998, pp. 86–87). The purpose here is only to give a concise introduction, for a more general presentation and details of the mathematical foundations see Lumley (1970), Monin & Yaglom (1975), Aubry *et al.* (1991), Aubry *et al.* (1992) and Berkooz *et al.* (1993), among others.

In typical vortex-meandering experiments, we are in possession of Eulerian velocity fields gathered in several streamwise measurement planes ( $z = \text{const}$ ) during some time  $T$ . (The following analysis uses the PIV measurements presented in appendix A.1.) In this case, the fluid domain  $M$  is a subset of the two-dimensional measurement plane and  $\mathbf{x} \in M$ . For all  $z \in \mathbb{Z}$  and  $\tilde{t} \in \mathbb{R}$  or  $\mathbb{Z}$ , let  $\mathbf{u}(\tilde{t}, z) \in L^2(M)$  be a vector-valued stochastic process with zero mean. We emphasize already that, in fact, the (measurement) time  $\tilde{t}$  merely is equivalent to a 'counter' of the random experiments by the ergodic hypothesis, while  $z$ , by Taylor's hypothesis –  $t = zU_\infty^{-1}$ , encompasses the actual meaning of 'temporal evolution'. For convenience, we suppress the dependence on  $z$ , since the analysis is the same for all measurement planes.

Since the space of square-integrable functions is separable (i.e. denumerably infinite), we can express every element of it in an infinite series of basis functions (Riesz & Sz-Nagy, 1956, pp. 64–70). The proper orthogonal decomposition then is defined as the expansion

$$(6.2) \quad \mathbf{u}(\tilde{t}) \in L^2(M) : \mathbf{u}(\tilde{t}, \mathbf{x}) = \sum_{l=1}^{\infty} a_l(\tilde{t}) \phi_l(\mathbf{x}) \quad \forall \mathbf{x} \in M \text{ and } z = \text{const},$$

whereas the expansion coefficients  $a_l(\tilde{t}) := (\mathbf{u}(\tilde{t}), \phi_l)_{L^2(M)}$  follow from projection (Holmes *et al.*, 1998, p. 90). The infinite-dimensional basis  $\{\phi_l\}_{l=1}^{\infty}$  is defined as the solutions of the

---

<sup>4</sup>This statement (as many others) lacks precision as to what exactly is meant by the 'vortex' – namely, where is its boundary or which fluid volume is considered to be the interior of the vortex? The same, it is not unambiguously clear what precisely is meant by free-stream 'coherent structures'.

eigenvalue problem

$$(6.3) \quad \mathbf{C}\phi_l = \lambda_l \phi_l \quad (l \in \mathbb{N})$$

where  $\mathbf{C} : L^2(M) \rightarrow L^2(M)$  is the covariance operator (Da Prato & Zabczyk, 1992, pp. 26–27). For  $\mathbf{C}$  being a compact self-adjoint operator, the spectral decomposition (6.3) into a set of mutually orthonormal functions  $(\phi_k, \phi_l)_{L^2(M)} = \delta_{kl}$  is guaranteed by Hilbert–Schmidt theory (Riesz & Sz-Nagy, 1956, pp. 233–234, 242–246; Kato, 1980, pp. 262–264). Equation (6.3) is symbolic for the Fredholm integral equation (Riesz & Sz-Nagy, 1956, p. 145)

$$(6.4) \quad \int_M d^d x' \mathbf{C}(\mathbf{x}, \mathbf{x}') \phi_l(\mathbf{x}') = \lambda_l \phi_l(\mathbf{x}) \quad \forall \mathbf{x} \in M \text{ and } z = \text{const} \quad (l \in \mathbb{N})$$

with symmetric kernel  $C_{\beta\gamma}(\mathbf{x}, \mathbf{x}') := \langle u_\beta(\mathbf{x}) u_\gamma^*(\mathbf{x}') \rangle$  ( $\beta, \gamma = 1, \dots, d$ ), called (two-point) covariance function (Monin & Yaglom, 1971, pp. 226–228).<sup>5</sup>

By appeal to variational calculus, it can be shown that the spectral decomposition (6.3) is equivalent to an optimization problem to identify the optimal (in the  $L^2(M)$ –sense) representation of the given  $\mathbf{u}(\tilde{t}) \in L^2(M)$  (Riesz & Sz-Nagy, 1956, pp. 232–233; Lumley, 1981, pp. 224–225; Holmes *et al.*, 1998, pp. 88–89). In the particular case that  $\mathbf{u}(\tilde{t}) \in L^2(M)$  is the velocity field, optimality is expressed by the relative energy content.

The energy content in the  $l$ -th POD mode is identical to the corresponding eigenvalue

$$(6.5) \quad \langle a_k a_l^* \rangle = (\phi_k, \mathbf{C}\phi_l)_{L^2(M)} = (\phi_k, \lambda_l \phi_l)_{L^2(M)} = \lambda_l \delta_{kl} \quad (k, l \in \mathbb{N}),$$

while the total energy content in the perturbation space equals the sum of all eigenvalues,

$$(6.6) \quad \langle \|\mathbf{u}\|_{L^2(M)}^2 \rangle = \left\langle \sum_{k,l=1}^{\infty} a_k a_l^* (\phi_k, \phi_l)_{L^2(M)} \right\rangle = \sum_{l=1}^{\infty} \langle a_l^2 \rangle = \sum_{l=1}^{\infty} \lambda_l,$$

using the fact that the decomposition (6.3) is into deterministic and orthonormal eigenfunctions, thus showing that the expansion coefficients are uncorrelated random variables with zero mean (see also Sirovich, 1987, p. 565). For convenience, we identify  $\lambda_0$  (the zeroth eigenvalue if the mean is not subtracted) with the energy of the mean flow  $\|\mathbf{U}\|_{L^2(M)}^2$  (supposing that it exists).

We define the relative energy content in the  $l$ -th POD mode by

$$(6.7) \quad \lambda_l^+(z) := \frac{\lambda_l(z)}{\sum_{k \in \mathbb{I}} \lambda_k(z)} \quad \forall z \geq 0 \text{ and } l \in \mathbb{I},$$

whereas  $\mathbb{I} \subseteq \mathbb{N}$  is a pertinent subset of the non-negative integers. Due to the normalization, (6.7) bears the interpretation of a probability on the function space (this was equally remarked by Aubry *et al.*, 1991; Sirovich, 1991, and used in sec. 5.1). The remaining eigenvalues are ordered in the decreasing sequence  $\lambda_0 \geq \lambda_1 \geq \dots \geq \lambda_n \geq 0$ , reminding that all positive eigenvalues have finite multiplicities and zero is the only accumulation point (Riesz & Sz-Nagy, 1956, pp. 232–242; Lumley, 1970, p. 58; Holmes *et al.*, 1998, pp. 90–91).

In practice, we solve (6.3) by the method of snapshots (Sirovich, 1987, pp. 567–568).

---

<sup>5</sup>The average is defined as  $\langle u \rangle := \lim_{T \rightarrow \infty} \frac{1}{T} \int_0^T d\tilde{t} u(\tilde{t})$  (if  $\tilde{t} \in \mathbb{R}$ ) or  $\langle u \rangle := \frac{1}{T} \lim_{T \rightarrow \infty} \sum_{\tilde{t}=1}^T u(\tilde{t})$  (if  $\tilde{t} \in \mathbb{Z}$ ), as the matter stands.

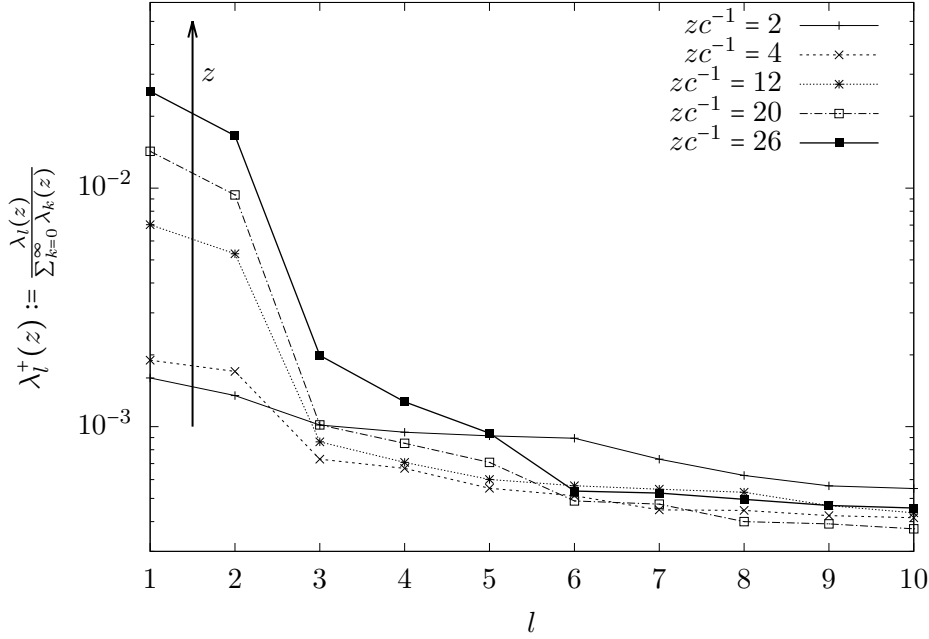


Figure 6.3: Downstream evolution of the first ten eigenvalues of the covariance operator (normalized with the eigenvalue sum *including* the zeroth order  $\lambda_0(z)$ ), showing gradual energy accumulation in the leading, nearly degenerate pair. (For the PIV measurements presented in appendix A.1.)

**Downstream evolution of the kinetic energy.** The energy partition over the first ten POD modes is shown in fig. 6.3 for experimental measurement planes located between  $2 \leq zc^{-1} \leq 26$ . It can be seen that the energy drops very quickly and then stabilizes at an almost constant level of  $10^{-3} \dots 10^{-4}$ . The perturbation space spanned by the first ten POD modes accommodates

$$\frac{\sum_{l=1}^{10} \lambda_l(z)}{\sum_{k=1}^{\infty} \lambda_k(z)} = 31\% \dots 65\% \quad (\text{for } zc^{-1} = 2 \dots 26)$$

of the total *fluctuation* kinetic energy (without  $\lambda_0$ ). The low values are due to the plateau beyond  $l \gtrsim 6$  such that a considerable portion of the energy persistently spreads over a large number of modes. It is a common expectation that the phase volume where the dynamics resides should be spanned by the leading modes containing practically all energy (e.g. Sirovich, 1987, p. 568; Sirovich, 1989, p. 139; Holmes *et al.*, 1998, p. 105).

Figure 6.3 then shows how the energy is distributed over the perturbation space ( $\lambda_l$  such that  $l > 0$ ) relative to the total energy of the system  $\sum_{k=0}^{\infty} \lambda_k$  – including the mean flow. Since  $\|\mathbf{U}(z)\|_{L^2(M)}^2 = \lambda_0^+(z) \approx 1$  for all  $zc^{-1} \in [2, 26]$ , the most energetic perturbation has about two to three orders of magnitude less energy than the mean flow. This suggests to think of the mean flow as an ‘inexhaustible energy reservoir’ (or ‘heat bath’ (*Wärmebad*) in the terminology of classical thermodynamics) that continually and unchangingly furnishes energy to the perturbation space.

The second important observation from fig. 6.3 is that, while energy is essentially equally distributed over all degrees of freedom at  $zc^{-1} = 2$ , it is gradually and systematically accumulated in the leading perturbation pair for  $zc^{-1} \geq 4$ . The remainder of the perturbation energy  $\lambda_l$  ( $l \geq 3$ ) does not evolve markedly. Beyond approximately  $zc^{-1} \approx 10 \dots 15$ , the energy in the leading pair ( $l = 1, 2$ ) is separated from the remainder ( $l \geq 3$ ) by a gap of about one order of magnitude. This suggests that the dimension (number of dynamically

active modes) of the perturbation space effectively decreases downstream. The persisting degeneracy of the leading perturbation pair is indicative of a translational symmetry or near streamwise homogeneity (Aubry *et al.*, 1992, § 3). A similar characteristic is observed in free-shear-flow turbulence (Rajaei *et al.*, 1994, pp. 9–10) and boundary-layer transition (Rempfer & Fasel, 1994, p. 360; Rempfer, 1996, p. 181), too. Rempfer & Fasel (1994, p. 359) define the span of the degenerate pairs of POD modes as ‘coherent structures’.

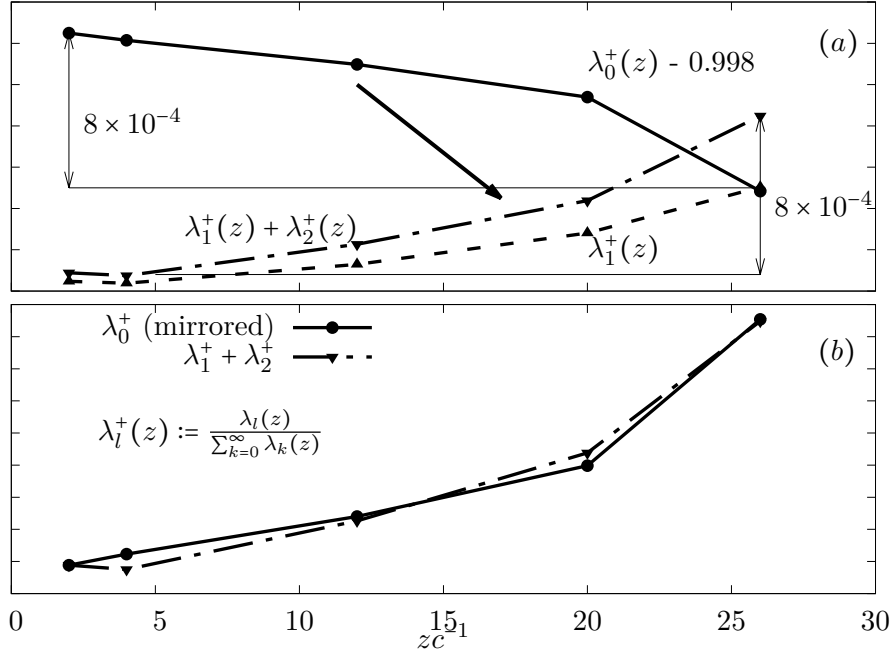


Figure 6.4: Downstream evolution of the leading eigenvalues of the covariance operator (normalized with the eigenvalue sum *including* the zeroth order). (a) Energy decay of the (shifted by  $-0.998$ ) mean  $\lambda_0(z)$  and amplification of the first and first two POD modes at the same rate, suggesting energy transfer from the mean to the two-dimensional perturbation subspace. (b) Superposition of the graphs in (a) reveals perfect correlation of the energy budgets. (For the PIV measurements presented in appendix A.1.)

We observe an increase of the energy in the perturbation space (fig. 6.3) (the near-wake growth is consistent with Edstrand *et al.*, 2016, fig. 5). Where does the energy come from? In order to answer this question, fig. 6.4a,b compares the downstream evolution of the integral energy in the mean flow and the perturbation space spanned by the first two POD modes, showing that the perturbation energy increases precisely at the expense of the mean flow. This correlation suggests that the energy in the perturbation space is completely provided by the mean flow (we give details below).<sup>6</sup>

The same graphs as in fig. 6.4b are reproduced in fig. 6.5 for varying fluid volumes, namely  $M, V_2, V_1$  as defined in sec. 2.2 and illustrated in the inset of fig. 6.5. Irrespective of the volume, the perturbation energy always increases precisely at the expense of the mean-flow energy. The smaller the volume, the more the energy is concentrated in the leading perturbation pair relative to the total energy contained in the volume.

The same mutual perturbation-energy growth at the expense of the mean energy can be deduced from the numerical experiment of Takahashi *et al.* (2005, figs. 10, 12).

<sup>6</sup>In principle, we must be extremely cautious with *correlations*, for they do not imply *causality*! This point was raised in footnote 27 on p. 25.

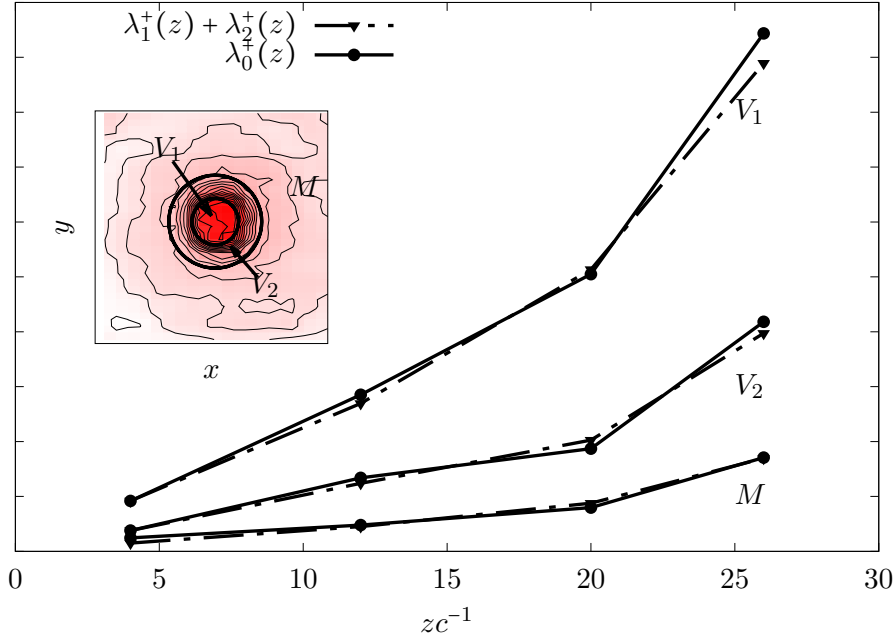


Figure 6.5: Downstream evolution of the leading eigenvalues of the covariance operator and the (reflected) mean energy (normalized with the eigenvalue sum *including* the zeroth order  $\lambda_0(z)$ ) for the different integration volumes  $M, V_2, V_1$  defined in sec. 2.2 and shown in the inset. In all cases the same correlation as in fig. 6.4 holds. (For the PIV measurements presented in appendix A.1.)

### Conclusion 6.2.1

The total energy in the perturbation space is at least two orders of magnitude less than in the mean flow. This suggests to idealize the mean flow as an inexhaustible energy reservoir which feeds the perturbation space. The system progressively increases its orderliness in the sense that the number of dynamically active modes decreases while the leading pair obeys a translation-invariance symmetry.

**The integral kinetic-energy budget.** Consider the fluid volume  $A$  defined to have no integral energy flux over its boundary  $\partial A$  on average. Let  $\mathcal{E}(t) := \nu \langle \|\mathbf{W}(t)\|_{L^2(A)}^2 \rangle$  and  $\varepsilon(t) := \nu \langle \|\mathbf{w}(t)\|_{L^2(A)}^2 \rangle$  be the average integral dissipation of the mean flow and perturbations, respectively. The average integral kinetic energy budgets of the mean and perturbations read (Tennekes & Lumley, 1973, pp. 62–62; Foias *et al.*, 2001, p. 28)

$$(6.8) \quad \partial_t \langle \|\mathbf{U}(t)\|_{L^2(A)}^2 \rangle = \langle (\mathbf{u}(t), \nabla \mathbf{U}(t) \mathbf{u}(t))_{L^2(A)} \rangle - \mathcal{E}(t),$$

$$(6.9) \quad \partial_t \langle \|\mathbf{u}(t)\|_{L^2(A)}^2 \rangle = -\langle (\mathbf{u}(t), \nabla \mathbf{U}(t) \mathbf{u}(t))_{L^2(A)} \rangle - \varepsilon(t).$$

Since by definition there is no energy flux over  $\partial A$ , Monin & Yaglom (1971, p. 368) resume that

... for flows of incompressible fluid in a field of nonfluctuating body forces, the only possible source of turbulent energy within a volume which has no influx of turbulent energy across its boundary is the transformation of the energy of the mean motion.

Thus, from figs. 6.4–6.5 and eqs. (6.8)–(6.9) we have evidence that, indeed, all the fluctuation energy is fed to the perturbation space by the mean and that all the considered volumes  $(M, V_2, V_1)$  are energetically closed in the sense that there is no flux over their boundaries (recall that  $t = zU_\infty^{-1}$ ). The mutual interaction term in (6.8)–(6.9) is  $\pm(\mathbf{u}(t), \nabla \mathbf{U}(t)\mathbf{u}(t))_{L^2(A)}$ , implying that the magnitude and direction of the energy transfer between the perturbations and the mean depends on the  $L^2$ –projection of the Reynolds stresses on the mean gradient. This means that besides the mean and the core perturbations there is a third actor – namely the Reynolds stress – which controls the energy exchange. It should be emphasized that this ‘control instance’ may have much less energy than the two primary actors (see also Wiener, 1988, p. 38). However, if any one of these elements is missing, the whole ceases to exist. This observation is strongly reminiscent of the mother–daughter mechanism elucidated by Boberg & Brosa (1988).

**Remark 6.1.** It should be emphasize here that a strikingly similar model is underlying the De-Broglie–Bohm mechanics of quantum physics.<sup>7</sup> In essence, a low-energetic non-local information field controls the much greater energy of a particle motion, whereas the energy supply comes from the particle itself (Bohm & Peat, 1987, pp. 90–94). The special form of the quantum potential (reminiscent of the numerical range) allots all importance to the information *form* rather than its *intensity* – this is called *active* information (Bohm & Peat, 1987, pp. 89, 93). This is precisely what happens in the Reynolds–Orr equation. The important non-local interaction is due to the appearance of the Laplacian in the bilinear form (Bohm & Peat, 1987, p. 89), whereas the typical vortex velocity gradient only permits effectively restricted interactions (as follows from spectral decomposition).

#### Conclusion 6.2.2: Closeness and control

A vortex is energetically closed in the sense that there is no integral energy transfer over its boundary on average. The accumulation of core energy is likely to be due to the mother–daughter mechanism, where external structures outside the vortex control the exchange without themselves providing energy, though.

Identification of meandering with the leading perturbation pair obtained from POD and the fact that energy enters the perturbation space at scales comparable to the integral scale (Tennekes & Lumley, 1973, p. 68) is consistent with the assumption that meandering is associated essentially with the large scales (cf. sec. 2.4.2). On a simplified level, the energy-input range (i.e. vortex meandering) is governed by the linear dynamics, while the pressure gradient and advective non-linearity are essentially responsible for inter-scale redistribution in the inertial range and viscous diffusion governs the dissipative range (Monin & Yaglom, 1971; Rotta, 1972; Tennekes & Lumley, 1973).

**The leading-order POD-mode dipole pattern.** The leading POD-mode pair computed from the vorticity field at  $zc^{-1} = 26$  is shown in fig. 6.6. POD analysis of vortex flow is commonly based on the vorticity field (Roy & Leweke, 2008, p. 22; Del Pino *et al.*, 2011, p. 6) rather than the velocity field. It should be kept in mind that then the eigenvalues do not represent physically kinetic fluctuation energy but enstrophy (Foiş *et al.*, 2001, p. 28). Nevertheless, POD of the vorticity and velocity fields are essentially comparable, showing the same trends and global behaviour.<sup>8</sup>

<sup>7</sup>Indeed, the conceptual connection between vortex dynamics and quantum mechanics seems to be quite tight (e.g. Hasimoto, 1972; Hirota, 1973; Klein & Majda, 1991).

<sup>8</sup>It should also be mentioned that POD analysis of the numerical data at far lower Reynolds numbers (provided by Navrose 2018, ONERA) by myself yielded qualitatively identical structures.

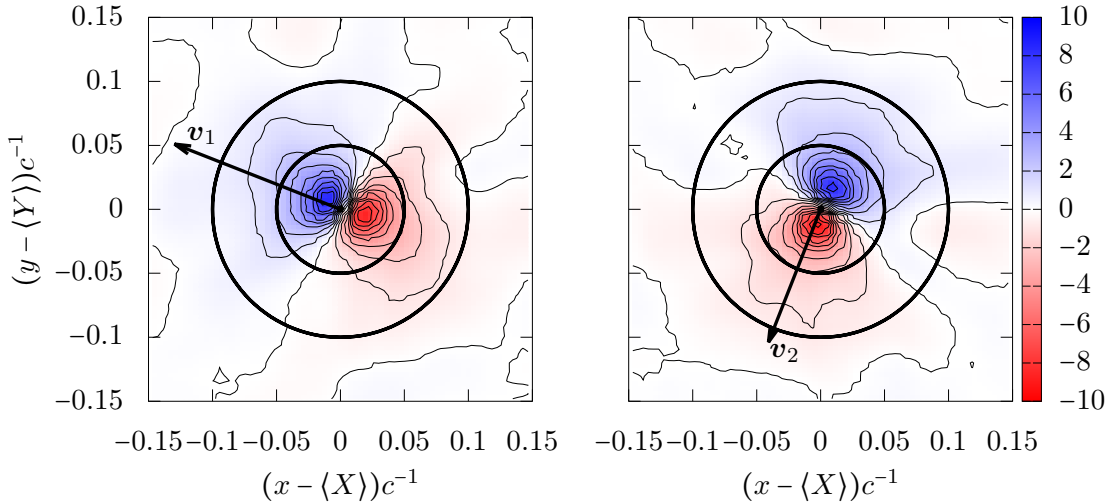


Figure 6.6: Leading POD modes  $\phi_l^w(\mathbf{x})$  ( $l = 1, 2$ ) at  $zc^{-1} = 26$  (normalized with  $t_c := cU_\infty^{-1}$ ). Inner and outer circle representing the vortex core and support. The principal axes  $\mathbf{v}_l$  ( $l = 1, 2$ ) from spectral decomposition of the centreline covariance tensor  $\langle \mathbf{X} \mathbf{X}^T \rangle$ . (For the PIV measurements presented in appendix A.1.)

The subsequent POD modes (not shown here) progressively (as  $l$  is increased beyond two) correspond to multi-pole structures (see Roy & Leweke, 2008; Del Pino *et al.*, 2011), reminiscent of the  $|m| \geq 2$  modes pertaining to the discrete spectrum of the Lamb–Oseen and Batchelor vortices (Mayer & Powell, 1992; Fabre & Jacquin, 2004; Fabre *et al.*, 2006).

The characteristic dipole structure of the leading POD modes has been taken as evidence that the most energetic contribution to vortex meandering corresponds to perturbation waves with helical  $|m| = 1$  symmetry (conj. 3.1 and Del Pino *et al.*, 2011, pp. 7, 10; Edstrand *et al.*, 2016, p. 7). The superposition of two  $|m| = 1$  Kelvin waves  $\phi_l^w$  ( $l = 1, 2$ ) mutually rotated by  $90^\circ$  is sufficient for arbitrary displacements in the plane (Roy & Leweke, 2008, p. 6). Since furthermore the inclination angle of the leading POD-mode pair coincides with the tilt derived from the vortex-centre correlation tensor (as shown in fig. 6.6), the meandering dynamics is believed to be characterized (entirely) by the leading POD-mode pair (Del Pino *et al.*, 2011, pp. 7, 10). This is further corroborated by observing that

$$x_l(t) = a_l(t) := (\mathbf{u}(t), \phi_l)_{L^2(M)} \quad \text{and} \quad E_{x_l}(\omega) = E_{a_l}(\omega) \quad (l = 1, 2)$$

holds, whereas  $x_l(t)$  are the realizations of the vortex-centre components with respect to the principal-axes system. That is, the time series obtained from projecting the velocity field on the  $l$ -th POD mode ( $l = 1, 2$ ), viz. the expansion coefficient, is identical with the realization of the vortex-centre time series in the direction of the principal axis  $\mathbf{v}_l$ . The same correspondence applies to the respective power spectral densities (the same observation was made by Del Pino *et al.*, 2011, p. 11). We conclude that the kinematic description of vortex meandering through the centreline time series  $\mathbf{X}(t)$  is equivalent to the dynamic representation in terms of the leading POD dipole pair.

Repeating the same analysis for the other measurement planes at  $zc^{-1} = 2, \dots, 20$  leads to qualitatively identical patterns and alignment with the principal direction of the vortex-centre time series. As an example, fig. 6.7 shows the leading POD-mode pair at  $zc^{-1} = 2$ .

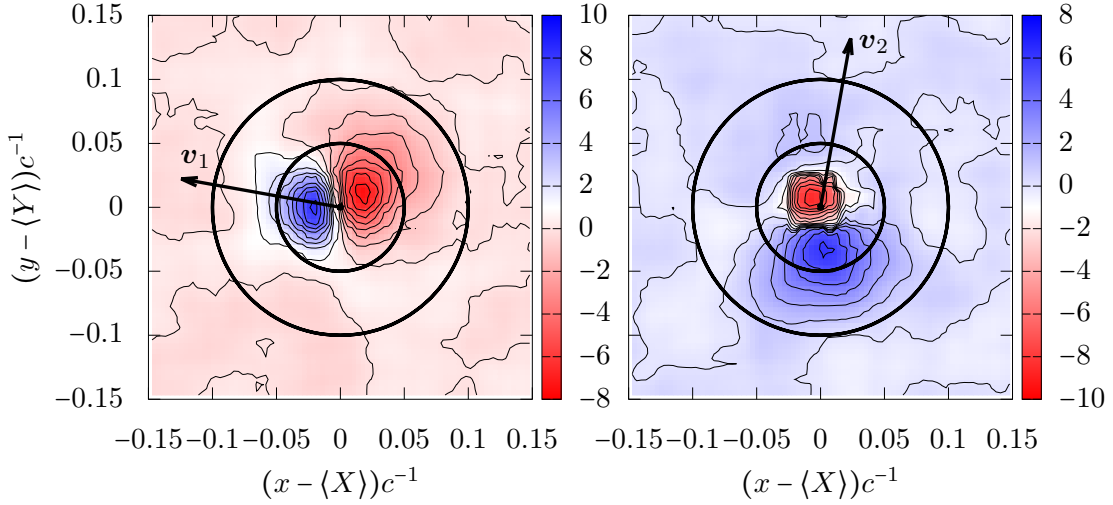


Figure 6.7: Leading POD modes  $\phi_l^w(\mathbf{x})$  ( $l = 1, 2$ ) at  $zc^{-1} = 2$  (normalized with  $t_c := cU_\infty^{-1}$ ). Otherwise same as fig. 6.6. (For the PIV measurements presented in appendix A.1.)

While the structures and inclinations are similar to fig. 6.6, we find the result to be much less representative of the actual vorticity field than farther downstream. This is evidenced by comparison with an instantaneous snapshot of the fluctuation vorticity  $w(t, \mathbf{x})$  ( $t$  fixed arbitrarily and  $\mathbf{x} \in M$ ) as shown in fig. 6.8 for  $zc^{-1} \in \{2, 26\}$ . We conclude that close to the wing the dynamics is not yet truly dominated by the leading dipole pair and that meandering – if we can already call it that – should be extremely weak (this is in agreement with Green & Acosta, 1991). This initial lack of a concise representation is consistent with the (quasi-uniform) spreading of the energy over multiple scales found in fig. 6.3. The quality of the representation of any (vorticity-field) realization by the leading POD modes becomes gradually more reliable as the energy content increases downstream.

The dynamics of the coherent structure itself is entirely represented by the ‘core dynamics’.<sup>9</sup> The core dynamics can be expressed as the unique superposition (Melander & Hussain, 1993b, p. 1996; Lesieur, 2008, pp. 163–166) and interaction of complex helical waves moving in opposite directions (eigenfunctions of operator  $\text{rot} := \nabla \times$ ) which, taken together, yield the actual entire vorticity field. This analysis reveals that ‘the deformation of the vortex column results primarily from the relative motion of two slowly deforming polarized vorticity structures’ (Melander & Hussain, 1993b, p. 2002).

**Reynolds stresses.** Recall that, in this section, we denote the measurement time by  $\tilde{t}$  and that  $\langle \cdot \rangle$  is the time average over the measurement duration  $T$ . We then recall the definition of the Reynolds stress as the second-order covariance tensor of the  $d$ -dimensional random field  $\mathbf{u}(\tilde{t}; z, \mathbf{x})$  (Monin & Yaglom, 1971, p. 261; Rotta, 1972, p. 56; Tennekes & Lumley, 1973, p. 32) –

$$(6.10) \quad R_{\beta\gamma}(z, \mathbf{x}) := \langle u_\beta(z, \mathbf{x}) u_\gamma^*(z, \mathbf{x}) \rangle \quad \forall (z, \mathbf{x}) \in [0, L] \times M \quad (\beta, \gamma = 1, \dots, d),$$

<sup>9</sup>Defined as the influence of the vortex’ own vorticity distribution on the dynamics (Melander & Hussain, 1994, p. 1).

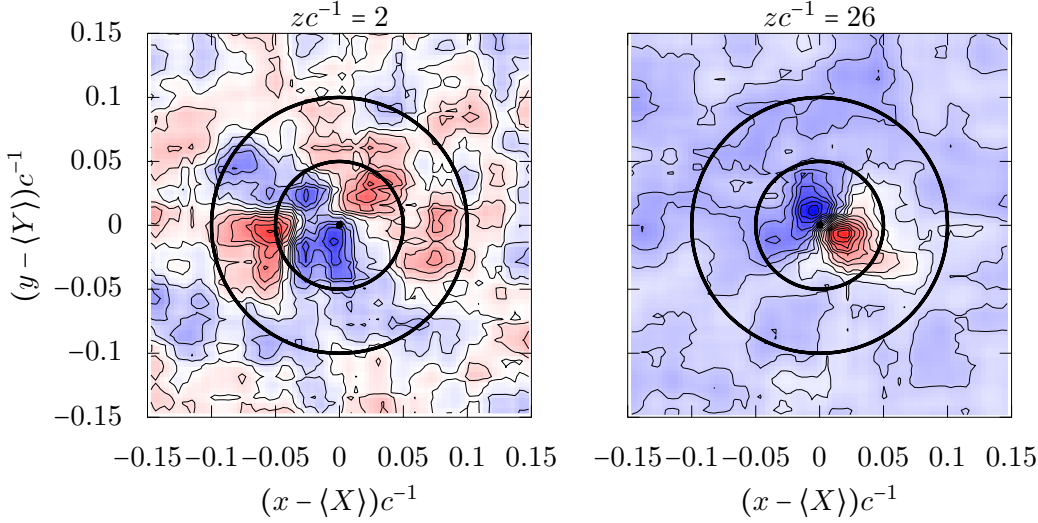


Figure 6.8: Instantaneous fluctuation vorticity at  $zc^{-1} = 2$  and  $zc^{-1} = 26$  (normalized with  $t_c$ ). Same colour on the right corresponds to twice the vorticity magnitude on the left. (For the PIV measurements presented in appendix A.1.)

where  $L$  is the length of the experimental test section (see fig. 2.1). In fact, for  $\mathbf{u}(\vec{t}) \in L^2(M)$ ,  $\mathbf{R} : L^2(M) \rightarrow L^2(M)$  is the special case of the covariance operator  $\mathbf{C}$  introduced above for  $\mathbf{x} = \mathbf{x}'$ . Equation (6.10) is then the symmetric (hermitian) kernel. The trace  $\text{tr } \mathbf{R}(z, \mathbf{x}) = \sum_{\beta=1}^d \langle u_\beta^2(z, \mathbf{x}) \rangle$  is therefore defined and is, by construction, identical with the total fluctuation kinetic energy  $\langle \|\mathbf{u}(z, \mathbf{x})\|_{\mathbb{R}^d}^2 \rangle$  (Kato, 1980, p. 521).

The sum of the normal Reynolds stresses, i.e. the trace or total kinetic energy, is shown in fig. 6.9 for  $zc^{-1} \in \{4, 26\}$ . In both measurement planes, the energy is essentially concentrated in the vortex core, whereas the bulk contribution comes from the transversal components. (The result is qualitatively the same for all other measurement planes in between.) Outside the core, the energy rapidly ceases while it amplifies by a factor of approximately ten within  $4 \leq zc^{-1} \leq 26$ . This is, of course, consistent with fig. 6.1.

The transversal Reynolds stresses naturally appear in the production (‘communication’) term of (6.8)–(6.9), thus ruling the energy exchange between the mean and the perturbations (cf. conclusion 6.2.1). As such, the decisive requirement for integral energy amplification on average is that the  $L^2$ -projection on the mean-velocity gradient be non-zero. In fact, since both arguments in the production bilinear form  $(\mathbf{u}, \nabla \mathbf{U} \mathbf{u})_{L^2(M)}$  are identical, only the symmetric part of  $\nabla \mathbf{U}$  can yield a non-zero contribution. We are thus led to analyse the possibility of projection on  $\mathbf{S} := 0.5(\nabla \mathbf{U} + \nabla \mathbf{U}^T)$ . For vortices, where generically  $\mathbf{U}(r) = U_\theta(r)\mathbf{e}_\theta + U_z(r)\mathbf{e}_z$ , we have (details are given in Bölle *et al.*, 2020)

$$(6.11) \quad \mathbf{S} = \frac{1}{2} \begin{bmatrix} 0 & r d\Omega/dr & dU_z/dr \\ r d\Omega/dr & 0 & 0 \\ dU_z/dr & 0 & 0 \end{bmatrix}.$$

This shows that the relevant Reynolds-stress components are  $\langle u_r u_\theta \rangle$  and  $\langle u_r u_z \rangle$  for projection on the symmetric gradient of the azimuthal and axial velocity, respectively. In

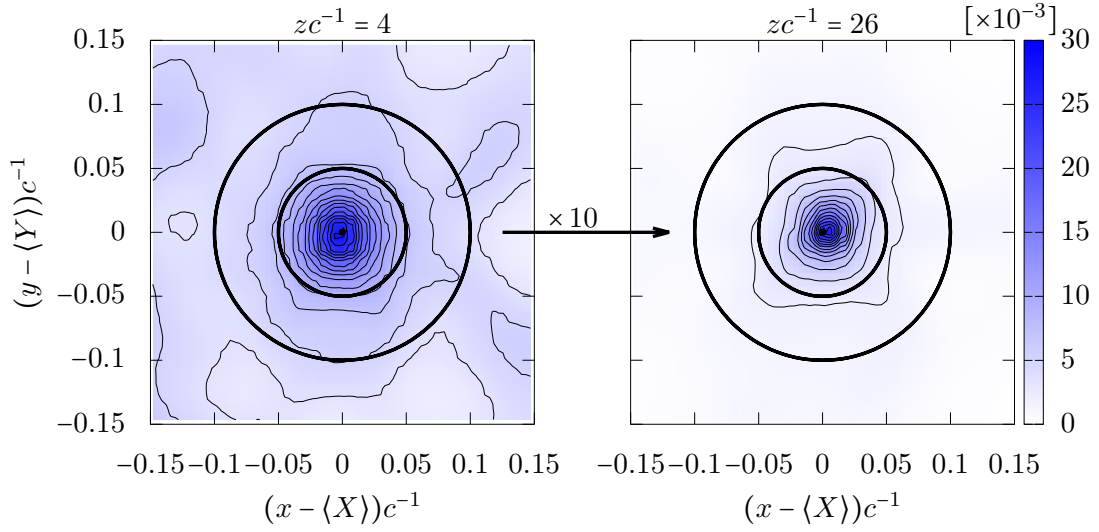


Figure 6.9: Normal Reynolds stress  $\sum_{\beta=1}^3 \langle u_{\beta}^2 \rangle$ . In both measurement planes the streamwise energy is more than an order of magnitude less than the transversal contributions  $\langle u_x^2 \rangle \sim \langle u_y^2 \rangle \sim 10^{1 \dots 2} \langle u_z^2 \rangle$ . (For the PIV measurements presented in appendix A.1.)

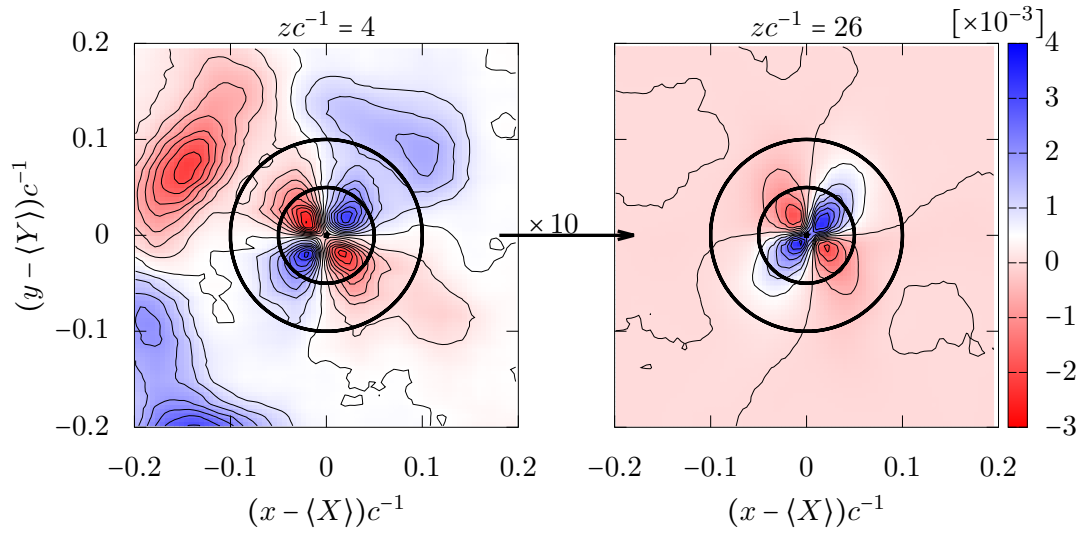


Figure 6.10: Transversal Reynolds stress  $\langle u_x u_y \rangle$ . (For the PIV measurements presented in appendix A.1.)

Cartesian coordinates, fig. 6.10 shows the in-plane transversal component and fig. 6.11 the combined transversal and normal component. The latter is much weaker and unlikely to play an important role at least at the first measurement station. In both cases, the Reynolds stresses are amplified by one order of magnitude over the measurement distance.

The same patterns of normal and transversal Reynolds stresses at  $zc^{-1} = 26$  are found in the PIV measurements of Heyes *et al.* (2004, fig. 7) at  $zc^{-1} = 22.9$  and Vandernoot *et al.* (2008, figs. 12, 16). In the experiments of Heyes *et al.*, the Reynolds-stress magnitude is about three times larger than shown in figs. 6.9–6.10, which is consistent with the fact that their turbulence intensity is also at least a factor two larger. The magnitudes detected by Vandernoot *et al.* are comparable, as is their turbulence intensity. Similar shapes and localization but weaker stresses are also observed by Phillips & Graham (1984, pp. 362–366). A qualitatively similar evolution as shown in fig. 6.10, namely the gradual concentration of transversal Reynolds stresses in the core downstream, is consistent with the simulations of Hussain *et al.* (2011, fig. 14b).

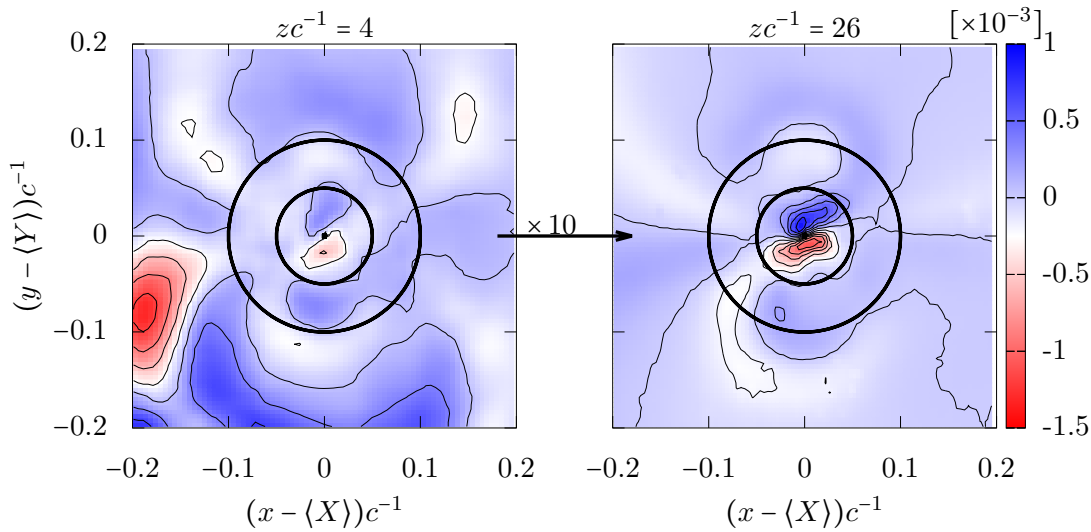


Figure 6.11: Reynolds stress  $\langle u_x u_z + u_y u_z \rangle$ . (For the PIV measurements presented in appendix A.1.)

### 6.3 Linear receptivity

... ein fehlerloses Vernunftsgelbte durchzusetzen,  
denn gerade seine fehlerlose Vollkommenheit ware  
seine todliche Luge und ein Zeichen der  
schrecklichsten Blindheit.

— F. Durrenmatt: Das Versprechen

The notion of receptivity was coined by I. Kant and derives from the Latin *recipiō*,<sup>10</sup> designating the sensitivity of an organism to external influences (*Empfanglichkeit*). In the *Kritik der reinen Vernunft*, I. Kant states that

Unsre Erkenntnis entspringt aus zwei Grundquellen des Gemuts, deren die erste ist, die Vorstellungen zu empfangen (die Rezeptivitat der Eindrucke), die

<sup>10</sup> *aufnehmen* (Stowasser, p. 429).

zweite das Vermögen, durch diese Vorstellungen einen Gegenstand zu erkennen (Spontaneität der Begriffe).<sup>11</sup>

That is, an action is the outcome of two complementary concepts. The passive receptivity, permitting to obtain external excitation, is followed by the active spontaneity of the organism. This is reminiscent of the duality observed in vortex meandering, namely the specific reaction (an intrinsic mechanism) to the principal exposition to external stimuli. To be precise, the common understanding of receptivity in fluid dynamics (introduced by Morkovin, 1969; Obremski *et al.*, 1969) is actually receptivity–spontaneity in the sense of Kant. Before discussing the linear receptivity of generic vortices in frequency space and subsequently in time domain, some comments are required.

The preceding chap. 5 suggests to formally identify the (manifesting) vortex with an (abstract) organism. (Greek *ὄργανισμός*, usually meaning a (living) entity or system.) The notion of a system here is to be distinguished (but is not disjoint) from the notion in chap. 5; the meaning here is rather in the thermodynamic sense (Atkins, 2010, p. 1; Klein & Nellis, 2012, p. 3). That is, the system (*viz.* the organism) is identified with a distinct geometrical space-time object (*i.e.* the vortex), delimited from its surrounding by the system boundary. This approach allows to distinguish the interior from the exterior of the system.

The external influence<sup>12</sup> should not be understood literally but rather abstractly, for the previous analysis suggests that the vortex is exposed to an information<sup>13</sup> field. This idea of the external excitation puts the emphasis on the content, form or kind, rather than magnitude in agreement with the before said (notably rem. 6.1). Metaphorically, the vortex *is* an organism ‘living’ in the fluid domain and subjected to the information field emanating from the surrounding free stream. Receptivity then determines the principal susceptibility to the various kinds of information and the vortex response is the spontaneity in the sense of Kant. The mutual communication between the vortex and the free stream will be shown to happen by appeal to secondary elements in the vortex periphery.

These considerations suggest that receptivity actually designates the process or action, rather than the state. As such, it is mathematically associated with transformations, or operators (Riesz & Sz-Nagy, 1956). In the henceforth discussed linear model, receptivity to the initial condition  $\mathbf{u}(0)$  or sustained forcing  $\mathbf{f}(t)$  is generically expressed by

$$\mathbf{u}(t) = \mathbb{T}(t)\mathbf{u}(0) + \int_0^t d\tau \mathbb{T}(t-\tau)\mathbf{f}(\tau) \quad \forall t \geq 0,$$

where  $t \mapsto \mathbb{T}(t)$  is the semigroup generated by the linearised Navier–Stokes operator  $\mathbf{L}$  (see appendix C and Engel & Nagel, 2000). Analysis of the semigroup will be the subject of sec. 6.3.2. The Laplace transform of the semigroup  $s \mapsto \mathbf{R}(s; \mathbf{L})$  is called resolvent and will be discussed in sec. 6.3.1 (Kato, 1980). However, it is clear that both analyses are different views of the same problem.

In both cases, the canonical decomposition of the linear operator families  $\mathbf{R}(s; \mathbf{L})$  and  $\mathbb{T}(t)$ , respectively, is used (the technical details necessary for the present work can be found in appendix C). Canonical decomposition amounts to a decomposition of the linear operator into a series of rank-1 operators (taking  $s, t$  as fixed parameters), ordered with respect to their energy amplification. The respective rank-1 operators can be understood as a (Hilbert-space) tensor product between the optimal input–output mode pairs. This

<sup>11</sup> Our knowledge springs from two fundamental sources of our soul; the first receives representations (receptivity of impressions), the second is the power of knowing an object by the representations (spontaneity of concepts).

<sup>12</sup>From the Latin *influō*, ‘to flow into’ (*hineinfließen*, *eindringen*; Stowasser, p. 262).

<sup>13</sup>From the Latin *fōrma*, shape (*Gestalt*, *Form*; Stowasser, p. 214)

analysis of the semigroup  $T(t)$  is called transient-growth analysis and the optimal input mode is referred to as (linear) optimal perturbation. Details can be found in Farrell & Ioannou (1996), Trefethen & Embree (2005), Schmid (2007) and Kerswell (2018) among many others.

### 6.3.1 Analysis in frequency space: the resolvent

Analysis of the linear receptivity in frequency space by means of the resolvent can be found in Bölle *et al.* (2020), which is appended in appendix C. Here, we merely add fig. 6.12 illustrating the mother–daughter mechanism adapted from Boberg & Brosa (1988) in the case of vortex dynamics. The daughters typify the core perturbations (figs. 6.6–6.7) which receive their energy  $u_T^2$  from the vortex mean flow (symbolized by an inexhaustible energy reservoir). The mothers take over the role of the control device which rules the transfer of energy, represented by a valve in the schematic. In the case of vortices, the mothers correspond to filaments wound up around the vortex core at a radial position identical with the critical layer. If this mechanism is responsible for the experimentally observed energy amplification in the vortex core, free-stream disturbances (with non-zero projection onto the shown excitation mode) are absolutely necessary, since otherwise no energy transfer is possible. It is, however, important to remember that the actual energy transfer is between the mean flow and the perturbation space, while the free-stream disturbances merely take the role of an indispensable mediator (*Vermittler*). In other words, the proposed mechanism implies that in a perfectly quiescent environment (or if the projection is zero), the vortex would not meander – not because there is no energy transfer from the free stream to the vortex, but because the external stimulus, which incites the perturbations to draw energy from the mean flow, is missing.

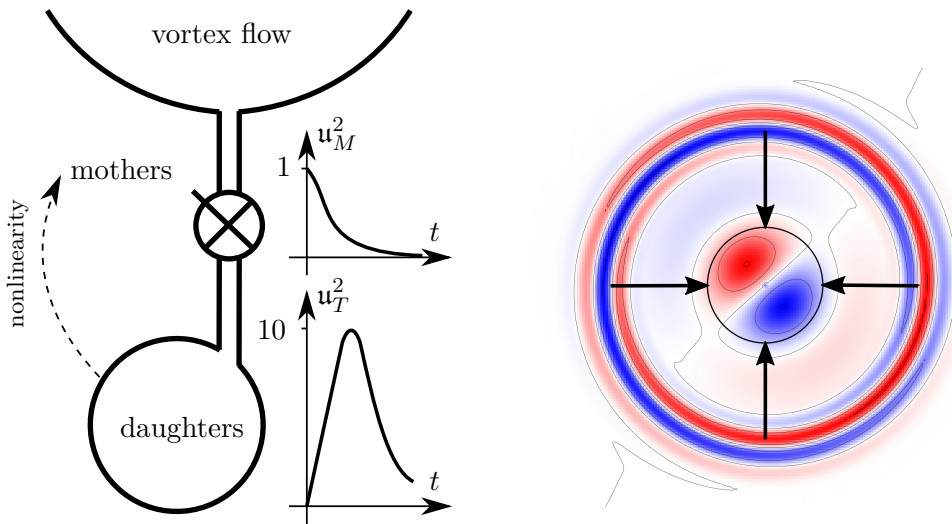


Figure 6.12: Mother–daughter mechanism. (a) Adaptation of the schematic elucidated by Boberg & Brosa (1988, fig. 1). (b) Critical-layer excitation of the Lamb–Oseen vortex derived from a canonical decomposition of the resolvent (Bölle *et al.*, 2020).

As in the case of Boberg & Brosa (1988), we add the typical qualitative energy evolution of the mothers and daughters. The factor ten is in principal agreement with the experimental finding shown in fig. 6.1 and re-emphasizes the fact that a comparably low-energetic ‘control unit’ is capable of ruling the energy budget of a high-energetic organism.

Eventually, Boberg & Brosa (1988) proposed that nonlinearity acts to re-establish the decaying daughters and therewith gives rise to a self-sustaining mechanism. It is not clear, whether this idea holds for vortices. Rather, the mothers would seem to be organized by the vortex mean flow and the nonlinearity might be considered as an abstract forcing. This is consistent with the previous remark that vortices tend to separate dynamic regimes into spatially distinct regions. It would also be consistent with a Brownian motion.

### 6.3.2 Analysis in time domain: transient growth

All approaches to vortex flow, such as experiments, simulation, linear dynamics of different reference flows etc., unanimously observe the preferred excitation of a few characteristic, possibly generic, wave modes, commonly believed to be related to a linear transient-growth mechanism (Hussain *et al.*, 2011, p. 305). Since the transient-growth dynamics of the Lamb–Oseen vortex essentially extends to the Batchelor vortex, we discuss both flows together. In particular, the peak due to resonance excitation (Antkowiak & Brancher, 2004) persists for all stable conditions at a comparable wave number (Heaton & Peake, 2007, fig. 7).

**Review of the theory.** We assume perturbations of the form

$$\phi(t, r, \theta, z) = \hat{\phi}(t, r) e^{i(m\theta + \alpha_z z)}$$

with wavenumbers  $m \in \mathbb{Z}$  and  $\alpha_z \in \mathbb{R}$ . The perturbation kinetic energy is defined by (for fixed  $m, \alpha_z$ )

$$(6.12) \quad E(t) := \|\mathbf{u}(t)\|_{L^2(M)}^2.$$

For fixed  $t > 0$ , the gain is defined as

$$(6.13) \quad G(t) := \max_{\mathbf{u}(0) \neq 0} \frac{E(t)}{E(0)},$$

that is, the maximum normalized amplification over all admissible initial conditions for the considered horizon time  $t$ . The maximum gain, or global optimum, is defined by  $G_{max} := \max_t G(t)$  and  $t_{max} := \arg \max_t G(t)$  (Pradeep & Hussain, 2006, p. 264; Heaton & Peake, 2007, p. 275). For later reference, the graph of the global optima  $G_{max}(\alpha_z)$  as a function of the streamwise wave number  $\alpha_z$  is reproduced in fig. 6.13 from Antkowiak & Brancher (2004, fig. 1). We discern two peaks at  $\alpha_z r_0 \approx 1.5$  and as  $\alpha_z \rightarrow 0$  which are natural candidates for meandering.

Antkowiak (2005) and Roy & Leweke (2008, fig. 25) extrapolate the optimal-time curves of Antkowiak & Brancher (2004, fig. 1) for the Lamb–Oseen vortex (fig. 6.13) in the same range of Reynolds numbers to observation times of their experiments for an estimated characteristic meandering wavelength of  $\lambda r_1^{-1} = 120$ . Roy & Leweke (2008, p. 9) suggest:

**Conjecture 6.1.** *Vortex meandering is due to transient growth of optimal perturbations ‘initiated by background noise in the flow or by turbulence in the wake of the wing’.*

Jacquin *et al.* (2007, p. 8) speculate that meandering in their jet–vortex interaction experiment is due to transient growth of core perturbations initiated by the jet turbulence. Assuming essential similarity between meandering of inlet and trailing vortices, Wang & Gursul (2012, pp. 16–17) also refer to a linear transient-growth mechanism to explain the observed long-wavelength vortex deformation.

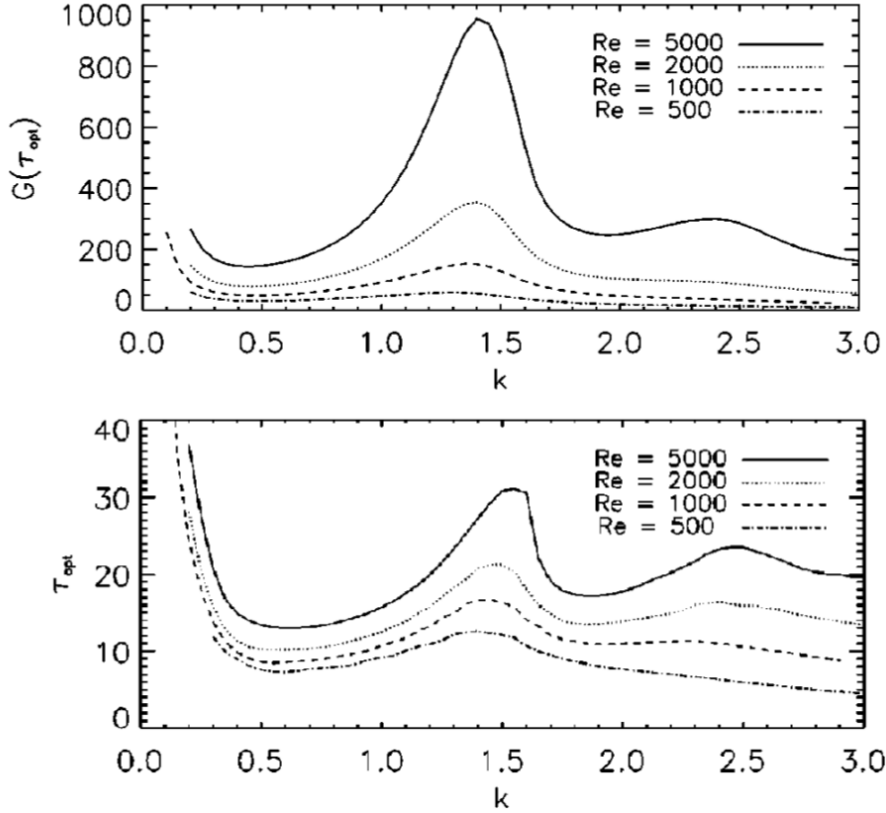


Figure 6.13: Top figure: maximum gain  $G_{max}$  (called  $G(\tau_{opt})$  here) over the wavenumber  $\alpha_z$  (called  $k$  here) for perturbations to the Lamb–Oseen vortex with  $m = 1$ . The Reynolds number is  $Re := r_0^2 \Omega_0 / \nu$ . Bottom figure: the associated horizon time  $t_{max}$  (called  $\tau_{opt}$  here) to reach the maximum gain. (Taken from Antkowiak & Brancher, 2004.)

**Scale estimates for resonant transient growth.** Increasing the Reynolds number leaves the wave-number location of the (resonance) peak almost unaffected while  $G_{max}$  grows since the governing mechanisms are essentially inviscid (Pradeep & Hussain, 2006, p. 279). For the Reynolds number  $\Gamma/\nu \sim 10^4$  the global optimum attains values of the order of  $G_{max} \sim 10^2 \dots 10^3$ . The time to reach this value also increases and is estimated to be beyond  $t_{max} = 30 t_r$  (extrapolated from the trend shown in Antkowiak & Brancher, 2004, fig. 1). This lower-bound estimate matches reasonably with the value of  $t_{max} t_r^{-1} \approx 10^2$  for the Batchelor-vortex resonant transient growth of the  $m = -1$  perturbation at  $\Gamma/\nu = 5 \times 10^3$  (Heaton & Peake, 2007, p. 291).

Assume  $t_{max} t_r^{-1} \sim 10^2$  for the time required to attain the global optimum due to resonance. The corresponding travelling distance of the vortex is  $z c^{-1} \sim 10^2 t_r t_c^{-1} \approx 20$ . It is not evident to decide whether the dynamics at about twenty chords is governed by (linear) transient growth of an optimal initial perturbation (see also Hussain *et al.*, 2011, p. 316).

**Scale estimates for  $\alpha_z \rightarrow 0$  transient growth.** Assuming perturbation dynamics of helical symmetry in the meridional plane, energy amplification is maximized by streamwise homogeneous (viz.  $\alpha_z = 0$ ) perturbations (Mao & Sherwin, 2012, p. 48). Ad idem, the global optima curves in Antkowiak & Brancher (2004, fig. 1), Pradeep & Hussain (2006, fig. 19) and Heaton & Peake (2007, fig. 7) all show significantly increased gain in the limit of very long wavelengths:  $G_{max}(\alpha_z) \rightarrow \infty$  as  $\alpha_z \rightarrow 0$  (Heaton *et al.*, 2009, p. 291). Infinite amplification is physically infeasible and is an artefact of vanishing viscous terms

for  $|m| = 1$  perturbations (Heaton & Peake, 2007, p. 293). However, the time to attain maximum amplification diverges  $t_{max}(\alpha_z) \rightarrow \infty$  as  $\alpha_z \rightarrow 0$  (Antkowiak & Brancher, 2004, fig. 1), which would seem to limit the physical significance of these modes. As a matter of fact, this formal divergence is a consequence of an extremely flat gain curve and Heaton & Peake (2007, pp. 293–294) state that

the growth rate for any transients should be reasonable for small- $\alpha_z$  bending modes, and indeed faster than the growth rates involved in the bending mode resonance [and] conclude that the small- $\alpha_z$  bending mode disturbances are capable of contributing significant transient growth . . . comparable to the resonant effect.

For  $\alpha_z r_0 \sim 10^{-1}$  and  $q = 4$ , the gain envelope has similar shape as compared to the resonance case for early times  $tt_r^{-1} \lesssim 10^2$  (Heaton & Peake, 2007, fig. 9). This suggests that the global optima and associated optimization times are an insufficient measure for the actually possible transient growth of long-wave perturbations. In fact, significant transient energy growth of the same order as for the resonant case within similar time may be expected (Heaton & Peake, 2007, pp. 293–294).

Energy amplification in the long-wave limit has been analysed by means of the two-dimensional linear perturbation equation (Antkowiak & Brancher, 2004; Johnson, 2016; Navrose *et al.*, 2018). In this case the  $m = 1$  optimal gain increases linearly with the optimization time and the slope depends on the Reynolds number. However, initial perturbations move away from the core as the time is increased (Antkowiak & Brancher, 2004, p. 3). This gradual outward motion limits the relevance in practical applications to  $tt_\delta^{-1} \lesssim 100$  (Mao & Sherwin, 2012, p. 56). With regards to this threshold value the required optimal time  $tt_r^{-1} = 150 \pm 10$  extrapolated by Roy & Leweke (2008, p. 30) would be achievable (cf. time-scale estimates in sec. 2.2). This behaviour is completely analogous to the gradual outward motion of the optimal forcing, obtained from canonical decomposition of the resolvent, as  $\omega \rightarrow 0$  (see appendix C).

### The nonlinear evolution of linear optimal perturbations

Integration of an isolated line vortex embedded into initially fine-scale turbulence of initial intensity  $uU_\infty^{-1} \approx 4 \times 10^{-2}$  (corresponding to 15% of  $U_{\theta,1}$ ) leads to the formation of non-axisymmetric perturbations of multiple axial wavelengths. Like in experiments, the dominant wavelength increases with time, thus promoting the enhanced relative importance of one particular wavelength (Hussain *et al.*, 2011, p. 309). The dominant perturbation mode has strong structural similarity with the resonantly excited linear optimal perturbation. The simulation time is  $tt_r \leq 250$  – by (2.22) corresponding to  $zc^{-1} = 250 tt_r t_c^{-1} \approx 50$ . For the given turbulence intensity, the spectral evolution manifests in the gradually increasing importance of one isolated peak (Hussain *et al.*, 2011, fig. 5), not usually observed in experiments (e.g. Bailey & Tavoularis, 2008, fig. 11).

**Resonant optimal perturbation.** Hussain *et al.* (2011, pp. 312–313, 317–318) and Stout & Hussain (2016) study the nonlinear evolution of the Lamb–Oseen vortex initially subjected to the resonant linear optimal perturbation (with  $\alpha_z r_0 = 1.4$ , located around the critical layer at about  $rr_0^{-1} \approx 2.5$ ) of amplitude  $uU_{\theta,1}^{-1} \approx 6 \times 10^{-2}$  (corresponding to the turbulence intensity  $uU_\infty^{-1} \approx 0.25 uU_{\theta,1}^{-1} \approx 1.25\%$ ). For  $\Gamma/\nu = 5 \times 10^3$ , this initial perturbation excites core perturbations with an order of magnitude larger kinetic energy ( $u(\langle \mathbf{X}(t) \rangle)U_{\theta,1}^{-1} \approx 40 \times 10^{-2}$  or  $u(\langle \mathbf{X}(t) \rangle)U_\infty^{-1} \approx 10\%$ ) during an integration time of  $50 tt_r$  (the equivalent of  $zc^{-1} \approx 10$ ), as shown in fig. 6.14.

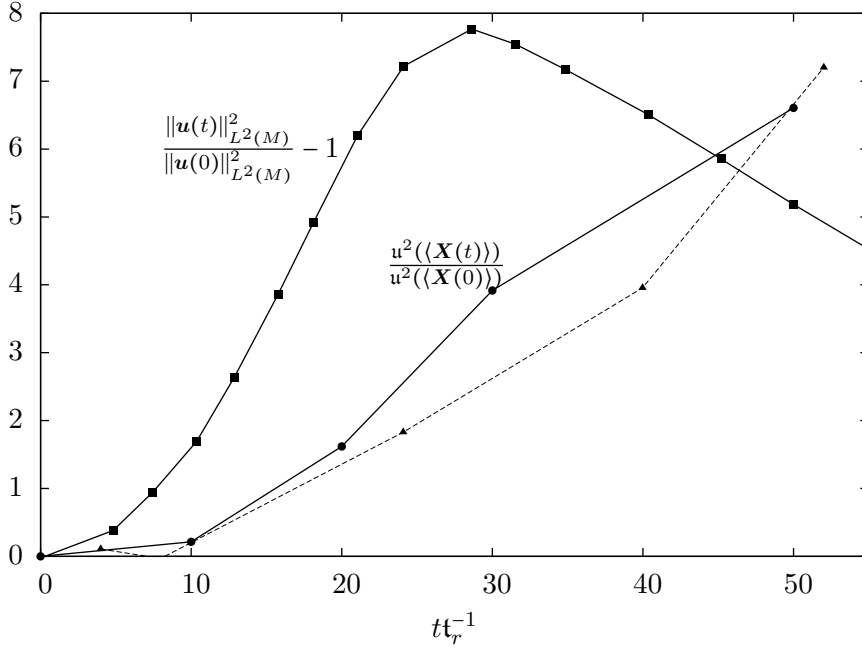


Figure 6.14: Perturbation kinetic energies in the Navier–Stokes DNS of Hussain *et al.* (2011, figs. 14 and 16). ■ integral kinetic energy; ● kinetic energy on the vortex axis (scaled by a factor 0.2); ▲ rescaled and shifted local energy from fig. 6.1.

Amplification by one order of magnitude over a downstream range of the order of ten chord lengths is in very good agreement with the observations in figs. 6.1 and 6.9. The final energy in the numerical experiment of Hussain *et al.* (2011) equals  $u^2(\langle \mathbf{X}(t) \rangle) U_\infty^{-2} = 10^{-2}$ . This is precisely the energy in the experiments of Heyes *et al.* (2004, fig. 7) and (as discussed above) a factor of three less than in figs. 6.1 and 6.9. However, this is not inconsistent, as the turbulence intensities in this latter experiment was about a factor three less than in the simulation. Moreover, the circulation-based Reynolds number in the experiment is approximately an order of magnitude larger, which indicates stronger resistance to deflection.

For comparison, the evolution of the kinetic energy (rescaled by a constant factor) at the vortex axis  $\langle \mathbf{X}(t) \rangle$  (fig. 6.1) is superposed on fig. 6.14. The agreement with the local kinetic energy in the simulation is reasonable.

**Long-wave optimal perturbation.** The axially homogeneous ( $\alpha_z = 0$ ) linear optimal perturbation leads to the most significant energy amplification (Antkowiak & Brancher, 2004; Heaton & Peake, 2007) and is therefore selected by Mao & Sherwin (2012, p. 51) for nonlinear time integration. Further linear and nonlinear transient-growth analysis of the two-dimensional dynamics is carried out by Navrose *et al.* (2018). In a linearised framework, the gain increases linearly with the specified finite time (in the optimization problem) (Antkowiak & Brancher, 2004, fig. 3; Navrose *et al.*, 2018, fig. 1).

The vortex-centre trajectory from the computations of Mao & Sherwin (2012, fig. 14c) is reproduced in fig. 6.15c. Mao & Sherwin (2012) assume  $R_\delta = 10^3$ ,  $q = 3$  and initialize the linear optimal perturbation with the energy<sup>14</sup>  $\|\mathbf{u}(0)\|_{L^2(M)}^2 = 10^{-3}$ ; the integration is carried out until  $tt_\delta^{-1} = 500$ . The perturbation-energy amplification follows the linearised dynamics

<sup>14</sup>Non-dimensionalized with  $|\delta U_z|$ .

for a substantial time before eventually saturating at about  $50 t_\delta$  (Mao & Sherwin, 2012, p. 55).

Navrose *et al.* (2018, p. 938) compare the nonlinear evolution of the two-dimensional Lamb–Oseen vortex initially perturbed by the linear and nonlinear optimal perturbation ( $R_\Gamma = 5 \times 10^3$ ), both initialized with a perturbation energy<sup>15</sup> of  $\|\mathbf{u}(0)\|_{L^2(M)}^2 = 10^{-2}$ . The resulting vortex-centre trajectories are shown in fig. 6.15*a, b, e, f*. Despite the different vortex models and parameter values, we observe essentially the same vortex motion as found by Mao & Sherwin (2012). Nonlinearity in the determination of the optimal perturbation seems to impact mainly the resulting energy amplitudes and sustainability, while it does not lead to a fundamentally different motion.

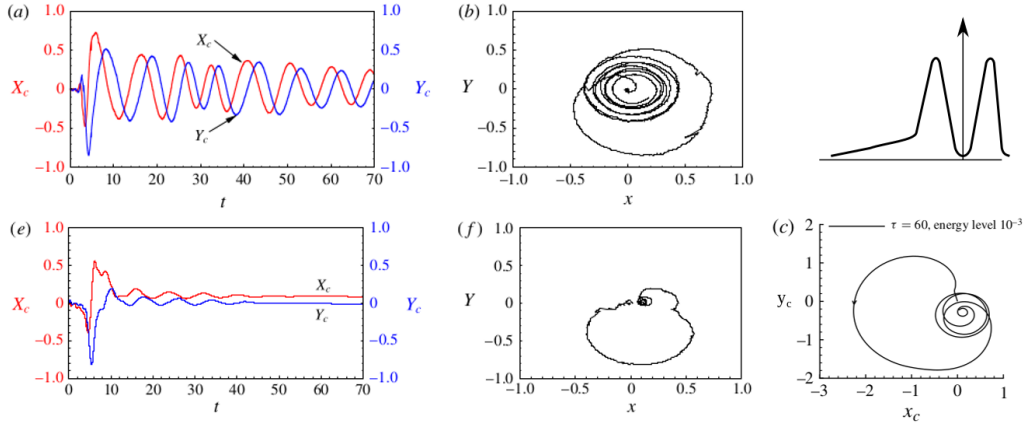


Figure 6.15: Vortex-centre trajectories. Nonlinear integration of the linear (bottom) and nonlinear (top) optimal perturbations to the Lamb–Oseen vortex (taken from Navrose *et al.*, 2018, fig. 14*e, f*, 15*a, b*). Nonlinear evolution of the linear optimal perturbation to the Batchelor vortex (reproduced from Mao & Sherwin, 2012, fig. 14*c*) and the corresponding schematic probability density.

Mao & Sherwin (2012, pp. 53–54) leave little doubt – ‘we see that this meandering is driven by the transient response of the vortex to the [linear,  $\alpha_z \rightarrow 0$ ] periphery perturbation, which is associated with the continuous spectra and induces perturbations inside the vortex core.’

However, comparing the centreline trajectories in fig. 6.15 to fig. 1.1, would not seem to describe the same motion – not even qualitatively. In fact, the most fundamental universal properties of experimental meandering are not met, namely amplitude growth and Gaussian statistics. By the law of large numbers, we expect the density of the trajectories to converge to the probability density of the vortex-centre position. Assume the trajectories in fig. 6.15 being statistically meaningful in this respect, the corresponding probability density of the vortex centre is sketched in fig. 6.15 (top right). Clearly, the spiralling motion (sinusoidal oscillation) in the numerical experiments corresponds to an  $M$ -shaped probability density rather than Gaussian statistics (Spalart, 1998, p. 112). As regards the experimental amplitude growth, we note two inconsistencies: the initial amplification is too fast, while the long-term dynamics is not sufficiently sustained.

It should probably also be noted, that the oscillatory motion in fig. 6.15, associated with meandering by Mao & Sherwin (2012) and Navrose *et al.* (2018), does not correspond to the ‘transient-growth phase’ *sensu stricto*. In fact, if meandering corresponds to the oscillatory motion, transient growth *literally* describes a transient here, merely driving the system to the meandering motion of interest. However in this case, meandering would

<sup>15</sup>Normalized with  $\Gamma/(2\pi r_0)$ .

not be directly related to transient growth, but rather sets in once the transient energy amplification phase is terminated. This puts not only into question the very motivation for doing transient-growth analysis but is also incompatible with the typical energy growth (cf. sec. 6.2).

**Remark 6.2.** The fact, that the linear response to the optimal perturbation visually resembles the ‘displacement mode’ of Fabre *et al.* (2006), led Navrose *et al.* (2018, p. 931) to conclude that the ‘displacement mode’ in fact must be in the span of the linear optimal perturbation. Recalling that the ‘displacement mode’ is associated with the discrete spectrum of the linearised Navier–Stokes operator, this conclusion is in stark contrast to the finding of Mao & Sherwin (2012, p. 42) (admittedly not for the same parameter values and base flow), that the linear optimal perturbations are constructed from the (inviscid) continuous spectrum. The analysis in sec. 6.3.1 shows that the communication between the vortex and the free stream is governed by the continuous spectrum (thus excluding the displacement mode, which pertains to the discrete spectrum). It should also be emphasized, that non-congruent input–output pairs are possible in a linear *non-normal* setting. In other words, the input and output spans can be different.

**Nonlinear evolution of the linearly initialized wake dynamics: evidence for vortex solitons?** Navrose *et al.* (2019) further compute the linear optimal perturbation of the flat-plate wake flow ( $\alpha = 5^\circ$ ,  $R_c = 10^3$ , corresponding to  $\Gamma/\nu \approx 170$ ; Navrose *et al.*, 2019, fig. 4). It is noted that the linear optimal perturbation to the trailing vortex is located around the vortex generator, i.e. upstream of the vortex formation (Navrose *et al.*, 2019, p. 411). Nonlinear integration of this linear optimal perturbation (initial energy  $\|\mathbf{u}(0)\|_{L^2(M)}^2 = 10^{-4} U_\infty^2 c^3$ ) leads to the propagation of a wave packet along the trailing vortex at a speed close to  $U_\infty$  (Navrose *et al.*, 2019, p. 413 and fig. 13). The phase shift between the perturbation velocities implies a helical core motion, such that the vortex centre traces an elliptical trajectory in a cross plane; this is reproduced in fig. 6.16a. Navrose *et al.* (2019, p. 421) propose the transient growth of perturbations located about the vortex generator as a candidate mechanism for vortex meandering. This identification of the observed dynamics with vortex meandering is probably based on a misconception of the experimental data shown in fig. 6.16b, in that Navrose *et al.* (2019) seem to infer an elliptical vortex-centre trajectory from the standard-deviation ellipse shown in red.

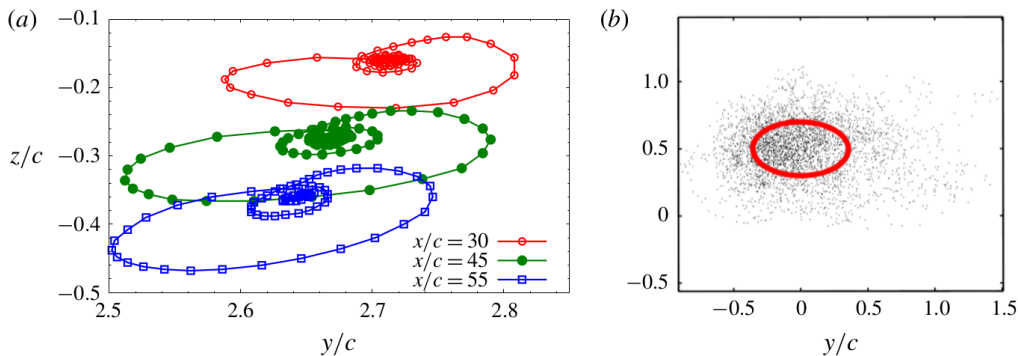


Figure 6.16: Vortex-axis trajectories in a cross plane. (a) Simulations of Navrose *et al.* (2019) and (b) Roy & Leweke (2008).

To be more precise, the motion shown in fig. 6.16 constitutes a valid manifestation of vortex meandering according to def. 2.6, yet it seems not to comply with the essential features of experimental *trailing-vortex* meandering (cf. sec. 2.4). It should be noted that the motion is qualitatively very similar to the trajectories shown in fig. 6.15. Furthermore,

Navier–Stokes DNS of the Lamb–Oseen vortex initially subjected to resonant linear optimal perturbation leads to a helical deflection of the vortex axis, too (Stout & Hussain, 2016, p. 361).

Indeed, this perturbation evolution seems rather reminiscent of soliton propagation on the vortex core than what is commonly referred to as meandering in trailing vortices. As shown by Hasimoto (1972), soliton perturbations of a vortex obey a non-linear Schrödinger equation for curvature and torsion of the vortex filament (see also Wu *et al.*, 2006, p. 404). This dynamics was observed experimentally on vortex columns in rotating turbulence (Hopfinger *et al.*, 1982; Maxworthy *et al.*, 1985).

**Critique of transient growth.** The normal distribution of the vortex centre is incompatible with the presence of a dominant helical vortex motion as it could result from an instability (Bailey & Tavoularis, 2008, p. 310).

The scale inconsistency between wrapped filaments in experiments and long-wavelength meandering on the one hand as well as long time scales of long-wavelength transient growth on the other hand led Bailey *et al.* (2018, p. 738) to conclude

it is unlikely that the observed long-wavelength meandering motions would be caused by transient growth.

The primary peak in the initial two-peak spectral signature of the no-grid case matches fairly well with the characteristic wavelength of resonance-induced transient growth at about  $\alpha r_1^{-1} \approx 1.4 \Leftrightarrow \lambda r_1^{-1} \approx 2\pi/1.4 \approx 4 \dots 5$ . Nevertheless, this wavelength is too short for ‘universal meandering’ and transient growth incapable to explain the shift in peak frequency; the associated perturbation is not sustained. Bailey *et al.* (2018, p. 736) speculate that this comparably short-wavelength critical-layer wave dissipates due to viscous diffusion. Almost identical energy content at subsequent stations suggests that a certain cross-feeding mechanism may be active (cf. sec. 2.4.2).

Pentelov (2014, p. 58), referring to Bailey *et al.* (2011), state that it exists ‘a regular helical component of vortex meandering, which is unaffected by the free-stream turbulence’.

Bailey *et al.* (2018, p. 744) observe that within the *stochastic meandering* it exists an azimuthal average motion reminiscent of a weak  $|m| = 1$  bending mode that did not scale on the turnover time. *On average*, the vortex was found to obey a *clockwise helical motion* along a path around the time-averaged axis, yet constituting a *rare event*. Put differently, ‘the vortex axis was on average in nearly rigid-body rotation about its average position ... covering the entire domain of its meandering’ (Bailey *et al.*, 2011, p. 6; Bailey *et al.*, 2018, pp. 740–743). They explain this (rare) motion in terms of a self-induced solid-body rotation of the vortex axis about its mean position on average (necessarily countergrade). Bailey *et al.* (2018, p. 743) come to the conclusion that

all these observations prove conclusively that the organized helical motion was only a small component of the overall meandering, which was largely stochastic.

This point of view corresponds to an ‘inverse’ scenario or causality (Bailey *et al.*, 2018, p. 745, cf. Alekseenko *et al.*, 2007):

**Conjecture 6.2.** *Meandering is first and foremost stochastic due to momentum exchange with impacting eddies. The interaction is limited by the turnover time (intrinsic scaling) privileging long-wavelength motion. As a consequence of this long-wave small-amplitude motion self induction is a generic feature which establishes a helical wave form on average as a rare event.*

Pentelov (2014, §5.1.3) (see also Bailey *et al.*, 2018, p. 731) found that the instantaneous axis deformation (reconstructed 9th-order polynomial from LIF) was *often* nearly planar with the plane including the mean axis but the orientation gradually changing among frames. Thus, arguing that a helical axis motion can be excluded as the most pertinent contribution to meandering. The deformed vortex axis *often* appeared to have a sinusoidal shape in these planes.

## 7 | Some final thoughts

Knowledge is a function of being.

---

— A. Huxley: The Perennial Philosophy

The Navier–Stokes dynamics is inherently nonlinear, so that meaningfulness and pertinence of a linear model can and perhaps should *a priori* be doubted. It is however true that highly important mechanisms can be unveiled from the linear dynamics which are of relevance for the full problem. This principal conflict is nicely expressed by F. Dürrenmatt (*Das Versprechen*) –

Ihr versucht nicht, euch mit der Realität herumzuschlagen, die sich uns immer wieder entzieht, sondern ihr stellt eine Welt auf, die zu bewältigen ist. Diese Welt mag vollkommen sein, möglich, aber sie ist eine Lüge. Laßt die Vollkommenheit fahren, wollt ihr weiterkommen, zu den Dingen, zu der Wirklichkeit, wie es sich für Männer schickt, sonst bleibt ihr sitzen, mit nutzlosen Stilübungen beschäftigt.<sup>1</sup>

A possible argument here for the validity of a linear model is provided by the often called intrinsic property of vortices to separate different regimes. As such, the *statistics* of meandering might be explainable by a linear reaction of ordered nature to random forcing by the free stream. Mathematically, the driving random force is associated with the advective nonlinearity  $\mathbf{f} := \langle \nabla_{\mathbf{u}} \mathbf{u} \rangle - \nabla_{\mathbf{u}} \mathbf{u}$  ( $\nabla_{\mathbf{u}}$  is the covariant derivative; Synge & Schild, 1978). This idea of turbulence as a driven linear system has been developed by Landahl (1967; 1975; 1989) and is frequently used in the mathematical theory of the Navier–Stokes equations (e.g. Sohr, 2001). Recent popularity is mainly due to mean-flow and resolvent analysis (McKeon, 2017; Jiménez, 2018, among many others).

We provided some evidence here that this idea and a linear model indeed holds (at least in some respects) for vortex meandering. To be precise, it would seem to be able to elucidate some important aspects of the dynamics which are related to amplitudes and energy, while it seems to fail for the question of ‘frequency selection’ (if it exists).

So far, the validity of linearity has been approved (exclusively) by its invariance with respect to scalar multiplication (i.e. finite vs infinitesimal perturbations). This is only one aspect of a linear transformation, and not necessarily the more relevant. By definition, an operator  $\mathbf{A} : X \rightarrow Y$  is linear if and only if

$$\mathbf{A}(\alpha_1 x_1 + \alpha_2 x_2) = \alpha_1 \mathbf{A}x_1 + \alpha_2 \mathbf{A}x_2$$

for all  $x_1, x_2 \in X$  and scalars  $\alpha_1, \alpha_2$  (Kato, 1980, p. 16). Perhaps, by carefully designing an experiment, the superposition principle could indicate a way to corroborate (or reject) linearity of vortex meandering.

---

<sup>1</sup> You do not try to deal with the reality that surrounds us, you set up a world that can be managed; this world may be perfect, but it’s a lie. Let perfection go, if you want to get ahead, to things, to the reality that is appropriate for men, otherwise you will remain seated, occupied with useless style exercises.

In any case, the fact that we systematically observe structurally similar responses (viz. the dipole pattern) in experiment and by various linear approaches is not conclusive. In the words of Schrödinger (1992, p. 47) –

The evidence that two features, similar in appearance, are based on the same principle, is always precarious as long as the principle itself is unknown.

Unlike the energy balance and amplitude growth, where reasonable agreement between theory and experiment has been obtained, the 'frequency selection' would not seem to be governed by a linear mechanism. The here held point of view is best illustrated by quoting A. Einstein in a conversation with W. Heisenberg (Heisenberg, 1969, p. 80) –

Erst die Theorie entscheidet darüber, was man beobachten kann.<sup>2</sup>

In the case of vortex meandering, this causality is observed in at least two respects. First, the general turbulence theory assumes a 'transition problem', where the laminar state passes over into a gradually more complex turbulent state. We suggest here that vortex dynamics does not follow the 'route to turbulence', but is atypical in the sense that it progressively increases its orderliness, while the dynamics is not of a simple diffusion kind.

The second aspect where the theory seems to dictate expectations in experiments which have not been satisfied yet, is the ongoing seek for coherence and '*the* meandering frequency'. It appears that the idea of coherence originated in the work of Bandyopadhyay *et al.* (1991) and is historically correlated with the emphasis on linear dynamics in general and particularly with considerable progress made in the understanding of linear stability and transient growth. As such, it seems that the expectation that there is *one* meandering frequency is largely induced by the contemporary theory. This is not far from the quotation of A. Huxley above.

---

<sup>2</sup>It is the theory which decides what we can observe.

## 8 | Conclusion

Zwischen dem Ähnlichsten gerade lügt der Schein  
am schönsten; denn die kleinste Kluft ist am  
schwersten zu überbrücken.

---

— F. Nietzsche: Also sprach Zarathustra

Vortex meandering is the principal manifestation of unsteadiness affecting experiments of vortex-dominated fluid flow. Despite recurrent observation of the phenomenon for trailing vortices since the 1970s, the governing physics and mechanisms continue to escape a through understanding as of this writing. The objective of the present work was formulated in the Introduction by the question – *Why do vortices meander?*

Before attempting an explanation of the origins of the phenomenon, we must *define* what vortex meandering consists of. Despite the multitude of studies, clear cut definitions are rare and even fundamental notions are often employed without proper introduction. We propose an elementary meandering definition, viz. the displacement of the vortex as a whole, which turns out to be not sufficiently sharp for practical purposes. Restricting to trailing vortices, we then isolated three fundamental characteristics which are generically and inevitably associated with meandering. Namely,

- (i) downstream amplitude growth
- (ii) apparent coherent–stochastic duality and
- (iii) progressive concentration and amplification of energy in the vortex core.

Before attempting explanations of these three main features of trailing-vortex meandering, we discussed the previously proposed explanation approaches. To a large extent, they fall into either one of the two categories called 'extrinsic' or 'intrinsic' mechanisms. That is, they seek to explain the phenomenon as either completely externally induced (e.g. by the surrounding turbulence) or as purely internally caused (e.g. as the consequence of an instability). Both restrictions seem inappropriate and rather meandering combines both aspects in an intricate manner. We propose to model meandering as a problem of *generalized receptivity*.

As regards the downstream amplitude growth, we have considerable experimental evidence for  $\sigma(t) \sim u\sqrt{t\Gamma^{-1}}$  ( $t = zU_\infty^{-1}$ ) to hold universally. This finding has several important implications. First, the meandering amplitude  $\sigma$  depends *linearly* on the turbulence intensity  $u$ , thus suggesting a linear excitation mechanism of the vortex by the free stream. Second, meandering is inversely and nonlinearly proportional to the vortex strength  $\Gamma$ , which hints at a combined intrinsic-extrinsic receptivity dynamics – a conflict between external excitation and internal resistance. This excitation-resistance duality together with the characteristic time dependence  $\sim \sqrt{t}$  of the vortex-centre standard deviation  $\sigma(t)$  is strongly reminiscent of a Brownian motion of the vortex as a whole. This is resumed in the metaphor (in the sense of D. Bohm) – a vortex *is* a particle and meandering *is* a Brownian motion.

The apparent coexistence of stochastic and coherent, ordered dynamics is probably the most puzzling and woolly aspect of vortex meandering. In essence, the broadband continuous spectral signature is commonly taken as evidence that the dynamics is stochastic. At the same time, meandering is usually associated only with the low-frequency range and visualizations suggest a rather organized nature. The idea of coherence is so profound that several previous studies attempted to identify *the* meandering frequency. The point we want to make in the present work is, that vortex meandering is the manifestation of a 'return-to-order' principle rather than a classical 'transition-to-turbulence' problem. This has important implications for modelling and breaks with previously and commonly held perceptions. We suggest a formulation as a generalized receptivity. Increasing orderliness is quantified by appeal to nonlinear time series and information entropy analysis (for the first time to the best of our knowledge). This analysis strongly shows that meandering is not stochastic, while it is not associated with a distinct frequency either. The progressive trend towards orderliness is reflected in the gradually decreasing phase volume which accommodates the dynamics, decreasing entropy and the characteristic recurrence structure. A provocative metaphor resuming the findings would be: a vortex *is* a 'living' organism.

The concentration and amplification of kinetic energy in the vortex core is a very unusual behaviour as compared to other open shear flows. In some sense, it is just a complementary perspective of the inherent ordering nature of vortices previously discussed. The progressive accumulation of fluctuation energy inside the vortex unlike global decay in wing wakes is just one example of the intrinsic tendency of vortices to separate different regimes inside from outside. Another such characteristic of first importance for meandering being the closeness with respect to mass transport. This general distinction suggests that the nonlinear advection in the Navier–Stokes equations is spatially associated with the free-stream turbulence, while the vortex-meandering dynamics are essentially linear. The very nature of vortex meandering suggests that the free-stream and core dynamics are indeed coupled by a linear transfer operator. This is the dynamic formulation of the problem of generalized receptivity, which we solve formally by appeal to the resolvent.

The essential outcome of this study is that linear receptivity of vortices to free-stream disturbances is intimately linked to the (inviscid) continuous spectrum. The thus identified three protagonists of vortex meandering are (*i*) the mean flow (inexhaustible energy reservoir), (*ii*) the (dipole-like) core perturbation (daughter) and (*iii*) filament-like periphery perturbations with non-zero  $L^2$ -projection onto the Reynolds stresses (mother). This interplay is precisely the mother–daughter mechanism proposed by Boberg & Brosa (1988). It further has crucial parallels with the De-Broglie–Bohm interpretation of quantum mechanics.

Complementary POD analysis of the experimental data confirms the theoretically predicted (dipole-like) response structure. More importantly, the perturbation energy amplification at the expense of the mean flow is entirely consistent with the suggested model. We would like to emphasize that the proposed model of an external low-energy information field (mother or forcing) remotely controlling the high-energy transfer between the mean and the core perturbations breaks with the commonly held idea of energy transfer between the free-stream and vortex-core perturbations directly.

Therefore, this study suggests – while the amplitude and core-energy amplification seem indeed to be governed by linear mechanisms to some extent (at least they seem to hint at the pertinent mechanisms), the 'frequency selection' is nonlinear. It appears that the scales are imposed by the vortex (inherently nonlinear), while the amplitudes are significantly determined by the surrounding flow, obeying an essentially linear dynamics.

# Bibliography

- Abarbanel, H. D. I. *et al.* (1993). ‘The analysis of observed chaotic data in physical systems’. In: *Reviews of Modern Physics* 65.4, pp. 1331–1392.
- Adrian, R. J. (1991). ‘Particle-Imaging Techniques for Experimental Fluid Mechanics’. In: *Annual Review of Fluid Mechanics* 23.1, pp. 261–304.
- Alekseenko, S. V., P. A. Kuibin & V. L. Okulov (2007). *Theory of concentrated vortices: an introduction*. Springer Science & Business Media.
- Antkowiak, A. (2005). ‘Dynamique aux temps courts d’un tourbillon isolé’. PhD thesis. Université Paul Sabatier de Toulouse.
- Antkowiak, A. & P. Brancher (2004). ‘Transient energy growth for the Lamb–Oseen vortex’. In: *Physics of Fluids* 16.1, pp. L1–L4.
- Aref, H. & E. P. Flinchem (1984). ‘Dynamics of a vortex filament in a shear flow’. In: *Journal of Fluid Mechanics* 148, pp. 477–497.
- Arendt, S., D. C. Fritts & Ø. Andreassen (1997). ‘The initial value problem for Kelvin vortex waves’. In: *Journal of Fluid Mechanics* 344, pp. 181–212.
- Ash, R. L. & M. R. Khorrami (1995). ‘Vortex stability’. In: *Fluid vortices*. Ed. by S. I. Green. Springer, pp. 317–372.
- Atkins, P. (1984). *The second law*. Scientific American Library.
- (2010). *The laws of thermodynamics: A very short introduction*. Oxford University Press.
- Aubry, N., R. Guyonnet & R. Lima (1991). ‘Spatiotemporal analysis of complex signals: theory and applications’. In: *Journal of Statistical Physics* 64.3-4, pp. 683–739.
- Aubry, N., R. Guyonnet & R. Lima (1992). ‘Spatio-temporal symmetries and bifurcations via bi-orthogonal decompositions’. In: *Journal of Nonlinear Science* 2.2, pp. 183–215.
- Bailey, S. C. C. & S. Tavoularis (2008). ‘Measurements of the velocity field of a wing-tip vortex, wandering in grid turbulence’. In: *Journal of Fluid Mechanics* 601, pp. 281–315.
- Bailey, S. C. C., S. Tavoularis & B. H. K. Lee (2006). ‘Effects of free-stream turbulence on wing-tip vortex formation and near field’. In: *Journal of Aircraft* 43.5, pp. 1282–1291.
- Bailey, S. C. C. *et al.* (2018). ‘Experimental investigation of the scaling of vortex wandering in turbulent surroundings’. In: *Journal of Fluid Mechanics* 843, pp. 722–747.
- Bailey, S. C. *et al.* (2011). ‘Long-wavelength vortex motion induced by free-stream turbulence’. In: *TSFP DIGITAL LIBRARY ONLINE*. Begel House Inc.

- Baker, G. R. *et al.* (1974). ‘Laser anemometer measurements of trailing vortices in water’. In: *Journal of Fluid Mechanics* 65.2, pp. 325–336.
- Bandyopadhyay, P. R., D. J. Stead & R. L. Ash (1991). ‘Organized nature of a turbulent trailing vortex’. In: *AIAA Journal* 29.10, pp. 1627–1633.
- Barenblatt, G. I. (1996). *Scaling, self-similarity, and intermediate asymptotics*. Cambridge University Press.
- Batchelor, G. K. (1953). *The theory of homogeneous turbulence*. Cambridge University Press.
- (1964). ‘Axial flow in trailing line vortices’. In: *Journal of Fluid Mechanics* 20, pp. 645–658.
- (2000). *An Introduction to Fluid Dynamics*. Cambridge University Press.
- Ben-Mizrachi, A., I. Procaccia & P. Grassberger (1984). ‘Characterization of experimental (noisy) strange attractors’. In: *Physical Review A* 29.2, pp. 975–977.
- Beninati, M. L. & J. S. Marshall (2005). ‘An experimental study of the effect of free-stream turbulence on a trailing vortex’. In: *Experiments in Fluids* 38.2, pp. 244–257.
- Beresh, S. J., J. F. Henfling & R. W. Spillers (2010). ‘Meander of a fin trailing vortex and the origin of its turbulence’. In: *Experiments in Fluids* 49.3, pp. 599–611.
- Berkooz, G., P. Holmes & J. L. Lumley (1993). ‘The Proper Orthogonal Decomposition in the Analysis of Turbulent Flows’. In: *Annual Review of Fluid Mechanics* 25, pp. 539–575.
- Birch, D. M. (2012). ‘Self-similarity of trailing vortices’. In: *Physics of Fluids* 24.2, p. 025105.
- Boberg, L. & U. Brosa (1988). ‘Onset of turbulence in a pipe’. In: *Zeitschrift für Naturforschung* 43.8–9, pp. 697–726.
- Boffetta, G. & R. E. Ecke (2012). ‘Two-dimensional turbulence’. In: *Annual Review of Fluid Mechanics* 44, pp. 427–451.
- Bohm, D. (1980). *Wholeness and the Implicate Order*. Routledge & Kegan Paul.
- Bohm, D. & F. D. Peat (1987). *Science, order, and creativity*. Bantam Books.
- Bölle, T. *et al.* (2020). ‘On the linear receptivity of trailing vortices’. In: *Journal of Fluid Mechanics* 908, p. 29.
- Bradley, E. & H. Kantz (2015). ‘Nonlinear time-series analysis revisited’. In: *Chaos: An Interdisciplinary Journal of Nonlinear Science* 25.9, p. 097610.
- Bradshaw, P (1969). ‘The analogy between streamline curvature and buoyancy in turbulent shear flow’. In: *Journal of Fluid Mechanics* 36.1, pp. 177–191.
- Buchhave, P., W. K. George & J. L. Lumley (1979). ‘The Measurement of Turbulence with the Laser-Doppler Anemometer’. In: *Annual Review of Fluid Mechanics* 11.1, pp. 443–503.
- Chigier, N. A. & V. R. Corsiglia (1971). *Tip vortices: Velocity distributions*. Tech. rep. National Aeronautics and Space Administration.
- (1972). ‘Wind-tunnel studies of wing wake turbulence’. In: *Journal of Aircraft* 9.12, pp. 820–825.

- Chow, J., G. Zilliac & P. Bradshaw (1997). *Turbulence measurements in the near field of a wingtip vortex*. National Aeronautics and Space Administration.
- Comte-Bellot, G. (1976). ‘Hot-Wire Anemometry’. In: *Annual Review of Fluid Mechanics* 8.1, pp. 209–231.
- Corsiglia, V. R., R. G. Schwind & N. A. Chigier (1973). ‘Rapid Scanning, Three-Dimensional Hot-Wire Anemometer Surveys of Wing-Tip Vortices’. In: *Journal of Aircraft* 10.12, pp. 752–757.
- Cotel, A. J. (2002). ‘Turbulence inside a vortex: Take two’. In: *Physics of Fluids* 14.8, pp. 2933–2934.
- Cotel, A. J. & R. E. Breidenthal (1999). ‘Turbulence inside a vortex’. In: *Physics of Fluids* 11.10, pp. 3026–3029.
- Crow, S. C. (1970). ‘Stability theory for a pair of trailing vortices’. In: *AIAA Journal* 8.12, pp. 2172–2179.
- Da Prato, G. & J. Zabczyk (1992). *Stochastic Equations in Infinite Dimensions*. Cambridge University Press.
- Dahmen, W. & A. Reusken (2008). *Numerik für Ingenieure und Naturwissenschaftler*. Springer.
- Deem, E. *et al.* (2013). ‘Deconvolution Correction for Wandering in Wingtip Vortex Flow-field Data’. In: *Journal of Fluid Science and Technology* 8.2, pp. 219–232.
- Del Pino, C. *et al.* (2011). ‘Dynamics of the wing-tip vortex in the near field of a NACA 0012 aerofoil’. In: *The Aeronautical Journal* 115.1166, pp. 229–239.
- Devaney, R. (1989). *An introduction to chaotic dynamical systems*. Westview press.
- Devenport, W. J. *et al.* (1996). ‘The structure and development of a wing-tip vortex’. In: *Journal of Fluid Mechanics* 312, pp. 67–106.
- Dürr, H.-P. (2009). *Warum es ums Ganze geht*. Oekom-Verlag.
- Eckmann, J.-P. & D. Ruelle (1985). ‘Ergodic theory of chaos and strange attractors’. In: *Reviews of Modern Physics* 57.3, pp. 617–656.
- Eckmann, J.-P., S. Oliffson Kamphorst & D. Ruelle (1987). ‘Recurrence Plots of Dynamical Systems’. In: *Europhysics Letters* 4.9, pp. 973–977.
- Edstrand, A. M. *et al.* (2016). ‘On the mechanism of trailing vortex wandering’. In: *Journal of Fluid Mechanics* 801.
- Edstrand, A. M. *et al.* (2018). ‘A parallel stability analysis of a trailing vortex wake’. In: *Journal of Fluid Mechanics* 837, pp. 858–895.
- Engel, K.-J. & R. Nagel (2000). *One-Parameter Semigroups for Linear Evolution Equations*. Springer-Verlag.
- Fabre, D. (2002). ‘Instabilités et instationnarités dans les tourbillons : Application aux sillages d’avions’. PhD thesis. Université Paris VI.
- Fabre, D. & L. Jacquin (2004). ‘Viscous instabilities in trailing vortices at large swirl numbers’. In: *Journal of Fluid Mechanics* 500, pp. 239–262.
- Fabre, D., D. Sipp & L. Jacquin (2006). ‘Kelvin waves and the singular modes of the Lamb-Oseen vortex’. In: *Journal of Fluid Mechanics* 551, pp. 235–274.

- Farrell, B. F. & P. J. Ioannou (1996). ‘Generalized stability theory. Part I: Autonomous operators’. In: *Journal of the atmospheric sciences* 53.14, pp. 2025–2040.
- Foias, C. *et al.* (2001). *Navier–Stokes Equations and Turbulence*. Encyclopedia of mathematics and its applications. Cambridge University Press.
- Foti, D. *et al.* (2016). ‘Wake meandering statistics of a model wind turbine: Insights gained by large eddy simulations’. In: *Physical Review Fluids* 1.4, p. 044407.
- Friedlander, S. & V. Yudovich (1999). ‘Instabilities in fluid motion’. In: *Notices of the AMS* 46.11, pp. 1358–1367.
- Friedlander, S., W. Strauss & M. Vishik (1997). ‘Nonlinear instability in an ideal fluid’. In: 14.2, pp. 187–209.
- Friedlander, S., N. Pavlović & R. Shvydkoy (2006). ‘Nonlinear instability for the Navier–Stokes equations’. In: *Communications in mathematical physics* 264.2, pp. 335–347.
- Frisch, U. (1995). *Turbulence: The legacy of A. N. Kolmogorov*. Cambridge University Press.
- Gallay, T. & D. Smets (2019). ‘On the linear stability of vortex columns in the energy space’. In: *Journal of Mathematical Fluid Mechanics* 21.4, pp. 1–27.
- (2020). ‘Spectral stability of inviscid columnar vortices’. In: *Analysis & PDE* 13.6, pp. 1777–1832.
- García-Ortiz, J. H. *et al.* (2019). ‘A complementary numerical and experimental study of the influence of Reynolds number on theoretical models for wingtip vortices’. In: *Computers & Fluids* 180, pp. 176–189.
- Georgescu, A. (1985). *Hydrodynamic stability theory*. Springer Science & Business Media.
- Gerz, T., F. Holzäpfel & D. Darracq (2002). ‘Commercial aircraft wake vortices’. In: *Progress in Aerospace Sciences* 38.3, pp. 181–208.
- Giuni, M. (2013). ‘Formation and early development of wingtip vortices’. University of Glasgow.
- Grassberger, P. & I. Procaccia (1983a). ‘Characterization of Strange Attractors’. In: *Physical Review Letters* 50.5, pp. 346–349.
- (1983b). ‘Estimation of the Kolmogorov entropy from a chaotic signal’. In: *Physical Review A* 28.4, p. 2591.
- (1983c). ‘Measuring the strangeness of strange attractors’. In: *Physica D* 9.1-2, pp. 189–208.
- Grassberger, P., T. Schreiber & C. Schaffrath (1991). ‘Nonlinear time sequence analysis’. In: *International Journal of Bifurcation and Chaos* 1.03, pp. 521–547.
- Green, S. I. & A. J. Acosta (1991). ‘Unsteady flow in trailing vortices’. In: *Journal of Fluid Mechanics* 227, pp. 107–134.
- Green, S. I. (1995). ‘Wing Tip Vortices’. In: *Fluid Vortices*. Ed. by S. I. Green. Springer, pp. 427–469.
- Gu, Y. (2013). ‘Statistics of optical vortex wander on propagation through atmospheric turbulence’. In: *JOSA A* 30.4, pp. 708–716.

- Guckenheimer, J. (1986). ‘Strange attractors in fluids: another view’. In: *Annual Review of Fluid Mechanics* 18.1, pp. 15–31.
- Gursul, I. & W. Xie (2000). ‘Origin of Vortex Wandering over Delta Wings’. In: *Journal of Aircraft* 37.2, pp. 348–350.
- Haller, G. *et al.* (2016). ‘Defining coherent vortices objectively from the vorticity’. In: *Journal of Fluid Mechanics* 795, pp. 136–173.
- Hasimoto, H. (1972). ‘A soliton on a vortex filament’. In: *Journal of Fluid Mechanics* 51.3, pp. 477–485.
- Heaton, C. J. (2007a). ‘Centre modes in inviscid swirling flows and their application to the stability of the Batchelor vortex’. In: *Journal of Fluid Mechanics* 576, pp. 325–348.
- (2007b). ‘Optimal growth of the Batchelor vortex viscous modes’. In: *Journal of Fluid Mechanics* 592, pp. 495–505.
- Heaton, C. J. & N. Peake (2007). ‘Transient growth in vortices with axial flow’. In: *Journal of Fluid Mechanics* 587, pp. 271–301.
- Heaton, C. J., J. W. Nichols & P. J. Schmid (2009). ‘Global linear stability of the non-parallel Batchelor vortex’. In: *Journal of Fluid Mechanics* 629, pp. 139–160.
- Heisenberg, W. (1959). *Physik und Philosophie*. Hirzel.
- (1969). *Der Teil und das Ganze: Gespräche im Umkreis der Atomphysik*. Piper Verlag.
- Helmholtz, H. (1858). ‘Über Integrale der hydrodynamischen Gleichungen, welche den Wirbelbewegungen entsprechen’. In: *Journal für die reine und angewandte Mathematik* 55, pp. 25–55.
- Heyes, A., R. Jones & D. Smith (2004). ‘Wandering of wing-tip vortices’. In: *International Symposia on Applications of Laser Techniques to Fluid Mechanics*, pp. 1–20.
- Hirota, R. (1973). ‘Exact envelope-soliton solutions of a nonlinear wave equation’. In: *Journal of Mathematical Physics* 14.7, pp. 805–809.
- Holmes, P., J. L. Lumley & G. Berkooz (1998). *Turbulence, coherent structures, dynamical systems and symmetry*. Cambridge University Press.
- Holzäpfel, F. *et al.* (2002). ‘Aircraft wake vortex evolution and decay in idealized and real environments: methodologies, benefits and limitations’. In: *Advances in LES of Complex Flows*. Springer, pp. 293–309.
- Holzäpfel, F. *et al.* (2003). ‘Analysis of wake vortex decay mechanisms in the atmosphere’. In: *Aerospace Science and Technology* 7.4, pp. 263–275.
- Hopf, E. (1948). ‘A mathematical example displaying features of turbulence’. In: *Communications on Pure and Applied Mathematics* 1.4, pp. 303–322.
- Hopfinger, E. J. & G. J. F. Van Heijst (1993). ‘Vortices in rotating fluids’. In: *Annual Review of Fluid Mechanics* 25.1, pp. 241–289.
- Hopfinger, E. J., F. K. Browand & Y. Gagne (1982). ‘Turbulence and waves in a rotating tank’. In: *Journal of Fluid Mechanics* 125, pp. 505–534.
- Hossain, M., W. H. Matthaeus & D. Montgomery (1983). ‘Long-time states of inverse cascades in the presence of a maximum length scale’. In: *Journal of plasma physics* 30.3, pp. 479–493.

- Huerre, P. & P. A. Monkewitz (1990). ‘Local and global instabilities in spatially developing flows’. In: *Annual review of fluid mechanics* 22.1, pp. 473–537.
- Hunt, J. C. R., A. A. Wray & P. Moin (1988). ‘Eddies, streams, and convergence zones in turbulent flows’. In: *Studying Turbulence Using Numerical Simulation Databases, 2. Proceedings of the 1988 Summer Program*, p. 193.
- Hussain, A. K. M. F. (1986). ‘Coherent structures and turbulence’. In: *Journal of Fluid Mechanics* 173, pp. 303–356.
- Hussain, F., D. S. Pradeep & E. Stout (2011). ‘Nonlinear transient growth in a vortex column’. In: *Journal of Fluid Mechanics* 682, pp. 304–331.
- Iungo, G. V. (2017). ‘Wandering of a Wing-Tip Vortex: Rapid Scanning and Correction of Fixed-Point Measurements’. In: *Journal of Aircraft* 54.5, pp. 1779–1790.
- Iungo, G. V., P. Skinner & G. Buresti (2009). ‘Correction of wandering smoothing effects on static measurements of a wing-tip vortex’. In: *Experiments in Fluids* 46.3, pp. 435–452.
- Iwanski, J. S. & E. Bradley (1998). ‘Recurrence plots of experimental data: To embed or not to embed?’ In: *Chaos: An Interdisciplinary Journal of Nonlinear Science* 8.4, pp. 861–871.
- Jacquín, L. & C. Pantano (2002). ‘On the persistence of trailing vortices’. In: *Journal of Fluid Mechanics* 471, pp. 159–168.
- Jacquín, L. *et al.* (2001). ‘The Properties of a Transport Aircraft Wake in the Extended Near Field : An Experimental Study’. In: *39th Aerospace Sciences Meeting and Exhibit*, p. 1038.
- Jacquín, L. *et al.* (2003). ‘Instability and unsteadiness of aircraft wake vortices’. In: *Aerospace Science and Technology* 7.8, pp. 577–593.
- Jacquín, L. (2005). ‘Aircraft trailing vortices: an introduction’. In: *Comptes Rendus Physique* 6.4-5, pp. 395–398.
- Jacquín, L. *et al.* (2005). ‘Unsteadiness, instability and turbulence in trailing vortices’. In: *Comptes Rendus Physique* 6.4-5, pp. 399–414.
- Jacquín, L. *et al.* (2007). ‘An Experiment on Jet-Wake Vortex Interaction’. In: *Collection of Technical Papers - 37th AIAA Fluid Dynamics Conference* 3.
- Jammy, S. P., N. Hills & D. M. Birch (2014). ‘Boundary conditions and vortex wandering’. In: *Journal of Fluid Mechanics* 747, pp. 350–368.
- Jeong, J. & F. Hussain (1995). ‘On the identification of a vortex’. In: *Journal of fluid mechanics* 285, pp. 69–94.
- Jiménez, J. *et al.* (1993). ‘The structure of intense vorticity in isotropic turbulence’. In: *Journal of Fluid Mechanics* 255, pp. 65–90.
- Jiménez, J. (2018). ‘Coherent structures in wall-bounded turbulence’. In: *Journal of Fluid Mechanics* 842.
- Johnson, H. (2016). ‘Nonlinear dynamics of wake vortices’. PhD thesis. Université Paris-Saclay.
- Joseph, D. D. (1976). *Stability of Fluid Motions I*. Springer.

- Kantz, H. & T. Schreiber (2004). *Nonlinear time series analysis*. Cambridge University Press.
- Kato, T. (1980). *Perturbation theory for linear operators*. Springer.
- Kerswell, R. (2018). ‘Nonlinear Nonmodal Stability Theory’. In: *Annual Review of Fluid Mechanics* 50.1, pp. 319–345.
- Khorrami, M. R. (1991). ‘On the viscous modes of instability of a trailing line vortex’. In: *Journal of Fluid Mechanics* 225, pp. 197–212.
- Klein, R. & A. J. Majda (1991). ‘Self-stretching of a perturbed vortex filament I. The asymptotic equation for deviations from a straight line’. In: *Physica D: Nonlinear Phenomena* 49.3, pp. 323–352.
- Klein, S. & G. Nellis (2012). *Thermodynamics*. Cambridge University Press.
- Kraichnan, R. H. (1967). ‘Inertial ranges in two-dimensional turbulence’. In: *The Physics of Fluids* 10.7, pp. 1417–1423.
- Kraichnan, R. H. & D. Montgomery (1980). ‘Two-dimensional turbulence’. In: *Reports on Progress in Physics* 43.5, pp. 547–619.
- Landahl, M. T. (1967). ‘A wave-guide model for turbulent shear flow’. In: *Journal of Fluid Mechanics* 29.3, pp. 441–459.
- (1975). ‘Wave breakdown and turbulence’. In: *SIAM Journal on Applied Mathematics* 28.4, pp. 735–756.
- (1989). ‘Boundary layer turbulence regarded as a driven linear system’. In: *Physica D: Nonlinear Phenomena* 37.1-3, pp. 11–19.
- Landau, L. D. & E. M. Lifšic (1959). *Fluid Mechanics*. Pergamon Press.
- (1980). *Statistical Physics*. Pergamon Press.
- Lanford, O. E. (1982). ‘The strange attractor theory of turbulence’. In: *Annual Review of Fluid Mechanics* 14.1, pp. 347–364.
- Larsen, G. C. *et al.* (2008). ‘Wake meandering: a pragmatic approach’. In: *Wind energy* 11.4, pp. 377–395.
- Lax, P. D. (2007). *Linear Algebra and Its Applications*. Wiley-Interscience.
- Lesieur, M. (2008). *Turbulence in Fluids*. 4th ed. Vol. 84. Springer.
- Lessen, M., P. J. Singh & F. Paillet (1974). ‘The stability of a trailing line vortex. Part 1. Inviscid theory’. In: *Journal of Fluid Mechanics* 63.4, pp. 753–763.
- Lingevitch, J. F. & A. J. Bernoff (1995). ‘Distortion and evolution of a localized vortex in an irrotational flow’. In: *Physics of Fluids* 7.5, pp. 1015–1026.
- Lugt, H. J. (1979). ‘The Dilemma of Defining a Vortex’. In: *Recent Developments in Theoretical and Experimental Fluid Mechanics: Compressible and Incompressible Flows*. Ed. by U. Müller, K. G. Roesner & B. Schmidt. Springer, pp. 309–321.
- Lumley, J. L. (1970). *Stochastic tools in turbulence*. Academic Press, Inc.
- Lumley, J. L. (1981). ‘Coherent structures in turbulence’. In: *Transition and Turbulence*. Ed. by R. E. Meyer, pp. 215–242.

- Lund, D. E. & J. T. Snow (1993). ‘Laser Doppler velocimeter measurements in tornadolike vortices’. In: *The Tornado: Its Structure, Dynamics, Prediction, and Hazards*, pp. 297–306.
- Malraison, B. *et al.* (1983). ‘Dimension of strange attractors: an experimental determination for the chaotic regime of two convective systems’. In: *Journal de Physique – Lettres* 44.22, pp. 897–902.
- Mao, X. & S. Sherwin (2012). ‘Transient growth associated with continuous spectra of the Batchelor vortex’. In: *Journal of Fluid Mechanics* 697, pp. 35–59.
- March, T. K., S. C. Chapman & R. O. Dendy (2005). ‘Recurrence plot statistics and the effect of embedding’. In: *Physica D: Nonlinear Phenomena* 200.1-2, pp. 171–184.
- Marshall, J. S. & M. L. Beninati (2005). ‘External turbulence interaction with a columnar vortex’. In: *Journal of Fluid Mechanics* 540, p. 221.
- Marshall, J. (1997). ‘The flow induced by periodic vortex rings wrapped around a columnar vortex core’. In: *Journal of Fluid Mechanics* 345, pp. 1–30.
- Marwan, N. *et al.* (2007). ‘Recurrence plots for the analysis of complex systems’. In: *Physics Reports* 438.5-6, pp. 237–329.
- Maxworthy, T., E. J. Hopfinger & L. G. Redekopp (1985). ‘Wave motions on vortex cores’. In: *Journal of Fluid Mechanics* 151, pp. 141–165.
- Mayer, E. W. & K. G. Powell (1992). ‘Viscous and inviscid instabilities of a trailing vortex’. In: *Journal of Fluid Mechanics* 245, pp. 91–114.
- McAlister, K. W. & R. Takahashi (1991). *NACA 0015 wing pressure and trailing vortex measurements*. Tech. rep. National Aeronautics and Space Administration.
- McKeon, B. J. (2017). ‘The engine behind (wall) turbulence: perspectives on scale interactions’. In: *Journal of Fluid Mechanics* 817.
- McWilliams, J. C. (1984). ‘The emergence of isolated coherent vortices in turbulent flow’. In: *Journal of Fluid Mechanics* 146, pp. 21–43.
- (1990). ‘The vortices of two-dimensional turbulence’. In: *Journal of Fluid Mechanics* 219, pp. 361–385.
- Melander, M. V. & F. Hussain (1993a). ‘Coupling between a coherent structure and fine-scale turbulence’. In: *Physical Review E* 48.4, p. 2669.
- (1993b). ‘Polarized vorticity dynamics on a vortex column’. In: *Physics of Fluids A: Fluid Dynamics* 5.8, pp. 1992–2003.
- (1994). ‘Core dynamics on a vortex column’. In: *Fluid dynamics research* 13.1, p. 1.
- Melander, M. V., J. C. McWilliams & N. J. Zabusky (1987). ‘Axisymmetrization and vorticity-gradient intensification of an isolated two-dimensional vortex through filamentation’. In: *Journal of Fluid Mechanics* 178, pp. 137–159.
- Menke, M. & I. Gursul (1997). ‘Unsteady nature of leading edge vortices’. In: *Physics of Fluids* 9.10, pp. 2960–2966.
- Miyazaki, T. & J. C. Hunt (2000). ‘Linear and nonlinear interactions between a columnar vortex and external turbulence’. In: *Journal of Fluid Mechanics* 402, pp. 349–378.

- Monin, A. S. & A. M. Yaglom (1971). *Statistical Fluid Mechanics, Volume I: Mechanics of Turbulence*. MIT Press.
- (1975). *Statistical Fluid Mechanics, Volume II: Mechanics of Turbulence*. MIT Press.
- Morkovin, M. V. (1969). ‘On the many faces of transition’. In: *Viscous drag reduction*. Springer, pp. 1–31.
- Navrose *et al.* (2018). ‘Optimal perturbation for two-dimensional vortex systems: route to non-axisymmetric state’. In: *Journal of Fluid Mechanics* 855, pp. 922–952.
- Navrose, V. Brion & L. Jacquin (2019). ‘Transient growth in the near wake region of the flow past a finite span wing’. In: *Journal of Fluid Mechanics* 866, pp. 399–430.
- Nolan, D. S. & B. F. Farrell (1999). ‘Generalized stability analyses of asymmetric disturbances in one-and two-celled vortices maintained by radial inflow’. In: *Journal of the atmospheric sciences* 56.10, pp. 1282–1307.
- Obremski, H. J. *et al.* (1969). *A portfolio of stability characteristics of incompressible boundary layers*. Tech. rep.
- Okubo, A. (1970). ‘Horizontal dispersion of floatable particles in the vicinity of velocity singularities such as convergences’. In: *Deep sea research and oceanographic abstracts*. Vol. 17. 3. Elsevier, pp. 445–454.
- Packard, N. H. *et al.* (1980). ‘Geometry from a time series’. In: *Physical Review Letters* 45.9, pp. 712–716.
- Pentelow, S. (2014). ‘Wing-tip vortex structure and wandering’. MA thesis. University of Ottawa.
- Perrin, J. (1913). *Les atomes*. Librairie Félix Alcan.
- Phillips, W. & J. Graham (1984). ‘Reynolds-stress measurements in a turbulent trailing vortex’. In: *Journal of Fluid Mechanics* 147, pp. 353–371.
- Pope, S. B. (2000). *Turbulent flows*. Cambridge University Press.
- Pradeep, D. S. & F. Hussain (2006). ‘Transient growth of perturbations in a vortex column’. In: *Journal of Fluid Mechanics* 550, 251–288.
- (2010). ‘Vortex dynamics of turbulence-coherent structure interaction’. In: *Theoretical and Computational Fluid Dynamics* 24.1-4, pp. 265–282.
- Prandtl, L. (1918). ‘Tragflügeltheorie. I. Mitteilung’. In: *Nachrichten der K. Gesellschaft der Wissenschaften zu Göttingen. Mathematisch-physikalische Klasse*, pp. 451–477.
- (1923). *Applications of modern hydrodynamics to aeronautics*. Tech. rep. 116. NASA, pp. 157–215.
- Provenzale, A. (1999). ‘Transport by coherent barotropic vortices’. In: *Annual Review of Fluid Mechanics* 31.1, pp. 55–93.
- Ragab, S. & M. Sreedhar (1995). ‘Numerical simulation of vortices with axial velocity deficits’. In: *Physics of fluids* 7.3, pp. 549–558.
- Rajaei, M., S. K. F. Karlsson & L. Sirovich (1994). ‘Low-dimensional description of free-shear-flow coherent structures and their dynamical behaviour’. In: *Journal of Fluid Mechanics* 258, pp. 1–29.

- Rempfer, D. (1996). ‘Investigations of boundary layer transition via Galerkin projections on empirical eigenfunctions’. In: *Physics of Fluids* 8.1, pp. 175–188.
- Rempfer, D. & H. F. Fasel (1994). ‘Evolution of three-dimensional coherent structures in a flat-plate boundary layer’. In: *Journal of Fluid Mechanics* 260, pp. 351–375.
- Reynolds, W. C. & A. K. M. F. Hussain (1972). ‘The mechanics of an organized wave in turbulent shear flow. Part 3. Theoretical models and comparisons with experiments’. In: *Journal of Fluid Mechanics* 54.2, pp. 263–288.
- Riesz, F. & B. Sz-Nagy (1956). *Functional analysis*. Blackie.
- Rokhsaz, K., S. R. Foster & L. S. Miller (2000). ‘Exploratory Study of Aircraft Wake Vortex Filaments in a Water Tunnel’. In: *Journal of Aircraft* 37.6, pp. 1022–1027.
- Rotta, J. C. (1972). *Turbulente Strömungen: Eine Einführung in die Theorie und ihre Anwendung*. Leitfäden der angewandten Mathematik und Mechanik. Stuttgart: Teubner.
- Roy, A. & G. Subramanian (2014). ‘Linearized oscillations of a vortex column: the singular eigenfunctions’. In: *Journal of Fluid Mechanics* 741, pp. 404–460.
- Roy, C. & T. Leweke (2008). *Experiments on vortex meandering*. FAR-Wake. Fundamental Research on Aircraft Wake Phenomena.
- Saffman, P. G. (1992). *Vortex Dynamics*. Cambridge Monographs on Mechanics. Cambridge University Press.
- Samelson, R. M. & S. Wiggins (2006). *Lagrangian transport in geophysical jets and waves: The dynamical systems approach*. Springer Science & Business Media.
- Sarpkaya, T. & J. J. Daly (1987). ‘Effect of Ambient Turbulence on Trailing Vortices’. In: *Journal of Aircraft* 24.6, pp. 399–404.
- Schlichting, H. (1997). *Grenzschicht-Theorie*. Springer.
- Schmid, P. J. (2007). ‘Nonmodal Stability Theory’. In: *Annual Review of Fluid Mechanics* 39, pp. 129–162.
- Schrödinger, E. (1992). *What is life? and Mind and Matter*. Cambridge University Press.
- (1996). *Nature and the Greeks and Science and Humanism*. Cambridge University Press.
- Sen, R. (1997). ‘Vortex-Oscillation Model of Airfoil Side-Edge Noise’. In: *AIAA Journal* 35.3, pp. 441–449.
- Shannon, C. E. (1948). ‘A Mathematical Theory of Communication’. In: *The Bell System Technical Journal* 27.3, pp. 379–423.
- (1949). ‘Communication in the Presence of Noise’. In: *Proc. Institute of Radio Engineers* 37.1, pp. 10–21.
- Singh, P. I. & M. S. Uberoi (1976). ‘Experiments on vortex stability’. In: *The Physics of Fluids* 19.12, pp. 1858–1863.
- Sirovich, L. (1987). ‘Turbulence and the dynamics of coherent structures. I. Coherent structures’. In: *Quarterly of applied mathematics* 45.3, pp. 561–571.
- (1989). ‘Chaotic dynamics of coherent structures’. In: *Physica D: Nonlinear Phenomena* 37.1, pp. 126–145.

- (1991). ‘Empirical Eigenfunctions and Low Dimensional Systems’. In: *New Perspectives in Turbulence*. Ed. by L. Sirovich.
- Sohr, H. (2001). *The Navier-Stokes equations: An elementary functional analytic approach*. Springer.
- Spalart, P. R. (1998). ‘Airplane Trailing Vortices’. In: *Annual Review of Fluid Mechanics* 30.1, pp. 107–138.
- Spurk, J. H. (2006). *Strömungslehre: Einführung in die Theorie der Strömungen*. Springer.
- Stout, E. & F. Hussain (2016). ‘External turbulence-induced axial flow and instability in a vortex’. In: *Journal of Fluid Mechanics* 793, pp. 353–379.
- Swinney, H. L. & J. P. Gollub (1986). ‘Characterization of hydrodynamic strange attractors’. In: *Physica D: Nonlinear Phenomena* 18.1-3, pp. 448–454.
- Synge, J. L. & A. Schild (1978). *Tensor calculus*. Dover Publications, Inc.
- Takahashi, N., H. Ishii & T. Miyazaki (2005). ‘The influence of turbulence on a columnar vortex’. In: *Physics of Fluids* 17.3, p. 035105.
- Takens, F. (1981). ‘Detecting strange attractors in turbulence’. In: *Dynamical systems and turbulence*. Springer, pp. 366–381.
- Taylor, G. I. (1921). ‘Diffusion by continuous movements’. In: *Proceedings of the London Mathematical Society*. 2nd ser. 20, pp. 196–212.
- Tennekes, H. & J. L. Lumley (1973). *A first course in turbulence*. MIT Press.
- Trefethen, L. N. & M. Embree (2005). *Spectra and pseudospectra: the behavior of nonnormal matrices and operators*. Princeton University Press.
- Truesdell, C. (1984). *Rational thermodynamics*. Springer-Verlag.
- Truesdell, C. (1954). *The kinematics of vorticity*. Indiana University Press.
- Vadarevu, S. B. (2017). ‘Exact Invariant Solutions for Grooved Couette and Channel Flows’. PhD thesis. University of Southampton.
- Van Jaarsveld, J. P. J. *et al.* (2011). ‘An experimental study of the effect of external turbulence on the decay of a single vortex and a vortex pair’. In: *Journal of Fluid Mechanics* 670, pp. 214–239.
- Vandernoot, F.-X. *et al.* (2008). ‘Mean and turbulence measurements of wake vortices. Wandering effects’. In: *Proceedings of the 14th International Symposium on Applications of Laser Techniques to Fluid Mechanics Lisbon, Portugal*.
- Viola, F., C. Arratia & F. Gallaire (2016). ‘Mode selection in trailing vortices: harmonic response of the non-parallel Batchelor vortex’. In: *Journal of Fluid Mechanics* 790, pp. 523–552.
- Wang, Z. & I. Gursul (2012). ‘Unsteady characteristics of inlet vortices’. In: *Experiments in fluids* 53.4, pp. 1015–1032.
- Weiss, J. (1991). ‘The dynamics of enstrophy transfer in two-dimensional hydrodynamics’. In: *Physica D: Nonlinear Phenomena* 48.2-3, pp. 273–294.
- Westerweel, J., G. E. Elsinga & R. J. Adrian (2013). ‘Particle Image Velocimetry for Complex and Turbulent Flows’. In: *Annual Review of Fluid Mechanics* 45, pp. 409–436.

- Wiener, N. (1988). *The Human Use of Human Beings: Cybernetics and Society*. Da Capo Press.
- Wu, J.-Z., H.-Y. Ma & M.-D. Zhou (2006). *Vorticity and vortex dynamics*. Springer.
- Yaglom, A. M. (1962). *An Introduction to the Theory of Stationary Random Functions*. Prentice-Hall, Inc.
- (2012). *Hydrodynamic Instability and Transition to Turbulence*. Ed. by U. Frisch. Springer.
- Yeung, K. A. F & K. B. Lee (1999). ‘Particle image velocimetry study of wing-tip vortices’. In: *Journal of aircraft* 36.2, pp. 482–484.
- Yudovich, V. I. (1989). *The linearization method in hydrodynamical stability theory*. American Mathematical Soc.
- Zeman, O (1995). ‘The persistence of trailing vortices: a modeling study’. In: *Physics of Fluids* 7.1, pp. 135–143.
- Zurheide, F. T., M. Meinke & W. Schröder (2009). ‘Meandering of Wing-Tip Vortices Interacting with a Cold Jet in the Extended Wake’. In: *High Performance Computing on Vector Systems 2008*. Springer, pp. 223–242.

# A | Details of the experiments

## A.1 Presentation of the experimental configuration

The experimental results are computed from several databases gathered in the F2 wind tunnel of ONERA at Fauga-Mauzac between 1998 and 2017. To a large extent, these experiments are presented in Jacquin *et al.* (2001), Fabre (2002) and Jacquin *et al.* (2007). The measurement techniques employed in all these studies were hot-wire anemometry (HWA) and laser-Doppler velocimetry (LDV) (for technical details see e.g. Comte-Bellot, 1976; Buchhave *et al.*, 1979). The setup in these experiments is illustrated in Jacquin *et al.* (2001, fig. 2 on p. 28).

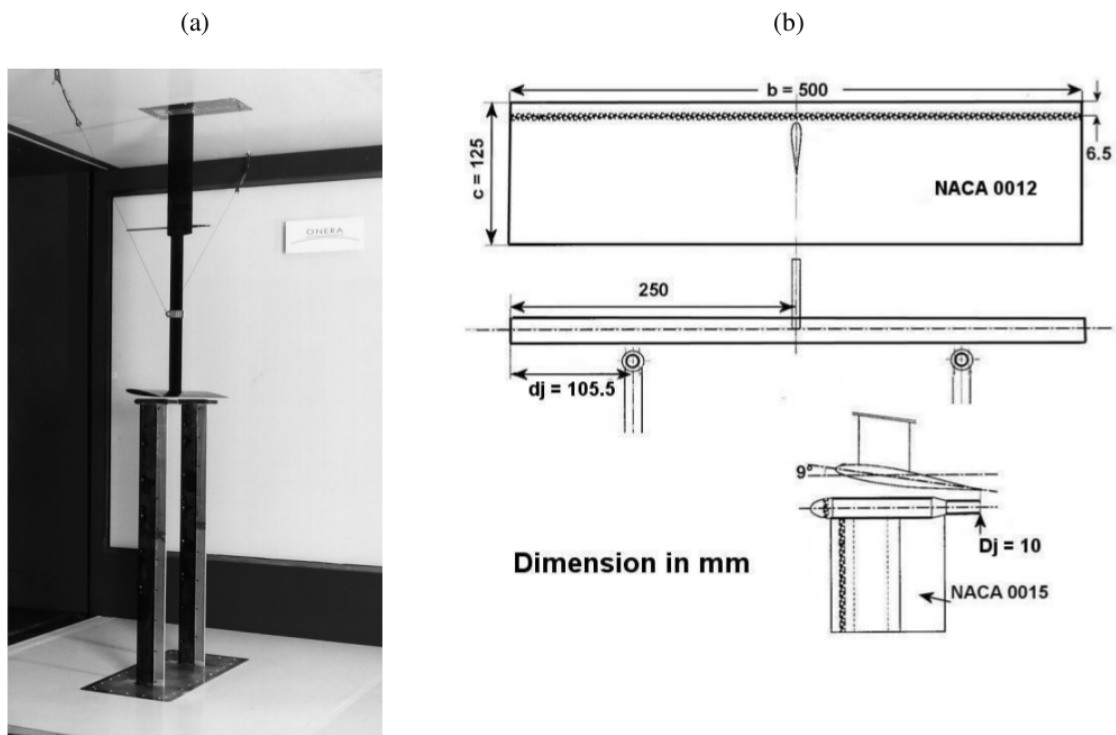


Figure A.1: Experimental setup (Jacquin *et al.*, 2007).

The majority of the experimental results is computed for an unpublished measurement campaign from 2017, where high-speed stereoscopic Particle Image Velocimetry (PIV) has been used (cf. Adrian, 1991; Westerweel *et al.*, 2013, for technical details). The configuration is the same as in the LDV measurements of Jacquin *et al.* (2007), for which the setup and essential geometrical dimensions of the model are shown in fig. A.1. In the present study, only the experimental runs *without* the additional jets shown in fig. A.1 are considered.

**Geometry of the facility and model.** The test section of the wind tunnel has a length of  $L = 5$  m and rectangular cross section of width  $B = 1.4$  m and height  $H = 1.8$  m (diagonal  $\sqrt{B^2 + H^2} = 2.3$  m) (cf. fig. 2.1). A wing with NACA 0012 profile is positioned in the test-section centre, 0.75 m downstream of the inlet, at an angle of incidence  $\alpha = 9^\circ$ . The chord length  $c = 0.125$  m and wing span  $b = 0.5$  m yield the aspect ratio  $bc^{-1} = 4$ . PIV measurements are taken in cross planes at  $zc^{-1} \in \{2, 4, 12, 20, 26\}$ . In each measurement plane 4100 snapshots of the velocity field are registered at an image sampling rate of  $f_s = 3$  kHz. It follows a measurement duration of approximately 1.4 s ( $\approx 220 t_c$ ).

**Fluid parameters.** The free-stream velocity is  $U_\infty = 20$  ms $^{-1}$ , which yields the chord-based Reynolds number  $R_c \approx 2 \times 10^5$ . Jacquin *et al.* (2007, p. 4) compute the circulation based Reynolds number  $R_\Gamma \approx 9 \times 10^3$ . The turbulence intensity in the F2 wind tunnel is  $uU_\infty^{-1} < 0.5\%$  (Jacquin *et al.*, 2001, p. 14; Jacquin *et al.*, 2007, p. 5).

**Some scale estimates.** If we suppose that the meandering dynamics is essentially associated with frequencies approximately below  $S_c := fcU_\infty^{-1} \lesssim 10$  (cf. conj. 2.6, figs. 2.8–2.9 and the discussion there), the resolution of the smallest characteristic meandering period  $T$  would be

$$\frac{T}{T_s} = T f_s = \frac{1}{10} \frac{c}{U_\infty} f_s \approx 2.$$

In other words, the smallest expected time scale of vortex meandering is sampled twice (or inversely,  $f_s = 2T^{-1}$ ), which is the theoretical limit according to the Nyquist–Shannon sampling theorem (Shannon, 1949).

It is convenient to define the integral scales of the whole dynamics by

$$l = c = 0.125 \text{ m} \quad \mathfrak{U} = U_\infty = 20 \text{ ms}^{-1}.$$

Using these estimates the production (equal to the dissipation; Tennekes & Lumley, 1973, p. 20) is of the order of

$$\varepsilon \sim \mathfrak{U}^3 l^{-1} = 6.4 \times 10^4 \text{ m}^2 \text{ s}^{-3}$$

and the viscosity of air is given in Spurk (2006, tab. D.2 on p. 555) for 290 K and 1 bar atmospheric pressure as (this value is in very good agreement with the Reynolds number)

$$\nu \approx 1.5 \times 10^{-5} \text{ m}^2 \text{ s}^{-1}.$$

Thereof, the Kolmogorov scales are estimated to be (Tennekes & Lumley, 1973, p. 20)

$$\begin{aligned} \eta &= (\nu^3 \varepsilon^{-1})^{1/4} \sim 1.3 \times 10^{-5} \text{ m} = 13 \mu\text{m} \\ \tau &= (\nu \varepsilon^{-1})^{1/2} \sim 1.5 \times 10^{-5} \text{ s} = 0.015 \text{ ms} \quad \Leftrightarrow \quad \tau^{-1} \sim 70 \text{ kHz} \\ v &= (\nu \varepsilon)^{1/4} \sim 1 \text{ ms}^{-1}. \end{aligned}$$

## A.2 Symbols of the experiments in figs. 2.2, 2.4 and 3.1

The symbols in figs. 2.2, 2.4 and 3.1 correspond to the following experiments:

- Chigier & Corsiglia (1971) = \*;
- Chigier & Corsiglia (1972) = ■;
- Baker *et al.* (1974) = ●;
- Chow *et al.*, 1997 = ▲;
- Devenport *et al.* (1996) = ▼;
- Jacquin *et al.* (2001) = ◆;

Beninati & Marshall (2005) =  ;

Jacquin *et al.* (2007) =  ;

Bailey & Tavoularis (2008) =  ;

Pentelow (2014) =  ;

Iungo (2017) =  .

### A.3 Details of the experiments in fig. 4.3

The symbols in fig. 4.3 correspond to the experiments listed in tab. A.1, together with the turbulence intensity and circulation. Additional experiments are added to tab. A.1 for which not all parameters were available. For the estimated values, those experiments collapse with the scaling law, too.

Table A.1: Experimental parameters for meandering-amplitude scaling.

		$uU_\infty^{-1}$	$\Gamma_0(cU_\infty)^{-1}$	$\alpha$
Devenport <i>et al.</i> (1996)		$10^{-3}$ (p. 70)	$6 \times 10^{-2}$ (p. 81)	$5^\circ$
		$10^{-3}$	$2 \times 10^{-2}$	$2.5^\circ$
		$10^{-3}$	$3 \times 10^{-2}$	$3.75^\circ$
		$10^{-3}$	$12 \times 10^{-2}$	$7.5^\circ$
Jacquin <i>et al.</i> (2007, PIV)		$10^{-3}$	$5.5 \times 10^{-2}$	$9^\circ$
Bailey & Tavoularis (2008)		$2 \times 10^{-3}$ (p. 284)	$18 \times 10^{-2}$ (fig. 21a)	$5^\circ$
		$15 \times 10^{-3}$ (estimated)	$12 \times 10^{-2}$ (fig. 21a)	$5^\circ$
		$25 \times 10^{-3}$ (p. 293)	$8 \times 10^{-2}$ (estimated)	$5^\circ$
Iungo <i>et al.</i> (2009)		$7.5 \times 10^{-3}$ (p. 437)	$9.5 \times 10^{-2}$ (tab. 1)	$8^\circ$
Van Jaarsveld <i>et al.</i> (2011)		$5 \times 10^{-3}$ (p. 217)	$37.5 \times 10^{-2}$ (p. 221)	–
Del Pino <i>et al.</i> (2011)		$20 \times 10^{-3}$ (p. 2)	$10 \times 10^{-2}$ (estimated)	$4 \dots 12^\circ$
Deem <i>et al.</i> (2013)		$7 \times 10^{-3}$ (p. 226)	$6 \times 10^{-2}$ (estimated)	$5^\circ$

### A.4 Details of the experiments in fig. 5.7

Power spectral densities are computed from the:

- axial velocity (Devenport *et al.*, 1996; Jacquin *et al.*, 2001);
- turbulent kinetic energy (Beninati & Marshall, 2005);
- transversal fluctuation velocity (Bailey & Tavoularis, 2008);
- vortex centreline (Bailey *et al.*, 2018).



## B | Brownian meandering

# On the statistics of vortex meandering as a Brownian motion

Tobias Bölle\*

DAAA, ONERA–The French Aerospace Lab  
8 Rue des Vertugadins, 92190 Meudon, France

(Dated: 23rd February 2021)

Vortex meandering denotes the apparently random lateral displacement of the vortex core as a whole, as such having an inherently Lagrangian notion. We derive an equation for the meandering amplitude  $\sigma(t)$  analogous to Brownian motion which explains the experimental findings that  $\sigma(t) \sim \sqrt{t}$ . Adopting a random-walk model, we argue that the commonly observed Gaussian statistics might be an artefact of the central-limit theorem.

## INTRODUCTION

Probably all vortices are affected by the apparently random lateral displacement of the vortex core as a whole, called meandering. This motion becomes particularly visible and problematic in large-scale configurations such as trailing vortices or tornadoes [1–3]. Despite its universal observation in experiments since the 70s, the governing physics remain poorly understood [4]. Nevertheless, we have considerable experimental evidence that the meandering amplitude  $\sigma(t)$  (defined below) always grows like  $\sigma(t) \sim \sqrt{t}$  downstream of the vortex generator [5, 6]. This characteristic is reminiscent of Brownian motion, which is an established fact for suspended and fluid particles [7, pp. 545, 580]. The identification of vortex meandering with a Brownian motion implies that vortex cores *as a whole* constitute (generalized) fluid particles.

In a first step, we derive a Langevin equation for the meandering amplitude which explains the experimental observations. Secondly, by appeal to a random-walk model, we argue that the universally observed Gaussian statistics may be an artefact of the central-limit theorem.

The meandering motion manifests in the  $(x, y)$ -planes orthogonal to the mean advection  $\mathbf{D}$  along  $z$ , see fig. 1a. It will thus be convenient to assume an  $(x^1, x^2)$ -frame of reference following the mean displacement  $\mathbf{D}$ . In this *laboratory frame* we identify the vortex core with a definite two-dimensional fluid volume (a disc say) whose position depends on time. Suppose the dynamics in the core is essentially due to meandering, then the vortex-centre time series  $\mathbf{X}(t, \mathbf{a})$  (with respect to the laboratory frame) is equivalent to the motion of the vortex as a whole. The essential point here is that the core is identified with a material fluid volume which evolves along the trajectory  $t \mapsto \mathbf{X}(t, \mathbf{a}) \in \mathbb{R}^2$ . This is a Lagrangian point of view where we identify the vortex core with a fluid particle labelled  $\mathbf{a}$ .

We shall assume that  $\mathbf{X}(t, \mathbf{a})$  is a (discrete or continuous) stochastic process ( $t \in \{\mathbb{Z}, \mathbb{R}\}$ ), denoting it with a capital letter, having probability density  $\mu_{\mathbf{X}}$  and  $\mathbf{x}^{(s)}(t)$  is the realization of the  $s$ -th experiment. The average of an observable  $\phi(t, \mathbf{X}(t))$  is defined by  $\langle \phi(t, \mathbf{X}(t)) \rangle := \int_{\mathbb{R}^2} d\mu_{\mathbf{X}}^t(\mathbf{x}) \phi(t, \mathbf{x})$  [8, pp. 19–20] [9]. The standard devi-

ation of  $\mathbf{X}(t, \mathbf{a})$  is called meandering amplitude [1].

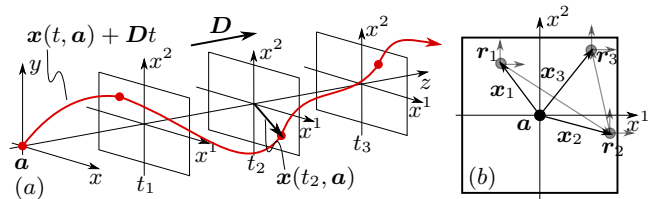


Figure 1. (a) Observation of a meandering realization  $\mathbf{x}(t, \mathbf{a}) + \mathbf{D}t$  in the earth-fixed frame  $(x, y, z)$  and laboratory frame  $(x^1, x^2)$  moving with  $\mathbf{D}$ . (b) Random-walk realization  $\mathbf{r}_i = \mathbf{r}(t, \mathbf{a})$  in the meandering frame  $(r^1, r^2)$  corresponding to vector-sum meandering  $\mathbf{x}_i = \mathbf{x}(t, \mathbf{a})$  in the laboratory frame.

The perception of vortex meandering as the Lagrangian dynamics of a fluid particle suggests a modified interpretation of the experiment. The conventional point of view is that we conduct *one* experiment, taking measurements in the  $n$  streamwise planes shown in fig. 1a, each during a time  $m$ . Consequently, the result consists of  $n$  vortex-centre sequences, each of the length  $m$ . The experimental outcome of one such sequence in one such plane is shown in fig. 3.

The Lagrangian point of view, however, suggests to define the experiment as follows. At some initial time we tag the vortex centre  $\mathbf{a}$  and follow its evolution in time. Keeping this initial condition fixed while repeating this same random experiment  $m$  times yields an ensemble of  $m$  different meandering trajectories (see fig. 1a). Assuming the same  $n$  measurement planes as before,  $(\mathbf{x}^{(s)}(t_1), \mathbf{x}^{(s)}(t_2), \dots, \mathbf{x}^{(s)}(t_n)) \in \mathbb{R}^{2 \times n}$  is then the outcome of the  $s$ -th experiment ( $s = 1, \dots, m$ ). This amounts to the ergodic hypothesis where we relate the measurement duration  $m$  with the number of realizations. In this view now, every point in fig. 3 corresponds to the detection of one out of  $m$  identically prepared random experiments for fixed  $t$ .

## BROWNIAN MEANDERING

Assume the vortex centre is material. The Lagrangian velocity reads  $d\mathbf{X}(t, \mathbf{a})/dt|_{\mathbf{a}} = \partial_t \mathbf{X}(t, \mathbf{a}) = \mathbf{v}(t, \mathbf{a})$  which

equals the Eulerian velocity  $\mathbf{u}(t, \mathbf{X}(t, \mathbf{a}))$  on the instantaneous centreline [7, p. 529]. Since by definition the vortex centre corresponds to the point of zero cross-flow velocity in the meandering frame [2],  $\mathbf{u}(t, \mathbf{X}(t, \mathbf{a}))$  is the velocity *only* due to the displacement of  $\mathbf{X}(t, \mathbf{a})$ . Measurement in the  $s$ -th experiment amounts to the position–velocity realization pair  $\{\mathbf{x}^{(s)}(t), \mathbf{u}^{(s)}(t, \mathbf{x}(t))\}$  at time  $t$ . Observing the realization pair at a certain position and with a certain velocity is determined by the probability distribution  $\mu_{\mathbf{X}}$ .

We note that [10]

$$\begin{aligned} \left( \mathbf{X}(t, \mathbf{a}), \frac{d\mathbf{u}(t, \mathbf{X}(t, \mathbf{a}))}{dt} \Big|_{\mathbf{a}} \right) &= \left( \mathbf{X}(t, \mathbf{a}), \frac{d^2\mathbf{X}(t, \mathbf{a})}{dt^2} \Big|_{\mathbf{a}} \right) = \\ &= \frac{d^2 \|\mathbf{X}(t, \mathbf{a})\|^2}{dt^2} \Big|_{\mathbf{a}} - \left\| \frac{d\mathbf{X}(t, \mathbf{a})}{dt} \Big|_{\mathbf{a}} \right\|^2. \end{aligned} \quad (1)$$

By the above definition of meandering, a measurement of the Eulerian velocity field taken in plane  $t$  corresponds to the superposition of the vortex-induced velocity  $\mathbf{U}(\mathbf{x} - \mathbf{X}(t, \mathbf{a}))$  centred around the instantaneous centre position  $\mathbf{X}(t, \mathbf{a})$  and a fluctuation field  $\mathbf{u}(t, \mathbf{x})$ . Precisely in the vortex centre  $\mathbf{u}(t, \mathbf{X}(t, \mathbf{a}))$  is identical to the Lagrangian velocity of vortex meandering and  $\mathbf{U}(0) = 0$  for all  $t$ , by definition. In general, the dynamics in the instantaneous vortex centre is governed by [7, p. 148]

$$\frac{\partial \mathbf{u}}{\partial t} + (\mathbf{u}, \nabla)\mathbf{u} + (\mathbf{U}, \nabla)\mathbf{u} = -\nabla\mathbf{U}\mathbf{u} - \nabla p + \nu\nabla^2\mathbf{u} \quad (2)$$

where for all  $t$  all terms are evaluated at  $\mathbf{X}(t, \mathbf{a})$ . By definition, in the vortex centre  $\mathbf{U} = 0$  and the third term on the left of (2) vanishes. We then identify  $\partial/\partial t + (\mathbf{u}, \nabla)$  in (2) with  $d/dt$  for fixed  $\mathbf{a}$  in (1) to obtain

$$\frac{d\mathbf{u}(t, \mathbf{X}(t))}{dt} = -\nabla\mathbf{U}|_{\mathbf{X}(t)}\mathbf{u}(t, \mathbf{X}(t)) + \mathbf{f}(t, \mathbf{X}(t)) \quad (3)$$

where we suppress dependence on  $\mathbf{a}$  for simplicity. Equation (3) has the form of a Langevin equation when we agree to assemble the pressure gradient and viscous diffusion in the (stochastic) forcing  $\mathbf{f} := -\nabla p + \nu\nabla^2\mathbf{u}$  ( $\nu^{-1}$  is the Reynolds number). While these terms might be significant for perturbation dynamics inside the core which do not displace the vortex, we expect them to have a negligible effect on the integral motion of the vortex as a whole. Considering meandering as an *integral* dynamics, the pressure gradient drops out in the energy balance of an incompressible fluid, while it depends crucially on the velocity gradient [11]. The relative unimportance of the pressure gradient for fluctuation-energy evolution is also stated in Ref. [7, pp. 382–383]. We therefore assume that  $\mathbf{X}(t)$  and  $\mathbf{f}(t)$  are stochastically independent such that  $\langle\langle \mathbf{X}, \mathbf{f} \rangle\rangle = \langle\langle \mathbf{X} \rangle\rangle, \langle\langle \mathbf{f} \rangle\rangle = 0$  [1].

The velocity gradient in the instantaneous vortex centre is the skew-adjoint matrix  $\mathbf{\Omega}$ . Graphical evaluation shows that the corresponding rigid-body rotation is

a good approximation up to approximately 0.5 core radii which is the order of typical meandering amplitudes [1].

Due to symmetry of the probability distribution (fig. 4), functions of the random process  $\mathbf{X}(t, \mathbf{a})$  are evaluated in the mean centre to leading order [12]. Combining (1) with (3) and averaging then yields [13]

$$\frac{d^2 \langle\langle \|\mathbf{X}(t)\|^2 \rangle\rangle}{dt^2} \frac{1}{2} + \mathbf{\Omega} \frac{d \langle\langle \|\mathbf{X}(t)\|^2 \rangle\rangle}{dt} \frac{1}{2} = \langle\langle \|\mathbf{u}(t, \langle\mathbf{X}\rangle)\|^2 \rangle\rangle. \quad (4)$$

Equation (4) is an inhomogeneous Cauchy problem for the ‘variance velocity’ with skew-adjoint generator  $\mathbf{\Omega}$  unlike (3) where  $\nabla\mathbf{U}|_{\mathbf{X}(t)}$  is non self-adjoint. The spectral theorem guarantees that  $\mathbf{\Omega}$  is unitary diagonalisable with imaginary eigenvalues  $\pm i\Omega_0$ . Transformation to the principal axes uncouples the problem but leaves the norm invariant (mere rotation).

For molecular Brownian motion in thermal equilibrium the equipartition theorem states that the kinetic energy of the particle can be expressed in terms of the energy of the surrounding fluid. By analogy, we pose

$$\langle\langle \|\mathbf{u}(t, \langle\mathbf{X}\rangle)\|^2 \rangle\rangle \sim \mathbf{u}^2(t) \quad (5)$$

where  $\mathbf{u}^2(t)$  is the characteristic turbulent kinetic energy of the free stream [14, p. 63]. If meandering was essentially an inactive buffeting of the core by the surrounding turbulence [1],  $\mathbf{u}^2(t)$  should constitute an upper bound for the centreline kinetic energy in some sense [2]. Boundedness should not be understood literally but rather emphasizes the experimental observation that meandering is driven by a balance between external excitation and internal resistance. The stronger the free-stream turbulence (i.e. the larger  $\mathbf{u}(t)$ ), the more the vortex will meander.

For simplicity, we assume isotropy in the principal-axes system and write  $\sigma^2(t) := \langle X^2(t) \rangle$  for the variance. Combining (4)–(5) yields ( $C = \text{const.}$ )

$$\frac{d^2 \sigma^2(t)}{dt^2} \frac{1}{2} + \Omega_0 \frac{d \sigma^2(t)}{dt} \frac{1}{2} = C\mathbf{u}^2(t). \quad (6)$$

Equation (6) is of Langevin type with time-dependent right-hand side describing Brownian-motion-like meandering-amplitude evolution.

*Comparison with experiment.* The generator  $\mathbf{\Omega}$  in (4) physically represents an ‘equivalent friction’ for the Brownian motion of a vortex particle. In the case of a vortex, diffusivity is proportional to the mean angular velocity on the mean centreline. This is a remarkable difference to actual molecular Brownian motion in that the vortex imposes its own intrinsic ‘equivalent friction’ to resist displacement.

The general solution of (6) can be written as the sum of the homogeneous and particular solution. The former governs the transient adjustment to the initial condition. We shall concentrate only on the particular solution

$$\sigma(t) \sim \sqrt{\frac{1}{\Omega_0} \int_0^t d\tau \mathbf{u}^2(\tau)} \stackrel{\mathbf{u} \neq \mathbf{u}(\tau)}{\sim} \mathbf{u} \sqrt{\frac{t}{\Omega_0}}. \quad (7)$$

Figure 2 shows a comparison of the scaling law (7) with a compilation of the data reported in the literature. We observe good principal agreement and trends, particularly for later times.

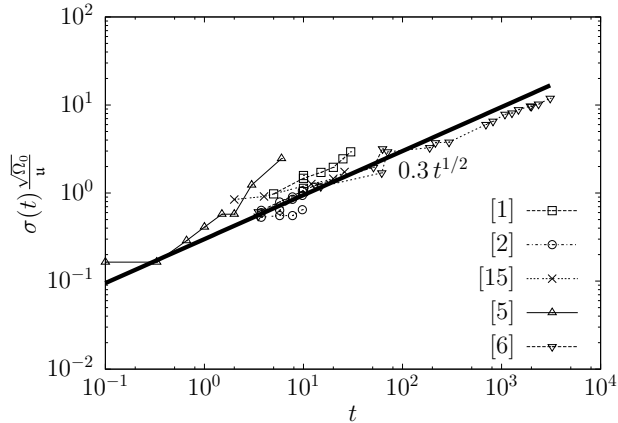


Figure 2. Temporal evolution of the normalised vortex-centre standard deviation  $\sigma(t)$  according to (7) (solid line) and compilation of experiments (symbols).

Comparing (7) to (8) suggests that the vortex imposes the Lagrangian time scale  $T_L \sim \Omega_0^{-1}$ , provided that (5) holds, viz.  $\mathbf{v} \sim \mathbf{u}$ . We can then estimate a typical experimental measurement duration to be of the order of  $10^2$  Lagrangian integral scales which justifies application of the central-limit theorem above [16]

Eventually, we shall show that (7) is compatible with the previously proposed meandering-amplitude models. The classical mixing-length argument identifies the characteristic turbulence scales with a net effect of enhanced diffusivity  $\mathbf{u}^2 T_L =: \nu_t$  where  $\nu_t$  is the eddy viscosity [14, p. 229]. Replacing in (7) yields  $\sigma(t) \sim \sqrt{\nu_t t}$  which is analogous to viscous vortex-core diffusion. Assuming meandering to be a passive buffeting of the vortex core by the surrounding turbulence of statistical strength  $\nu_t$  this relation has been proposed in Ref. [4]. Equation (4) is also consistent with the meandering-amplitude guess  $\sigma^l \sim \mathbf{u}^l (\partial \mathbf{u}^l / \partial r)^{-1}$ ,  $l = 1, 2$  (evaluated on the mean centreline) employed in the correction algorithm of Ref. [1]. Essentially the same scaling law as (7) has been suggested recently in Ref. [6] upon merely replacing the Lagrangian integral scale by the vortex-rotation period.

### CENTRAL-LIMIT THEOREM

Besides the laboratory frame, we shall use the *meandering frame* which is attached to the vortex-core motion (the small grey coordinate systems shown in fig. 1b). Let  $\mathbf{R}(t, \mathbf{a})$  denote the vortex-centre motion in the meandering frame, which is assumed to be a discrete random pro-

cess ( $t \in \mathbb{Z}$ ). We shall assume  $\mathbf{R}(t, \mathbf{a})$  being stochastically independent and identically distributed [17]. Thus, the probability density  $\mu_{\mathbf{R}}$  of  $\mathbf{R}(t, \mathbf{a})$  is invariant in time which implies that the standard deviation  $\sigma_{\mathbf{R}} = \text{const}$ . An observer in the meandering frame sees meandering as a sequence of random steps. That is, being in  $\mathbf{r}(t, \mathbf{a})$  at some time  $t$  the vortex will effectuate a step in some direction  $\mathbf{r}(t + \delta t, \mathbf{a})$  away from the present position according to the (local) probability distribution  $\mu_{\mathbf{R}}$  (fig. 1b). This is the problem of the random walk [18].

The laboratory-fixed observer as defined in the Introduction follows the mean motion of the vortex centre. In general, this means advection in the streamwise direction, downwash and drift towards the symmetry plane of the trailing-vortex system. Let us assume that the combined translation  $\mathbf{D}$  represents a uniform rectilinear motion. The laboratory frame of reference is related to the earth fixed frame by Galilean transformation and, hence, is an inertial frame of reference (fig. 1a). A laboratory-fixed observer recognises a random process being the vector sum of the meandering observer  $\mathbf{X}(t, \mathbf{a}) := \sum_{q=1}^t \mathbf{R}(q, \mathbf{a}) + \mathbf{a}$  ([7, p. 540], [14, pp. 224–225]). We suppose that  $\langle \mathbf{R}(t, \mathbf{a}) \rangle = 0$  for all  $t$ , meaning that Lagrangian meandering has no preferred direction, which yields  $\langle \mathbf{X}(t, \mathbf{a}) \rangle = \mathbf{a}$ .

The central-limit theorem states that the limiting probability distribution of  $\mathbf{X}(t, \mathbf{a})$  approaches a normal distribution  $\mathcal{N}(0, \sigma_{\mathbf{X}}(t))$ , where  $\sigma_{\mathbf{X}}(t) = \sigma_{\mathbf{R}} t^{1/2}$ , as  $t \rightarrow \infty$  [8, pp. 30–31]. We notice from this result that unlike  $\mathbf{R}(t, \mathbf{a})$  the statistics of  $\mathbf{X}(t, \mathbf{a})$  are not stationary and that the actually measured standard deviation  $\sigma_{\mathbf{X}}(t)$  is proportional to  $\sigma_{\mathbf{R}}$ . In the limit of long experimental runs (in terms of the Lagrangian integral scale; [14, p. 46]), the laboratory-fixed observer should observe meandering being normally distributed. This is indeed the case in experiments as shown in figs. 3–4.

We modelled meandering as a discrete random process with stochastically independent elements. The central-limit theorem also holds for a continuous random process if  $(t \in \mathbb{R}) \gg T_L$  where  $T_L$  is the Lagrangian integral scale [19]. We estimate validity of this condition below.

It is in fact the probability distribution of the "true" Lagrangian meandering  $\mu_{\mathbf{R}}$  which determines the next step in a random walk. While  $\mu_{\mathbf{X}}$  is sufficient in practice (e.g. for correction of mean velocity profiles [1]), it does not illuminate the governing dynamics which is represented by  $\mu_{\mathbf{R}}$  [see also 14, p. 216].

The vortex trajectory is the integral curve  $\mathbf{X}(t, \mathbf{a}) = \int_0^t d\tau \mathbf{v}(\tau, \mathbf{a})$  where  $\mathbf{v}(t, \mathbf{a})$  denotes the Lagrangian velocity (see also below). The variance of  $\mathbf{X}(t, \mathbf{a})$  for stationary velocity has been derived by Taylor:

$$\langle (X^l)^2(t) \rangle = 2 \langle (v^l)^2 \rangle t \int_0^t d\tau \frac{t-\tau}{t} \rho(\tau) \approx 2 (\mathbf{v}^l)^2 T_L^l t, \quad (8)$$

where  $\rho(\tau)$  is the correlation coefficient [14, p. 225] and  $l = 1, 2$  is the component index. The difficulty with (8)

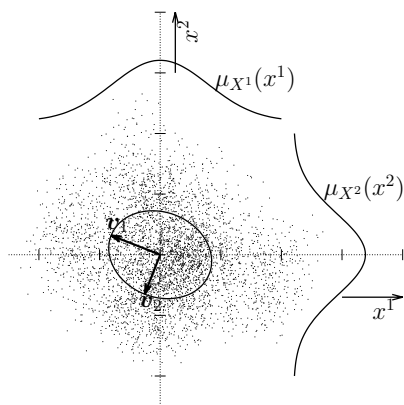


Figure 3. Experimentally detected cloud of realizations of  $\mathbf{x}(t, \mathbf{a})$  for some fixed  $t > 0$  and the associated marginal probability densities obeying normal distributions  $\mathcal{N}(0, \sigma_{X^i})$  ( $t$  fixed). The principal axes  $\mathbf{v}_1, \mathbf{v}_2$  spanning the standard-deviation ellipse (meandering amplitude) [15].

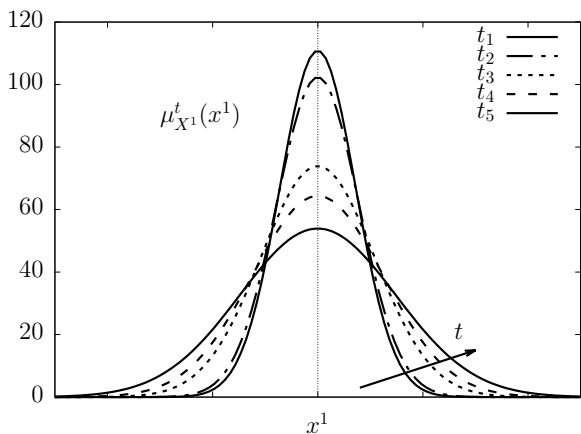


Figure 4. Diffusion of the marginal probability density  $\mu_{X^1}^t(x^1) \sim \mathcal{N}(0, \sigma_{R^1}^1 t^{1/2})$  for the five measurement stations in the experiment [15].

is that it is not evident how the Lagrangian quantities  $(\mathbf{v}^l)^2 := \langle (v^l)^2 \rangle$  and  $T_L^l$  are related to Eulerian statistics in general. We look at this below.

This work has been supported by the French Ministry of Civil Aviation (DGAC) under PHYWAKE (PHYSics of WAKE vortices) research program.

\* tobias.bolle@onera.fr

- [1] W. J. Devenport, M. C. Rife, S. I. Liapis, and G. J. Follin, *J. Fluid Mech.* **312**, 67 (1996).
- [2] S. C. C. Bailey and S. Tavoularis, *J. Fluid Mech.* **601**, 281 (2008).
- [3] M. Karami, H. Hangan, L. Carassale, and H. Peerhossaini, *Physics of Fluids* **31**, 085118 (2019).
- [4] G. R. Baker, S. J. Barker, K. K. Bofah, and P. G. Saffman, *J. Fluid Mech.* **65**, 325 (1974).
- [5] G. V. Iungo, P. Skinner, and G. Buresti, *Exp. in Fluids* **46**, 435 (2009).
- [6] J. P. J. Van Jaarsveld, A. P. C. Holten, A. Elsenaar, R. R. Triefling, and G. J. F. Van Heijst, *J. Fluid Mech.* **670**, 214 (2011).
- [7] A. S. Monin and A. Yaglom, *Statistical Fluid Mechanics. Mechanics of Turbulence*, Vol. 1 (MIT Press, 1971).
- [8] J. L. Lumley, *Stochastic Tools in Turbulence* (Academic Press, Inc., 1970).
- [9] See also the identity in E. Hopf, *J. Rat. Mech. Anal.* **1**, 87 (1952) p. 91
- [10] We designate by  $(\cdot, \cdot)$  and  $\|\cdot\|$  the usual Euclidean inner product and induced norm. The derivatives are defined in C. Truesdell, *The Kinematics of Vorticity* (Indiana University Press, 1954) pp. 37–39
- [11] T. Bölle, V. Brion, J.-C. Robinet, D. Sipp, and L. Jacquin, *J. Fluid Mech.* **908**, A8 (2021).
- [12] Let  $\mu_{\mathbf{X}}^t$  be symmetric. The expected value of the random function  $\phi(t, \mathbf{X}(t))$  reads

$$\begin{aligned} \langle \phi(t) \rangle &= \int_{\mathbb{R}^2} d\mu_{\mathbf{X}}^t(\mathbf{x}) \phi(t, \mathbf{x}) = \\ &= \int_{\mathbb{R}^2} d\mu_{\mathbf{X}}^t(\mathbf{x}) \{ \phi(t, \langle \mathbf{X} \rangle) + (\nabla \phi|_{\langle \mathbf{X} \rangle})(t, \mathbf{x}) + \dots \} \end{aligned}$$

using Taylor series expansion about the mean vortex centre. Due to symmetry only even terms contribute:

$$\langle \phi(t) \rangle = \int_{\mathbb{R}^2} d\mu_{\mathbf{X}}^t(\mathbf{x}) \phi(t, \langle \mathbf{X} \rangle) + O(\|\mathbf{x}\|^2) \quad (\|\mathbf{x}\| \rightarrow 0).$$

- [13] Averaging and time derivatives are assumed to commute [7, pp. 206–207].
- [14] H. Tennekes and J. L. Lumley, *A First Course in Turbulence* (MIT press, 1972).
- [15] The shown experimental data has been obtained from Particle Image Velocimetry in the facility and configuration described in L. Jacquin, P. Molton, P. Loiret, and E. Coustols, in *37th AIAA Fluid Dynamics Conference and Exhibit* (2007) p. 4363.
- [16] Considering Ref. [1, pp. 80–81],  $zU_{\infty}^{-1} \sim 10^{-1}$  s and  $T_L \sim \Omega_0^{-1} \sim r_1/U_1^{\theta} \sim 10^{-3}$  s yields  $zU_{\infty}^{-1}T_L^{-1} \sim 10^2$  and similarly in [2, 15].
- [17] The central-limit theorem still holds if both assumptions are relaxed [8, pp. 30–33, 84–93].
- [18] K. Pearson, *Nature* **72**, 342 (1905).
- [19] A time-continuous process can be traced back to a discrete sequence upon conceiving every step as the integral over a time interval of the length of the integral scale ([7, p. 541], [14, pp. 216–220]).



# C | The linear receptivity of vortices in frequency space

# On the linear receptivity of trailing vortices

Tobias Bölle<sup>1</sup>†, Vincent Brion<sup>1</sup>, Jean-Christophe Robinet<sup>2</sup>, Denis Sipp<sup>1</sup> and Laurent Jacquin<sup>1</sup>

<sup>1</sup>DAAA, ONERA-The French Aerospace Lab, Université Paris Saclay, 92190 Meudon, France

<sup>2</sup>DynFLuid, Arts et Métiers Institute of Technology, CNAM, HESAM University, 75013 Paris, France

(Received xx; revised xx; accepted xx)

The present work investigates the excitation process by which freestream disturbances are transformed into vortex-core perturbations. This problem of receptivity is modelled in terms of the resolvent in frequency space as the linear response to forcing. This formulation of receptivity suggests that nonnormality of the resolvent is necessary to allow freestream disturbances to excite the vortex core. Considering a local (in frequency) measure of nonnormality, we show that vortices are frequency-selectively nonnormal on a narrow frequency band of retrograde perturbations while the rest of the range is governed by an effectively normal operator, thus not contributing to receptivity. Canonical decomposition of the resolvent reveals that vortices are most susceptible to coiled filaments localised about the critical layer that induce bending waves on the core. Considering Lamb-Oseen, Batchelor and Moore-Saffman vortices as reference-flow models, we find freestream receptivity to be essentially generic and independent of the axial wavelength on the considered range. A stochastic interpretation of the results could be a model for trailing-vortex meandering.

## 1. Introduction

Trailing-vortex experiments systematically display unsteady dynamics manifesting as the lateral displacement of the vortex, called meandering. Despite having broadband spectral signature, kinetic energy is typically essentially concentrated in a low-frequency bending wave (Devenport *et al.* 1996; Jacquin *et al.* 2001; Bailey *et al.* 2018). Similar dynamics is observed for related configurations such as inlet vortices or tornadoes (Wang & Gursul 2012; Karami *et al.* 2019) as well as in the interaction of canonical vortices with turbulence (Melander & Hussain 1993; Marshall & Beninati 2005). For this reason, we only consider helical perturbations with  $|m| = 1$  ( $m$  is the azimuthal wavenumber).

Discussion of the origin of vortex unsteadiness divides researchers into two camps, who attribute it either to intrinsic or extrinsic mechanisms. The former approach assumes that dynamics is governed in essence by the vortex in isolation, *e.g.* instability or self-induction (Fabre & Jacquin 2004; Ting *et al.* 2007). We assume the second approach, assessing vortex unsteadiness as a consequence of external disturbances (*e.g.* residual turbulence in wind tunnels or the atmosphere or residual vortex sheets from the roll-up of the vortex itself). The excitation of vortex-core perturbations by the surrounding freestream is a (generalised) receptivity problem.

There is no reason to believe that receptivity in general should be a linear mechanism (Saric *et al.* 2002) and nonlinear studies have been pursued. Nevertheless, trailing-vortex experiments provide evidence that variation of the freestream-turbulence intensity only affects the displacement amplitude linearly (Van Jaarsveld *et al.* 2011, p. 222) while

† Email address for correspondence: tobias.bolle@onera.fr

the dominant meandering frequency is universal irrespective of the turbulence intensity (Bailey *et al.* 2018, fig. 7). These findings altogether suggest that vortices tend to spatially separate dynamical regimes which interact linearly (at least for the question of meandering). That is, on the one hand freestream dynamics is nonlinear and complex whereas on the other hand the vortex response is governed by core dynamics of organised nature (Bandyopadhyay *et al.* 1991; Devenport *et al.* 1996; Jacquin *et al.* 2001). This distinction is generic and independent of the (structural) details of freestream turbulence (at least sufficiently far from the wing, about five chord lengths, say). For this reason, we neglect all internal structure and interactions of the advective nonlinearity ( $\sim \nabla_{\mathbf{u}}\mathbf{u}$ ,  $\mathbf{u}$  being the perturbation velocity about the reference state  $\mathbf{U}$ ) but simply consider its compiled action in terms of the forcing field  $\mathbf{f} = \mathbf{f}(\mathbf{u})$  (Kato & Fujita 1962, p. 244; Landahl 1967, p. 456; Sharma *et al.* 2016, p. 6). Identification of the freestream with the given forcing field  $\mathbf{f}(t)$ , the exact evolution equation for perturbations  $\mathbf{u}(t)$  (*cf.* Joseph 1976, p. 8) takes on the form of an inhomogeneous linear abstract Cauchy problem. The general solution in time domain is the sum of the homogeneous  $\mathbf{u}_h(t)$  and a particular solution  $\mathbf{u}_p(t)$ . By Duhamel's principle,

$$\mathbf{u}(t) = \mathbf{u}_h(t) + \mathbf{u}_p(t) = \mathbb{T}(t)\mathbf{u}(0) + \int_0^t d\tau \mathbb{T}(t-\tau)\mathbf{f}(\tau), \quad t \geq 0, \quad (1.1)$$

where  $t \mapsto \mathbb{T}(t)$  is the propagator (semigroup) generated by the linearised Navier-Stokes operator  $\mathbb{L}$  (Kato 1980, p. 488, Engel & Nagel 2000, p. 436; see also Kato & Fujita 1962, pp. 244–245 and Sohr 2001, p. 8).

Alternatively, the solution in frequency space is obtained by Laplace transform of (1.1),

$$\hat{\mathbf{u}}(s) = \mathbb{R}(s)(\mathbf{u}(0) + \hat{\mathbf{f}}(s)) \quad \text{for admissible frequency } s \in \mathbb{C}. \quad (1.2)$$

The family of transfer operators  $s \mapsto \mathbb{R}(s) = \int_0^\infty dt \exp(-st)\mathbb{T}(t)$  is called the resolvent (Kato 1980, p. 484, Engel & Nagel 2000, p. 58). Equation 1.2 shows that the resolvent determines the homogeneous *and* particular solution in frequency space. The steady-state response of an asymptotically stable system (the case here) corresponds to the particular solution in (1.1) and is characterised in frequency space by taking the Fourier transform. Roughly speaking, setting  $s = i\omega$ ,  $\omega \in \mathbb{R}$  in (1.2) and  $\mathbf{u}(0) = 0$  we study response to harmonic forcing.

So far, most analysis of linear vortex dynamics concentrated on the representation in time domain. The homogeneous solution of (1.1) governs transient dynamics for all  $t \geq 0$  while asymptotic stability (as  $t \rightarrow \infty$ ) is determined by the spectrum of  $\mathbb{L}$  (Joseph 1976, p. 9; Arnol'd 1992, p. 212). Linear stability of Lamb-Oseen, Batchelor and Moore-Saffman vortices has been studied by Fabre *et al.* (2006), Fabre & Jacquin (2004) and Feys & Maslowe (2014) among others. From these studies, one concludes that vortices are asymptotically stable for typical parameters of aeronautical applications. More importantly, the spectrum is the union of a discrete spectrum of isolated eigenvalues (governing asymptotic stability) and two continuous spectra due to spatial unboundedness and an inviscid singularity, respectively (strictly speaking, continuity of the latter is true only in the inviscid limit; Heaton & Peake 2007). It is in fact this latter inviscid continuous spectrum which seems to be of primary importance for transient dynamics (Heaton & Peake 2007, p. 294, Mao & Sherwin 2012, p. 42).

As a matter of fact, despite asymptotic stability, transient energy growth is possible if the linear operator  $\mathbb{L}$  is nonnormal (*i.e.* it does not commute with its adjoint) (Farrell & Ioannou 1996; Trefethen & Embree 2005, § 14). Canonical decomposition (as in § 3.2) of the propagator  $\mathbb{T}(t)$  for fixed  $t > 0$  identifies those pairs of optimal initial and associated final-time perturbations which maximise energy growth for the given  $t$ . The possibility of

transient growth has been shown numerically for Lamb-Oseen and Batchelor vortices by Antkowiak & Brancher (2004), Pradeep & Hussain (2006), Heaton & Peake (2007) and Mao & Sherwin (2012) among others. For helical perturbations with  $|m| = 1$ , the main finding is the resonant excitation of core bending waves by remote filaments in the core periphery (Antkowiak & Brancher 2004). This mechanism also applies for the Batchelor vortex (Heaton & Peake 2007, p. 295).

Stochastic-forcing analysis in the time domain is concerned with the particular solution of (1.1) assuming stationary dynamics, *viz.* considering the  $t \rightarrow \infty$  limit (Farrell & Ioannou 1996). The probability distribution of  $\mathbf{f}(t)$  is *a priori* unknown and the forcing is usually assumed to be Gaussian spatio-temporal white noise (Farrell & Ioannou 1996; Fontane *et al.* 2008; Towne *et al.* 2018). Stochastic-forcing analysis has been conducted by Fontane *et al.* (2008) and Guo *et al.* (2011) for the Lamb-Oseen and Batchelor vortex, respectively. These studies identify the same resonance prototype as in transient-growth analyses to contribute most to stationary kinetic perturbation energy and covariance.

Fewer studies dealt with the solution in frequency space (1.2). Instead of analysing the propagator, transient dynamics can be described from tracing out contours of the resolvent norm, *i.e.* the pseudospectrum, in the complex plane (Trefethen & Embree 2005, pp. 31, 135). To the best of our knowledge, pseudospectra have only been computed for axisymmetric ( $m = 0$ ) perturbations of the Batchelor vortex (Mao & Sherwin 2011). We compute the pseudospectrum of the Lamb-Oseen vortex for  $m = 1$  and show that it is qualitatively identical to the results of Mao & Sherwin (2011) despite the important parametric difference.

However, by appeal to the above motivated physical model of trailing-vortex dynamics, the majority of our analysis concerns response to harmonic forcing (*i.e.* for  $s = i\omega$ ,  $\omega \in \mathbb{R}$  in (1.2) and  $\mathbf{u}(0) = 0$ ). As in transient-growth studies, canonical decomposition (§ 3.2) of the resolvent  $R(i\omega)$  for fixed  $\omega \in \mathbb{R}$  yields pairs of spatial forcing and response structures which are optimal in terms of energy amplification. Canonical decomposition of the resolvent has been computed previously for Lamb-Oseen and Batchelor vortices by Guo & Sun (2011) and Blanco-Rodríguez *et al.* (2017) for  $|m| \in \{0, 1, 2\}$ . However, no thorough attempt has been made to relate these results to physics and linear dynamics in general. Recently, Viola *et al.* (2016) analysed the resolvent of perturbation dynamics about the non-parallel, convectively unstable Batchelor vortex in a global approach and compared their results to linear stability analysis and nonlinear simulations of the Navier-Stokes equations. Their work focused on mode selection (*i.e.* identification of dominant azimuthal wavenumbers) and concludes applicability of the resolvent for this question.

The resolvent for harmonic forcing is a convenient model for linear receptivity to sustained excitation by the freestream (*cf.* also McKeon & Sharma 2010, p. 342). Assuming the forcing to be the compiled action of the (turbulent) freestream that we have no further knowledge of,  $\mathbf{f}(t)$  is naturally modelled as a random process. In this case the response  $\mathbf{u}(t)$  is also a stochastic process ( $T(t)$ ,  $R(s)$  are deterministic) and  $\mathbf{U} = \text{const.}$  is the *mean* state. It should be noted that  $\mathbf{U} + \mathbf{u}(t)$  is the Reynolds decomposition where the perturbation may be finite (Towne *et al.* 2018, p. 836). This setting is to be contrasted with traditional linear analysis where  $\mathbf{U}$  is the *base* flow (*i.e.* a fixed point of the Navier-Stokes equations; Arnol'd 1992, p. 210) and  $\mathbf{u}(t)$  is an infinitesimal deterministic process. Despite the motivation, the mathematical framework we employ does not distinguish between deterministic or stochastic forcing, neither is the restriction to freestream disturbances essential and  $\mathbf{f}(t)$  could conceptually represent *e.g.* control. Our analysis only addresses the operator properties of the (deterministic) resolvent, specifically its nonnormality.

The notion of freestream receptivity crucially relies on remote excitation in the sense

that forcing and response have spatially distinct support. Nonnormality of the resolvent is a means to excite core perturbations by radially disjoint forcing structures (*cf.* also Trefethen & Embree 2005, p. 201). We conclude that nonnormality is necessary for linear freestream receptivity (conj. 1, § 2). Since nonnormality is the essential feature of linear vortex dynamics in general, we expect our results to be of fundamental interest beyond the particular question of freestream receptivity.

Against this backdrop, the main objective must be a thorough understanding and quantification of the resolvent nonnormality. Various scalar measures have been proposed (*cf.* Trefethen & Embree 2005, § 48) which, though, might significantly overestimate effective nonnormality and hence be misleading for actual dynamics. Trefethen & Embree (2005, p. 446) conclude that ‘nonnormality is too complex to be summarized in a single number’. We make use of resolvent bounds to classify nonnormality of linear vortex dynamics in frequency domain. While the governing operator is nonnormal, it will be shown that the *effective* behaviour for vortices depends on the excitation frequency, we call this *selective nonnormality* (conj. 2, §§ 3–4). First studying the linearised operator  $L$  for a generic vortex in § 4.1, we deduce that nonnormality should be maximal for forcing localised about the critical layer (radial location where the phase velocity equals advection by the mean; Le Dizès 2004, p. 319). Assuming the (parallel) Lamb-Oseen vortex as a reference state (base-flow model), we confirm this result numerically in §§ 4.2–4.4.

The second objective is the corroboration of these results under variation of the reference flow and the axial wavenumber. For this purpose, we analyse the resolvent for (parallel) Batchelor and Moore-Saffman vortices in § 5 which constitute approximations to experimental mean flow (see § 2.2). This sequence of reference states serves two purposes, namely to assess differences between dynamics about base and mean flow as motivated above and to evaluate the impact of (weak) axial mean velocity in the vortex core. We discuss the relation to previous linear studies throughout.

Lastly, results in frequency space are often easier related to experiments than time-domain analysis. Still, idealising vortex meandering as a monochromatic wave, the associated frequency in experiments corresponds to an infinity of wavenumber-frequency pairs in theory by the Doppler relation. Nevertheless, by appeal to our results of selective nonnormality, in § 6 we show how the actually contributing frequency range can be significantly reduced.

## 2. Linear receptivity in the resolvent formalism

Let the fluid domain be the entire Euclidean space  $\mathbb{R}^3$  with cylindrical coordinates  $\mathbf{x} = (r, \theta, z)$  and corresponding velocities  $\mathbf{v} = (v_r, v_\theta, v_z)$ . The  $z$  coordinate is chosen to coincide with the axis of mean rotation,  $r$  pointing radially outwards and  $\theta$  being such that  $\{r, \theta, z\}$  yields a right-handed system. The fluid is assumed incompressible with constant, homogeneous material properties.

All physical quantities are non-dimensionalised on the length scale  $r_0 = 2\sqrt{\nu t_0}$ , where  $t_0 > 0$  determines the vortex age and is chosen such that  $r_0 := 1$  without loss of generality, and the azimuthal mean velocity at this radius  $(2\pi r_0)^{-1} \Gamma_0 := 1$ . It follows the circulation-based Reynolds number  $R_\Gamma := \Gamma_0 / (2\pi\nu) = \nu^{-1}$ .

### 2.1. Trailing vortex dynamics as a generalised receptivity problem

The dynamics of trailing vortices in experiments is dominated by low-frequency displacement waves (vortex meandering). In the intermediate wake ( $z \leq 10b$ ,  $b$  is the

wingspan; Jacquin *et al.* 2001, p. 5) destabilising effects from consideration of the counter-rotating pair are of second order (Crow  $\sim b^{-2}$ ; Jacquin *et al.* 2001, p. 17) and the isolated line vortex is asymptotically stable for parameters of typical aeronautic applications (Fabre & Jacquin 2004, p. 259). Rather it appears that the observed dynamics is due to temporally sustained excitation of the vortex by the surrounding freestream (as already suggested by Baker *et al.* 1974, p. 331). This *internalisation* of *external* disturbances is reminiscent of receptivity.

While strictly speaking the classical notion of receptivity applies to the transition problem and the excitation of instability modes (Morkovin 1988, p. 76), it is used here to describe the general reaction of a system to initial or temporally sustained external disturbances (see also Fontane *et al.* 2008, p. 236). For these reasons, let us refer to the problem of receptivity in the following generalised sense which is not restricted to laminar reference states but straightforwardly extends to turbulent mean flows. (This generalised perception of receptivity is also implicitly understood in McKeon & Sharma 2010, p. 342 and Towne *et al.* 2018, §5.1 among others.)

**DEFINITION 1.** *The excitation of general perturbations inside the vortex by external disturbances is called (freestream) receptivity.*

The essential aspect of receptivity according to def. 1 is *perturbation internalisation* in the sense that *external* disturbances in the freestream are converted into *internal* perturbations inside the vortex. For this excitation to be well-defined, we must partition the fluid domain into a subset  $\mathbb{V}$  identified with the interior of the vortex and its complement  $\mathbb{R}^3 \setminus \mathbb{V}$ , *viz.* the freestream.

Trailing-vortex experiments provide considerable evidence that rather rapidly (within about two wing chords  $c$  at chord-based Reynolds number  $R_c := U_\infty c / \nu \sim 10^5$ ; Devenport *et al.* 1996, p. 68) the flow develops a coherent vortex in the sense of a single concentration of streamwise vorticity which is axisymmetric and parallel to leading order. For definiteness, we define the system boundary as a concentric cylinder at the *vortex-core radius*  $r_1 = 1.12$ , corresponding to the location of the maximum azimuthal velocity of a Gaussian vortex. Similar identification of the vortex core is used by Pradeep & Hussain (2006, p. 266) and Takahashi *et al.* (2005, p. 6) for example. Thus, perturbations with radial support less than  $r_1$  are interior to the vortex while those disturbances supported on  $r > r_1$  are external, *viz.* in the freestream. It must be stressed that the notion of internalisation here only serves the purpose to highlight the essential aspect of receptivity (according to def. 1) of being inherently related to a spatial shift between forcing and response in the (spatio-temporal) fluid domain. In fact, as discussed in § 3.1, freestream receptivity may not require actual transport (*e.g.* of energy) over the system boundary.

## 2.2. Choice of the reference flow

Trailing vortices are generically associated with an axisymmetric mean velocity of the form  $\mathbf{U}(r) = U_\theta(r)\mathbf{e}_\theta + U_z(r)\mathbf{e}_z$ , blending rotational and jet kinematics. Restriction to parallel vortices is justified by previous studies of Antkowiak (2005, fig. 3.18), Heaton *et al.* (2009) and Viola *et al.* (2016, fig. 5), showing numerically that consideration of base-flow diffusion does not alter considerably transient-growth and stability properties.

We consider receptivity of Lamb-Oseen, Batchelor and Moore-Saffman vortices. The motivation for this sequence of reference flows is twofold. Firstly, it gradually shifts between different conceptual points of view, *viz.* from base to mean flow. Considering the Lamb-Oseen vortex as (an approximation to) a base flow yields receptivity of the laminar state. On the other hand, the Moore-Saffman vortex rather constitutes an approximation to the mean flow thus building on the above generalised notion of

receptivity in a turbulent (stochastic) framework. Secondly, the effect of including an axial mean velocity on freestream receptivity can be assessed (we assume weak axial mean velocity as discussed below).

The parallel approximation of the Batchelor vortex (Batchelor 1964) reads (see also Fabre & Jacquin 2004, p. 242 and Heaton & Peake 2007, p. 285)

$$U_r(r) = 0, \quad U_\theta(r) = \frac{1 - e^{-r^2}}{r}, \quad U_z(r) = q^{-1} e^{-r^2}. \quad (2.1)$$

Equation (2.1) is parametrised by the swirl number  $q \neq 0$  (the ratio of mean azimuthal to axial velocity; Jacquin *et al.* 2001, p. 15). The Lamb-Oseen vortex is formally obtained as the  $|q| \rightarrow \infty$  limit of the Batchelor vortex (2.1).

The parallel approximation of the Batchelor vortex is typically considered as a base flow in stability analysis. Nevertheless, Iungo (2017, p. 1785) observe the Batchelor vortex to fit experimental data well, which is also claimed by Heaton & Peake (2007, p. 272). Qualitative matching is equally reported in numerical studies of Takahashi *et al.* (2005, p. 5) and Heaton *et al.* (2009, pp. 142, 144). At least, the Batchelor vortex constitutes a useful prototype, containing the essential aspects of trailing-vortex mean velocity.

The Moore-Saffman vortex is defined by a system of differential equations (Moore & Saffman 1973) which is solved numerically. From a practical point of view the important aspect of this model is its parametrisation by the real value  $n \in (0, 1)$  which determines the radial decay of the velocity profiles and leads to jet-wake coexistence for sufficiently small values. Generally, the Moore-Saffman vortex is observed to be a good fit to experimental mean velocity. There is considerable experimental evidence that a representative value is about  $n \gtrsim 0.75$  for trailing vortices. For instance, experiments conducted at ONERA suggest a calibration with  $n \in \{0.79, 0.72, 0.80\}$  in the streamwise range of one to five wingspans (private communication). Similarly, experiments and iLES of García-Ortiz *et al.* (2019, fig. 6(b)) report a range of roughly  $n \in [0.8, 0.95]$  over a streamwise range of 40 chords and chord Reynolds number  $R_c \sim 10^4$ . For these representative values of  $n$  departure from a Gaussian vortex is essentially negligible.

### 2.3. Resolvent for the linear dynamics of a trailing vortex

Let there be given a time-invariant reference state  $(\mathbf{U}, P)$  of the form  $\mathbf{U}(r) = U_\theta(r)\mathbf{e}_\theta + U_z(r)\mathbf{e}_z$  and  $P = P(r)$  (the pressure) defining the vortex in the sense of § 2.1 by one of the reference states of § 2.2, subjected to the perturbation  $(\mathbf{u}, p)$  such that  $(\mathbf{U} + \mathbf{u}, P + p)$  solves the Navier-Stokes equations. Consider perturbations in the form of Fourier modes  $\mathbf{u}(t, r, \theta, z) = \hat{\mathbf{u}}(s, r, m, \alpha) \exp(i(m\theta + \alpha z) - st) + \text{c.c.}$  whereas  $m \in \mathbb{Z}$ ,  $\alpha \in \mathbb{R}$  and  $s = s_r + is_i \in \mathbb{C}$  and equivalently for the pressure. For convenience, parameters in the Fourier amplitudes will be dropped if unambiguous. Complex frequencies  $s$  are used in the computation of spectra and pseudospectra (defined below) while the response to temporally-sustained forcing assumes purely imaginary values  $s = i\omega, \omega \in \mathbb{R}$ . We seek perturbations with finite kinetic energy, thus endowing the solution space with the inner product

$$(\hat{\mathbf{u}}, \hat{\mathbf{v}}) := \int_0^\infty dr r \sum_{l=1}^3 \overline{\hat{u}_l(r)} \hat{v}_l(r), \quad (2.2)$$

where an overbar  $\overline{(\cdot)}$  denotes complex conjugation.

Inserting the decomposition  $(\mathbf{U} + \mathbf{u}, P + p)$  into the Navier-Stokes equations and subtracting the equation for the reference flow yields a nonlinear transport equation for the perturbation. Restriction only to linear terms yields the linearised perturbation transport equation (Joseph 1976, pp. 7–8). In studying receptivity, we suppose a non-

vanishing inhomogeneity  $\mathbf{f}$  to drive the system. Introducing the above Fourier ansatz into the linear perturbation transport equation yields a boundary-value problem on  $r \in [0, \infty)$  for the system of linear ordinary differential equations, parametrised by the wavenumbers  $m \in \mathbb{Z}, \alpha \in \mathbb{R}$  and frequency  $s \in \mathbb{C}$ . For  $m = \pm 1$ ,

$$(\mathbf{L} - s\mathbf{P}) \begin{pmatrix} \hat{\mathbf{u}} \\ \hat{\mathbf{p}} \end{pmatrix} = \begin{pmatrix} \hat{\mathbf{f}} \\ 0 \end{pmatrix} \text{ such that } \begin{cases} d\hat{u}_r/dr|_0 \text{ and } d\hat{u}_\theta/dr|_0 = 0 \\ \hat{u}_z(0) = \hat{p}(0) = 0 \end{cases}, \quad \begin{pmatrix} \hat{\mathbf{u}} \\ \hat{\mathbf{p}} \end{pmatrix} (r \rightarrow \infty) \rightarrow 0. \quad (2.3)$$

The restriction to perturbations with finite kinetic energy on an unbounded domain requires faster than algebraic decay as  $r \rightarrow \infty$  (Ash & Khorrami 1995, pp. 339–342). The linear operators in (2.3) are formally given by the projection

$$\mathbf{P} := \begin{bmatrix} 1 & 0 & 0 & 0 \\ 0 & 1 & 0 & 0 \\ 0 & 0 & 1 & 0 \\ 0 & 0 & 0 & 0 \end{bmatrix} = \begin{bmatrix} 1 & 0 & 0 \\ 0 & 1 & 0 \\ 0 & 0 & 1 \\ 0 & 0 & 0 \end{bmatrix} \begin{bmatrix} 1 & 0 & 0 & 0 \\ 0 & 1 & 0 & 0 \\ 0 & 0 & 1 & 0 \\ 0 & 0 & 1 & 0 \end{bmatrix} =: \mathbf{B}\mathbf{B}^\dagger$$

and

$$\mathbf{L} := \begin{bmatrix} im\Omega + i\alpha U_z - \nu(\Delta - r^{-2}) & -2\Omega + 2\nu imr^{-2} & 0 & d/dr \\ W_z - 2\nu imr^{-2} & im\Omega + i\alpha U_z - \nu(\Delta - r^{-2}) & 0 & imr^{-1} \\ dU_z/dr & 0 & im\Omega + i\alpha U_z - \nu\Delta & i\alpha \\ -r^{-1} - d/dr & -imr^{-1} & -i\alpha & 0 \end{bmatrix}$$

whereas

$$\Delta := \frac{d^2}{dr^2} + \frac{1}{r} \frac{d}{dr} - \left(\frac{m}{r}\right)^2 - \alpha^2 \quad \text{and} \quad \Omega := \frac{U_\theta}{r}, \quad W_z := \Omega + \frac{dU_\theta}{dr}$$

are the Laplace operator of a scalar field, the angular velocity and axial vorticity of the reference flow, respectively. The radius  $r_c \in \mathbb{R}$  for which mean advection  $m\Omega(r_c) + \alpha U_z(r_c)$  equals the perturbation frequency  $\omega = s_i \in \mathbb{R}$  is called critical layer (Le Dizès 2004, p. 319).

Suppose the inverse of (2.3) exists, then the solution formally reads

$$\hat{\mathbf{u}}(s) = \mathbf{B}^\dagger (\mathbf{L} - s\mathbf{P})^{-1} \mathbf{B} \hat{\mathbf{f}}(s) \quad \text{for all } s \in \rho(\mathbf{L}) \quad (2.4)$$

and the operator-valued one-parameter family  $s \mapsto \mathbf{R}(s; \mathbf{L}) := \mathbf{B}^\dagger (\mathbf{L} - s\mathbf{P})^{-1} \mathbf{B}$  is referred to as the resolvent (Kato 1980, p. 173). Bounded inversion exists for frequencies which do not pertain to the spectrum  $\sigma(\mathbf{L})$ . The subset of the complex plane for which the resolvent is defined *and* bounded is called resolvent set  $\rho(\mathbf{L})$  (Riesz & Sz.-Nagy 1956, §132). For the here considered asymptotically stable systems  $i\mathbb{R} \subset \rho(\mathbf{L})$  holds and the resolvent is defined on the entire imaginary axis. The pseudospectrum is defined by  $\sigma_\epsilon(\mathbf{L}) := \{s \in \mathbb{C} \mid \|\mathbf{R}(s; \mathbf{L})\| > \epsilon^{-1}\}$  as contours of the resolvent norm (defined in § 3.2) for fixed values of  $\epsilon > 0$  (Trefethen & Embree 2005, p. 31).

The resolvent (2.4) is obtained numerically from finite-element discretisation of (2.3) and inversion of the corresponding matrix, see app. A.

Due to symmetries of the linearised perturbation equation (2.3) the parameter space can be reduced. For the Lamb-Oseen vortex it is sufficient to consider  $m, \alpha \geq 0$  and  $\omega \in \mathbb{R}$  (Fabre *et al.* 2006, pp. 241–242). Inclusion of an axial velocity component breaks azimuthal symmetry, making a distinction between positive and negative azimuthal wavenumbers necessary (Fabre & Jacquin 2004, p. 247; Heaton & Peake 2007, p. 289).

### 3. Estimation of linear receptivity by analysis of the nonnormality

Let  $A$  be a formal operator on a Hilbert space (see *e.g.* Kato 1980, p. 146 for this terminology) and denote by  $A^\dagger$  its formal adjoint. Then  $A$  is formally normal if the commutator  $[\cdot, \cdot]$  of  $A$  and  $A^\dagger$  is equal to zero, *i.e.*  $[A, A^\dagger] := AA^\dagger - A^\dagger A = 0$  (Riesz & Sz.-Nagy 1956, p. 284; Kato 1980, p. 276).

#### 3.1. Necessity of nonnormality for linear freestream receptivity

Receptivity according to def. 1 is intimately linked to the excitation of vortex-core perturbations by spatially remote disturbances. For receptivity of vortices to freestream disturbances this implies a radial perturbation shift in order to internalise external disturbances. Now, if the linear receptivity problem (2.4) is associated with a *normal* operator  $R(i\omega; L)$  any forcing-response pair  $\{\hat{\mathbf{f}}(\omega), \hat{\mathbf{u}}(\omega)\}$  should have the same radial support. On the other hand, Trefethen & Embree (2005, p. 10) states that resonance of *nonnormal* systems is the fundamental principle in receptivity. Indeed, the following may be suggested (see also Roy & Subramanian 2014, p. 405).

CONJECTURE 1. *Let perturbations have finite kinetic energy, then nonnormality of  $R(i\omega; L)$  is necessary for the linear model of vortex receptivity to freestream disturbances.*

Assuming linear dynamics, vortices are receptive to freestream disturbances by two distinct mechanisms, namely through (i) generalised eigenvectors pertaining to the continuous spectrum  $\sigma_c^\infty(L)$  (defined in § 4.2) and (ii) critical-layer forcing discussed in §§ 4.2–4.3. Efficiency of the former is typically significantly diminished due to shear sheltering such that disturbances only slightly penetrate the core (Jacobs & Durbin 1998). In fact, the penetration mechanism is viscous (no penetration in the inviscid limit; Jacobs & Durbin 1998, p. 2010) and should not be significant for high Reynolds numbers in experiments. Restriction to perturbations with finite kinetic energy in conj. 1 excludes receptivity associated with generalised eigenvectors pertaining to  $\sigma_c^\infty(L)$ .

There is considerable evidence that a vortex essentially constitutes a material subset of the fluid domain which does not exchange fluid particles with its surrounding (Haller *et al.* 2016). Therefore, perturbation-energy amplification in the core must preclude significant mass or momentum transport, *e.g.* through intermittent vorticity stripping or ejection, as proposed by Bandyopadhyay *et al.* (1991, pp. 1629, 1633). Indeed, strong ambient turbulence intensity is required to enable exchange of core fluid with the freestream (Marshall & Beninati 2005, pp. 231, 233). For low to moderate levels, numerical experiments indicate that coiled vorticity filaments in the freestream cannot penetrate into the core (Jacobs & Durbin 1998, p. 2006; Takahashi *et al.* 2005, p. 12). Low turbulence intensities in experiments therefore call for receptivity mechanisms which excite core perturbations without significant mass transport. The proposed receptivity mechanism by nonnormality does not require physical exchange of fluid, hence, constitutes a candidate in moderate-turbulence regimes.

#### 3.2. Canonical decomposition and bounds on the resolvent

The present study uses canonical decomposition of the resolvent, *cf.* (2.4). Let  $R(s; L)$  be a compact linear operator and  $n > 0$ . Then, for all admissible forcing fields  $\hat{\mathbf{f}}$ , the expansion

$$\hat{\mathbf{u}}(s) = R(s; L) \hat{\mathbf{f}}(s) = \sum_{k=1}^n \mu_k(s) \mathbf{u}_k(s) (\mathbf{f}_k(s), \hat{\mathbf{f}}(s)), \quad s \in \rho(L), \quad (3.1)$$

converges, whereas orthogonality  $(\mathbf{f}_k(s), \mathbf{f}_l(s)) = (\mathbf{u}_k(s), \mathbf{u}_l(s)) = \delta_{kl}$  holds and  $\mu_1(s) \geq \mu_2(s) \geq \dots \geq \mu_n(s) > 0$  (Riesz & Sz.-Nagy 1956, p. 203; Kato 1980, pp. 160–161 and 260–262). The pair  $\{\mathbf{u}_k(s), \mathbf{f}_k(s)\}$  defines a hierarchy of rank-1 operators and  $\mu_k(s)$  is referred to as singular value. From a physics point of view, each pair defines the radial pattern of the  $k$ th-optimal response  $\mathbf{u}_k(s)$  to forcing  $\mathbf{f}_k(s)$ . We call  $\mathbf{f}_k(s)$ ,  $\mathbf{u}_k(s)$  forcing and response structures, respectively. The respective singular values  $\mu_k(s)$  signify the  $k$ th-optimal energy amplifications and the leading singular value is identical to the norm of the resolvent  $\mu_1^2(s) = \|\mathbf{R}(s; \mathbf{L})\|^2$  which can be interpreted as the maximum amplification obtained for all admissible forcing fields (Riesz & Sz.-Nagy 1956, p. 149).

The canonical decomposition (3.1) is inherently related to the respectively self-adjoint eigenvalue problems (Kato 1980, p. 261)

$$\mathbf{R}^\dagger \mathbf{R} \mathbf{f}_k = \mu_k^2 \mathbf{f}_k \quad \text{and} \quad \mathbf{R} \mathbf{R}^\dagger \mathbf{u}_k = \mu_k^2 \mathbf{u}_k \quad \text{with} \quad \mathbf{u}_k := \mu_k^{-1} \mathbf{R} \mathbf{f}_k, \quad \mu_k \neq 0.$$

If  $\mathbf{R}(s; \mathbf{L})$  is normal the two eigenvalue problems can be identified, implying that forcing and response are structurally identical. By def. 1, receptivity relies on perturbation internalisation, hence, forcing and response structures must have different spatial support. This is possible if the resolvent is nonnormal; *cf.* conj. 1. The degree of nonnormality can be estimated from bounds on the resolvent norm.

Let  $\phi(\mathbf{L}) := \text{cl}\{s \in \mathbb{C} \mid s = (\mathbf{q}, \mathbf{P}\mathbf{L}\mathbf{q}), \mathbf{q} = (\mathbf{u}, p)^T \text{ such that } \text{div } \mathbf{u} = \text{div } \mathbf{B}^\dagger \mathbf{L}\mathbf{q} = 0, \|\mathbf{u}\| = 1\}$  be the closure  $\text{cl}\{\cdot\}$  of the numerical range (Kato 1980, p. 267; Gustafson & Rao 1997, p. 1). Then, for all  $s \in \rho(\mathbf{L})$  which are in the complement of  $\phi(\mathbf{L})$ ,

$$\frac{1}{d(s, \sigma(\mathbf{L}))} \leq \|\mathbf{R}(s; \mathbf{L})\| \leq \frac{1}{d(s, \phi(\mathbf{L}))}, \quad (3.2)$$

where  $d(s, \sigma(\mathbf{L})) := \inf_{\lambda \in \sigma(\mathbf{L})} |s - \lambda| > 0$  defines the distance of  $s \in \rho(\mathbf{L})$  from the closest element in the spectrum and analogously for  $d(s, \phi(\mathbf{L}))$  with  $s \notin \phi(\mathbf{L})$  (Kato 1980, Thm. 3.2; Gustafson & Rao 1997, eq. (4.6-7) and Lem. 6.1-4). Equality with the lower bound holds in (3.2) if the resolvent is normal (Kato 1980, pp. 272, 277).

From a physical point of view, the left-hand side of (3.2) describes the "classical" resonance behaviour of the equivalent normal operator (solely determined by its spectrum) as the excitation frequency  $s$  differs from elements of the spectrum (Arnol'd 1992, p. 235). In contrast, nonnormal operators are principally amenable to significant amplification even far from the spectrum (Trefethen & Embree 2005, p. 10). Contours of the resolvent norm (*i.e.* the pseudospectrum) therefore represent generalised resonance (pseudo-resonance) of the system. Comparison of the graphs of the lower bound with the resolvent norm along the imaginary axis ( $s = i\omega$ ) therefore reveals frequency ranges where the resolvent is nonnormal and thus pseudo-resonance outweighs "classical" resonance (*cf.* fig. 3).

The right-hand side of (3.2), defining the distance to the numerical range  $\phi(\mathbf{L})$ , is physically not associated with resonance but related to the capacity of energy growth which we use in § 4.1 to derive the location of the instantaneously most amplified perturbation. Despite identical structure of the two bounds in (3.2), it should be emphasized that we cannot use the upper bound to draw a meaningful graph (similar to fig. 3(a)) which bounds pseudo-resonance  $\|\mathbf{R}(s = i\omega; \mathbf{L})\|$  from above along the imaginary axis. Rather the intention is to gain insight into nonnormality from patterns the linear operator  $\mathbf{L}$  defines in the complex plane. The smallest set characterising  $\mathbf{L}$  (sufficient for the dynamics of normal operators) is the spectrum  $\sigma(\mathbf{L})$  while the numerical range  $\phi(\mathbf{L})$  is the largest set determining dynamics. Pseudospectra  $\sigma_\epsilon(\mathbf{L}) \subset \mathbb{C}$ , determining transient dynamics, continuously fill the gap whereas  $\lim_{\epsilon \rightarrow 0} \sigma_\epsilon(\mathbf{L}) \leftrightarrow \sigma(\mathbf{L})$  and  $\lim_{\epsilon \rightarrow \infty} \sigma_\epsilon(\mathbf{L}) \leftrightarrow \phi(\mathbf{L})$  (Gustafson & Rao 1997, p. 106; Trefethen & Embree 2005, p. 172). We expect that resolvent nonnormality can be inferred from differences in these sets.

#### 4. Selective nonnormality of linear vortex dynamics

Hill (1995, p. 183) noted that receptivity is determined by geometry, physical location and frequency of the source as well as the reference-flow characteristics. Indeed, wind-tunnel and numerical experiments provide evidence that vortices favour a response at distinguished frequencies and to particular disturbance patterns (*e.g.* Marshall & Beninati 2005; Bailey *et al.* 2018). Adopting the linear model developed in §2.3 the last of Hill's points is obvious since the formal operator is essentially determined by the reference-flow profile as discussed below. Further assessment shows that the reference flow also imposes a preferred position and frequency for disturbances contributing to freestream receptivity; we find that vortices are generally most susceptible to the archetypal forcing pattern of coiled filaments aligned with the critical layer. As stated in conj. 1 nonnormality is a necessary requirement for linear receptivity to freestream turbulence and hence to quantify the above aspects; we thus conclude the main result of this section:

**CONJECTURE 2.** *Linear perturbation dynamics about axisymmetric vortices satisfying  $\mathbf{U}(r) = U_\theta(r)\mathbf{e}_\theta + U_z(r)\mathbf{e}_z$  are governed by an  $\omega$ -selectively nonnormal linear operator. In the inviscid limit, nonnormality is maximised for critical-layer perturbations.*

##### 4.1. Analysis of the formal operator and its numerical range

To the best of our knowledge no analytic expression of the resolvent for three-dimensional inhomogeneous perturbations about smooth viscous vortices exists today (*e.g.* Ash & Khorrami 1995, p. 321; Roy & Subramanian 2014, p. 439). However, it can be shown that normality of a linear operator implies normality of its resolvent (Kato 1980, pp. 276–277) so that we proceed by analysing  $\mathbf{L}$ , expecting similar properties to hold for  $\mathbf{R}(i\omega; \mathbf{L})$ , too.

In order to attribute nonnormality a physical significance, the linear operator in (2.3) is written as the sum

$$\mathbf{L} = \nabla_{\mathbf{U}} + \nabla\mathbf{U} + \mathbf{A}, \quad (4.1)$$

comprising contributions from advection  $\nabla_{\mathbf{U}}$ , mean-velocity gradient  $\nabla\mathbf{U}$  and the Stokes operator  $\mathbf{A}$  (governing the Stokes system; Sohr 2001, §4), respectively. Pressure gradient and continuity equation are contained in the Stokes operator by definition.

The formal adjoint of (4.1) is defined through the Lagrange identity (Friedman 1962, p. 148) and reads

$$\mathbf{L}^\dagger = \nabla_{\mathbf{U}}^\dagger + (\nabla\mathbf{U})^\dagger + \mathbf{A}^\dagger = -\nabla_{\mathbf{U}} + (\nabla\mathbf{U})^\dagger + \mathbf{A}. \quad (4.2)$$

Comparing (4.1) and (4.2) element-wise, it is evident that the Stokes operator  $\mathbf{A}$  is (formally) self-adjoint and hence normal. Taken independently, the advection operator  $\nabla_{\mathbf{U}}$  is formally skew-adjoint thus also normal.† While dynamics on unbounded or periodic fluid domains (in the direction of the mean flow) seems to promote actual self-adjointness, realisations on bounded domains are associated with (inflow-outflow) boundary conditions which break the formal behaviour. In terms of physics, this latter *advective nonnormality* known in the *global* approach manifests as the spatial separation (in  $z$ ) of the direct and adjoint eigenfunctions (Sipp *et al.* 2010, p. 7). From the three terms in (4.1) only the velocity-gradient operator  $\nabla\mathbf{U}$  is inherently nonnormal in isolation.

Since the Stokes operator is normal (independently) and increasing viscosity consistently found to dampen nonnormal dynamics, nonnormality of  $\mathbf{L}$  should result from the inviscid advection and mean-velocity gradient operators (Antkowiak 2005, p. 3; Pradeep

† A skew-adjoint operator generates a unitary (inner-product preserving) propagator, *viz.*  $\mathbf{T}(t)^\dagger = \mathbf{T}(t)^{-1}$  for all  $t$  (Engel & Nagel 2000, p. 20).

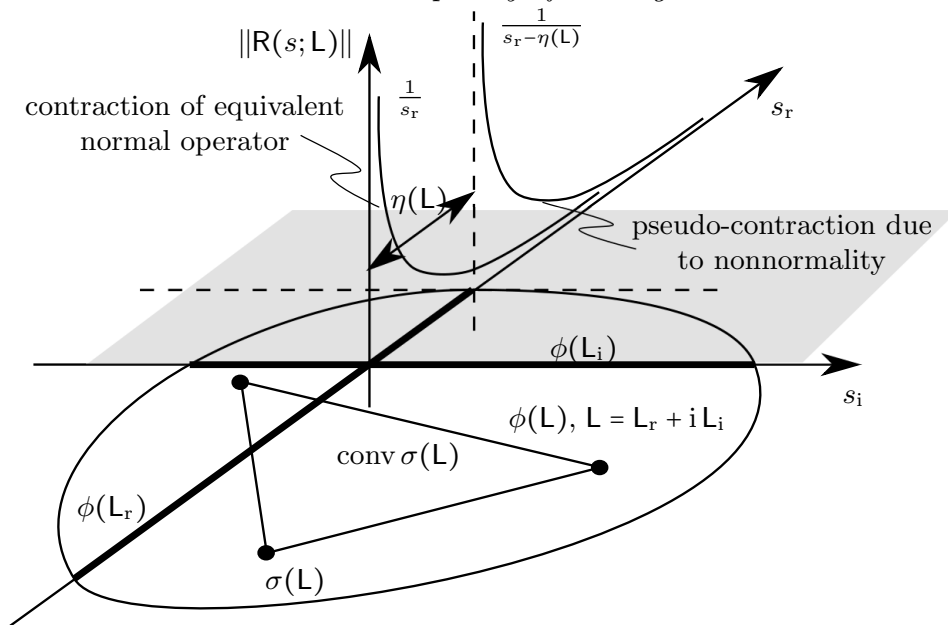


Figure 1: Schematic comparison of the dissipative dynamics (contraction) generated by the equivalent normal operator (*i.e.* solely defined by its spectrum  $\sigma(\mathbf{L})$  and its convex hull  $\text{conv } \sigma(\mathbf{L})$ ) with the actual dynamics (determined by the numerical range  $\phi(\mathbf{L})$ ) showing that nonnormality is associated with the numerical abscissa  $\eta(\mathbf{L})$  (see (4.5)). The unstable half plane is visualised by grey shading.

& Hussain 2006, p. 279; Heaton & Peake 2007, p. 278). It should be noted though that the sum of normal operators is not necessarily normal, as shown *e.g.* for the advection-diffusion operator by Reddy & Trefethen (1994, p. 1647).

Neglecting  $\mathbf{A}$  in (4.1) and (4.2), formal nonnormality of the advection-velocity-gradient operator is associated with the commutator  $[\mathbf{L}, \mathbf{L}^\dagger] \rightarrow [\nabla_{\mathbf{U}}, 2\mathbf{S}] + [\nabla\mathbf{U}, (\nabla\mathbf{U})^\dagger]$  (recalling that advection is formally normal) where  $\mathbf{S} := (\nabla\mathbf{U} + (\nabla\mathbf{U})^\dagger)/2$  denotes the hermitian part of the velocity gradient. Explicitly,

$$[\mathbf{L}, \mathbf{L}^\dagger] \rightarrow \begin{bmatrix} -(W_z + 2\Omega)r d\Omega/dr - (dU_z/dr)^2 & 0 & 0 \\ 0 & (W_z + 2\Omega)r d\Omega/dr & \Omega dU_z/dr \\ 0 & \Omega dU_z/dr & (dU_z/dr)^2 \end{bmatrix}. \quad (4.3)$$

Writing  $(W_z + 2\Omega)r d\Omega/dr = W_z^2 - (2\Omega)^2$  readily shows that dynamics is formally normal if the reference flow is that of a rigid-body rotation and translation (*i.e.*  $W_z = 2\Omega$  and  $U_z = \text{const.}$ ). In other words, nonnormality is unaffected by the superposition of rotation or translation as a rigid body and, in particular, indistinguishable for observers being in rigid-body rotation or translation to one another, *e.g.* between aeroplane cruise condition and laboratory experiment.

To get a deeper understanding of the resolvent nonnormality, let us now consider the upper bound in (3.2), which, as we re-emphasize, is not amenable to the same physical and graphical interpretation as the lower bound in terms of resonance but rather the intention is the assessment of nonnormality. In fact, the upper bound merely means that the pseudospectrum  $\sigma_\epsilon(\mathbf{L})$  cannot be much larger than the numerical range  $\phi(\mathbf{L})$  (Trefethen & Embree 2005, p. 169). Figure 1 shows a qualitative sketch illustrating the principal terminology used thereafter.

We write  $\mathbf{L} = \mathbf{L}_r + i\mathbf{L}_i$  with the hermitian part  $\mathbf{L}_r := (\mathbf{L} + \mathbf{L}^\dagger)/2$  and the skew-hermitian part  $\mathbf{L}_i := (\mathbf{L} - \mathbf{L}^\dagger)/(2i)$ , respectively. This decomposition implies the inclusion the spectrum in the numerical range,  $\sigma(\mathbf{L}) \subset \phi(\mathbf{L}_r + i\mathbf{L}_i) \subset \phi(\mathbf{L}_r) + i\phi(\mathbf{L}_i)$ , which is shown in fig. 1 (Kato

1980, pp. 309–310; Gustafson & Rao 1997, pp. 6, 103). From a physical point of view, the hermitian part  $L_r = S + A$  determines energy growth while the skew-hermitian part  $L_i = -i\nabla_U + W$  ( $\nabla_U = S + iW$  where  $W$  is the skew-hermitian mean-vorticity operator) is associated with conservative redistribution (*cf.* also the remark in the context of  $\nabla_U$  above). In agreement, Pradeep & Hussain (2006, p. 264) conclude that mean vorticity promotes vortex waves which do not contribute to energy growth. *A priori* this does not tell us anything about the origin of nonnormality, however, our interest in energy amplification suggests closer examination of  $\phi(L_r)$ .

This reasoning is reflected in the Hille-Yosida generation theorem (Engel & Nagel 2000, pp. 73–76). Let  $c \in \mathbb{R}$  be a constant (which we identify with the numerical abscissa  $\eta(L)$  below), then the propagator  $T(t)$  is a *pseudo-contraction* if and only if

$$\|T(t)\| \leq e^{ct} \quad \forall t \geq 0 \quad \Leftrightarrow \quad \|R(s; L)\| \leq \frac{1}{s_r - c}, \quad s_r > c. \quad (4.4)$$

By definition, the associated generator  $L$  is contractive if its numerical range does not protrude into the unstable half plane while it is pseudo-contractive if it becomes contractive upon a constant shift  $L - c$  (Kato 1980, pp. 278–279; Engel & Nagel 2000, p. 75). Physically, a contractive propagator represents dissipation (of energy;  $c = 0 \Rightarrow \|T(t)\| \leq 1$ ) whereas a pseudo-contraction is dissipative beyond a certain threshold  $c$ .

If  $L$  was a normal operator, the numerical range would be the convex hull of its spectrum  $\phi(L) = \text{conv } \sigma(L)$  as sketched in fig. 1 (Gustafson & Rao 1997, Thm. 1.4-4). Since the considered vortices are asymptotically stable this would imply  $c = 0$  in (4.4) and the equivalent normal operator would describe pure dissipation. The present deviation from this equivalent normal dynamics is a consequence of nonnormality and in a sense proportional to the protrusion of the numerical range into the unstable half plane. The maximum protrusion (recall that  $\text{div } \mathbf{u} = 0$ )

$$\eta(L) := \sup_{s \in \phi(L)} s_r = \sup_{\mathbf{u} \neq 0} \frac{(\mathbf{u}, L_r \mathbf{u})}{\|\mathbf{u}\|^2} = \sup_{\mathbf{u} \neq 0} \frac{(\mathbf{u}, (S - \nu \Delta) \mathbf{u})}{\|\mathbf{u}\|^2} \quad (4.5)$$

is called the numerical abscissa (Trefethen & Embree 2005, p. 174). The operator  $S - \nu \Delta$  in (4.5) is self-adjoint and the numerical abscissa is identical to its largest eigenvalue. Since the viscous term is necessarily negative (Sohr 2001, p. 101) and by the above remarks on the damping effect of viscosity for nonnormal dynamics, we assume an inviscid fluid in the following.

In terms of physics, the numerical abscissa represents the maximum instantaneous energy growth. Let  $\nu = 0$  in (4.5), then the momentary change of integral energy is governed by the inviscid Reynolds-Orr equation for all  $t \geq 0$  (Joseph 1976, p. 10)

$$\frac{d}{dt} \frac{\|\mathbf{u}(t)\|^2}{2} = (\mathbf{u}(t), \frac{1}{2} \begin{bmatrix} 0 & rd\Omega/dr & dU_z/dr \\ rd\Omega/dr & 0 & 0 \\ dU_z/dr & 0 & 0 \end{bmatrix} \mathbf{u}(t)), \quad \|\mathbf{u}(0)\| = 1, \quad (4.6)$$

assuming the generic reference flow  $\mathbf{U}(r) = U_\theta(r)\mathbf{e}_\theta + U_z(r)\mathbf{e}_z$ . Searching for the maximum of (4.6), the right-hand side is seen to coincide with the definition of the numerical abscissa (4.5) in the limit as  $t \rightarrow 0$ . This is equivalent to  $d\|T(t \rightarrow 0)\|/dt = \eta(L)$  where the numerical abscissa is the largest eigenvalue of  $S$  for an inviscid fluid (see also Trefethen & Embree 2005, Thm. 17.4). Comparing (4.6) with the commutator (4.3) confirms that energy growth in an asymptotically stable system is possible only for reference states which are not in rigid-body motion (*cf.* also Joseph 1976, p. 10). The actual maximum energy-amplification capacity serves as a measure to assess nonnormality.

The hermitian part of the velocity gradient is self-adjoint, hence, the spectral theorem

guarantees existence of real eigenvalues  $\lambda_1 = 0$ ,  $\lambda_{2,3} := \pm\lambda = \pm\frac{1}{2}\sqrt{(rd\Omega/dr)^2 + (dU_z/dr)^2}$  and mutually orthogonal eigenvectors

$$\mathbf{v}_1 = \begin{pmatrix} 0 \\ -dU_z/dr \\ rd\Omega/dr \end{pmatrix}, \quad \mathbf{v}_{2,3} = \begin{pmatrix} \pm 2\lambda \\ rd\Omega/dr \\ dU_z/dr \end{pmatrix}. \quad (4.7)$$

Physically, the eigenvectors (4.7) span three orthogonal eigenspaces for which the production bilinear form in (4.6) vanishes (zero strain) and is negative/positive, respectively. The maximum eigenvalue corresponds to the numerical abscissa which is attained if the perturbation projects identically on the associated eigenvector  $\mathbf{v}_3$ .

Eigenvectors  $\mathbf{v}_{2,3}$  only differ in the sign of the radial component while their projections onto a cylinder of radius  $r$ ,  $\mathbf{v} := \mathbf{v}_{2,3} - \mathbf{e}_r(\mathbf{e}_r, \mathbf{v}_{2,3})$  say, are identical and are conveniently represented in terms of their streamlines  $rd\theta/v_\theta = dz/v_z$ . On the other hand, an analogous representation on the cylinder holds for arbitrary perturbations  $\hat{\mathbf{u}}$  and the streamlines take on the form of helices due to the assumed symmetry. The pitch of the perturbation streamlines (streamwise increment  $dz$  per azimuthal increment  $rd\theta$ ) defines the angle

$$\frac{1}{r} \frac{dz}{d\theta} = -\frac{m}{r\alpha} \quad \text{while} \quad \frac{1}{r} \frac{dz}{d\theta} = \frac{1}{r} \frac{dU_z/dr}{dr\Omega/dr}$$

is the streamline angle of the eigenvector projection. In order that perturbation and eigenvector align, it is necessary that the above angles match, *i.e.*

$$-\frac{m}{r\alpha} = \frac{1}{r} \frac{dU_z/dr}{dr\Omega/dr} \Leftrightarrow \frac{d}{dr}(m\Omega + \alpha U_z) = 0 \Leftrightarrow m\Omega + \alpha U_z = \omega = \text{const.} \quad (4.8)$$

which is precisely the critical-layer condition (*cf.* § 2.3). Perturbation alignment on the cylinder is necessary but not sufficient for energy growth. It is in fact the radial component  $\pm\lambda$  in (4.7) that decides whether energy is amplified or attenuated. The situation of energy attenuation through critical-layer perturbations is known as Landau damping (Antkowiak 2005, p. 13; Fabre *et al.* 2006, p. 255).

The importance of stationary values of  $m\Omega(r) + \alpha U_z(r) - \omega$  for inviscid instability was previously shown by Leibovich & Stewartson (1983) (see also Ash & Khorrami 1995, p. 332). Approximate alignment of viscous and inviscid instability modes with the principal eigenvector was shown by Abid (2008, p. 28) for the Batchelor vortex and increases with  $q \leq 1$  (see (2.1)). Nevertheless, while perturbation alignment has been identified as the condition for maximum energy growth before, it seems that equivalence with the critical-layer condition (4.8) has not been stated explicitly, yet. Moreover, we are not aware of any previous result relating critical-layer perturbations directly to nonnormality.

In order to quantify nonnormality for Batchelor (Lamb-Oseen) and Moore-Saffman vortices, fig. 2 shows graphs of the mean profiles  $U_z(r)$ ,  $dU_z(r)/dr$ ,  $\Omega(r)$  and  $W_z(r)$ .

With regards to axial mean velocity and its gradient, shown in fig. 2(a) for the Batchelor and Moore-Saffman vortex, the most essential aspect for the present work is *substantial localisation* in the vortex core. For the Batchelor vortex (2.1),  $U_z^B$  is exponentially confined to the core. For the Moore-Saffman vortex  $U_z^{MS}(r) \sim (n^{-1} - 1)r^{-2n}$  as  $r \rightarrow \infty$  holds by definition (Moore & Saffman 1973, eq. (3.5)). Nevertheless, jet-wake coexistence renders this asymptotic irrelevant for the practically pertinent behaviour in the core vicinity where the Moore-Saffman vortex behaves effectively identically as the Batchelor vortex. This substantial confinement of axial mean velocity is in agreement with its importance for the discrete spectrum (discussed in § 4.2) and suggests negligible pertinence for disturbances located in the freestream. The critical-layer location for peak amplification of the Batchelor (Lamb-Oseen) vortex ( $m = 1, \omega = 0.1, q = 4$ ) is indicated

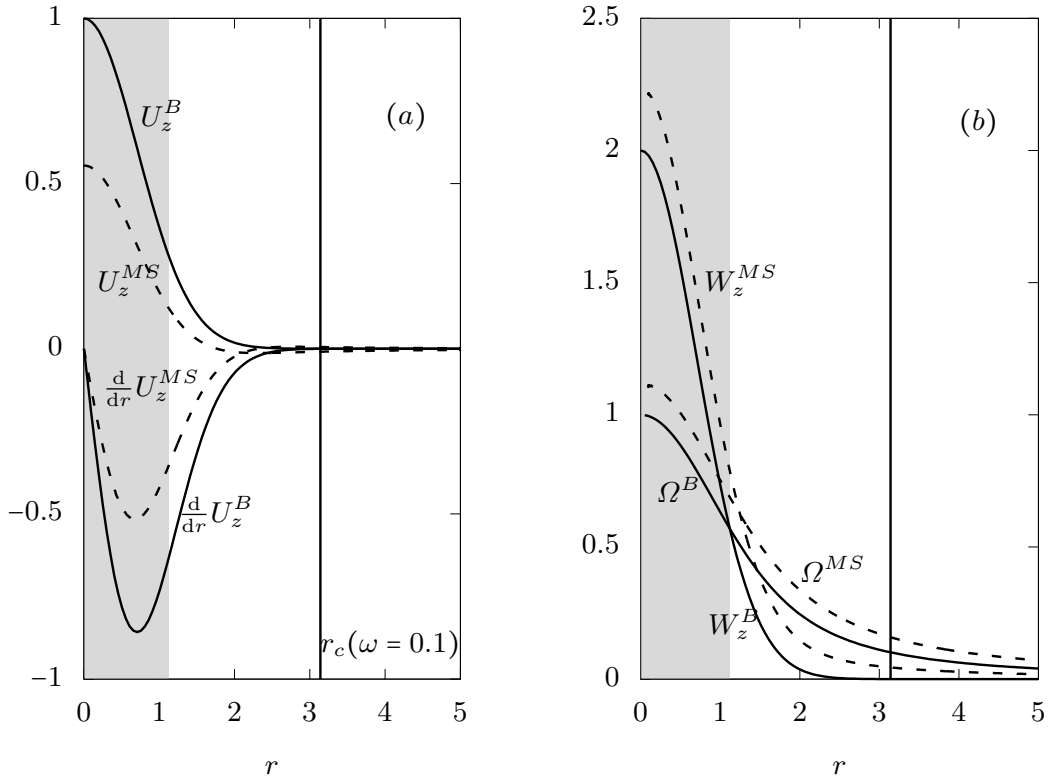


Figure 2: Comparison of radial mean-flow profiles for Batchelor (B) and Moore-Saffman (MS) vortices ( $n = 0.75$ ). Axial velocity and mean-shear profiles on the left show (at least visually) exponential localisation in the core region, restricting significant contribution to  $r \lesssim 2$ . Mean angular velocity  $\Omega$  and axial vorticity  $W_z$  on the right panel show essentially identical behaviour for the two models, the latter being also strongly localised. For reference the vortex core is shown in gray shading as well as the critical layer  $r_c$  of the Lamb-Oseen vortex for  $\omega = 0.1, m = 1$ .

by a straight line at  $r_c \approx \pi$  where no measurable effect of the axial mean flow is to be expected any more.

The second direct source of nonnormality is by differential mean angular velocity  $\Omega \neq \text{const.}$  and mean streamwise vorticity  $W_z$ , shown in fig. 2(b). Vorticity is again substantially localised in the core, obeying an exponential law for the Batchelor (Lamb-Oseen) vortex (2.1) and qualitatively similar behaviour for the Moore-Saffman vortex. From the characteristic reference-flow profiles shown in fig. 2, angular velocity  $\Omega$  is the only quantity which is not (almost) exponentially decreasing. As a matter of fact,  $\Omega(r) \sim r^{-n-1}$  as  $r \rightarrow \infty$  holds for all models, whereas  $n = 1$  corresponds to the Batchelor (Lamb-Oseen) vortex (Moore & Saffman 1973, eq. (3.5)) and  $n = 0.75$  is a lower bound for the Moore-Saffman vortex fitting experimental trailing vortices (see § 2.2).

We conclude that receptivity to the freestream should be largely independent of the vortex model and subsequent discussion will focus on the Lamb-Oseen vortex. Variation of the reference flow will be further discussed in § 5.

#### 4.2. Selective nonnormality of the Lamb-Oseen vortex

According to the left-hand side of (3.2), the difference between the resolvent norm and the reciprocal of the shortest distance of any given frequency  $i\omega \in \rho(\mathbf{L})$  to the spectrum is a local measure for nonnormality. Comparing graphs of these two functions

we find vortices to be effectively nonnormal only on a narrow frequency band (termed ( $\omega$ -)selective nonnormality).

All results of this section are obtained for the Lamb-Oseen vortex and  $R_\Gamma = 5000$ ,  $m = 1$ ,  $\alpha = 1.55$  as in Guo & Sun (2011, p. 3191). By (3.1) a compact resolvent can be expanded in a convergent series of rank-1 operators, weighted by the associated singular value. We find the singular values to be rapidly decreasing for all considered frequencies, thus, restricting to leading-order structures henceforth (constituting the rank-1 approximation of the resolvent by (3.1)). It should be noted though that this is not true for steady perturbations ( $\omega \approx 0$ ) due to the continuous spectrum  $\sigma_c^\infty(\mathbf{L})$  introduced below.

Figure 3(b) shows nested isocontours of the pseudospectrum in the complex  $s$ -plane for values of  $\epsilon = \|\mathbf{R}(s; \mathbf{L})\|^{-1} \in \{10^n : n = -1, -1.5, -2, -2.5, -3, -4, -5\}$ , effectively approaching the spectrum shown by dots (for details on pseudospectra see *e.g.* Trefethen & Embree 2005). The particular case of  $s = i\omega$  is shown in fig. 3(a) and will be discussed thereafter.

It should be noted that the spectrum is organised into the same branching structure as the spectrum shown in Fabre *et al.* (2006, fig. 7) for the Lamb-Oseen vortex with  $m = 1$ ,  $\alpha = 3$  and  $R_\Gamma = 1000$ . Even more, qualitatively the same pseudospectrum and eigenvalue scattering is reported in Mao & Sherwin (2011, p. 8) for the Batchelor vortex with  $m = 0$ ,  $\alpha = 10$ ,  $R_\Gamma \approx 2000$  and  $q = 3$ . These findings provide further support for conj. 3 that linear vortex dynamics is generic as discussed in § 5.

The spectrum of the linear operator  $\mathbf{L}$  governing three-dimensional perturbation dynamics about vortices comprises contributions from discrete eigenvalues  $\sigma_d(\mathbf{L})$  as well as a (semi-infinite) continuous spectrum  $\sigma_c^\infty(\mathbf{L})$  due to spatial unboundedness. The latter is argued to be  $\sigma_c^\infty(\mathbf{L}) = \{s = s_r + is_i \in \mathbb{C} \mid \alpha^2\nu < s_r < \infty, s_i = 0\}$  (Fabre *et al.* 2006, app. A; Mao & Sherwin 2011, p. 14 and app. B) and can be anticipated from eigenvalue and contour clustering along the real axis in fig. 3(b). Receptivity of the Batchelor vortex to axisymmetric disturbances has previously been related to long-wavelength generalised eigenmodes pertaining to  $\sigma_c^\infty(\mathbf{L})$  which penetrate into the core (Mao & Sherwin 2011, pp. 1, 10 and fig. 3). We exclude this mechanism by restricting to finite kinetic energy solutions and rather emphasize remote receptivity without mass transport across the system boundary (*cf.* discussion at the end of §2.1). Rather  $\sigma_c^\infty(\mathbf{L})$  is an artefact of the mathematical model of an unbounded domain and the associated perturbations are considered irrelevant here (*cf.* also Heaton & Peake 2007, pp. 275, 295).

Considering an inviscid fluid, an additional *inviscid* continuous spectrum  $\sigma_c^0 = \{s \in \mathbb{C} \mid s_i = \omega = m\Omega(r), s_r = 0\}$  exists as a consequence of a critical-layer singularity of the homogeneous problem (Le Dizès 2004, p. 319; Roy & Subramanian 2014, §3.2). For non-vanishing viscosity it degenerates to a discrete spectrum of a large number of stable discrete modes (Heaton & Peake 2007, p. 282) which are algebraically localised in the core vicinity, referred to as potential modes by Mao & Sherwin (2011, p. 2). This viscous remnant of the inviscid continuous spectrum, denoted  $\sigma_c^\nu(\mathbf{L})$ , is observed as the apparently random eigenvalue scattering in the rectangular central part of fig. 3(b). Small values and shape of the ( $\epsilon = 10^{-5}$ )-pseudospectrum (innermost thick contour in fig. 3(b)) led Mao & Sherwin (2011, p. 10) to speculate that the spectrum in fact remains continuous.

The distinguished situation of neutral harmonic perturbations corresponds to a cut at  $s_i = \omega$ ,  $s_r = 0$  which yields the resolvent norm shown in fig. 3(a) in comparison with the graph of the reciprocal distance. By (3.2) we observe the resolvent to be selectively nonnormal in a frequency band of roughly  $0 \lesssim \omega \lesssim 1$  while it is effectively normal outside this range. Considering the associated perturbation structures we will show in § 4.3 that the nonnormality frequency interval is essentially correlated with the critical layer, as already anticipated from analysis of the operator structure in § 4.1.

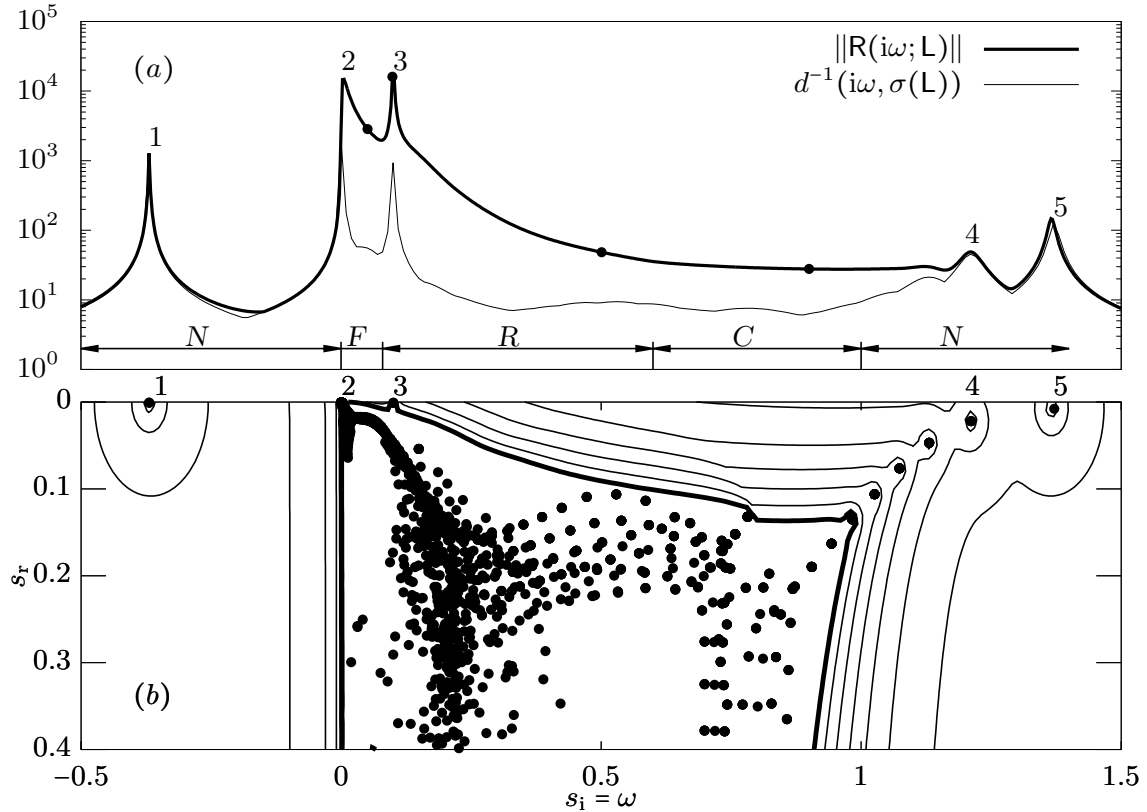


Figure 3: Comparison of the resolvent norm for the Lamb-Oseen vortex ( $m = 1$ ,  $\alpha = 1.55$ ,  $R_\Gamma = 5000$ ) with the reciprocal distance in (a) assuming a harmonic ansatz  $\omega = s_i \in \mathbb{R}$  and  $s_r = 0$ , revealing  $\omega$ -selective nonnormality roughly for  $0 \lesssim \omega \lesssim 1$ . Distinction of dynamical regimes of the resolvent:  $N$  signifying a nominally normal operator and  $\{F, R, C\}$  being associated with nonnormality due to critical-layer singularity. The latter distinguish dynamics essentially situated in the far field ( $F$ ) and core ( $C$ ), respectively, while only the intermediate range critical-layer forcing ( $R$ ) is associated with receptivity. Solid dots mark frequencies of forcing/response structures shown in fig. 4. Numbering refers to the (pseudo)spectrum in (b), showing nested isocontours of the resolvent norm and the spectrum (solid dots) in the complex  $s$ -plane.

Applying the same numbering in figs. 3(a,b) indicates that peaks in the resolvent norm match with the least damped elements of the spectrum. Furthermore, the response modes associated with peaks 1, 4 and 5 belong to the D-, V- and C-families in the classification of Fabre *et al.* (2006) and are equivalent to the modes obtained from the eigenvalue problem for  $L$ . The associated peak forcing structures are identical to the eigenmodes of the adjoint  $L^\dagger$ . A thorough classification of perturbations in the  $(\omega, \alpha)$ -plane is postponed to §5 (*cf.* also figs. 7–9).

These observations suggest that perturbations for which roughly  $\omega \notin [0, 1]$  the dynamics is governed by an effectively normal operator and hence irrelevant for receptivity according to def. 1 by conj. 1. From a physical standpoint, the dynamic regimes labelled  $N$  in fig. 3(a) constitute classical resonance between congruent perturbation patterns, e.g.  $\mathbf{f}_1(\omega_l) \cong \mathbf{u}_1(\omega_l)$  where  $l \in \{1, 4, 5\}$  labels the peaks. Amplification away from the singularity is simply  $d^{-1}(i\omega, \{\omega_l\})$ ,  $\omega \in \mathbb{R}$ , in these cases (*cf.* (3.2)).

In order to gain further insight into the mechanisms of freestream receptivity, let us now turn to the perturbation structures. Typical patterns of forcing-response pairs  $\{\mathbf{u}_1(\omega), \mathbf{f}_1(\omega)\}$  for gradually increasing frequencies  $\omega \in \{0.05, 0.1, 0.5, 0.9\}$  are shown

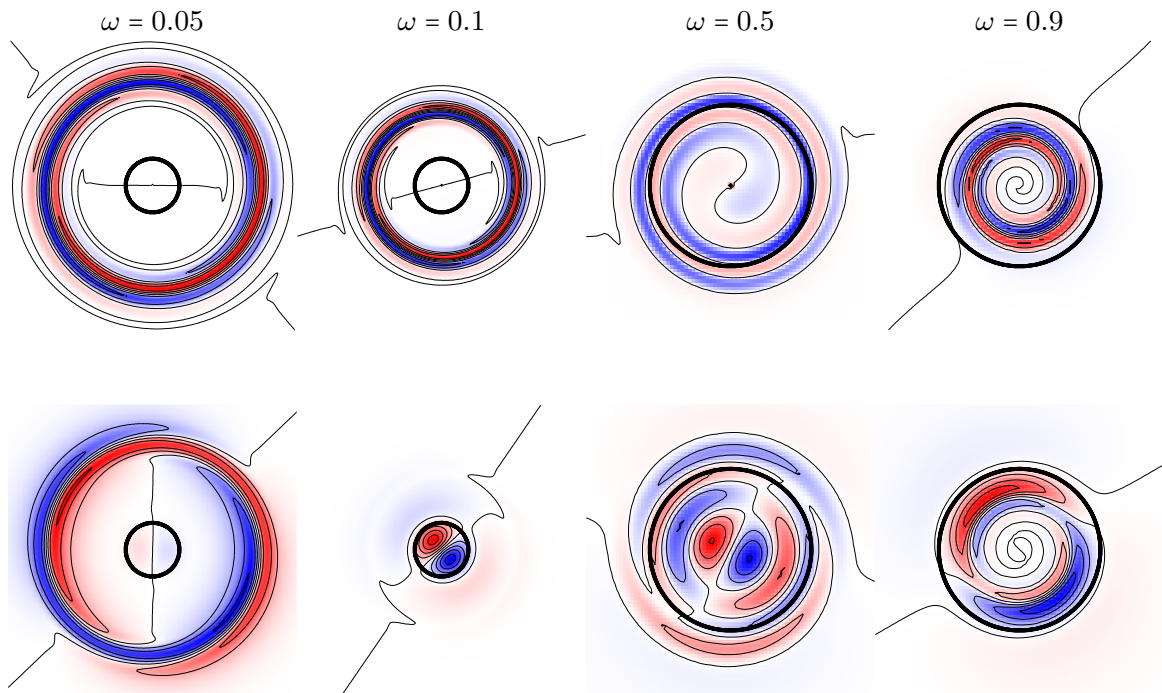


Figure 4: Streamwise component of  $\text{rot } \mathbf{f}_1(\omega)$  and  $\text{rot } \mathbf{u}_1(\omega)$  for  $\omega \in \{0.05, 0.1, 0.5, 0.9\}$  (solid dots in fig. 3(a)) in the top and bottom row, respectively, for the Lamb-Oseen vortex ( $m = 1$ ,  $\alpha = 1.55$ ,  $R_F = 5000$ ). Positive and negative values corresponding to blue and red colouring, the scale not being chosen uniformly across different panels. The solid circle of radius  $r_1 = 1.12$  indicates the vortex-core boundary.

in the top and bottom row of fig. 4. Contours and colouring represent the streamwise component of the curl of the forcing and response structures. Magnitudes are understood to be qualitative and not uniform across panels to emphasize the relative locations and perturbation patterns. For this purpose a solid circle of radius  $r_1 = 1.12$  indicates the vortex boundary, revealing that forcing structures are gradually located closer to the core as the frequency is increased. The forcing structure crosses the vortex boundary at a frequency of  $\omega \approx 0.5$  and hence disqualifies perturbations from  $\omega \gtrsim 0.6$  (say) from contributing to freestream receptivity as defined in def. 1 for the absence of radial transport, despite local nonnormality. Associated forcing-response pairs are not congruent but systematically located in the vortex core and, for this reason, are referred to as *C*-regime, cf. fig. 3(a).

Significant amplification is observed for quasi-steady excitation  $\omega \approx 0$  in fig. 3(a). Considering the sequence  $\omega \searrow 0$ , the associated forcing *and* response structures are found to be located at increasingly large radii as shown in fig. 4. The most important implication for receptivity is that below a certain frequency forcing and response structures take on the form of localised wave packets of comparable shape that are *both* far outside the vortex core, labelled *F*-regime in fig. 3(a). This kind of forcing, although causing large amplification, is unable to cause (at least directly) core perturbations. For this reason it is assumed to be irrelevant for linear receptivity. The two cases of *F*- and *C*-regimes underline that by conj. 1 nonnormality is *necessary* but not *sufficient*, the actual range of freestream receptivity (*R*-regime) is indicated in fig. 3. This considerable restriction of

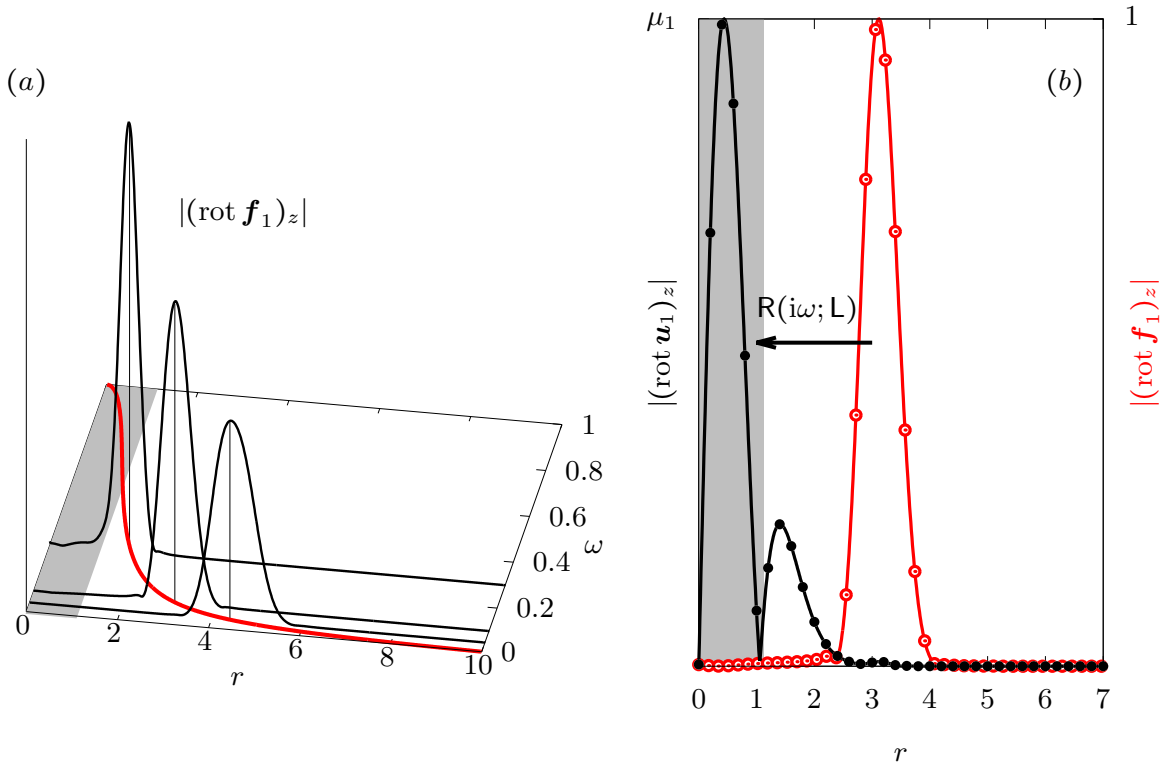


Figure 5: Archetypal critical-layer perturbations of the Lamb-Oseen vortex for  $\alpha = 1.55$ ,  $m = 1$ ,  $R_T = 5000$ . Candidate wave frequencies  $\omega$  in the critical layer (red line) and modulus of the streamwise component of  $\text{rot } \mathbf{f}_1(\omega)$  for selected forcing structures (thick black graphs) being centred around the critical layer and getting sharper as  $\omega$  increases (as they approach the core) in (a). Prototype of the critical-layer forcing-response pair at  $\omega = 0.1$  showing the perturbation shift from the critical layer into the vortex core in (b). The shaded region signifying the vortex core delimited by  $r_1 = 1.12$  in panels (a, b).

the receptivity frequency band suggests that vortices behave like strongly selective filters to freestream turbulence (see also Antkowiak 2005, p. 72).

#### 4.3. Critical-layer alignment of the forcing structures

As shown in §§ 4.1 and 4.2, the range of effective nonnormality is essentially correlated with the inviscid continuous spectrum. The inviscid nature of linear nonnormal dynamics and the retained importance of the singular continuous spectrum even for a viscous fluid (*cf.* also Heaton & Peake 2007, pp. 278–279, 287) is underscored by tracking the radial location of the forcing structures as a function of frequency, closely following the critical layer, in fig. 5.

In § 2.3 we recalled the definition of the critical layer as the radial location where mean advection equals perturbation propagation. Using the spatio-temporal Fourier ansatz of § 2.3 the material-derivative operator (including streamwise transport for now) becomes a multiplication operator associated with the symbol

$$\frac{\partial}{\partial t} + \Omega(r) \frac{\partial}{\partial \theta} + U_z(r) \frac{\partial}{\partial z} \rightarrow m\Omega(r) + \alpha U_z(r) - \omega.$$

Discussion in § 2.2 suggests that  $U_z$  is (nearly) exponentially localised in the core such that for disturbances in the freestream

$$m\Omega(r) + \alpha U_z(r) - \omega \approx m\Omega(r) - \omega$$

and receptivity to critical-layer forcing should be essentially independent from the axial mean velocity in practice. Thus, Lamb-Oseen, Batchelor and Moore-Saffman vortices are expected to have essentially identical critical-layer dynamics with regards to receptivity. Let  $m = 1$ , the critical layer of the Lamb-Oseen vortex becomes the locus  $\{r \in (0, \infty) \mid \Omega(r) - \omega = 0\}$ , shown in fig. 5(a) as a thick red line. The associated frequency range for critical-layer forcing is somewhat smaller than the range of nonnormality shown in fig. 3(a). Deviations from the Lamb-Oseen critical layer in fig. 5(a) due to axial mean velocity (Batchelor or Moore-Saffman vortex) are essentially restricted to the core, unless  $\alpha \gg 0$  or  $q \rightarrow 0$ . Both situations are excluded here since trailing-vortex dynamics is of long wavelength (meandering) and dominated by mean rotation rather than axial velocity (*i.e.* jet behaviour).

Forcing structures in fig. 5(a) are indeed systematically localised about the critical layer which strongly suggests a relation to the inviscid continuous spectrum and critical-layer forcing as the essential mechanism for receptivity. Archetypal freestream receptivity is associated with the characteristic forcing-response patterns displayed in fig. 5(b), showing the modulus of the streamwise curl component in fig. 4 for  $\omega = 0.1$ . The most important aspect qualifying this forcing-response pair as a candidate for freestream receptivity is the fact that forcing and response structures have (almost) disjoint radial support, showing that vortices are susceptible to disturbances which do not physically penetrate the core.

The receptivity prototype shown in figs. 4 for  $\omega = 0.1$  and 5(b), *i.e.* coiled forcing filaments in the critical layer resonantly exciting a core bending wave, is analogous to findings in transient-growth studies (Antkowiak & Brancher 2004; Pradeep & Hussain 2006). Its importance for receptivity to sustained (stochastic) forcing has been pointed out previously by Fontane *et al.* (2008, p. 250) who speculated that it might constitute a potential mechanism for vortex meandering (see also Viola *et al.* 2016, p. 545). While these two approaches formally discuss solutions to (2.3) in the time domain, the resolvent provides an analysis in frequency space (*cf.* (1.1)–(1.2) in § 1). All three approaches are mathematically related since the resolvent is the Laplace transform of the propagator (*cf.* § 1). All linear studies are complementary and analysis in frequency space (as opposed to time domain) has the same principal advantages and inconveniences as in the analysis of a time signal, for example. Specifically, it identifies those frequencies which contribute most to complex temporal dynamics (such as vortex meandering). As such, it is the natural framework for receptivity, characterising the vortex as a selective filter with frequency-dependent susceptibility.

#### 4.4. Variation of the axial wavenumber

So far, (arbitrarily) fixing  $\alpha = 1.55$  we showed that vortices are receptive in a narrow frequency band to a particular disturbance pattern localised in a certain radial range of the freestream. Despite this selectivity in  $\omega$  and  $r$ , we will provide evidence that receptivity is largely insensitive to variations in the axial wavelength. To illustrate that the choice of  $\alpha$  is not essential for values on the considered interval, fig. 6 shows the variation of forcing-response pairs taken for  $\alpha \in \{0, 1, 2, 3\}$  keeping  $\omega = 0.1 = \text{const.}$  in comparison with the receptivity prototype at  $\alpha = 1.55$  (thick line). Apparently, forcing structures (red lines, hollow symbols) are almost indistinguishable for all cases and localised about the critical layer. The excited responses (black lines, solid symbols of same shape) all have radially disjoint support and are localised in the core (indicated by grey shading). Nevertheless, the complexity of the response, measured in terms of its roots, say, is seen to increase with the axial wavenumber.

This finding provides evidence for the archetypal receptivity structures shown in fig. 5(b) existing in principle over the considered range of wavenumbers irrespective

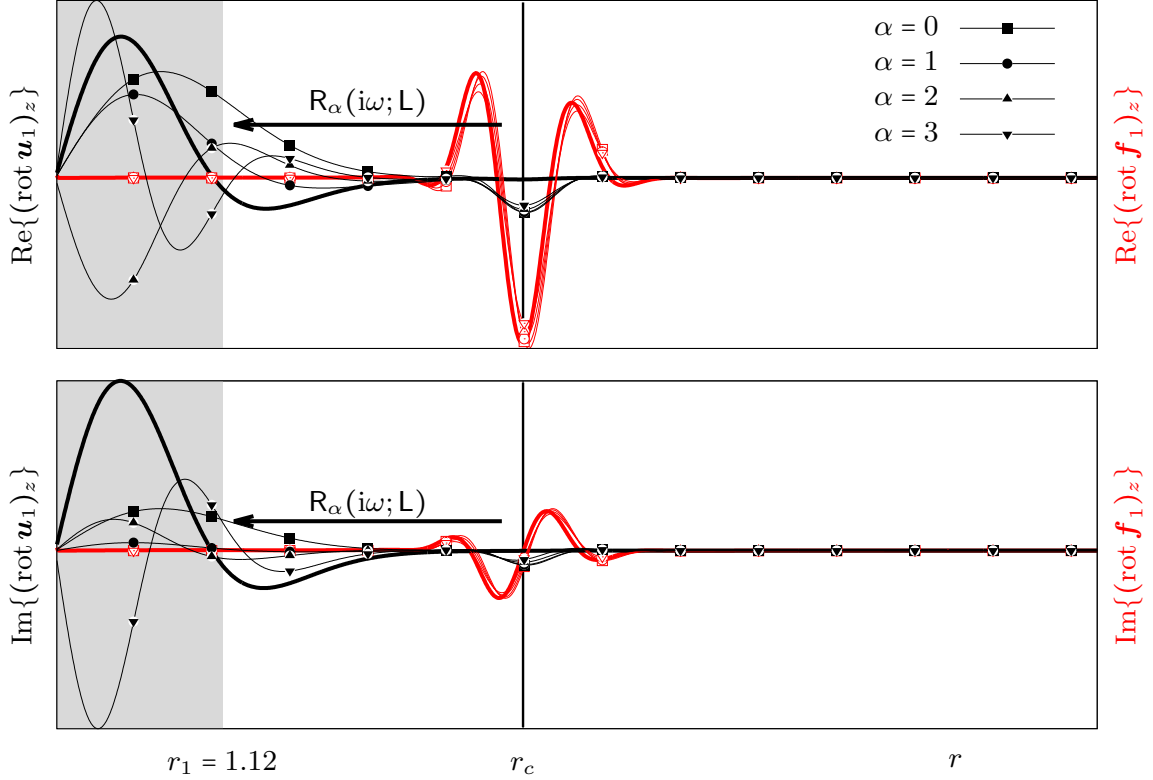


Figure 6: Real and imaginary part of the leading-order forcing and response structures (hollow red and solid black symbols, respectively) for the Lamb-Oseen vortex ( $m = 1$ ,  $R_T = 5000$ ) at  $\omega = 0.1$  and  $\alpha \in \{0, 1, 2, 3\}$  in comparison with the archetype at  $\alpha = 1.55$  (thick line; cf. also fig. 5). The characteristic forcing structures have essentially identical radial patterns in the vicinity of the critical layer at  $r_c \approx \pi$ . Resonantly excited forcing structures show comparable behaviour with spatial complexity increasing with  $\alpha$ .

whether the resolvent norm peaks or not and further underscores the generality of the mechanism. It would appear that our conclusion is consistent with Antkowiak (2005, fig. 3.26), yet contrary to previous statements that receptivity characteristics depend on  $\alpha$  (e.g. Fontane *et al.* 2008, p. 245). Further corroboration of insensitivity to variations in  $\alpha$  will be presented in § 5 when discussing resolvent-norm surfaces over  $(\omega, \alpha)$  in fig. 7.

The observed selectivity in  $\omega$  and  $r$  but not in  $\alpha$  is consistent with the matching of critical layers for all vortex models discussed in § 4.3.

## 5. Robustness of linear vortex receptivity

It is well-known that a sufficiently strong jet component in the core is necessary to destabilise an isolated unstrained vortex. This fact suggests that linear stability (*i.e.* the discrete spectrum) quite crucially depends on the precise vortex structure. In contrast, receptivity according to def. 1 is rather insensitive to major changes in the reference flow as will be affirmed henceforth by comparing different vortex models. We believe that this makes sustained forcing a better candidate to explain trailing-vortex dynamics which is found to obey universal characteristics, too.

Assessment of Lamb-Oseen, Batchelor and Moore-Saffman vortices as reference-flow models suggests the following generality conjecture which will be detailed thereafter.

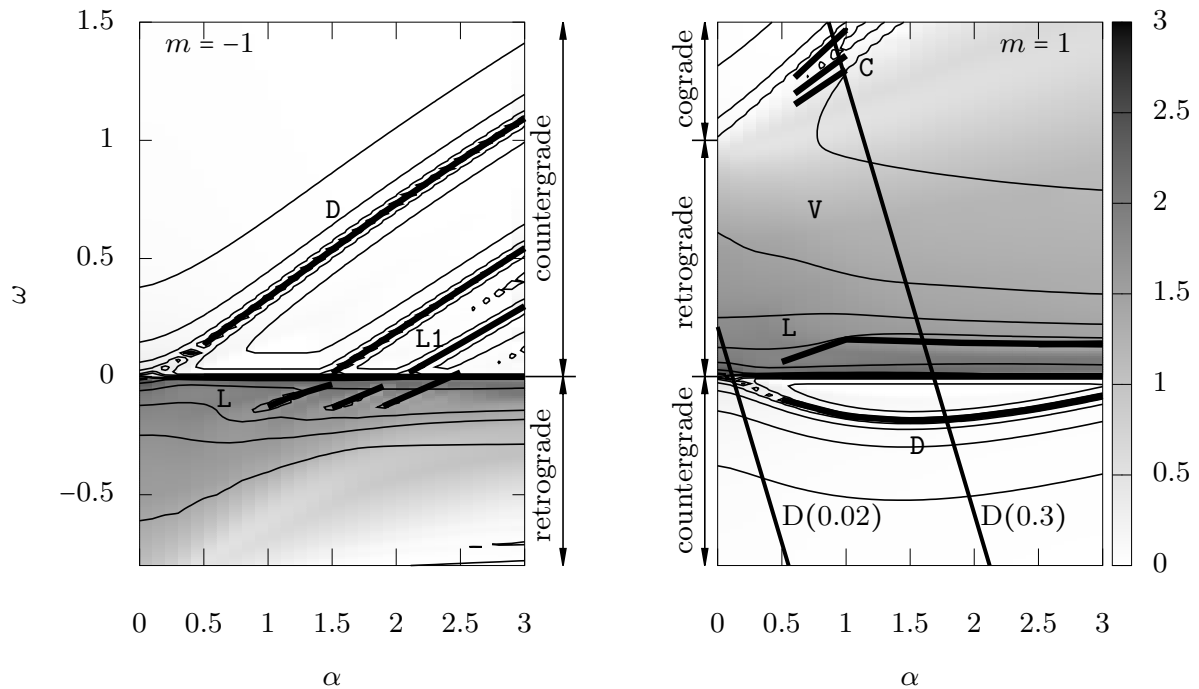


Figure 7: Resolvent norm of the Batchelor vortex in the  $(\alpha, \omega)$ -plane for  $R_\Gamma = 6000$  and  $q = 4$  showing (thin) nested contours for amplification levels  $\{10^n : n = 0.5, 1.0, 1.5, \dots, 4.5\}$  peaking at the thick lines, comparing  $m = -1$  (left) and  $m = 1$  (right). Superposition of the least damped eigenvalues obtained from solution of the eigenvalue problem (thick lines) reveals alignment with the peaks of the resolvent norm. Grey shading measures effective local nonnormality defined by  $\log_{10} \|R_{m,\alpha}(i\omega; \mathbf{L})\|/d(\omega, \sigma_{m,\alpha}(\mathbf{L}))^{-1} \in [0, \infty)$ ,  $\alpha \in [0, 3]$ , the lower bound being perfect local normality (white). Nonnormality happens to be essentially correlated with the possibility of having critical-layer forcing. Inclined graphs  $D = D(S_m)$  indicate the loci of candidate  $(\omega, \alpha)$ -pairs for the experimental meandering frequency  $S_m$  (from Bailey *et al.* 2018, fig. 7(a)) obtained from the Doppler relation.

**CONJECTURE 3.** *Receptivity of a trailing vortex to freestream disturbances (as defined in § 2.1) in the framework of § 2.3 is generic for the reference flows introduced in § 2.2.*

Results for the Batchelor vortex have been computed for the case discussed in Fabre & Jacquin (2004, p. 259) with regards to the vortex-meandering experiments of Jacquin *et al.* (2001) with  $q = 4$  and  $R_\delta = 1500$ , corresponding to  $R_\Gamma = 6000$ .<sup>†</sup> The Moore-Saffman vortex is parametrised on  $n \in \{0.7, 0.8\}$ . While parameters in § 4 were chosen for the sake of comparability to other theoretical approaches, the present choice is realistic for wind-tunnel experiments.

Contours (thin lines) of the resolvent norm in the  $(\alpha, \omega)$ -plane are shown in fig. 7 for  $m = \pm 1$  in comparison with curves of the least damped eigenvalues (thick lines). Essentially the same amplification contours and perturbation families are obtained for the Lamb-Oseen and Moore-Saffman vortex (not shown). This already suggests some generality of perturbation dynamics with  $\alpha > 0$ ,  $m = 1$  and for  $q, R_\Gamma$  sufficiently large.

Perturbations are conventionally classified according to their relative motion with

<sup>†</sup>  $R_\delta := r_0 \delta U_z / \nu$  is related to  $R_\Gamma$  through the swirl number as  $R_\Gamma = |q| R_\delta$  (Fabre & Jacquin 2004, p. 242).

respect to the reference flow. Thus, comparing signs of the azimuthal phase and mean velocity we define modes with  $\text{sgn } \omega/m \neq \text{sgn } U_\theta$  as *countergrade*, modes with  $\text{sgn } \omega/m = \text{sgn } U_\theta$  and  $|\omega/m| \in [0, 1]$  as *retrograde* and modes with  $\text{sgn } \omega/m = \text{sgn } U_\theta$  and  $|\omega/m| > 1$  as *cograde* (cf. Fabre *et al.* 2006, p. 241). The different regimes are indicated in figs. 7 and 8. As for the Lamb-Oseen vortex, one broadly distinguishes four families of perturbation structures, namely of core C, viscous V, displacement D and mixed L type (see Fabre *et al.* 2006, pp. 247–255). Countergrade perturbations with  $m = -1$  belong to the D and L1 families (Fabre *et al.* 2006, fig. 14(a)) with increasing structural complexity in  $r$  for subsequent branches as  $\alpha$  is increased. Generally, forcing structures having  $n > 0$  zero crossings induce response with  $n \geq 0$  roots, both being essentially localised in the core.

Different shapes of the resolvent norm  $\|\mathbf{R}_{m,\alpha}(i\omega; \mathbf{L})\|$  for  $m = \pm 1$  are due to the axial mean velocity breaking azimuthal symmetry (cf. § 2.3). However, this distinction seems to be not fundamental since co-, retro- and countergrade perturbations are always associated with essentially the same families. This similarity between results for  $m = \pm 1$  is further highlighted in fig. 8.

Selective nonnormality can be quantified by inspection of the quantity

$$\log_{10} \frac{\|\mathbf{R}_{m,\alpha}(i\omega; \mathbf{L})\|}{d(\omega, \sigma_{m,\alpha}(\mathbf{L}))^{-1}} \in [0, \infty), \quad \alpha \in [0, 3], \quad m = \pm 1.$$

By the left-hand side of (3.2) the argument is identically unity if  $\mathbf{R}_{m,\alpha}(i\omega; \mathbf{L})$  is (locally) effectively normal, hence, corresponding to the lower bound. As for the Lamb-Oseen vortex, countergrade waves are *always* associated with an effectively normal resolvent. On the other hand, for retrograde waves, pseudo-resonance exceeds classical resonance of the equivalent normal operator by up to three orders of magnitude. Most importantly, fig. 7 confirms conj. 2 that effective nonnormality, and thus receptivity, are strongly confined to a small frequency band, correlated with the critical layer. These findings hold irrespective of the considered vortex model,  $m = \pm 1$  and  $\alpha$ .

Figure 7 clearly shows that the resolvent norm of the Batchelor vortex develops sharp distinguished crests, all being aligned with the least stable eigenvalues. Each of the crests induces a dynamic regime in its neighbourhood such that the entire  $(\omega, \alpha)$ -plane is partitioned into different parameter subsets associated with distinguished dynamic behaviour. Therefore, the spectral signature ( $\omega$  and  $\alpha$ ) of the forcing field will in general matter as it favours a response to different perturbation subspaces (D, L, etc.). However, as already anticipated in fig. 6, grey shading in fig. 7 affirms that receptivity is confined to a universal frequency band and the generic family of critical-layer waves with only small variations in alpha.

In order to gain further insight into axial-flow induced nonnormality, fig. 8 shows a comparison of the resolvent norm extracted from fig. 7 at  $\alpha = 1.55$  for  $m = \pm 1$  and for the Lamb-Oseen vortex. For the ease of comparison, the  $m = -1$  spectrum is plotted on the negative frequency (*i.e.* reflected along the vertical axis at  $\omega = 0$ ). In all cases the central peaks of the L family are *universally* observed as well as the general behaviour away from steady forcing. Receptivity candidates at higher frequencies are labelled V as in Fabre *et al.* (2006, p. 252) to emphasize their viscous nature. In fact, the discussion in §4 indicates that they are transitional structures between the pure critical-layer receptivity structures L and core perturbations C. The only noticeable difference in the three cases is the location of the peaks of the D and L1 families. In the light of the above discussion this suggests that for vortices *nonnormal dynamics is generic* while *normal dynamics is more sensitive to the reference state*.

Generality and robustness is further highlighted in fig. 9, showing a comparison of the resolvent norm for the three different reference states and  $m = 1$ . The essential behaviour

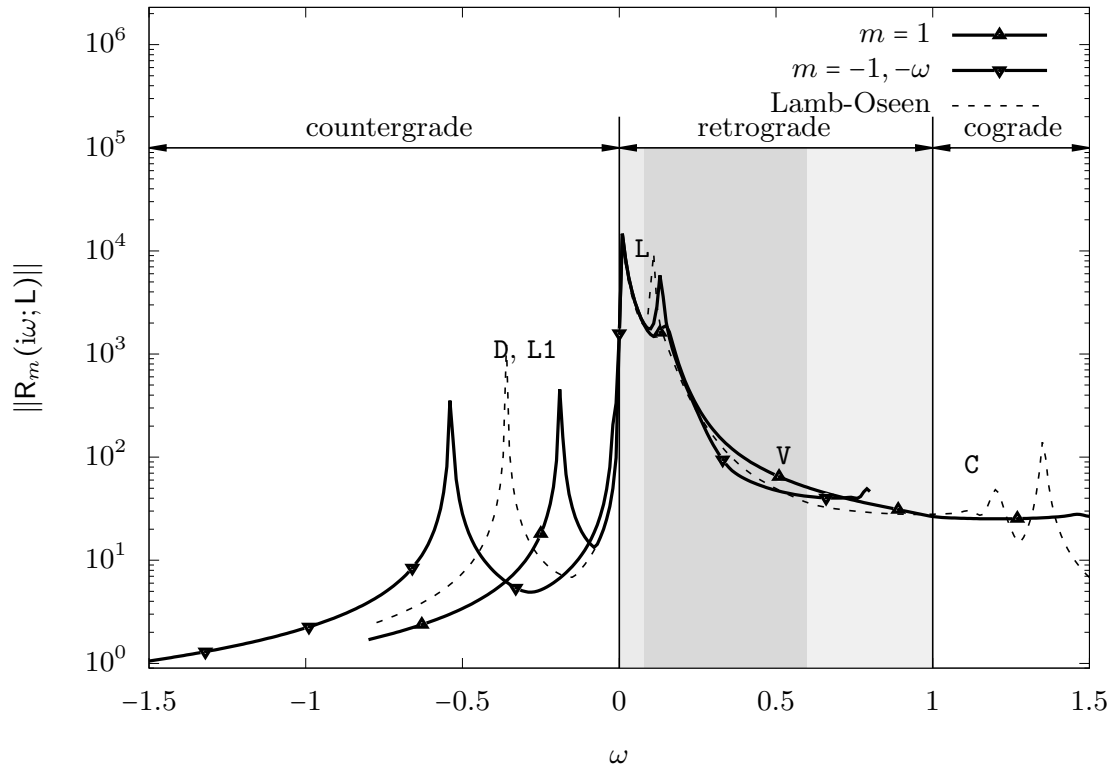


Figure 8: Resolvent norm of the Batchelor vortex for  $R_F = 6000$  and  $q = 4$  comparing  $m = -1$  (plotted on the negative frequency axis  $-\omega$ ) and  $m = 1$  for  $\alpha = 1.55$ , as well as the resolvent norm for the Lamb-Oseen vortex ( $R_F = 5000$ ). The critical-layer region of candidate receptivity is shaded in gray while the darker subset indicates the receptivity regime  $R$  indicated in fig. 3.

is unchanged by modification of the reference flow. As to be expected from discussion of the linear operator in § 4.1, differences mostly manifest for core perturbations associated with the C family.

Together, figs. 8 and 9 provide evidence that for vortex receptivity, and thus presumably vortex meandering, the detailed core structure of the reference state is of minor importance. These considerations support conj. 3, at least for the considered dynamics, and hence *a posteriori* justify limitation to the canonical case of a Lamb-Oseen vortex in § 4. It should be noted that this conclusion is in agreement with Antkowiak (2005, p. 47) and Pradeep & Hussain (2006, p. 252).

Our study affirms that generally vortices are most receptive to disturbances in the critical layer. Heaton & Peake (2007, p. 272) and Mao & Sherwin (2012, pp. 42, 44) come to the related conclusion that transient growth of the Batchelor vortex is essentially a consequence of the interaction of non-orthogonal eigenvectors pertaining to the inviscid continuous spectrum, with negligible contributions from the discrete spectrum. (Different from Antkowiak 2005, stating that combination of discrete and (unbounded) continuous spectrum.) Roy & Subramanian (2014, p. 405) demonstrate how the inclusion of singular modes pertaining to the inviscid continuous spectrum enables interaction between vortex and freestream, suggesting that a linear model of receptivity to ambient turbulence is intimately related to the inviscid continuous spectrum.

More generally, optimal localisation of input disturbances in the critical layer is universally observed in shear flows. In the context of boundary-layer flow, analysis of the eigenmodes of the adjoint, led Hill (1995, p. 185) to conclude that perturbations are

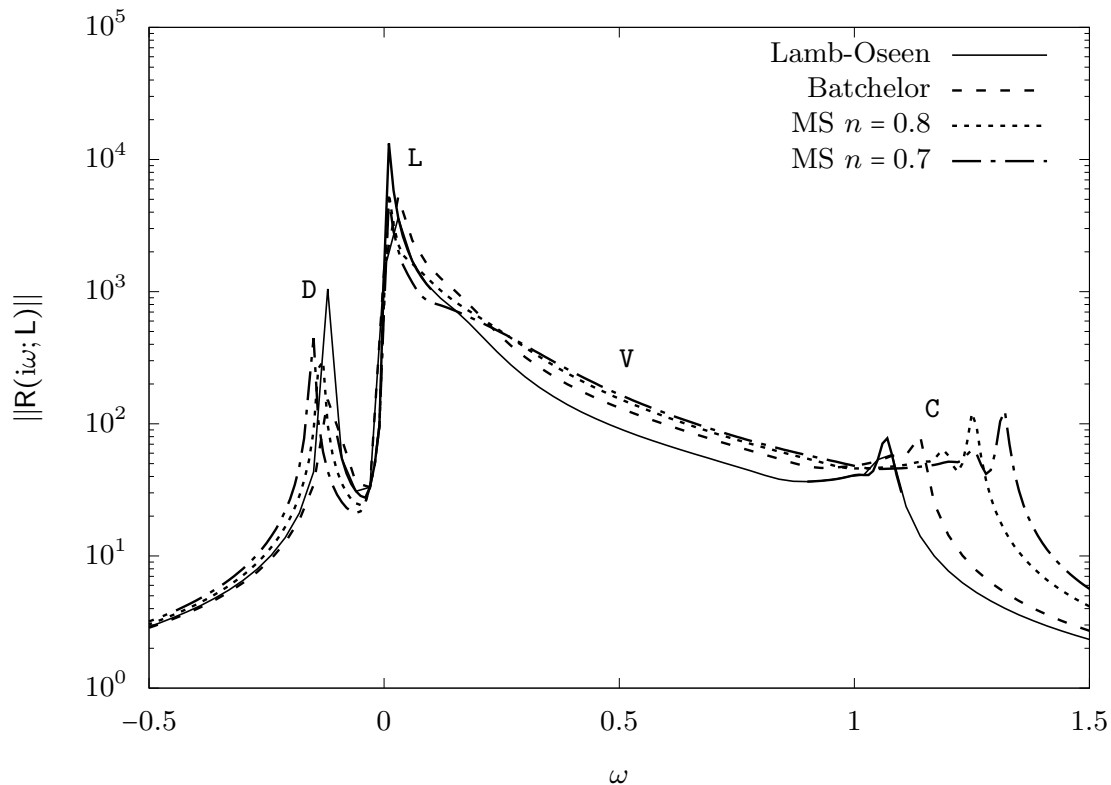


Figure 9: Comparison of resolvent-norm spectra for the Lamb-Oseen, Batchelor and Moore-Saffman (MS) vortices for  $\alpha = 0.5$ ,  $m = 1$ ,  $R_\Gamma = 5000$ ,  $R_\delta = 1000$  and  $q = 10$ , showing that axial velocity has a significant effect for perturbations in the core only.

most sensitive to forcing in the critical layer. Systematic alignment of perturbations with the critical layer in boundary-layer flow similarly to our fig. 5(a) is equally shown in McKeon (2017, figs. 7, 8, 10). The importance of critical-layer dynamics is also reported for pipe and Couette flow as well as for exact coherent states (*e.g.* McKeon & Sharma 2010; Hall & Sherwin 2010).

## 6. Frequency selection in meandering experiments

Trailing-vortex experiments reveal that meandering is principally associated with a broadband power spectral density (Devenport *et al.* 1996, p. 93), however, the principal energy-carrying structures are confined to a narrow frequency band (Jacquin *et al.* 2001; Bailey *et al.* 2018). Sufficiently far downstream (more than five chord lengths, say), experiments consistently report convergence towards the universal Strouhal number of  $S_m := f_m r_1 / U_\infty \sim 10^{-2}$  ( $m$  stands for meandering), while closer to the wing, energy may be concentrated at a higher frequency (Bailey *et al.* 2018, fig. 7). Hence, despite its formal broadband nature, trailing-vortex dynamics bears spectral coherence in the sense that the most energetic feature (*i.e.* meandering) happens at a specific frequency irrespective of freestream intensity, suggesting idealisation in terms of a monochromatic wave. Experiments of Bailey *et al.* (2018, fig. 7) identify the peak frequencies  $S_m \in \{0.02, 0.3\}$  for measurement stations  $z \lesssim 5c$  and  $z \gtrsim 5c$ , respectively.

Direct comparison of these characteristic experimental frequencies with the spectral signature of the resolvent is, however, complicated since the two analyses do not use the same reference frames. The principal issue is a manifestation of the Doppler effect for space-time signals (Landau & Lifshitz 1959, §68). In experiments, probing a spatio-

temporally varying signal at a fixed position in space, spatial and temporal variations are indistinguishably recognised as temporal unsteadiness. Consequently, the experimentally obtained frequencies in fact correspond to the locus  $D(S_m) := \{(\omega, \alpha) \in \mathbb{R}^2 \mid S_m - (\omega + \alpha U_\infty)/(2\pi) = 0\}$  (up to changes in non-dimensionalisation;  $r_1/r_0 = 1.12$ ), assuming constant background advection  $U_\infty/(\Gamma_0/(2\pi r_0)) = 1.83$  (Bailey *et al.* 2018). The loci  $D(S_m) \subset \mathbb{R}^2$  for  $S_m \in \{0.02, 0.3\}$  are shown in fig. 7 for the case of the Batchelor vortex.

If vortex meandering is due to generalised receptivity, assessment of the effective local nonnormality (shown in grey shading in fig. 7) allows us to restrict considerably the range of candidate  $(\omega, \alpha)$ -pairs identified from the Doppler relation. Taking into account that receptivity relies on radial perturbation transport,  $S_m = 0.3$  would be composed from  $1.3 \lesssim \alpha \lesssim 1.7$  and  $0 < \omega \lesssim 0.6$  while  $S_m = 0.02$  would have contributions from  $0 \lesssim \alpha \lesssim 0.1$  and  $0 < \omega \lesssim 0.3$ . It should be noted that (nearly) steady excitation is excluded since the associated forcing-response structures are both localised in the freestream. The resolvent norm along the Doppler curve for  $S_m = 0.3$  is qualitatively identical to that shown in fig. 8. Since the resolvent norm peaks sharply at the frequency-wavenumber pair of  $(\omega, \alpha) \approx (0.15, 1.6)$  it is expected that the response should be dominated by this monochromatic contribution.

## 7. Conclusion

We have investigated linear vortex receptivity by means of the resolvent (*i.e.* a family of transfer operators mapping the external forcing to the vortex response in frequency space). Discussion of (1.1) and (1.2) makes clear that the present study is complementary to previous linear approaches. In fact, the resolvent is at the root of all linear theories. Similarity of our results with those reported in the literature is therefore of structural rather than physical origin. Nevertheless, analysis of the resolvent is best suited for the question of freestream receptivity. Furthermore, analysis in frequency space allows us to relate the spectrum (determining the equivalent normal dynamics) and nonnormal dynamics. Our findings confirm previous results of Heaton & Peake (2007) and Mao & Sherwin (2012) in time domain (analysis of the propagator  $T(t)$ ).

The essential prerequisite for linear receptivity is nonnormality. Formulation of the problem in terms of the resolvent is appropriate to quantify nonnormality locally (in frequency space). Despite the governing operator being nonnormal, it was shown that the effective behaviour for vortices depends on the excitation frequency (called selective nonnormality). To the best of our knowledge, this work contains the first systematic use of resolvent bounds to classify nonnormality of linear vortex dynamics (considerable use of these bounds can be found in *e.g.* Reddy *et al.* 1993, too).

We found nonnormality of linear vortex dynamics to be essentially restricted to frequencies aligned with the inviscid continuous spectrum (characterising perturbation dynamics with stationary material advection). Accordingly, the associated forcing structures are localised in the critical layer. Using an upper bound of nonnormality in terms of the numerical range, we showed that disturbance alignment with the critical layer is necessary to maximise nonnormality. This finding is given physical meaning by consideration of the instantaneous variation of the integral kinetic energy.

Considering Lamb-Oseen, Batchelor and Moore-Saffman vortices as reference states, we found the above features of nonnormality to be robust. In particular, irrespective of the vortex model, linear dynamics turns out to be frequency-selectively nonnormal on the same range with forcing structures being systematically localised about the critical layer. On the contrary, nonnormality is almost invariant under variations of the axial wavenumber on the considered range. We conclude that freestream receptivity as a

consequence of nonnormal dynamics is largely independent of the precise vortex-core structure and in particular does not rely on axial mean velocity. This is in stark contrast to results of asymptotic stability (discrete spectrum) which crucially depends on the vortex model. Yet, universality of experimental trailing-vortex dynamics suggests that it should be associated with a robust mechanism, common for a large class of vortices. As motivated in § 1, we suggest a model of trailing-vortex dynamics as a linear system driven by the advective nonlinearity.

Declaration of Interests. The authors report no conflict of interest.

## Acknowledgements

This work has been supported by the French Ministry of Civil Aviation (DGAC) under PHYWAKE (PHYSics of WAKE vortices) research program. We are grateful to the anonymous referees for their exceptional investment and insightful suggestions.

## Appendix A. Numerical implementation, verification and validation

The present study relies on canonical and spectral decomposition of the linear operators  $R(s; L)$ ,  $L$  and  $L^\dagger$  as given in (2.3) which are approximated using a finite-element discretisation (see § 2 of Sipp & Marquet 2013 for details). The implementation uses `freefem++` (Hecht 2018) which uses the ARPACK library to solve eigenvalue problems (Lehoucq *et al.* 1997). Finite-element functions are fixed to the linear P1 and quadratic P2 Lagrangian finite elements for pressure and velocity, respectively (Hecht 2018, pp. 174–175). The radial domain in all computations is  $R = (0, r_{max}) = (0, 1] \cup (1, 6] \cup (6, r_{max}) = R_1 \cup R_2 \cup R_3$  with  $r_{max} = 30$ . The number of elements in each part of this partition is 200, 200 and 150 for  $R_1$ ,  $R_2$  and  $R_3$ , respectively. Grid refinement studies have been done for verification and convergence of the presented results is assured by variation of the maximum radius  $r_{max} \in [30, 200]$ .

The results of the canonical decomposition of the resolvent have been validated against the studies of Guo & Sun (2011) and Blanco-Rodríguez *et al.* (2017). Spectral decomposition of  $L$  is validated by comparing with the results of Fabre *et al.* (2006). To the best of our knowledge spectral decomposition of the adjoint  $L^\dagger$  has not been reported for vortices before; validation of the computation is therefore obtained by assuring condition (i)  $\sigma(L) = \sigma(L^\dagger)$  on the spectra and (ii) bi-orthogonality to hold (Kato 1980, Thm. 6.22; Friedman 1962, p. 112).

## REFERENCES

- ABID, M. 2008 Nonlinear mode selection in a model of trailing line vortices. *Journal of Fluid Mechanics* **605**, 19–45.
- ANTKOWIAK, A. 2005 Dynamique aux temps courts d’un tourbillon isolé. PhD thesis, Université Paul Sabatier de Toulouse.
- ANTKOWIAK, A. & BRANCHER, P. 2004 Transient energy growth for the Lamb-Oseen vortex. *Physics of Fluids* **16** (1), L1–L4.
- ARNOL’D, V. I. 1992 *Ordinary Differential Equations*. Springer.
- ASH, R. L. & KHORRAMI, M. R. 1995 Vortex stability. In *Fluid Vortices*, pp. 317–372. Springer.
- BAILEY, S. C. C., PENTELOW, S., GHIMIRE, H. C., ESTEJAB, B., GREEN, M. A. & TAVOULARIS, S. 2018 Experimental investigation of the scaling of vortex wandering in turbulent surroundings. *Journal of Fluid Mechanics* **843**, 722–747.
- BAKER, G. R., BARKER, S. J., BOFAH, K. K. & SAFFMAN, P. G. 1974 Laser anemometer measurements of trailing vortices in water. *Journal of Fluid Mechanics* **65**, 325–336.

- BANDYOPADHYAY, P. R., STEAD, D. J. & ASH, R. L. 1991 Organized nature of a turbulent trailing vortex. *AIAA Journal* **29** (10), 1627–1633.
- BATCHELOR, G. K. 1964 Axial flow in trailing line vortices. *Journal of Fluid Mechanics* **20**, 645–658.
- BLANCO-RODRÍGUEZ, F. J., RODRÍGUEZ-GARCÍA, J. O., PARRAS, L. & DEL PINO, C. 2017 Optimal response of Batchelor vortex. *Physics of Fluids* **29** (6), 064108.
- DEVENPORT, W. J., RIFE, M. C., LIAPIS, S. I. & FOLLIN, G. J. 1996 The structure and development of a wing-tip vortex. *Journal of Fluid Mechanics* **312**, 67–106.
- ENGEL, K.-J. & NAGEL, R. 2000 *One-Parameter Semigroups for Linear Evolution Equations*. Springer.
- FABRE, D. & JACQUIN, L. 2004 Viscous instabilities in trailing vortices at large swirl numbers. *Journal of Fluid Mechanics* **500**, 239–262.
- FABRE, D., SIPP, D. & JACQUIN, L. 2006 Kelvin waves and the singular modes of the Lamb-Oseen vortex. *Journal of Fluid Mechanics* **551**, 235–274.
- FARRELL, B. F. & IOANNOU, P. J. 1996 Generalized stability theory. part I: Autonomous operators. *Journal of the Atmospheric Sciences* **53** (14), 2025–2040.
- FEYS, J. & MASLOWE, S. A. 2014 Linear stability of the Moore-Saffman model for a trailing wingtip vortex. *Physics of Fluids* **26** (2), 024108.
- FONTANE, J., BRANCHER, P. & FABRE, D. 2008 Stochastic forcing of the Lamb-Oseen vortex. *Journal of Fluid Mechanics* **613**, 233–254.
- FRIEDMAN, B. 1962 *Principles and techniques of applied mathematics*. Courier Dover Publications.
- GARCÍA-ORTIZ, J. H., DOMINGUEZ-VAZQUEZ, A., SERRANO-AGUILERA, J. J., PARRAS, L. & DEL PINO, C. 2019 A complementary numerical and experimental study of the influence of Reynolds number on theoretical models for wingtip vortices. *Computers & Fluids* **180**, 176–189.
- GUO, Z.-W., CHEN, C. & SUN, D.-J. 2011 Stochastic forcing of the Batchelor vortex. In *AIP Conference Proceedings*, , vol. 1376, pp. 302–304. AIP.
- GUO, Z.-W. & SUN, D.-J. 2011 Optimal response in the Lamb-Oseen vortex. *Physics Letters A* **375** (36), 3191–3195.
- GUSTAFSON, K. E. & RAO, D. K. M. 1997 *Numerical Range. The Field of Values of Linear Operators and Matrices*. Springer.
- HALL, P. & SHERWIN, S. 2010 Streamwise vortices in shear flows: Harbingers of transition and the skeleton of coherent structures. *Journal of Fluid Mechanics* **661**, 178–205.
- HALLER, G., HADJIGHASEM, A., FARAZMAND, M. & HUHN, F. 2016 Defining coherent vortices objectively from the vorticity. *Journal of Fluid Mechanics* **795**, 136–173.
- HEATON, C. J., NICHOLS, J. W. & SCHMID, P. J. 2009 Global linear stability of the non-parallel Batchelor vortex. *Journal of Fluid Mechanics* **629**, 139–160.
- HEATON, C. J. & PEAKE, N. 2007 Transient growth in vortices with axial flow. *Journal of Fluid Mechanics* **587**, 271–301.
- HECHT, F. 2018 *Freefem++*. Version 3.56-2, 3rd edn. Laboratoire Jacques-Louis Lions, Université Pierre et Marie Curie, Paris.
- HILL, D. C. 1995 Adjoint systems and their role in the receptivity problem for boundary layers. *Journal of Fluid Mechanics* **292**, 183–204.
- IUNGO, G. V. 2017 Wandering of a wing-tip vortex: Rapid scanning and correction of fixed-point measurements. *Journal of Aircraft* **54** (5), 1779–1790.
- JACOBS, R. G. & DURBIN, P. A. 1998 Shear sheltering and the continuous spectrum of the Orr-Sommerfeld equation. *Physics of Fluids* **10** (8), 2006–2011.
- JACQUIN, L., FABRE, D., GEFFROY, P. & COUSTOLS, E. 2001 The properties of a transport aircraft wake in the extended near field: An experimental study. In *39th AIAA Aerospace Sciences Meeting and Exhibit*, p. 1038.
- JOSEPH, D. D. 1976 *Stability of Fluid Motions I*. Springer.
- KARAMI, M., HANGAN, H., CARASSALE, L. & PEERHOSSAINI, H. 2019 Coherent structures in tornado-like vortices. *Physics of Fluids* **31** (8), 085118.
- KATO, T. 1980 *Perturbation theory for linear operators*. Springer.
- KATO, T. & FUJITA, H. 1962 On the nonstationary Navier-Stokes system. *Rendiconti del Seminario Matematico della Università di Padova* **32**, 243–260.

- LANDAHL, M. T. 1967 A wave-guide model for turbulent shear flow. *Journal of Fluid Mechanics* **29**, 441–459.
- LANDAU, L. D. & LIFSHITZ, E. M. 1959 *Fluid mechanics*. Pergamon Press.
- LE DIZÈS, S. 2004 Viscous critical-layer analysis of vortex normal modes. *Studies in Applied Mathematics* **112** (4), 315–332.
- LEHOUCQ, R. B., SORENSEN, D. C. & YANG, C. 1997 Arpack users guide: Solution of large scale eigenvalue problems by implicitly restarted arnoldi methods.
- LEIBOVICH, S. & STEWARTSON, K. 1983 A sufficient condition for the instability of columnar vortices. *Journal of Fluid Mechanics* **126**, 335–356.
- MAO, X. & SHERWIN, S. 2011 Continuous spectra of the Batchelor vortex. *Journal of Fluid Mechanics* **681**, 1–23.
- MAO, X. & SHERWIN, S. 2012 Transient growth associated with continuous spectra of the Batchelor vortex. *Journal of Fluid Mechanics* **697**, 35–59.
- MARSHALL, J. S. & BENINATI, M. L. 2005 External turbulence interaction with a columnar vortex. *Journal of Fluid Mechanics* **540**, 221–245.
- MCKEON, B. J. 2017 The engine behind (wall) turbulence: Perspectives on scale interactions. *Journal of Fluid Mechanics* **817**, 1–86.
- MCKEON, B. J. & SHARMA, A. S. 2010 A critical-layer framework for turbulent pipe flow. *Journal of Fluid Mechanics* **658**, 336–382.
- MELANDER, M. V. & HUSSAIN, F. 1993 Coupling between a coherent structure and fine-scale turbulence. *Physical Review E* **48** (4), 2669.
- MOORE, D. W. & SAFFMAN, P. G. 1973 Axial flow in laminar trailing vortices. *Proceedings of the Royal Society of London. A. Mathematical and Physical Sciences* **333** (1595), 491–508.
- MORKOVIN, M. V. 1988 *Recent insights into instability and transition to turbulence in open-flow systems*. Institute for Computer Applications in Science and Engineering, NASA Langley Research Center.
- PRADEEP, D. S. & HUSSAIN, F. 2006 Transient growth of perturbations in a vortex column. *Journal of Fluid Mechanics* **550**, 251–288.
- REDDY, S. C., SCHMID, P. J. & HENNINGSON, D. S. 1993 Pseudospectra of the Orr-Sommerfeld operator. *SIAM Journal on Applied Mathematics* **53** (1), 15–47.
- REDDY, S. C. & TREFETHEN, L. N. 1994 Pseudospectra of the convection-diffusion operator. *SIAM Journal on Applied Mathematics* **54** (6), 1634–1649.
- RIESZ, F. & SZ.-NAGY, B. 1956 *Functional analysis*. Blackie.
- ROY, A. & SUBRAMANIAN, G. 2014 Linearized oscillations of a vortex column: The singular eigenfunctions. *Journal of Fluid Mechanics* **741**, 404–460.
- SARIC, W. S., REED, H. L. & KERSCHEN, E. J. 2002 Boundary-layer receptivity to freestream disturbances. *Annual Review of Fluid Mechanics* **34** (1), 291–319.
- SHARMA, A. S., MEZIĆ, I. & MCKEON, B. J. 2016 Correspondence between Koopman mode decomposition, resolvent mode decomposition, and invariant solutions of the Navier-Stokes equations. *Physical Review Fluids* **1**, 032402.
- SIPP, D. & MARQUET, O. 2013 Characterization of noise amplifiers with global singular modes: The case of the leading-edge flat-plate boundary layer. *Theoretical and Computational Fluid Dynamics* **27** (5), 617–635.
- SIPP, D., MARQUET, O., MELIGA, P. & BARBAGALLO, A. 2010 Dynamics and control of global instabilities in open-flows: A linearized approach. *Applied Mechanics Reviews* **63** (3), 1–26.
- SOHR, H. 2001 *The Navier-Stokes equations: An elementary functional analytic approach*. Springer.
- TAKAHASHI, N., ISHII, H. & MIYAZAKI, T. 2005 The influence of turbulence on a columnar vortex. *Physics of Fluids* **17** (3), 035105.
- TING, L., KLEIN, R. & KNIO, O. M. 2007 *Vortex Dominated Flows: Analysis and Computation for Multiple Scale Phenomena*. Springer Science & Business Media.
- TOWNE, A., SCHMIDT, O. T. & COLONIUS, T. 2018 Spectral proper orthogonal decomposition and its relationship to dynamic mode decomposition and resolvent analysis. *Journal of Fluid Mechanics* **847**, 821–867.
- TREFETHEN, L. N. & EMBREE, M. 2005 *Spectra and pseudospectra: The behavior of nonnormal matrices and operators*. Princeton University Press.
- VAN JAARSVELD, J. P. J., HOLTEN, A. P. C., ELSENAAR, A., TRIELING, R. R. & VAN HEIJST, R.

- G. J. F. 2011 An experimental study of the effect of external turbulence on the decay of a single vortex and a vortex pair. *Journal of Fluid Mechanics* **670**, 214–239.
- VIOLA, F., ARRATIA, C. & GALLAIRE, F. 2016 Mode selection in trailing vortices: Harmonic response of the non-parallel Batchelor vortex. *Journal of Fluid Mechanics* **790**, 523–552.
- WANG, Z. & GURSUL, I. 2012 Unsteady characteristics of inlet vortices. *Experiments in Fluids* **53** (4), 1015–1032.

## D | Long French résumé

Le flottement tourbillonnaire (*vortex meandering* en anglais) est une manifestation de l'instationarité tourbillonnaire observée dans les expériences depuis les années 1970. Celle-ci échappe encore aujourd'hui à une compréhension solide des mécanismes qui la sous-tendent. L'objectif de la présente thèse est de décrire et d'expliquer ces mécanismes. A ce titre, les travaux sont guidés par les questions suivantes :

– Pourquoi les tourbillons flottent-ils ? – Quelle est l'origine de ce phénomène ? – Quels sont les mécanismes essentiels ? – Quelles sont les caractéristiques récurrentes ? – Qu'est-ce qui est indispensable pour son occurrence ?

Le "meandering" du tourbillon, dans sa forme la plus générale, est le déplacement latéral et apparemment aléatoire du tourbillon dans son ensemble. Le phénomène est documenté pour divers écoulements dominés par les tourbillons, notamment dans l'aéronautique (tourbillon marginal et d'entrée des moteurs jet) et la géophysique (tornades et cyclones); on peut toutefois s'attendre à ce que les tourbillons soient affectés à toutes les échelles. Dans le cas particulier du "meandering" du tourbillon marginal, auquel on s'intéresse ici, la dynamique est toujours associée aux trois caractéristiques suivantes :

- (i) croissance de l'amplitude,
- (ii) coexistence d'une signature spectrale universelle à large bande et manifestation d'une cohérence ou d'une organisation progressive,
- (iii) concentration progressive et amplification de l'énergie de fluctuation dans le (cœur du) tourbillon.

La signature spectrale (c'est-à-dire l'accumulation progressive d'énergie dans le domaine des basses fréquences) témoigne du "retour à l'ordre" ; cela signifie que l'évolution typique des sillages de l'aile s'oppose au problème de transition vers la turbulence ("route vers la turbulence"), augmentant plutôt progressivement l'ordre à partir d'un état non ordonné et initialement complexe près de l'aile. Nous quantifions le niveau d'ordre en faisant appel à l'entropie et à l'analyse des séries temporelles non linéaires (à savoir, par des estimations de la dimension de "l'attracteur du meandering" et à partir de la structure caractéristique des récurrences). Une analyse du nombre de Rossby révèle des parallèles avec les caractéristiques de l'évolution de la turbulence dans les expériences d'écoulement en rotation.

En ce qui concerne la croissance de l'amplitude, nous avons des preuves expérimentales importantes que "amplitude  $\sim$  intensité de la turbulence  $\times \sqrt{\text{temps}/\text{circulation}}$ " est valable universellement. Ce comportement rappelle fortement un mouvement Brownien du tourbillon dans son ensemble. Nous soulignons deux observations importantes de cette loi – la réponse du tourbillon est *linéairement* forcée par l'intensité de la turbulence externe tandis que le tourbillon résiste à la déformation d'autant plus qu'il est fort (mesuré par la circulation).

Dans l'ensemble, nous proposons de modéliser la dynamique du tourbillon marginal en tant que *réceptivité généralisée* du tourbillon à l'excitation de l'écoulement libre (*free stream* en anglais) de manière à concentrer l'énergie de fluctuation dans le cœur tout en s'efforçant

d'obtenir un ordre général. Une décomposition en modes orthogonaux (POD) de la base de données expérimentale montre que les principales perturbations correspondent à une paire de dipôles localisés dans le cœur. L'énergie cinétique dans l'espace de perturbation couvert par ces deux modes croît en aval précisément au détriment de l'écoulement moyen.

Comme modèle théorique, nous partons des équations de Navier–Stokes linéarisées, que nous résolvons formellement dans l'espace de Fourier avec la résolvante. Dans un cadre d'opérateur de transfert linéaire, la *non-normalité est nécessaire pour la réceptivité* du tourbillon à l'excitation dans l'écoulement libre car, sinon, l'excitation et la réponse partagent inévitablement la même localisation. Cette condition préalable conduit à une restriction importante de la bande de fréquence admissible, qui est entièrement corrélée à un forçage de couche critique (c'est-à-dire le spectre continu non visqueux). L'archétype de la réceptivité (et probablement du "meandering") obéit au mécanisme mère–fille élucidé par Boberg & Brosa (1988).<sup>1</sup> C'est-à-dire des filaments à faible énergie (*mères*) enroulés autour de la couche critique dans la (proche) périphérie du cœur du tourbillon excitent par résonance des perturbations du cœur dipolaire (*sœurs*), aspirant l'énergie de l'écoulement moyen. Ce mécanisme est valable pour différents modèles de tourbillon et est donc un bon candidat pour le "meandering" des tourbillons observés de manière universelle.

---

<sup>1</sup>Boberg, L. & Brosa, U. (1988). Onset of turbulence in a pipe. *Zeitschrift für Naturforschung A*, **43**(8–9), 697–726.

**Titre** : Étude sur le flottement tourbillonnaire

**Mots clés** : flottement tourbillonnaire, résolvente, analyse du série temporelle, mouvement Brownien

**Résumé** : Le "meandering" est une manifestation de l'instationarité tourbillonnaire, observée dans les expériences depuis les années 1970, qui reste mal comprise. L'objectif de la présente étude est de décrire et d'expliquer le phénomène.

Le "meandering" est le déplacement latéral, apparemment aléatoire, du tourbillon dans son ensemble, connu pour divers écoulements tourbillonnaires. Dans le cas d'un tourbillon marginal, le mouvement est toujours associé avec les caractéristiques suivantes :

- (i) croissance d'amplitude en aval,
- (ii) coexistence d'une signature spectrale large bande universelle et d'une organisation progressive,
- (iii) concentration et amplification graduelles de l'énergie de fluctuation dans le tourbillon.

La signature spectrale est un témoignage du "retour à l'ordre" ; c'est-à-dire que l'évolution typique du sillage augmente progressivement l'ordre en dehors d'une dynamique complexe proche de l'aile. Nous quantifions le niveau d'ordre en faisant appel à l'entropie et à l'analyse des séries temporelles non-linéaires. Une analyse du nombre de Rossby révèle des parallèles avec l'évolution de la turbulence dans les expériences

d'écoulement en rotation.

En ce qui concerne la croissance d'amplitude, nous avons des preuves expérimentales que "amplitude  $\sim$  intensité de la turbulence  $\times \sqrt{\text{temps/circulation}}$ " est universellement valable. Cette loi suggère un mouvement Brownien du tourbillon dans son ensemble.

Nous modélisons la dynamique des tourbillons marginaux comme la *réceptivité généralisée* du tourbillon à l'excitation de l'écoulement libre. Une décomposition en modes orthogonaux (POD) de la base de données expérimentale montre que les principales perturbations correspondent à une paire de dipôles de déplacement dans le cœur. L'énergie des perturbations croît en aval au détriment du champ moyen.

Théoriquement, nous résolvons formellement les équations de Navier–Stokes linéarisées dans l'espace de Fourier avec la résolvente. Dans ce cadre, *la non-normalité est nécessaire pour la réceptivité*. Ce prérequis montre que le forçage pertinent est corrélé à la couche critique. L'archétype de réceptivité est constitué de filaments de faible énergie enroulés autour de la couche critique, qui excitent les perturbations du cœur, aspirant l'énergie du champ moyen.

**Title** : Treatise on the Meandering of Vortices

**Keywords** : Vortex meandering, resolvent, nonlinear time-series analysis, Brownian motion

**Abstract** : Meandering is a manifestation of vortex unsteadiness observed in experiments since the 1970s which remains puzzling in essential aspects. The objective of the present study is to describe and explain the subject matter – *Why meander vortices?*

Vortex meandering is the lateral, apparently random motion of the vortex as a whole, documented for various flows. In the case of trailing vortices, the motion is always associated with the following characteristics:

- (i) downstream amplitude growth,
- (ii) coexistence of a universal broadband spectral signature and progressive organization,
- (iii) gradual concentration and amplification of the fluctuation energy in the vortex.

The spectral signature is a testimony of the 'return to order'; that is, the typical evolution of wing wakes progressively increases orderliness out of a complex state close to the wing. We quantify the level of orderliness by appeal to the entropy and nonlinear time-series analysis. An analysis of the Rossby number reveals striking parallels to the turbulence evolution in rotating-tank experiments.

As regards the amplitude growth, we have considerable experimental evidence that 'amplitude  $\sim$  turbulence intensity  $\times \sqrt{\text{time/circulation}}$ ' holds universally. This behaviour is strongly reminiscent of a Brownian motion of the vortex as a whole.

We model trailing-vortex dynamics as the *generalized receptivity* of the vortex to excitation from the free stream. Proper Orthogonal Decomposition of the experimental database shows that the leading perturbations correspond to a pair of displacement-wave dipole patterns in the core. The energy in the perturbation space spanned by these two modes grows downstream at the expense of the mean flow.

As a theoretical model, we formally solve the linearised Navier–Stokes equations in Fourier space using the resolvent. In this framework, *non-normality is necessary for receptivity*. This prerequisite shows that the pertinent forcing is correlated with the critical layer. The receptivity archetype consists of low-energy filaments around the critical layer, which excite core perturbations, sucking energy from the mean flow.